The University of Hull

Active Fault-Tolerant Control of Nonlinear Systems with Wind Turbine Application

Being a thesis submitted for the degree of PhD

in the University of Hull

by

MONTADHER SAMI SHAKER

MSc Electronics (Baghdad)

October 2012

Acknowledgements

It is a pleasure to thank those who made this thesis possible. First, I owe many thanks for all the moral support, academic guidance that was given me by my supervisor, Professor Ron J Patton, in different matter during my study. Many thanks for his supervision expertise with numerous invaluable discussions and advice sessions that taught me how to do engineering research. It is really a wonderful feeling and honour to do research under his supervision.

I would like to thank all colleagues at the Department of Engineering, especially people in the Control and Intelligent Systems Engineering (Control Group), the University of Hull. I want to express my gratitude to my friend Ishaq Larbah, for his friendship during all these years.

I gratefully acknowledge the financial support of my PhD study from the Iraqi ministry of higher education and scientific research.

I also owe a great debt of gratitude to my dearest ones my parent, my brother Wesam, my wife, my daughters, and my parent in-law for their love and patient.

Abstract

The thesis concerns the theoretical development of Active Fault-Tolerant Control (AFTC) methods for nonlinear system via T-S multiple-modelling approach. The thesis adopted the estimation and compensation approach to AFTC within a tracking control framework. In this framework, the thesis considers several approaches to robust T-S fuzzy control and T-S fuzzy estimation: T-S fuzzy proportional multiple integral observer (PMIO); T-S fuzzy proportional-proportional integral observer (PPIO); T-S fuzzy virtual sensor (VS) based AFTC; T-S fuzzy Dynamic Output Feedback Control TSDOFC; T-S observer-based feedback control; Sliding Mode Control (SMC). The theoretical concepts have been applied to an offshore wind turbine (OWT) application study. The key developments that present in this thesis are:

- The development of three active Fault Tolerant Tracking Control (FTTC) strategies for nonlinear systems described via T-S fuzzy inference modelling. The proposals combine the use of Linear Reference Model Fuzzy Control (LRMFC) with either the estimation and compensation concept or the control reconfiguration concept.
- The development of T-S fuzzy observer-based state estimate fuzzy control strategy for nonlinear systems. The developed strategy has the capability to tolerate simultaneous actuator and sensor faults within tracking and regulating control framework. Additionally, a proposal to recover the Separation Principle has also been developed via the use of TSDOFC within the FTTC framework.
- The proposals of two FTTC strategies based on the estimation and compensation concept for sustainable OWTs control. The proposals have introduced a significant attribute to the literature of sustainable OWTs control via (1) Obviating the need for Fault Detection and Diagnosis (FDD) unit, (2) Providing useful information to evaluate fault severity via the fault estimation signals.
- The development of FTTC architecture for OWTs that combines the use of TSDOFC and a form of cascaded observers (cascaded analytical redundancy). This architecture is proposed in order to ensure the robustness of both the TSDOFC and the EWS estimator against the generator and rotor speed sensor faults.
- A sliding mode baseline controller has been proposed within three FTTC strategies for sustainable OWTs control. The proposals utilise the inherent robustness of the SMC to tolerate some matched faults without the need for analytical redundancy.

Following this, the combination of SMC and estimation and compensation framework proposed to ensure the close-loop system robustness to various faults.

- Within the framework of the developed T-S fuzzy based FTTC strategies, a new perspective to reduce the T-S fuzzy control design conservatism problem has been proposed via the use of different control techniques that demand less design constraints. Moreover, within the SMC based FTTC, an investigation is given to demonstrate the SMC robustness against a wider than usual set of faults is enhanced via designing the sliding surface with minimum dimension of the feedback signals.

Table of Contents

List of Abbreviations

Abbreviations

AFTC	Active fault tolerant control
EWS	Effective wind speed
FDD	Fault detection and diagnosis
FDI	Fault detection and isolation
FTC	Fault tolerant control
FTTC	Fault tolerant tracking control
LMI	Linear matrix inequality
LRMFC	Linear Reference Model Fuzzy Control
OWT	Offshore wind turbine
PFTC	Passive fault tolerant control
PIM	Pseudo inverse methods
PMF	Perfect model-following
PMIO	Proportional multiple integral observer
PPIO	Proportional-proportional integral observer
PV	Photovoltaic
SMC	Sliding mode control
SPD	symmetric positive definite
T-S	Takagi-Sugeno
TSDOFC	Takagi-Sugeno dynamic output feedback control
TSR	Tip-speed-ratio
VS	Virtual sensor

List of Publications

Within the period of this research the following works were published:

1. Sami, M. & Patton, R. J. 2012. Fault tolerant adaptive sliding mode controller for wind turbine power maximisation. 7th IFAC Symposium on Robust Control Design, Aalborg Congress & Culture Centre, Denmark, 499-504. 20-22 Jun.
2. Sami, M. & Patton, R. J. 2012. A multiple-model approach to fault tolerant tracking control for non-linear systems. 20th Mediterranean Conference on Control & Automation, Barcelona, 498-503. 3-6 July.
3. Sami, M. & Patton, R. J. 2012. Fault tolerant output feedback tracking control for nonlinear systems via T-S fuzzy modelling. 8th IFAC Symposium on Fault Detection, Supervision and Safety of Technical Processes, Mexico City, Mexico, 999-1004. 29-31 Aug.
4. Sami, M. & Patton, R. J. 2012. An FTC approach to wind turbine power maximisation via T-S fuzzy modelling and control. 8th IFAC Symposium on Fault Detection, Supervision and Safety of Technical Processes, Mexico City, Mexico, 349-354. 29-31 Aug.
5. Sami, M. & Patton, R. J. 2012. Global wind turbine FTC via T-S fuzzy modelling and control. 8th IFAC Symposium on Fault Detection, Supervision and Safety of Technical Processes, Mexico City, Mexico, 325-330. 29-31 Aug.
6. Sami, M. & Patton, R. J. 2012. Wind turbine power maximisation based on adaptive sensor fault tolerant sliding mode control. 20th Mediterranean Conference on Control & Automation, Barcelona, 1183-1188. 3-6 July.
7. Sami, M. & Patton, R. J. 2012. Wind turbine sensor fault tolerant control via a multiple-model approach. The 2012 UKACC International Conference on Control, Cardiff, 3-5 Sep.
8. Sami, M. & Patton, R. J. 2012. A fault tolerant approach to sustainable control of offshore wind turbines. 2nd International Symposium on Environment Friendly Energies and Applications, Northumbria University, UK, 25–27 June.
9. Sami, M. & Patton, R. J. 2012. Active Fault Tolerant Control for Non-linear Systems with Simultaneous Actuator and Sensor Fault. Int. J. Adapt. Control & signal processing, submitted.

Chapter 1 : Introduction

1-1. Introduction

Owing to the increasing demand on maintaining acceptable system performances in wide operating conditions, it becomes very important to design controllers so that the system under control maintains nominal performance (with acceptable degrade) when malfunction occurs. These controllers are known as fault tolerant controllers and have the ability to deal with systems that are subjected to faults. While the classical controller design only considers systems during nominal operation, the fault tolerant control (FTC) design explicitly includes the effects of faults on the behaviour of the system (Patton, 1997a, Blanke, Kinnaert, Lunze and Staroswiecki, 2006, Zhang and Jiang, 2008).

An increased interest in designing FTC and fault detection and diagnosis (FDD) systems has appeared in the last two decades, one can notice this through the publications which consider these topics in different application studies (Gertler, 1998, Chen and Patton, 1999, Chiang, Russell and Braatz, 2001, Blanke, Kinnaert, Lunze and Staroswiecki, 2006, Ding, 2008, Ducard, 2009, Noura, Theilliol, Ponsart and Chamseddine, 2009, Tehrani and Khorasani, 2009, Edwards, Lombaerts and Smaili, 2010, Jelali and Huang, 2010, Yang, Jiang and Cocquempot, 2010, Alwi, Edwards and Tan, 2011, Meskin and Khorasani, 2011, Richter, 2011, Song and Hedrick, 2011, Yang and Ye, 2011).

Historically, safety critical systems have stimulated a significant amount of research in FTC systems. Specifically, aviation accidents at the end of the 1970's have initiated the need for FTC design problem (Patton, 1997a, Zhang and Jiang, 2008). Extensive survey of aircraft accidents and history of flight reconfigurable control have been presented in (Steinberg, 2005, Edwards, Lombaerts and Smaili, 2010). However, FTC has begun to stimulate research in a different industrial community, particularly, the systems that demand high degree of reliability and availability (sustainability) and at the same time are characterised by expensive and safety critical maintenance work. In fact, there is clear conflict between ensuring a high degree of availability and reducing costly maintenance times. However, the recently developed offshore wind turbines (OWTs)

are the foremost example of systems for which this conflict has arisen since wind turbines have a stochastic and uncontrollable driving force as input in the form of wind speed. The OWT site accessibility is not always ensured during malfunctions. Therefore, system availability is highly affected by malfunctions and weather conditions. On the other hand, OWT maintenance work is more expensive to perform by a factor of 5-10 times compared with their onshore counterparts. Additionally, the cost (day rate) of general purpose lifting equipments required for OWTs is higher than that for the onshore wind turbine by a factor of 10 (van Bussel and Zaaijer, 2001). Thus, a reduction of maintenance effort to a minimum level is essential for OWTs.

Figure 1-1: OWTs maintenance (www.siemens.co.uk, 2012, www.smart-energy.com, 2012)

Several problems add credibility to the points raised above. For example, a megawatt turbine in Canada developed a gearbox bearing fault in January 2004, requiring complete overhaul of the gearbox, which demanded replacement of the existing gearbox with a new one. The 300 ton capacity crane was ordered as well as a replacement gearbox. Unfortunately, the crane arrived and bad weather set in. The work was suspended for the next 3 weeks because of weather and hazardous work conditions. The result was that the crane costs exceeded $ 150,000, an energy loss of $26,000 was incurred, and replacement of the gearbox, cost over $ 250,000 (The World Wind Energy Association, 2012). Analysis on wind farm maintenance costs has shown that unscheduled maintenance visits account for approximately 75% of the total wind turbine maintenance costs, whilst preventive visits and major planned overhauls account

for 20% and 5%, respectively (The World Wind Energy Association, 2012). Furthermore, wind turbine maintenance is a very dangerous process; several accidents have been reported during maintenance and some of these were fatal. Details of wind turbine accidents up to 31 March 2012 are available in (www.caithnesswindfarms.co.uk, 2012).

Consequently, improvements in reliability and availability and the requirement to minimize the complexity and cost of maintenance operations of OWTs are combined challenges that serve to enhance the importance of FDD and FTC for wind turbines. In fact, early or prompt fault detection and fault isolation for the mechanical and electrical subsystems of wind turbines can help to ensure that major component failures are avoided as well as preventing side effects that can lead to other component malfunctions. Since fault detection can be performed while the malfunctioning component is still operational, this will avoid unscheduled maintenance. Furthermore, avoiding unscheduled maintenance is of vital important for offshore wind farms, where bad weather conditions can prevent any repair actions for several weeks (van Bussel and Zaaijer, 2001, Ribrant and Bertling, 2007). Moreover, based on the information provided by FDD, an FTC scheme can trigger specific control actions to prevent damage of plant components and ensure system availability during malfunctions. Thus, overall maintenance costs and off-time of wind turbines can be significantly reduced. In the literature, FTC and its complementary FDD system have been recognised to be the proper solution of ensuring these requirements (kk-electronic, Wei and Verhaegen, 2008, Amirat et al., 2009, Bin, Yaoyu, Xin and Zhongzhou, 2009, Hameed et al., 2009, Odgaard, Stoustrup and Kinnaert, 2009, Wei and Liu, 2010, Sloth, Esbensen and Stoustrup, 2011, Kamal, Aitouche, Ghorbani and Bayart, 2012).

Moreover, FTC methods represent promising approaches for handling several practical fault scenarios for real system applications. For example, in (Patton, Putra and Klinkhieo, 2010b), FTC is utilised to compensate the effect of existing friction in mechatronic systems. In (Sung, Lee and Bien, 2005) FTC is used to enhance the performance of an electromagnetic suspension system through tolerating the effect of air gap sensor fault and an accelerometer fault. In (Podder and Sarkar, 2001) a way of tolerating the effect of a faulty thruster is proposed through reallocation of thruster forces of an autonomous underwater vehicle. (Ducard, 2009) describes the application

of FTC methods for flight control of unmanned airborne vehicles. FTC for a power plant application is also presented in (Luqing et al., 2001).

The importance of the FTC for different application studies, specifically OWTs, has been the main motivation for this research, providing investigation of different fault impacts, the main approaches for FTC, and some new methods in FTC of nonlinear systems. The rest of this Chapter introduces some fundamental terminology, main approaches, and basic building blocks of FTC and FDD topics.

1-2. Fault definition, classification, and modelling

A fault is an uncontrollable defect in the system structure or parameter that eventually leads to degradation in the closed-loop system performance or even the loss of the system function (failure). The literature various definitions for faults and failures. For example, (Blanke, Kinnaert, Lunze and Staroswiecki, 2006) defined a fault as '*…a deviation in the system structure or the system parameters from the nominal situation …*'. (Isermann, 2006) defined a fault as '*… a non-permitted deviation of a characteristic property (feature), of the system from the acceptable, usual, standard condition…*'. A failure, on the other hand, is defined as '*… A failure is a permanent interruption of a system's ability to perform a required function under specified operating conditions ...*'(Isermann, 2006).

Clearly, a failure is a much more severe concept than a fault. Although the fault causes the deviation of nominal system performance, the nominal controller can be equipped with some remedial activities to overcome the fault effects and hence maintain acceptable performance. On the other hand, when a failure occurs, a totally different component is needed to be able to retain the nominal performance, so that a form of redundancy becomes necessary.

Faults are classified according to their time characteristics as abrupt (non-smooth time behaviour), incipient (smooth time behaviour), and intermittent (pulsating time behaviour) (Isermann, 2006) (see Figure 1-2).

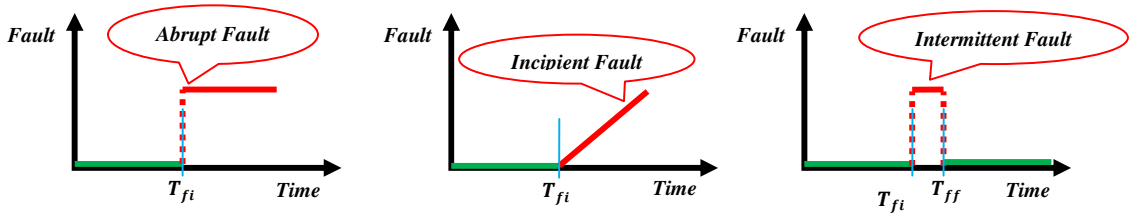

Figure 1-2: Fault classification with respect to time

Based on the location of the faults acting within a dynamical system, the faults are classified as actuator faults, sensor faults, or process faults. This classification is widely used in the FTC literature (Chen and Patton, 1999). Figure 1-3 below illustrates these faults classes.

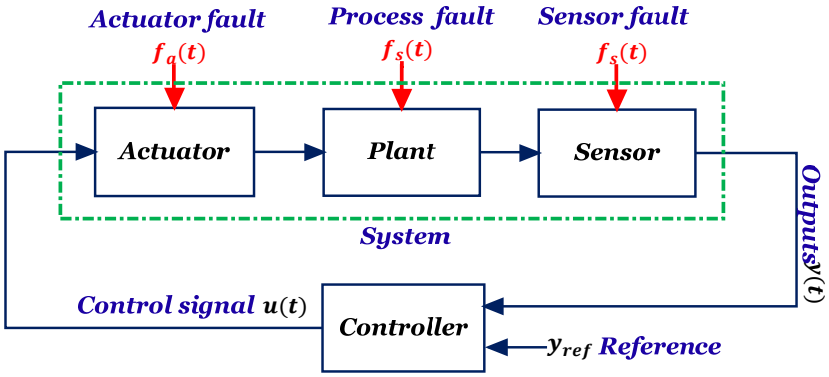

Figure 1-3: Fault classification with respect to their location

- ***Actuator Fault*** ($f_a(t)$): This fault corresponds to variations of the control input applied to the controlled system either completely or partially. The complete actuator faults means that the actuator produces no actuation regardless of the input applied to it. This can occur as a result of breakage, or burn out wiring. Partial actuator faults are cases in which the actuator has a slower response or become less effective and hence provides the plant with part of the normal actuation signal.
- ***Sensor Fault*** ($f_s(t)$): The sensors are any equipment that takes a measurement or observation from the system, e.g. potentiometers, accelerometers, tachometers, pressure gauges, strain gauges, etc. Sensor faults imply that incorrect readings or measurements are taken from the real dynamical system. This fault can also be subdivided into either complete or partial sensor faults. The complete sensor fault is the case in which the sensor provides readings that no longer correspond to the required physical parameters. The partial sensor fault is the case in which the sensor still provides inaccurate readings that contains the required physical parameters such that the required reading could be retrieved.
- ***Process Fault*** ($f_p(t)$): These faults directly affect the physical parameters of the system and in turn the input/output properties of the system. Process faults are often termed *component faults*, arising as variations from the structure or parameters used during system modelling, and as such cover a wide class of possible faults e.g. dirty water having a different heat transfer coefficient compared to when it is clean, or

changes in the viscosity of a liquid or components slowly degrading over time through wear and tear, aging or environmental effects, etc.

Some literature further classifies the faults according to the way they are modelled as either additive or multiplicative faults. Fault modelling is concerned with the representation of the real physical faults and their effects on the mathematical model of the system. The importance of fault modelling comes from the fact that all remedial actions taken to compensate the fault are based on the most appropriate form of modelling (Chen and Patton, 1999).

Fault effects appear in mathematical system models either as additive (signal change) or multiplicative (parameter change) terms. For example, actuator faults deform the control signal required to actuate the system. Mathematically, an actuator fault appears in the system model as follows:

$$u^f = \varepsilon^a u \tag{1-1}$$

where ε^a is a diagonal matrix with diagonal elements $0 \leq \varepsilon_i^a \leq 1, i = 1, 2, \ldots m$. Here, each element of the ε^a matrix determines the intensity of the fault in the i^{th} actuator with $\varepsilon_i^a = 0$ indicating a complete i^{th} actuator fault (failure), whereas $\varepsilon_i^a = 1$ implies that the i^{th} actuator operates normally. Any ε_i^a between 0 and 1 implies the presence of partial faults. Suppose that the state space model of the nominal system is given by:

$$\left.\begin{aligned} \dot{x} &= Ax + Bu \\ y &= Cx \end{aligned}\right\} \tag{1-2}$$

The state space model of the system dynamics with actuator faults will be:

$$\left.\begin{aligned} \dot{x} &= Ax + B\varepsilon^a u \\ y &= Cx \end{aligned}\right\} \tag{1-3}$$

This form of faulty models can represent a so called multiplicative fault and is useful in implementing FTC loops (Theilliol et al., 2008). Similarly, multiplicative sensor faults can be modelled as:

$$y^f = \varepsilon^s y \tag{1-4}$$

The effect of the sensor fault appears in the system model as follows:

$$\left.\begin{aligned} \dot{x} &= Ax + Bu \\ y^f &= \varepsilon^s Cx \end{aligned}\right\} \tag{1-5}$$

where ε^s is a diagonal matrix with diagonal elements $0 \leq \varepsilon_i^s \leq 1$, $i = 1, 2, \ldots p$. Here, each element of the matrix ε^s determines the intensity of the fault in the i^{th} sensor with $\varepsilon_i^s = 0$ denoting that a complete i^{th} sensor fault has occurred. $\varepsilon_i^s = 1$ implies that the i^{th} sensor operates normally, and any ε_i^s values between 0 and 1 imply that partial sensor faults have occurred.

Another way of introducing the effects of actuator, sensor and component faults into system model is by adding (additive fault) a new term to the dynamics of Eq. (1-1) as illustrated in Eq. (1-6):

$$\left.\begin{aligned} \dot{x} &= Ax + Bu + F_x f \\ y &= Cx + F_y f \end{aligned}\right\} \tag{1-6}$$

where f is the fault signal, F_x and F_y are the fault distribution matrices. It should be noted that additive faults representation best describes the cases in which the fault is independent of the system input and/or state such as plant leaks. On the other hand a multiplicative fault reflects the situation in which the plant parameters change and this is a good way to describe the deterioration of plant equipments, i.e. via parametric variations.

Remark: In Chapter 3, a new approach to fault modelling is presented in which, from an FTC stand point, the additive fault model can be considered as a generalized fault representation. Hence, only the additive fault model is considered in this thesis.

1-3. Structure and Approaches to FTC Systems

Generally, the nominal controller (sometimes referred to as the "baseline" controller, see Patton, 1997) aims to stabilize and achieve the required closed-loop performance during normal operation conditions. To give the controlled system the ability to tolerate fault effects, additional inherent ability of the controller and/or extra assistant blocks should be inserted in the control loop. Figure 1-4 illustrates the main structure of the fault tolerant system.

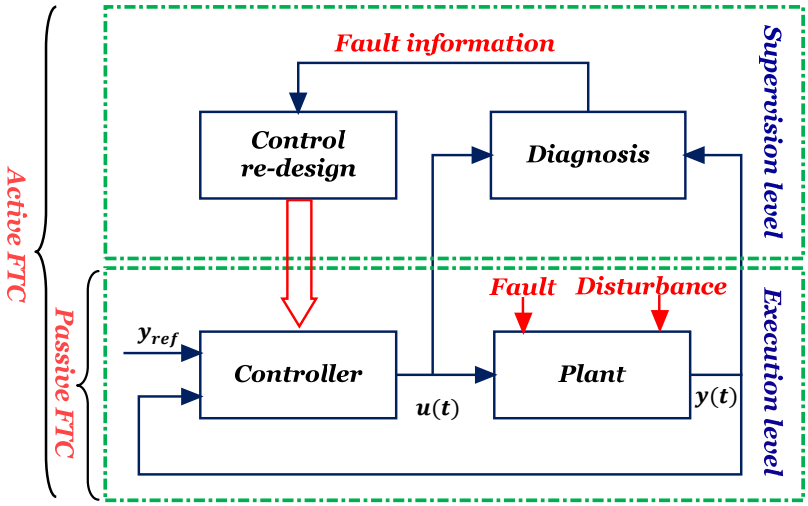

Figure 1-4: Schematic of the fault tolerant system (Blanke, Kinnaert, Lunze and Staroswiecki, 2006)

Generally, two steps are required to provide the system with the capability to tolerate faults:

- Equip the system with some mechanism to make it able to detect the fault once it occurs, provide information about the location, identification of faulty component, and decide the required remedial action in order to maintain acceptable operation performance (Supervision level).
- Make use of the information obtained from the supervision level and adapt the controller parameters and/or reconfigure the structure of the controller so that the required remedial activity can be achieved (Control reconfiguration level).

Hence, the FTC loop extends the usual feedback controller by a *supervision level*. In the absence of a fault, the system matches its nominal response so that the nominal controller attenuates the disturbance and ensures good reference following and other requirements on the closed-loop system. In this situation, the diagnostic block recognizes that the closed-loop system is fault-free and no change of the control law is necessary.

If a fault occurs, the *supervision level* makes the control loop fault-tolerant. The diagnosis block identifies the fault and the control re-design block adjusts the controller to the new controller parameter set. Following this, the reconfigured system continues to satisfy the control target.

Thus, FTC is the control loop that has the ability to fulfil the required system performances even if faults occur through utilizing the help provided by the supervision level. Approaches for synthesizing the FTC loop are classified as either a passive FTC (PFTC) or active FTC (AFTC). In the PFTC approach, the control loop is designed to tolerate some anticipated types of faults. The effectiveness of this strategy, that usually handles anticipated faults scenarios, depends upon the robustness of the nominal closed-loop system. Additionally, since the robustness of the closed-loop system to the fault is considered during the design cycle of the nominal controller, this may lead to post-fault degraded performance of the closed-loop system. However, it is interesting to note that the PFTC system does not require the FDD and controller reconfiguration and hence it has the ability to avoid the time delay due to online diagnosis of the faults and reconfiguration of the controller. In fact, this is very important in practice where the time windows during which the system remains stabilisable in the presence of faults are very short, e.g. the unstable double inverted pendulum example (Niemann and Stoustrup, 2005, Weng, Patton and Cui, 2007). Most of the PFTC methods have been proposed mainly based on robust control theory. However, the fundamental difference between the traditional robust control and the PFTC lies in the fact that robust control deals with small parameter variations or model uncertainties, whilst PFTC deals with more drastic changes in system configuration caused by faults (Šiljak, 1980, Veillette, Medanic and Perkins, 1992, Veillette, 1995, Seo and Kim, 1996, Guang-Hong, Si-Yang, Lam and Jianliang, 1998, Zhao and Jiang, 1998, Geromel, Bernussou and de Oliveira, 1999, Wang and Shao, 2000, Yang, Wang and Soh, 2000, Yew-Wen, Der-Cheng and Ti-Chung, 2000, Puig and Quevedo, 2001, Fang, Jian Liang and Guang-Hong, 2002, Hsieh, 2002, Benosman and Lum, 2010, Guang-Hong and Dan, 2010). It should be noted that in the early literature the PFTC approach was referred to as “reliable control” (Veillette, Medanic and Perkins, 1992, Veillette, 1995).

In order to improve the post-fault control performance and cope with severe faults that break the control loop, it is commonly advantageous to switch to a new controller that is on-line or designed off-line to control the faulty plant.

In the AFTC approach, two conceptual steps are required: *FDD* and *controller adjustment* so that the control law is reconfigured to achieve performance requirements, subsequent to faults (Patton, 1997a, Blanke, Staroswiecki and Wu, 2001, Blanke, Kinnaert, Lunze and Staroswiecki, 2006, Zhang and Jiang, 2008, Richter, 2011). An

AFTC system compensates for faults either by selecting a pre-computed control law (projection-based approaches) (Pogoda and Maybeck, 1989, Maybeck and Stevens, 1991, Rauch, 1995, Boskovic and Mehra, 1999, Zhang and Jiang, 2001, Seron, De Dona and Martinez, 2009, Shengqi, Liang, Cuijuan and Wenwei, 2009, Sanchez-Parra, Suarez and Verde, 2011) or by synthesizing a new control strategy on-line (on-line automatic controller redesign approaches) (Ahmed-Zaid, Ioannou, Gousman and Rooney, 1991, Tao, Joshi and Ma, 2001, Zhang and Jiang, 2002, Yen and Liang-Wei, 2003, Lunze and Steffen, 2006, Richter, Schlage and Lunze, 2007, Alwi and Edwards, 2008, Sijun, Youmin, Xinmin and Rabbath, 2009, Gayaka and Bin, 2011, Hamayun, Edwards and Alwi, 2011, Zou and Kumar, 2011, Li and Yang, 2012). Another widely studied method is the fault compensation approach, where a fault compensation input is superimposed on the nominal control input (Theilliol, Noura and Sauter, 1998, Noura, Sauter, Hamelin and Theilliol, 2000, Boskovic and Mehra, 2002, Bin, Staroswiecki and Cocquempot, 2006, Gao and Ding, 2007a, Gao and Ding, 2007b, Jiang, Gao, Shi and Xu, 2010, Zhang, Jiang and Staroswiecki, 2010).(Patton, Putra and Klinkhieo, 2010a)

It should be noted that owing to the ability of the traditional adaptive control methods to automatically adapt controller parameters to changes in system parameters, adaptive control has been considered as a special case of AFTC that obviates the need for diagnosis and controller re-design steps (Tao, Joshi and Ma, 2001, Tao, Chen, Tang and Joshi, 2004, Ye and Guang-Hong, 2006, Yang and Ye, 2011). However, adaptive control is best suited for application to plants that have slowly varying parameters, whilst, plants under the influence of faults typically have a nonlinear behaviour with sudden parameter changes since the faults cause nonlinear effects as the system moves away from its known equilibrium point. Furthermore, obviously adaptive control based AFTC can actively tolerate actuator and system faults, but it is not capable of tolerating sensor faults since in this situation the controller adapt its parameters according to the faulty measurements and hence causes the closed-loop system to deviate from correct operation. Therefore, for the case of sensor fault and FDD unit is required to detect, isolate, identify and then compensate the fault.

1-4. Fault Detection and Diagnosis

Fault detection and diagnosis (FDD) concerns procedures for determining whether or not a fault has occurred (fault detection) and judging the level of severity of the fault

and it's likely consequence (fault diagnosis), based on the available input and output signals. In the literature, another terminology has been popular for more than 25 years (Patton, Frank and Clark, 1989), this is fault detection and isolation (FDI) in which the fault is not only detected but also located in the system (or the fault is "isolated"). Sometimes the combined actions of fault isolation and fault identification are referred to as the diagnosis component of an FDD scheme (Gertler, 1998). The FDD function plays a vital role since the reconfiguration process, involved within the AFTC framework, depends on the information delivered by the FDD unit and hence the overall robustness of the AFTC design is strongly affected by the robustness of the FDD unit.

The process of FDD includes successive steps with each step serving the next until a diagnosis is achieved (Gertler, 1998, Chen and Patton, 1999, Blanke, Kinnaert, Lunze and Staroswiecki, 2006, Isermann, 2006, Ding, 2008, Meskin and Khorasani, 2011). These steps are:

Fault Detection: This step determines the occurrence of the fault by generating a signal that is affected by the faults only, this signal is called the *residual*. Therefore, in some literature this step is named as the *residual generation* step.

Fault Isolation (Localization): This step determines the component in which the fault has occurred.

Fault Identification (Analysis): This step determines the fault type and its consequences.

In fact, fault isolation and identification are based on processing the residual signal to extract the information about the fault of interests. Therefore in the literature, faults isolation and identification are sometimes referred to as *decision making* or the *residual evaluation* step (Patton, Frank and Clark, 1989, Patton, Frank and Clark, 2000).

The importance of detecting and diagnosing system faults comes from the fact that every controlled system can be subjected to faults occurring at unexpected time instants, making each fault difficult to predict and prevent. System faults can lead to catastrophic effects on human life, they can damage the environment, and lead to unsuitable plant economics. Whilst the occurrence of a fault cannot be prevented, the early detection of faults can lead to avoiding the fault consequences or at least minimise the severity of fault consequences. In fact, from a practical stand point, the topics of FDI and FDD have led to very interesting and challenging directions for theoretical and applied research in the control community. For example: the detection of faults, to be useful in

practice, should be achieved early by detecting "incipient" effects associated with the fault before its effects become serious (Patton, Frank and Clark, 1989, Patton and Chen, 1993, Zolghadri, Henry and Monsion, 1996, Patton, 1997b, Edwards, Spurgeon and Patton, 2000, Patton, Frank and Clark, 2000, Goh, Spurgeon and Jones, 2002, Tan and Edwards, 2002, Henry and Zolghadri, 2005, Marcos, Ganguli and Balas, 2005, Henry, 2007, Rodrigues, Theilliol, Adam-Medina and Sauter, 2008, Simani and Patton, 2008, Alwi, Edwards and Tan, 2009, Patton, Uppal, Simani and Polle, 2010).

Hardware and analytical redundancies are very important aspects of FDD. Hardware redundancy implies the addition of redundant physical components in order to increase the reliability of a closed-loop system. For example, two or three sensors are used to measure the same state to ensure reliable measurements in the case of a fault. On the other hand, analytical redundancy makes use of observers to provide estimates of the signal of interest instead of using redundant hardware. Hence, analytical redundancy obviates the need for extra hardware which in turn reduces the manufacturing costs. Figure 1-5 schematically illustrates these concepts.

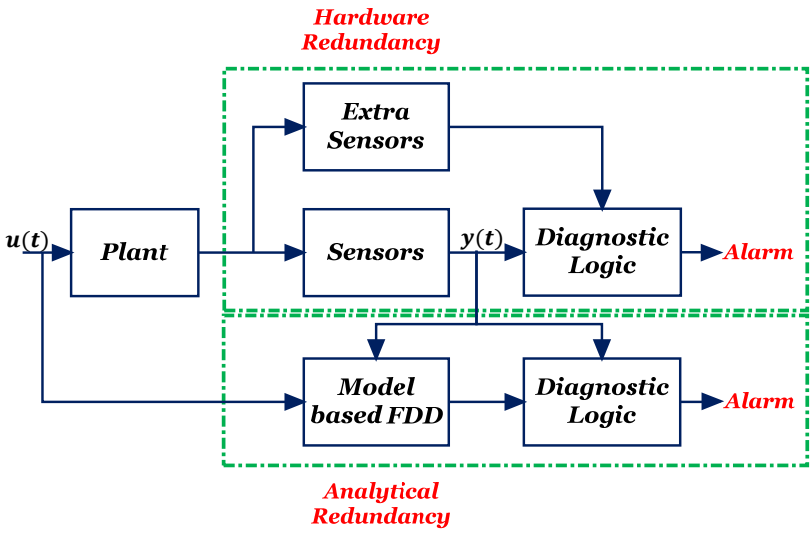

Figure 1-5: Hardware and analytical redundancy (Ding, 2008)

Generally, FDD methods are classified as to whether or not they utilise the mathematical model of the monitored plant. FDD methods which use an explicit mathematical model of the plant are often preferred (Patton, Frank and Clark, 1989, Gertler, 1998, Chen and Patton, 1999, Patton, Frank and Clark, 2000, Isermann, 2006, Ding, 2008). FDD techniques that do not require the use of models are often referred to as "model-free" FDD methods and can be classified as:

1. **Physical redundancy**: Multiple sets of sensors are installed to measure the same sets of variables. Any inconsistency between the measurements indicates a sensor fault. Clearly, increasing the level of redundancy implies that more information about the fault can be utilised. For example, with two parallel sets of measurements fault isolation is not possible, whereas, with three set of measurements, a voting scheme can be formed to isolate the faulty sensor.
2. **Limit checking**: This is the most frequently used in practice in which plant measurements are compared by computer to preset limits. Fault indication activates if the measurements exceeds the predefined threshold. The serious drawback of this method is that a single component fault may propagate through many plant variables which in turn could cause a significant number of system signals to exceed their limits and appear as multiple faults, leading to a very challenging fault isolation problem.
3. **Frequency spectral analysis**: This approach is based on observing the consistency between frequency spectra of plant measurements and the spectrum of normal operation conditions; any inconsistency represents an indication of abnormality. Fault isolation is also possible if they have their distinctive mark in the spectrum.

On the other hand, the intuitive idea of the model-based approach to FDD is appealing as this approach makes use of the concept of analytical redundancy in which the plant model runs in parallel with the real plant and is provided with the same inputs and outputs as the real plant. The differences between the sensor measurements and the analytically computed values of the respective variables, are referred to as *residual*, and these are indicators of the presence of faults in the system. In the literature, the procedure for extracting fault symptoms from the system, with the fault symptoms represented by a residual signal is called *residual generation*. On the other hand, the algorithm used to generate a residual is called a *residual generator* (Patton, Frank and Clark, 1989, Chen and Patton, 1999, Ding, 2008).

Owing to the presence of noise and modelling errors, the residual generation process needs to be followed by *residual evaluation* which is responsible for evaluating the residuals and monitor if and where a fault has occurred. This process may make use of a simple threshold test on the instantaneous values of the residual, or it may consist of methods of statistical decision theory (Chen and Patton, 1999). Figure 1-6 shows the

schematic outline of fault diagnosis showing the residual generation and residual evaluation functions.

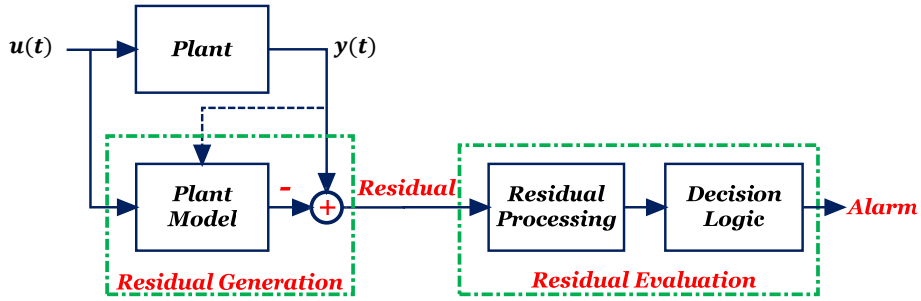

Figure 1-6: Schematic of model-based fault diagnosis adapted from (Ding, 2008)

The most important issue in model-based fault diagnosis is the robustness against modelling uncertainty which arises from inaccurate modelling of the monitored process, measurement noise, and disturbance. During the last 25 years robust fault diagnosis has steadily become a very significant research issue (Chen and Patton, 1999, Patton, Frank and Clark, 2000, Ding, 2008, Tehrani and Khorasani, 2009, Falcoz, Henry and Zolghadri, 2010, Patton, Uppal, Simani and Polle, 2010, Qing and Mehrdad, 2010).

In the literature, there are *three* different approaches used for residual generation in model-based FDD (Gertler, 1998, Chen and Patton, 1999, Ding, 2008):

1. *Observer-based FDD:* In this approach the observer is used to provide estimation of the actual system output. The residual signal is generated via the weighted output estimation error between the measured output and the estimated output. The available flexibility in selecting observer gains and the wide usage of observers in control theory and application has motivated interest in this approach.
2. *Parity relation based FDD:* In this approach, the residual signals are generated based upon a consistency check on system input and output data over a given time window. Several researchers have proved that the parity equation approach has some correspondence with certain types of observer-based FDD/FDI approaches (Chen and Patton, 1999, Isermann, 2006, Ding, 2008).
3. *Parameter estimation approach:* This approach is developed based on system identification techniques. The faults are reflected in the physical system parameters and then the idea of the fault detection is based on the comparison between the online estimation of system parameter and the parameter of the fault-free reference model.

It is also interesting to note that model-based FDD methods can be based on the use of an "implicit model", rather than the more usually understood explicit model-based methods outlined above. In this case the model is implicitly represented using either a dynamical or recurrent neural network or a fuzzy logic fault diagnosis scheme (Calado et al., 2001) or via a combination in the form of a neuro-fuzzy structure (Uppal and Patton, 2005).

1-5. Thesis Structure

The main trend of the work is the proposal of AFTC methods for nonlinear systems using the estimation and compensation methodology. The remainder of the thesis is arranged as follows:

Chapter 2 gives a generic literature review of the main FTC strategies, as well as an investigation of their advantages and limitations. Since the main trend of the work is based on multiple-model approach, Section 2-3 describes the main concepts of the T-S fuzzy based nonlinear system modelling and control and the literature of research studies that use the T-S fuzzy framework in FTC of nonlinear systems. The survey presented in Chapter 2 has established good foundations to highlight the challenges in the FTC framework to be considered in the next Chapters.

The work presented in **Chapter 3** is motivated by the lack of literature investigating the following points:

1. The relative impacts of the sensor and actuator faults on regulator control problems.
2. The relative impacts of the sensor and actuator faults on tracking control problems.
3. The advantageous features of the use of Linear Reference Model Fuzzy Control (LRMFC) within multiple-models (specifically T-S fuzzy approach) and in an FTC framework.

To attain the aim of this Chapter, the LMI-based design of the model reference state tracking T-S fuzzy controller is designed first to be the basis for illustrating the investigations. The main contributions of this Chapter are:

- The proposal of the use of an LRMFC strategy as an alternative approach to the LMI-based pole-clustering closed-loop performance specification. This achieves significant attributes to the T-S fuzzy modelling and control via: (i) governing the closed-loop performance of nonlinear system without the use of additional (e.g.

pole-clustering) LMIs. (ii) Offering precise allocation of closed-loop system eigenvalues. Following this a new research trend is established based on modifying the control strategies to minimise design constraints.

- Investigate the relative impacts of actuator and sensor faults within the tracking and regulator control framework. This is a significant attribute in the FTC literature since the solutions to the challenges that arise in Chapter3 have not been considered in the FTC literature.
- Introduce the concept of additive fault modelling as a generalised fault model within the fault estimation framework.

Following the investigations presented in Chapter 3, the sensor FTTC is the most challenging fault scenario. Hence the main contributions in **Chapter 4** are:

a. The proposal of the LMI-based design of active sensor fault tolerant model reference tracking control for nonlinear systems described via T-S fuzzy inference modelling. The designed strategy is based on the use of the VS method based on-line control reconfiguration. From the simulation results, the limitations of using this method within T-S fuzzy framework have been examined. These limitations are the main motivation to set the thesis direction towards the estimation and compensation based approach to AFTC.
b. The proposal of an LMI-based design of active sensor fault tolerant model reference tracking control for nonlinear systems described via T-S fuzzy modelling. The strategy combines the design of H_∞ fuzzy PMIO, fuzzy state feedback control, and linear reference modelling to form a new sensor fault estimation and hiding (*'implicit compensation'*) based FTTC. The use of an H_∞ T-S fuzzy PMIO is also proposed to overcome the problems of uncertain fault time behaviour and provide simultaneous state and sensor fault estimation. Furthermore, compared with the literature of T-S fuzzy model reference AFTC, the proposed method considers the case of an unmatched reference model.
c. The proposal of an LMI-based design of active actuator fault tolerant model reference tracking control for nonlinear system described via T-S fuzzy model. The strategy combines the design of H_∞ fuzzy PPIO, fuzzy state feedback control, and linear reference model to form new actuator fault estimation and compensation based FTTC. The use of H_∞ T-S fuzzy PPIO is proposed to overcome the uncertain fault time behaviour and provide simultaneous state and actuator fault estimation.

The simulation results have clearly shown the ability of the LRMFC to maintain acceptable closed-loop performance for some minor actuator faults.

The proposed strategies are illustrated via a nonlinear inverted pendulum example with control objective to force the pendulum cart position to follow a reference position in both faulty sensor and fault-free cases.

Based on the investigations of the proposed methods presented in Chapter 4, the advantages and limitations of the methods are investigated and stimulate the use of observer-based fault estimation and compensation approaches in Chapter 5 and 6.

Chapter 5 proposes a novel LMI-based design for observer-based state feedback tracking and regulator FTC for nonlinear systems affected by simultaneous actuator and sensor faults. The proposed strategy is based on the use of interacting multi-observers, one dedicated for sensor faults and the other focussed on actuator faults. Each of the observers is designed to be robust against the estimation error of the other observer. The sensor fault estimation observer is responsible for hiding the sensor fault from both the controller and the actuator fault estimator. On the other hand, the estimated actuator fault signal is used to compensate the effect of the actuator fault. The proposed strategy is applied to different nonlinear systems affected by simultaneous actuator and sensor faults.

The main contributions involved in this strategy are:

- The proposal of an LMI-based design for observer-based active FTTC and FTC strategy for nonlinear systems subjected to simultaneous actuator and sensor faults using the estimation and compensation idea.
- An enhancement to the T-S PMIO design proposed in Chapter 4 by adding an adaptive term in order to ensure observer robustness against unanticipated faults.
- Proposal of a method for de-coupling the design of the fault estimation observers and hence minimise the effects of each fault on the alternative observer.

The two proposed LMI-based T-S fuzzy FTTC and FTC schemes are applied to two different nonlinear systems affected by simultaneous actuator and sensor faults.

Chapter 6 proposes a novel LMI-based design for TSDOFC based FTTC for nonlinear systems subject to simultaneous actuator and sensor faults. The proposed strategy follows the idea presented in Chapter 5. However, due to global stability constraints

required for the T-S fuzzy observer and/or control design problem, it is generally not possible to assign the observer and/or controlled system closed-loop eigenvalues anywhere in the stable complex plane. Hence, following this in the fuzzy observer-based state estimates feedback control, observer dynamics are not guaranteed to have fast enough dynamics compared with controller dynamics even if the Separation Principle holds. This limitation may lead to degradation of the closed-loop system tracking performance. Therefore, the main contributions of this Chapter are:

1. Proposal of a generic LMI-based design for TSDOFC based FTTC for nonlinear systems subject to simultaneous actuator and sensor faults using the concept of estimation and compensation.
2. An enhancement of the T-S PPIO design proposed in Chapter 4 via adding an adaptive term in order to ensure observer robustness against unanticipated faults.

The proposed LMI-based design strategy is applied to a nonlinear system affected by simultaneous actuator and sensor faults.

Chapter 7 presents an investigation into different aspects of wind turbine operation and the wind turbine control design problem. Specifically, the Chapter includes the following topics:

- The presentation of a mathematical model of an offshore wind turbine dynamical system that combines the constituent subsystem models together that make up the overall wind turbine dynamics.
- A description of the basic characteristics of the wind to be exploited to produce electrical power, different components of wind speed, and the effects of wind turbine structure and sizes on the uncertainty of the measured wind speed.
- The description of wind turbine control within low and high wind speed ranges.
- The main challenges for the deployment of wind turbine systems and the different approaches proposed to make wind energy systems competitive with other energy sources.
- Investigation of the importance of FTC for wind turbine systems and specifically the OWTs.
- Investigate the state space model of a wind turbine and based on this the motivation of using T-S fuzzy inference modelling within the wind turbine control problem. Following this, the derivation of the T-S fuzzy model of the wind turbine system.

The material included in Chapter7, alongside with the 5MW wind turbine benchmark (Odgaard, Stoustrup and Kinnaert, 2009), form the basis of the work in Chapters 8 and 9.

Chapter 8 proposes three new observer-based sensor FTTC approaches for wind turbine systems. Compared with the literature of wind turbine sensor FTC, the proposed strategy overcomes the complexity of the fault tolerant strategy and provides further information about the fault via the fault estimation signal.

The main contributions of this Chapter are:

1. An investigation into the effects of different fault scenarios on the wind turbine power extraction efficiency and drive train loading.
2. The proposal of a state feedback sensor FTTC using the sensor fault hiding (*'implicit compensation'*) approach of Chapter 4 to obviate the residual evaluation block described in the literature for tolerating the fault in a wind turbine FTC system, via a generalised observer method.
3. The proposal of a T-S fuzzy dynamic output feedback sensor FTTC strategy to tolerate the effects of generator and rotor rotational speed sensor faults on the performance of the wind turbine.
4. The proposal of a generic T-S fuzzy dynamic output feedback approach for sensor FTTC of wind turbine system with simultaneous EWS estimation and generator and rotor rotation speed sensor faults. This strategy is based on the architecture proposed in Chapter 6

Chapter 9 proposes *three* new methods that utilize the inherent robustness of SMC within an AFTC framework for wind turbine systems. Clearly, the main challenge involved within the development of FTC for wind turbines is that the number of unknown input and output signals exceed the number of measurements making a challenging closed-loop robustness problem against unknown input and output signals. This Chapter focuses on an approach for handling this challenging operation scenario via utilizing the inherent robustness of an SMC strategy within the AFTC framework for power maximization in the OWT benchmark. Within this framework, the Chapter introduces a new perspective to the sliding mode surface design problem from an FTC stand point. This new perspective simply requires the design of the sliding surface with

the minimum number of possible feedback signals. In doing so, the robustness of the SMC is ensured over a wider than usual range of fault scenarios.

The first strategy uses the inherent robustness of a simple adaptive gain SMC against matched faults as a basis for FTC of OWT. Although the proposed method is simple and obviates the need for the sensor fault hiding observer, the main challenges lies in the need to optimise the sensitivity of the sliding surface to unknown outputs (measurement noises and/or faults). Hence, the second strategy combines the use of SMC and the estimation and compensation concept to enhance the overall robustness of the SMC control against faults that affect the sliding surface. In the third strategy, the SMC based AFTC is proposed using the spirit of Chapter 5 to overcome the sliding surface sensitivity to measurement noise and faults and provide robust estimation of the EWS. The proposed strategies are illustrated via FTC design for the 5MW OWT benchmark system.

The main contributions of this Chapter are:

1. An investigation of the robustness of SMC within the FTC framework via a tutorial example.
2. The proposal for an adaptive SMC to tolerate the effects of the generator speed sensor fault. In fact, via designing the sliding surface with minimum feedback signals, some sensor faults (i.e. the generator speed sensor fault) become similar to the case of matched uncertainty and hence the robustness of the SMC can tolerate this effect (as the generator speed fault is de-coupled during sliding).
3. The proposal of an AFTC strategy based on the combination of SMC and fault estimation and the fault compensation concept in order to ensure the robustness of the sliding motion against the rotor speed sensor fault.
4. The proposal of a generic approach for simultaneous sensor faults and EWS estimation so that the robustness of the sliding surface against the unknown outputs (sensor fault and/or noise) is ensured by making use of the spirit of the methods proposed in Chapter 5 & 6.

Chapter 10 summarises and concludes the overall work described by the thesis and makes suggestions and recommendations as to how the research can be further developed in the future.

Chapter 2 : A generic overview of FTC methods

2-1. Introduction

The design of FTC systems has attracted more and more attention in both industry and academic communities due to the increased demands for safety, high system performance, availability and operating efficiency in a wider range of engineering applications, not limited to traditional safety-critical systems.

Many FTC design approaches have been proposed in the literature, with each approach having some advantages and some limitations that should be well understood in order to decide the best approach to handle a specific fault in a specific application study. This Chapter provides a generic overview of the main FTC approaches.

2-2. Overview of the FTC design approaches

The FTC methods are generally classified into PFTC and AFTC methods. These classes are achieved via different control techniques. Figure 2-1 shows a general overview of the main approaches used to achieve FTC for each class.

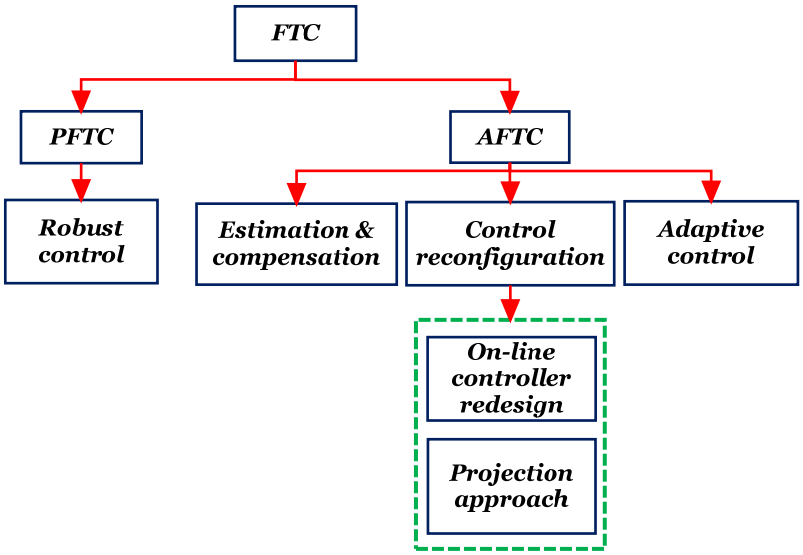

Figure 2-1: General classification of FTC methods

The following subsections present the FTC methods that belong to the main classifications given in Figure 2-1.

2-2-1. Model-following

The main idea and aim of the use of a model-following approach to FTC or reconfigurable control is to determine a reconfiguring controller gain that is able to provide a control signal that enables the following post-fault closed-loop behaviour:

$$\dot{x}_f = A_f x_f + B_f u_f \tag{2-1}$$

to follow a reference model defined by Eq. (2-2) as follows:

$$\dot{x}_m = A_m x_m + B_m u_m \tag{2-2}$$

According to the model-matching requirement different model-following control mechanisms are possible. For example, the so-called perfect model-following (PMF) (Gao and Antsaklis, 1992) or the pseudo inverse method (PIM) (Gao and Antsaklis, 1991) propose a control reconfiguration methodology to achieve best matching between the nominal and the post-fault closed-loop matrix. The PIM based reconfiguration methodology requires the nominal closed-loop system matrix to compute the new controller gain, whilst the PMF presents a more general reconfiguration methodology in which the reference model (e.g. the nominal closed-loop system) is implemented as part of the controller (Gao and Antsaklis, 1992).

Based on Eqs. ((2-1 & (2-2), the error dynamics ($e = x_m - x_f$) between the nominal and faulty plant can be stated as:

$$\dot{e} = A_f e + \big(A_m - A_f\big)x_m + B_m u_m - B_f u_f \tag{2-3}$$

For PMF the control signal would be of the form:

$$u_f = K_e e + K_m x_m + K_u u_m \tag{2-4}$$

where $K_e, K_m,\ and\ K_u$ are the design matrices which can be determined as follows (Gao and Antsaklis, 1992):

$$\left.\begin{aligned} K_m &= B_f^{\dagger}\big(A_m - A_f\big) \\ K_u &= B_f^{\dagger} B_m \end{aligned}\right\} \tag{2-5}$$

And the gain K_e is selected such that $A_f - B_f K_e$ is a stable matrix. Using the controller gains given in Eq. (2-5), the dynamic error equation becomes:

$$\dot{e} = \big(A_f - B_f K_e\big)e + (I - B_f B_f^{\dagger})\big(A_m - A_f\big)x_m + (I - B_f B_f^{\dagger})B_m u_m \tag{2-6}$$

Based on the last equation, the perfect PMF requires that:

$$\left.\begin{aligned}\left(I - B_f B_f^{\dagger}\right)\left(A_m - A_f\right) = 0 \\ \left(I - B_f B_f^{\dagger}\right)B_m = 0\end{aligned}\right\} \tag{2-7}$$

On the other hand, PIM actually does not require full interaction with the reference model (Gao and Antsaklis, 1992). However, only the reference closed-loop system matrix is required to compute the system reconfiguration gain:

$$A_f + B_f K_f = A_m + B_m K_m$$
$$K_f = B_f^{\dagger}(A_m - A_f + B_m K_m) \tag{2-8}$$

Hence the error dynamics for the PIM simply become:

$$\dot{e} = (A_m + B_m K_m)e + (I - B_f B_f^{\dagger})\left(A_m - A_f + B_m K_m\right)x_f \tag{2-9}$$

Generally, the exact model matching may be too demanding. Therefore, approximate model matching is of more interest and can be reached through finding the value of (K_f) that minimizes the following Frobenius norm (Gao and Antsaklis, 1991):

$$\left\|A_m + B_m K_m - A_f - B_f K_f\right\|_F^2 \tag{2-10}$$

Beside the similarity between the PMF and PIM methodology, the essential research features are: (1) The guarantee of the stability of the reconfigured closed-loop system, (2) Minimization of the time consumed to approach the acceptable matching, and/or (3) Achieving the perfect matching through the use of different control methodologies. For example, a modified PIM algorithm was proposed in (Gao and Antsaklis, 1991) to guarantee the stability of the reconfigured closed-loop system. To relax the matching condition, (Staroswiecki, 2005, Staroswiecki, 2006) proposed an *admissible model matching* approach

Although PMF and PIM are characterized by their reconfiguration simplicity, the main limitations are:(i) The robustness issues against model uncertainty and exogenous inputs are not considered in the reconfiguration process, (ii) The methods are highly dependent on accurate post-fault model provided by the FDD unit, (iii) A trade-off exists between the reconfiguration time and an urgent requirement for a multi-objective minimization algorithm, (iv) The reconfiguration algorithm always gives solutions for the minimum distance between the pre- and post-fault closed-loop systems and this indicates that the post-fault system dynamic response cannot be determined.

2-2-2. Eigenstructure assignment

The spirit of the eigenstructure assignment based approach to reconfigurable control follows the framework of model-following based FTC. The controller should be reconfigured so that the post-fault closed-loop system eigenstructure matches the pre-fault closed-loop system eigenstructure, i.e. in order to recover the approximate dynamic performance of the closed-loop fault-free system. The new "*should be fast computed"* controller computed so that at least the dominant faulty closed-loop system eigenvalues are preserved to be as close as possible to the dominant fault-free closed-loop system eigenvalues. On the other hand, the new eigenvectors have to be close to those of the corresponding nominal eigenvalues.

Assume that the closed-loop system has eigenvalues $\lambda_i, i = 1, 2, \dots, n$ then in the case of the faulty system the feedback gain matrix (K_f) should achieve the following:

$$\lambda_i^f = \lambda_i \tag{2-11}$$

$$\left.\begin{aligned} (A_f + B_f K_f) v_i^f &= \lambda_i v_i^f \quad , i = 1, 2, \dots, n \\ v_i^f &= (\lambda_i I - A_f)^{-1} B_f K_f v_i^f \end{aligned}\right\} \tag{2-12}$$

$$v_i^f = \arg min_{v_i^f} \| v_i - v_i^f \| \tag{2-13}$$

v_i and v_i^f are the pre- and post-fault eigenvectors. The λ_i^f are the eigenvalues of the faulty closed-loop system, A_f and B_f are the post-fault system matrices, and K_f is the reconfigured controller gain.

An eigenstructure assignment-based approach to FTC was first proposed in (Jiang, 1994). This work describes how the stability of the system after reconfiguration as well as the time consumed to determine the best possible reconfigured controller parameters are evaluated as the main focus of interest in this approach. In the literature, either static state or output feedback controllers have been proposed. When full state feedback control is used, the stability of the reconfigured system will be guaranteed as there will be freedom to assign all the closed-loop system eigenvalues (Jiang, 1994). On the other hand, if static output feedback control is used, only part of the post-fault closed-loop eigenvalues can be assigned. Consequently the reconfigured closed-loop system stability cannot be guaranteed. Hence, more constraints are required to guarantee the post-fault system stability (Jiang, 1994, Ashari and Sedigh, 2004). The reconfiguration algorithm proposed in (Konstantopoulos and Antsaklis, 1996, Konstantopoulos and

Antsaklis, 1999) uses a Lyapunov equation as an additional constraint to guarantee closed-loop system stability. An integrated FDD based FTC design is proposed in (Zhang and Jiang, 2002), in which the reconfigured state feedback controller is computed based on the information provided by the fault detection unit.

Owing to the fact that the achievable eigenvectors are a linear combination of the columns of the matrix $(\lambda_i I - A_f)^{-1} B_f$, the main challenge in this method is that the computation of the controller gain (whether using output or state feedback) is based on the assumption that there is no intersection between the open-loop and closed-loop eigenvalues. However, this assumption is violated if there are uncontrollable mode(s), in this case the term $(\lambda_i I - A_f)^{-1}$ will be singular. The same problem arises if, due to a fault, some of the pre-fault dominant eigenvalues become identical with the post- fault system open-loop eigenvalues.

2-2-3. Multiple-model approaches

The multiple-models belong to the model-based AFTC method in which a local controller is designed off-line to guarantee acceptable performance and stability for each anticipated faulty system model. In the literature, fault tolerance can be achieved by developing an on-line procedure that produces a control action representing a weighted combination of the local control signals as follows:

$$u(t) = \sum_{i=1}^{n} \mu_i u_i(t) \ , \sum_{i=1}^{n} \mu_i = 1 \qquad (2\text{-}14)$$

where u_i is the local control signal and $\mu_i$is its weight. Usually the weight is computed based on a residual signal generated by taking the difference between the measured system outputs and the estimated outputs produced by an observer designed off-line for each local model (anticipated faulty model). Figure 2-2 shows the schematic of the multiple-model approach to AFTC.

The research in the literature mainly focuses on: (i) The tolerance of a large range of fault scenarios, (ii) making use of different local control methods, and (iii) ensuring the robustness of the weighting signal against unknown signals. A multiple-model method for FTC was proposed by (Pogoda and Maybeck, 1989, Maybeck and Stevens, 1991, Rauch, 1995) to tolerate single or multiple sensor and/or actuator faults. In developments by (Yen and Liang-Wei, 2003, Jin and Youmin, 2006, Efimov, Cieslak

and Henry, 2012) more attention has been focussed on methods to ensure robustness of the controller weight generation algorithm.

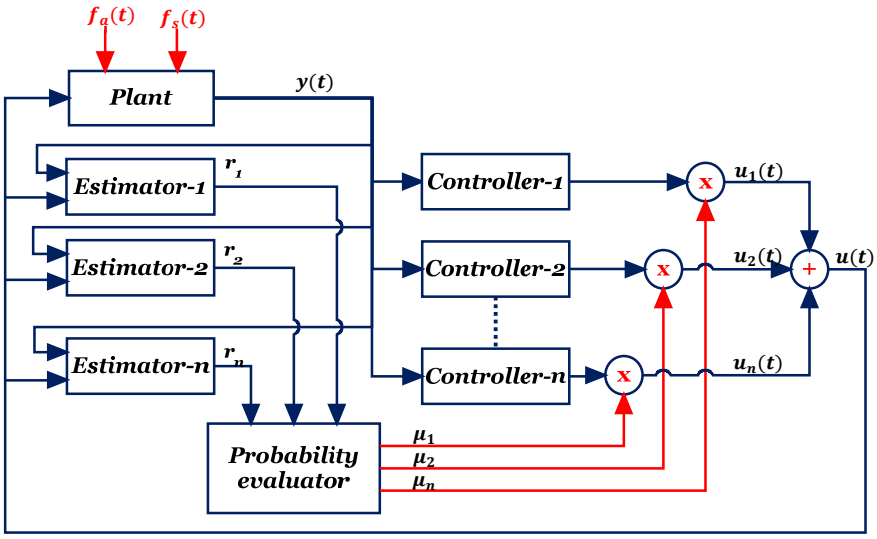

Figure 2-2: Schematic of multiple-model approach to AFTC

Another approach of multiple-model-based FTC obviates the weighting of local control signals so that a single controller is activated at each time instant (see Figure 2-3). This approach of multiple-models presented in (Gopinathan, Boskovic, Mehra and Rago, 1998, Xin and Guang-Hong, 2007, Seron, De Dona and Martinez, 2009, Sanchez-Parra, Suarez and Verde, 2011).

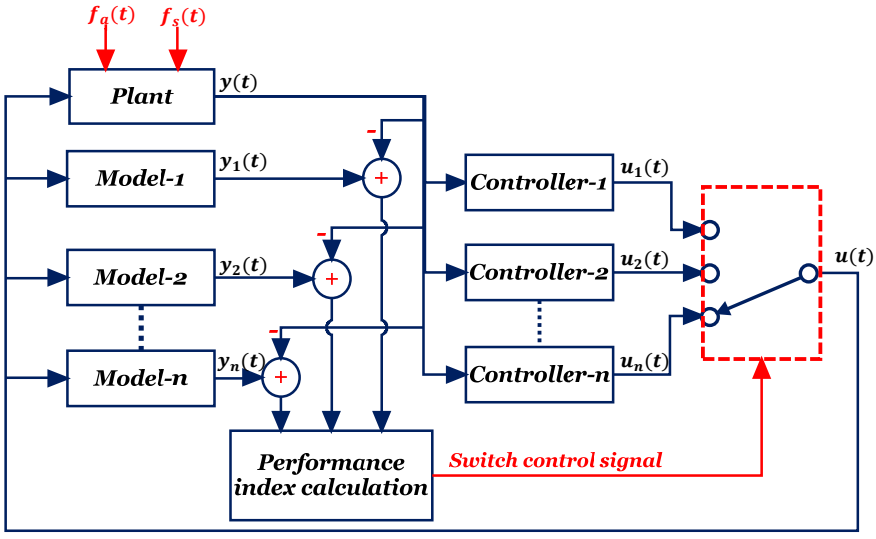

Figure 2-3: Schematic of multiple-model AFTC based on switching between controllers

The main limitation of this method is usually that the reconfiguration strategy considers a finite number of anticipated faults. Furthermore, due to the inevitable model

uncertainty and/or unanticipated faults the combined local control signals will not in general, provide an optimal signal for the system, with the inevitable consequence of closed-loop performance degradation.

2-2-4. Fault hiding

The concept of the fault hiding approach is centred on achieving FTC loop goals such that the nominal control loop remains unchanged. One way to achieve this is through the use of analytical redundancy known as virtual actuators or sensors before and after the nominal controller. Some basic details of this approach can be found in (Blanke, Kinnaert, Lunze and Staroswiecki, 2006).

The virtual actuators (VA) or virtual sensors (VS) is a dynamic system depends mainly on the difference between the nominal and faulty system state to changes in its dynamics such that the required control objectives are continuously achieved even if a fault occurs. In the sensor fault case the VS masks the effect of the fault from the input of the controller. However, in the actuator fault case, the virtual actuator compensates the effect of the fault. The literature for this method is mainly covered by the papers (Lunze and Steffen, 2006, Richter, Schlage and Lunze, 2007, Richter, Heemels, van de Wouw and Lunze, 2008, Seron and De Dona, 2009, Richter, Heemels, van de Wouw and Lunze, 2011). Although this method depends completely on the fault model provided by the FDD unit, the literature lacks any attempt to build an integrated FDD and virtual actuator and/or virtual sensor. It is always assumed that the FDD/fault estimation scheme is available! However, leaving out this information leaves an unpublished aspect of research as the robust fault estimation problem associated with the virtual actuator/virtual sensor approach to FTC is an important and challenging topic of considerable practical value. A proposal of VS approach to FTTC for nonlinear systems is given in chapter 4. Moreover, Chapter 4 has also shown how the simultaneous state and fault estimate capability of the PMIO can be used as integrated fault estimate/VS into the FTTC loop

2-2-5. FTC via generalized observer

The FTC via the use of generalized observers is a viable approach for building sensor fault-tolerance into an FTC system. The concept of the generalized observer was first proposed as a fault detection strategy (Patton, Frank and Clark, 1989). The concept is

based on analytical redundancy in which a set of observers are designed based on individual measurements. In the case of sensor faults, a residual evaluation unit compares the residual signals generated by each observer to identify the faulty measurements. Recently, some researchers have used this technique to design an observer-based state feedback sensor fault FTC scheme in which the residual evaluation unit simply switches the state estimation from the faulty observer to a fault-free one (Oudghiri, Chadli and El Hajjaji, 2008, Kamal, Aitouche, Ghorbani and Bayart, 2012). The main limitations of this approach are (a) there is a need for the system to be observable from each measurement set, and (b) the requirement of a residual evaluation unit with an accompanying need for system switching, and finally (c) it can only be used for sensor FTC problems.

2-2-6. Sliding mode control (SMC)

Due to the inherent robustness of SMC against matched model uncertainty and faults, SMC offers a promising basis for an important approach to FTC. As a result, the numbers of publications that use the SMC method for FTC have increased substantially, considering various application problems. The earliest SMC based FTC study can be attributed to (Ting, Tosunoglu and Fernandez, 1994) wherein the robustness of the SMC against matched unknown inputs has been used to tolerate actuator faults and the pre-fault path recovery is investigated on a four degrees of freedom planar serial robot. The combination of the estimation and compensation concept within the SMC framework in the presence of matched and/or unmatched faults is suggested in (Patton, Putra and Klinkhieo, 2010a). The idea of tolerating actuator faults by redistributing the control signal over other fault-free actuators (*'known as control allocation'*) within an SMC framework has been dealt with in several publications (Corradini, Orlando and Parlangeli, 2005, Alwi and Edwards, 2008, Sijun, Youmin, Xinmin and Rabbath, 2009, Fu, Cheng, Jiang and Yang, 2011). Current research in SMC based FTC is mainly focussed on exploiting the advantage of integral SMC to achieve enhanced reliability of the FTC loop (Alwi, Edwards and Hamayun, 2011, Hamayun, Edwards and Alwi, 2011, Larbah and Patton, 2012).

The common weakness of the SMC approach to FTC is that the sensitivity of the sliding mode surface to unknown output signals (sensor faults and/or measurement noise) tends to be ignored. In fact, the sliding mode surface represents the heart of the SMC and

hence the design of an SMC based FTC with due care for unknown outputs greatly contributes to the SMC FTC methodology. This problem is studied carefully in Chapter 8 of this thesis wherein the unknown output hiding approach is used to render the sliding surface immune to unknown outputs.

2-2-7. Adaptive control

Owing to the ability to regulate controller parameters on-line based on signals in the system, adaptive control has been extensively used as an AFTC method. In fact, the raw adaptive controller's operation philosophy best coincides with the philosophy of AFTC. Clearly, using adaptive control methods as an approach to FTC can lead to obviate the need for and FDD unit (either based on fault residual signals or on fault estimation). The main features of research in adaptive control based AFTC are focused on proposing methods that can handle different scenarios of system and/or actuator faults as well as robustness against exogenous input effects. The early use of adaptive control based FTC is due mainly to work by (Ahmed-Zaid, Ioannou, Gousman and Rooney, 1991) in which an adaptive control was a supplementary controller to help the nominal controller of an F-16 fighter aircraft to accommodate to some faults effects. To ensure stability and acceptable performance over a large class of faults which may lead to large variations in system dynamics encountered in a flight control application, (Boskovic and Mehra, 1999) proposed multiple fault tolerant adaptive controllers with each controller designed to handle a specific fault scenario. More recently, various investigators have developed schemes for adapting controller parameters to tolerate the effects of actuator faults, plant uncertainty, and/or exogenous inputs (Tao, Joshi and Ma, 2001, Jin and Yang, 2009, Gayaka and Bin, 2011, Zou and Kumar, 2011). These approaches have become the characterizing features of fault tolerant adaptive control research.

Clearly, fault tolerant adaptive control methods have always appeared to be appropriate for handling system and/or actuator fault problems. However, in this method, sensor FTC represents the most challenging fault scenario and has been rarely considered in fault tolerant adaptive control methods. For example, output feedback adaptive control can tolerate actuator and/or system faults, whereas, if sensor faults have occurred the adaptation will force the faulty outputs to follow the reference signals and hence, the control signal is no longer suitable for the system under control. Therefore, sensor fault

tolerant adaptive control requires an FDD unit to help the adaptive control to handle sensor faults.

2-2-8. Estimation and compensation

Traditionally, FTC requires the activity of a nominal controller and an FDD unit (Patton, 1997a). Either the controller reconfiguration or fault compensation is performed based on the residual evaluation and parameter identification provided by the FDD unit. However, the main challenge of this general FTC methodology lies in the requirement for a robust and fast FDD unit. As an extension to this FDD concept the estimation and compensation approach to FTC is based on the computation of fault estimates and a mechanism to compensate these fault effects by the addition of a new compensating control law to the nominal one as shown in Eqs. (2-15) and (2-16):

$$u = u_n + u_{ad} \tag{2-15}$$

$$\left.\begin{aligned} u_{ad} &= K_f \hat{f} && f \neq 0 \\ u_{ad} &= 0 && f = 0 \end{aligned}\right\} \tag{2-16}$$

u_n is the nominal control signal, u_{ad} is the additive control signal responsible for fault compensation, K_f is the additive control signal gain, and f and $\hat{f}$ are the fault and fault estimation, respectively.

Clearly, this approach obviates the need for residual evaluation and parameter identification and hence requires no time consuming algorithms for maintaining the performance of the nominal system control law. Consequently, this FTC strategy can be implemented quite easily. Following this reasoning, the number of FTC publications that follow this approach has steadily increased in the last decade. This approach was first proposed in (Theilliol, Noura and Sauter, 1998) to compensate the effect of additive or multiplicative actuator and/or system component faults. In (Noura, Sauter, Hamelin and Theilliol, 2000) the estimation and compensation approach has been used to compensate the effect of winding machine actuator faults. The features of the estimation and compensation research mainly deals with the problem of robust fault estimation against exogenous inputs, the modification of the nominal control strategy to enhance the overall closed-loop system performance, ensure the stability of the post-fault closed-loop system for different fault scenarios, and extension of the proposed method to nonlinear systems. For example, in (Gao and Ding, 2007b) the estimation and

compensation method has been used to tolerate actuator faults for generalized systems. Also to cope with the time varying nature of the faults a proportional, multiple-integral and derivative observer is proposed which leads to an enhancement of the fault tolerance performance. To obviate the need for explicit friction modelling for robust on-line friction compensation, (Patton and Klinkhieo, 2009) make use of the estimation and compensation idea to tolerate the effect of friction, considering the friction phenomenon as an unwanted fault effect The estimation and compensation method has also been extended to deal with FTC for nonlinear systems (Gao and Ding, 2007a, Jiang, Gao, Shi and Xu, 2010, Zhang, Jiang and Staroswiecki, 2010).

Clearly, post-fault system performance using this approach is highly affected by the estimation of the fault signal. On the other hand, the fault is an unpredictable event in both its occurring time and its behaviour. Therefore, to ensure good closed-loop system performance over a wide range of fault scenarios, the estimation strategy must have due care for the time varying nature of the fault and the robustness against exogenous inputs.

2-3. FTC via T-S fuzzy modelling and control

The Takagi-Sugeno (T-S) fuzzy inference modelling approach for dynamical systems (Takagi and Sugeno, 1985) is an important and systematic tool for approximating a nonlinear function that can be very useful in model-based FDD and FTC. The T-S fuzzy model consists of a set of IF-THEN rules which represent local linear input-output relations of the nonlinear system. The main feature of this approach is that it can express the local dynamics of each fuzzy rule by a linear system model. The overall fuzzy model is achieved by connecting the local linear model of each rule by membership functions yielding the global model of the system. A typical fuzzy rule in this approach has the following form:

Model i

IF $p_1(t)$ is M_{i1} and ..... and $p_p(t)$ is M_{ip}

THEN

$$\left.\begin{aligned} \dot{x}(t) &= A_i x(t) + B_i u(t) \\ y(t) &= C_i x \end{aligned} \qquad i = 1, 2, .. r \right\} \tag{2-17}$$

here, M_{ij} is the fuzzy set and r is the number of model rules. Matrices $A \in \mathcal{R}^{n*n}$, $B \in \mathcal{R}^{n*m}$, and $C \in \mathcal{R}^{l*n}$ is the system, input, and the output matrices; $p_1(t) \dots p_p(t)$ are *premise variables* that may be functions of the state variables, or external disturbances. Each linear consequent equation is called a subsystem. The final outputs of the fuzzy systems are inferred as follows:

$$\left.\begin{aligned} \dot{x}(t) &= \sum_{i=1}^{r} h_i\big(p(t)\big)\{A_i x(t) + B_i u(t)\} \\ y(t) &= \sum_{i=1}^{r} h_i\,(p(t))\{C\,x(t)\} \end{aligned} \right\} \quad i = 1, 2, .. r \tag{2-18}$$

where

$$p(t) = [p_1(t),\ \dots, p_p(t)] \ \ , \ h_i\big(p(t)\big) = \frac{w_i\,(p(t))}{\sum_{i=1}^{r} w_i\,(p(t))} \ \ , w_i\,\big(p(t)\big) = \prod_{j=1}^{p} M_{ij}(\,p_j(t))$$

The term $M_{ij}(\,p_j(t))$ is the grade of membership of $p_j(t)$ in M_{ij}, since:

$$\left.\begin{aligned} &\sum_{i=1}^{r} w_i\,\big(p(t)\big) > 0 \\ &w_i\,\big(p(t)\big) \geq 0 \end{aligned} \right\} \quad i = 1, 2, .. r \tag{2-19}$$

then

$$\left.\begin{aligned} &\sum_{i=1}^{r} h_i\,\big(p(t)\big) = 1 \\ &h_i\,\big(p(t)\big) \geq 0 \end{aligned} \right\} \quad i = 1, 2, .. r \tag{2-20}$$

for all t.

2-3-1. T-S fuzzy model construction

It is important to note that a T-S fuzzy controller is a model-based approach to control. The procedure of obtaining a T-S fuzzy model for a nonlinear system is the corner stone in this control approach. Generally, there are two approaches for constructing a T-S fuzzy model. (1) The identification using input-output data. (2) Derivation from given nonlinear system equations. The two approaches are schematically shown in Figure 2-4 below.

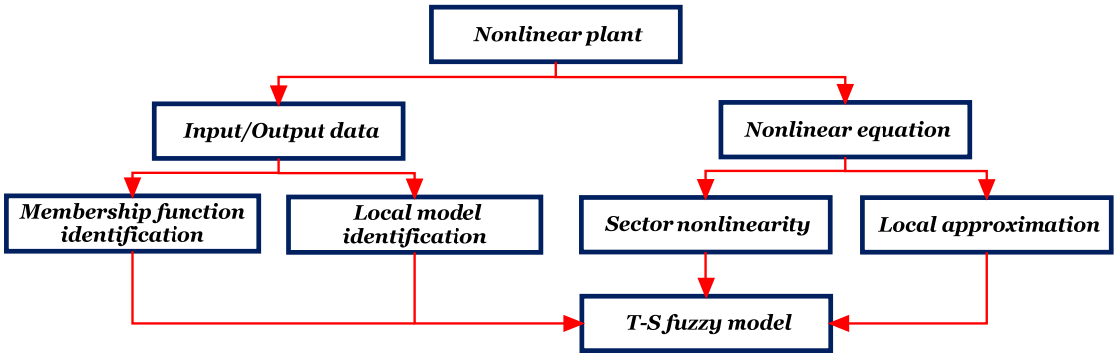

Figure 2-4: Construction methods for T-S fuzzy models

The fuzzy model identification approach is suitable for plants that are too difficult to be embodied in analytical models. In the literature, this fuzzy modelling approach is referred to as Takagi-Sugeno-Kang fuzzy model (TSK fuzzy model) (Sugeno and Kang, 1988). On the other hand, the second approach, which derives the fuzzy model from given nonlinear dynamical models, is more appropriate and utilizes the concept of *sector nonlinearity* or *local approximation*. In section 2-3-3 a tutorial example is given to illustrate how to construct fuzzy models based on the second approach.

2-3-2. Sector nonlinearity

This approach to T-S fuzzy model construction is based on the concept of considering a scalar non-linear smooth and differentiable function $f(x)$ in terms of its bounded values within a sector of the graph of $f(x)$ against x as shown in Figure 2-5 (Tanaka and Wang, 2001). It is assumed that the nonlinearity is guaranteed to exactly represent the nonlinear function $f(x)$ within the sector defined by the straight lines: $a_1 x$ and $a_2 x$. The sector bounding can be global or semi-global (local sector nonlinearity). Based on the values of a_1, a_2, and $f(x)$, the membership functions $h_1(x)$ and $h_2(x)$ used to approximate the function $f(x)$, are constructed as follows:

$$h_2(x) = \frac{f(x) - a_2 x}{(a_1 - a_2)x} \quad , h_1(x) = \frac{a_1 x - f(x)}{(a_1 - a_2)x}$$

where $h_1(x) + h_2(x) = 1$ and $h_1(x), h_2(x) \geq 0$ for all x.

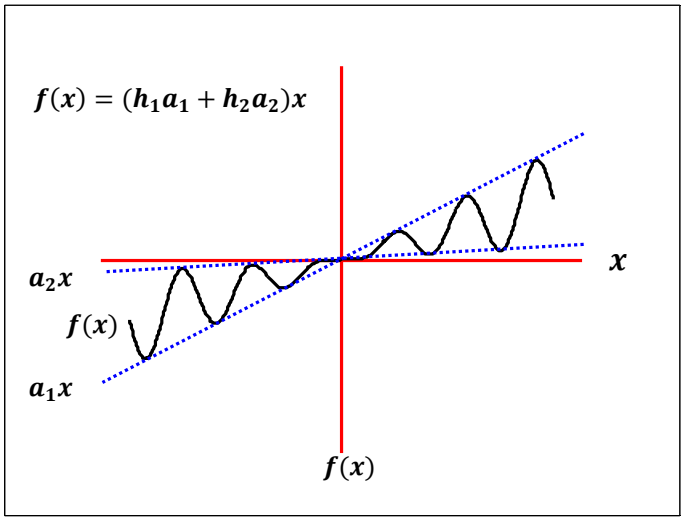

Figure 2-5: Global sector nonlinearity

It is sometimes difficult to find global sectors to cover the dynamics. However, it is possible to find local sectors that cover a specific bound. This is reasonable since variables of physical systems are always bounded. Figure 2-6 shows the local sector nonlinearity in which two lines become the local sectors under $-b < x < b$.

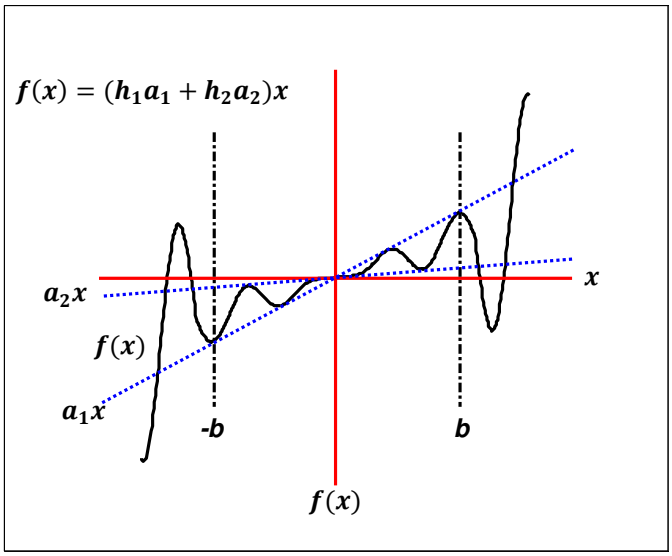

Figure 2-6: Local sector nonlinearity

Although the sector nonlinearity approach offers a tool for exact global or semi-global fuzzy modelling of the nonlinear system, it is often preferable to simplify the original nonlinear model as much as possible because it always leads to the reduction of the number of model rules, which reduces the effort for analysis and design of control systems.

2-3-3. Local approximation in fuzzy partition spaces

In order to reduce the number of local models, the T-S model of the nonlinear system obtained uses the local approximation approach. The spirit of this approach is to approximate the smooth nonlinear terms by linearizing the given nonlinear model around a number of operating points of interest (Tanaka and Wang, 2001). In this approach, the membership functions are always defined as triangular, trapezoidal, or Gaussian types. On the other hand, the membership functions for the sector bounded nonlinearity approach are obtained so as to exactly represent the nonlinear system. (Teixeira and Zak, 1999) suggest a modified local approximation approach based on linearization and optimization to minimise the expected modelling error.

Example 1: A nonlinear inverted pendulum T-S fuzzy model via sector nonlinearity.

A non-linear state space model of the inverted pendulum on a moving cart is considered as follows (Teixeira and Zak, 1999):

$$\begin{bmatrix}\dot{x}_1\\ \dot{x}_2\\ \dot{x}_3\\ \dot{x}_4\end{bmatrix} = \begin{bmatrix} 0 & 0 & 1 & 0\\ 0 & 0 & 0 & 1\\ \frac{g\,sin(x_1)}{4l/3-mla(cos(x_1))^2}\frac{1}{x_1} & 0 & \frac{-mlax_3 sin(2x_1)/2}{4l/3-mla(cos(x_1))^2} & 0\\ \frac{-mag\,sin(2x_1)\,/2\;\;1}{4/3-ma(cos(x_1))^2 x_1} & 0 & \frac{alx_3\,sin(x_1)4m/3}{4/3-ma(cos(x_1))^2} & 0 \end{bmatrix}\begin{bmatrix}x_1\\ x_2\\ x_3\\ x_4\end{bmatrix} + \begin{bmatrix} 0\\ 0\\ \frac{-a\,cos(x_1)}{4l/3-mla(cos(x_1))^2}\\ \frac{4a/3}{4/3-ma(cos(x_1))^2}\end{bmatrix}(u) \tag{2-21}$$

where $x_1, x_2, x_3,$ and x_4 are the pendulum angular position, cart position, pendulum angular velocity, and cart velocity, respectively. The nonlinear terms in Eq. (2-21) can then be defined as follows:

$$\left.\begin{aligned} z_1 &= 1/(4l/3 - mla(cos(x_1))^2)\\ z_2 &= sin(x_1)/x_1\\ z_3 &= x_3\,sin(x_1)\\ z_4 &= cos(x_1)\end{aligned}\right\} \tag{2-22}$$

Suppose further that $x_1 \in [-88^o, 88^o]$ and $x_3 \in [-\beta, \beta]$. The maximum and minimum values of each nonlinear term under the specified period are calculated as follows:

Max	Min	Max	Min
$z_{11} = \frac{1}{4l/3 - mla(cos(88))^2}$	$z_{12} = \frac{1}{4l/3 - mla}$	$z_{21} = 1$	$z_{22} = \frac{sin(88)}{88}$
$z_{31} = \beta$	$z_{32} = -\beta$	$z_{41} = 1$	$z_{42} = cos(88)$

From the maximum and minimum values, the nonlinear system can be locally represented in terms of membership functions and maximum and minimum values as follows:

$$\left.\begin{aligned} z_1 &= M_1 * z_{11} + M_2 * z_{12} \\ z_2 &= N_1 * z_{21} + N_2 * z_{22} \\ z_3 &= E_1 * z_{31} + E_2 * z_{32} \\ z_4 &= S_1 * z_{41} + S_2 * z_{42} \end{aligned}\right\} \tag{2-23}$$

where

$$M_1 + M_2 = 1 \qquad N_1 + N_2 = 1 \qquad E_1 + E_2 = 1 \qquad S_1 + S_2 = 1$$

Therefore the membership functions can be calculated as:

$$M_1 = \frac{z_1 - z_{12}}{z_{11} - z_{12}} \qquad M_2 = \frac{z_{11} - z_1}{z_{11} - z_{12}} \qquad N_1 = \frac{z_2 - z_{22}}{z_{21} - z_{22}} \qquad N_2 = \frac{z_{21} - z_2}{z_{21} - z_{22}}$$

$$E_1 = \frac{z_3 - z_{32}}{z_{31} - z_{32}} \qquad E_2 = \frac{z_{31} - z_3}{z_{31} - z_{32}} \qquad S_1 = \frac{z_4 - z_{42}}{z_{41} - z_{42}} \qquad S_2 = \frac{z_{41} - z_4}{z_{41} - z_{42}}$$

Hence, the T-S fuzzy model for the inverted pendulum is determined as follows:

$$\begin{bmatrix} \dot{x}_1 \\ \dot{x}_2 \\ \dot{x}_3 \\ \dot{x}_4 \end{bmatrix} = \sum_{i=1}^{2}\sum_{j=1}^{2}\sum_{k=1}^{2}\sum_{l=1}^{2} M_i N_j E_k S_l \left(\begin{bmatrix} 0 & 0 & 1 & 0 \\ 0 & 0 & 0 & 1 \\ g z_{1i} z_{2j} & 0 & -mla z_{1i} z_{3k} z_{4l} & 0 \\ -magl z_{1i} z_{2j} z_{4l} & 0 & \frac{4}{3} ml^2 a z_{1i} z_{3k} & 0 \end{bmatrix} \begin{bmatrix} x_1 \\ x_2 \\ x_3 \\ x_4 \end{bmatrix} + \begin{bmatrix} 0 \\ 0 \\ -a z_{1i} z_{4l} \\ \frac{4}{3} a l z_{1i} \end{bmatrix} (u) \right) \tag{2-24}$$

Although the T-S fuzzy model given in Eq. (2-24) exactly represents the nonlinear model in Eq. (2-21) in the specified range of operation, two important points must be highlighted: (1) Accurate modelling always leads to complex controller design since the number of local models increases, also (2) Accurate fuzzy models require more premise variables which may be unmeasured variables and hence complicate the controller design problem.

Example 2: A stand alone solar power generation system consists of a photovoltaic (PV) array and a dc/dc buck converter (Chian-Song, 2010).

The solar power uses the PV effect to convert solar energy into electrical energy; the PV panel is a nonlinear power source. The solar power circuit diagram with DC-DC buck converter is shown in Figure 2-7.

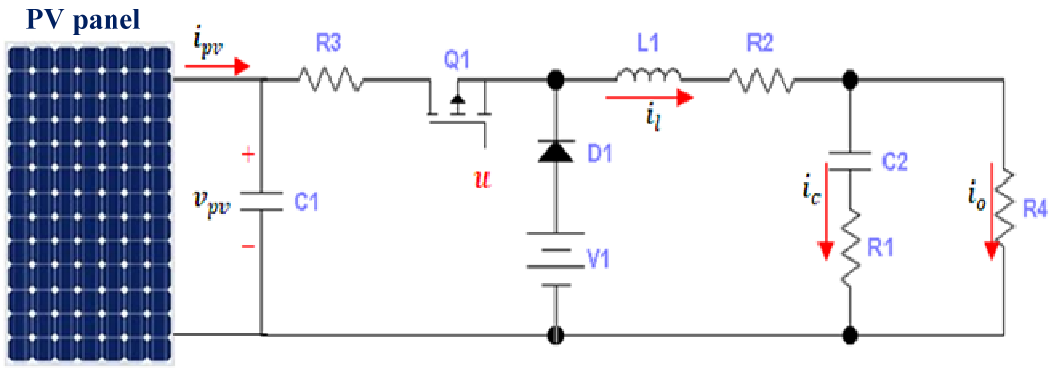

Figure 2-7: PV with DC-DC buck converter (adapted from (Chian-Song, 2010))

The output power of a PV panel array depends on the PV voltage and unpredictable weather conditions. In order to optimize the ratio between the output power and installation cost, dc/dc converters are used to draw maximum power from the PV panel array. Power maximisation is achieved by adjusting the duty cycle of the convertor in order to track the maximum power point.

Using Kirchhoff's current and voltage laws, the dynamic model of this system is derived and summarised below:

$$\begin{bmatrix} \dot{i}_l \\ \dot{v}_{c2} \\ \dot{v}_{pv} \end{bmatrix} = \begin{bmatrix} \frac{-1}{L1}[R_2 + \frac{R_4 R_1}{R_4+R_1}] & \frac{-1}{L1}[\frac{R_4}{R_4+R_1}] & 0 \\ \frac{1}{C2}[\frac{R_4}{R_4+R_1}] & \frac{-1}{C2}[\frac{1}{R_4+R_1}] & 0 \\ 0 & 0 & \frac{1}{C1}[\frac{i_{pv}}{v_{pv}}] \end{bmatrix} \begin{bmatrix} i_l \\ v_{c2} \\ v_{pv} \end{bmatrix} + \begin{bmatrix} \frac{-1}{L1}[R_3 i_l - v_{pv} - V_1] \\ 0 \\ \frac{-1}{C1} i_l \end{bmatrix} (u) + \begin{bmatrix} \frac{-V_1}{L1} \\ 0 \\ 0 \end{bmatrix} \quad (2\text{-}25)$$

where i_l, v_{c2}, v_{pv} and i_{pv} are the inductance (L1) current, capacitance (C2) voltage, the photovoltaic array voltage, and the PV current. V_1 is the power diode (D1) forward voltage, R_1 and R_2 are the parasitic resistances of the capacitance (C2) and inductance,

R_3 is the drain to source static resistance, and R_4 is the load resistance. Defining the variables as:

$$z_1 = i_l \qquad z_2 = v_{pv} \qquad z_3 = \frac{i_{pv}}{v_{pv}}$$

Also, assume the following bounds on these variables: $i_l \in [i_{lmax} = z_{11}, i_{lmin} = z_{12}]$, $v_{pv} \in [v_{pvmax} = z_{21}, v_{pvmin} = z_{22}]$, and $\frac{i_{pv}}{v_{pv}} \in [\frac{i_{pv}}{v_{pv}}_{max} = z_{31}, \frac{i_{pv}}{v_{pv}}_{min} = z_{32}]$.

Hence, based on the specified bounds, z_1, z_2, and z_3 can be represented as follows:

$$\left.\begin{aligned} z_1 &= M_1 * z_{11} + M_2 * z_{12} \\ z_2 &= N_1 * z_{21} + N_2 * z_{22} \\ z_3 &= E_1 * z_{31} + E_2 * z_{32} \end{aligned}\right\} \tag{2-26}$$

where

$$M_1 + M_2 = 1 \qquad N_1 + N_2 = 1 \qquad E_1 + E_2 = 1$$

Therefore the membership functions can be calculated as:

$$M_1 = \frac{z_1 - z_{12}}{z_{11} - z_{12}} \qquad M_2 = \frac{z_{11} - z_1}{z_{11} - z_{12}}$$

$$N_1 = \frac{z_2 - z_{22}}{z_{21} - z_{22}} \qquad N_2 = \frac{z_{21} - z_2}{z_{21} - z_{22}}$$

$$E_1 = \frac{z_3 - z_{32}}{z_{31} - z_{32}} \qquad E_2 = \frac{z_{31} - z_3}{z_{31} - z_{32}}$$

Hence, the T-S fuzzy model for the photovoltaic array with buck DC-DC converter become as follows:

$$\begin{bmatrix} \dot{i}_l \\ \dot{v}_{c2} \\ \dot{v}_{pv} \end{bmatrix} = \sum_{i=1}^{2}\sum_{j=1}^{2}\sum_{k=1}^{2} M_i N_j E_k \left(\begin{bmatrix} \frac{-1}{L1}[R_2 + \frac{R_4 R_1}{R_4 + R_1}] & \frac{-1}{L1}[\frac{R_4}{R_4 + R_1}] & 0 \\ \frac{1}{C2}[\frac{R_4}{R_4 + R_1}] & \frac{-1}{C2}[\frac{1}{R_4 + R_1}] & 0 \\ 0 & 0 & \frac{1}{C1} z_{3k} \end{bmatrix} \begin{bmatrix} i_l \\ v_{c2} \\ v_{pv} \end{bmatrix} + \begin{bmatrix} \frac{-1}{L1}[R_3 z_{1i} - z_2 j - V_1] \\ 0 \\ \frac{-1}{C1} z_{1i} \end{bmatrix} (u) \right) + \begin{bmatrix} \frac{-V_1}{L1} \\ 0 \\ 0 \end{bmatrix} \tag{2-27}$$

Hence, the T-S fuzzy model of the stand alone solar power system consists of *eight* local models.

2-3-4. Research trends in T-S fuzzy control

The attention on T-S fuzzy model approaches has increased in parallel with the development of the use of LMI (Boyd, El Ghaoui, Feron and Balakrishnan, 1994) as an efficient tool to design controllers and prove the stability of a multiple-model system. Compared with linear model-based control, the T-S approach has the potential for minimizing the modelling uncertainty of nonlinear systems (Tanaka and Wang, 2001), (Feng, 2010). The diagram shown in Figure 2-8 illustrates the main directions of research based on T-S fuzzy control.

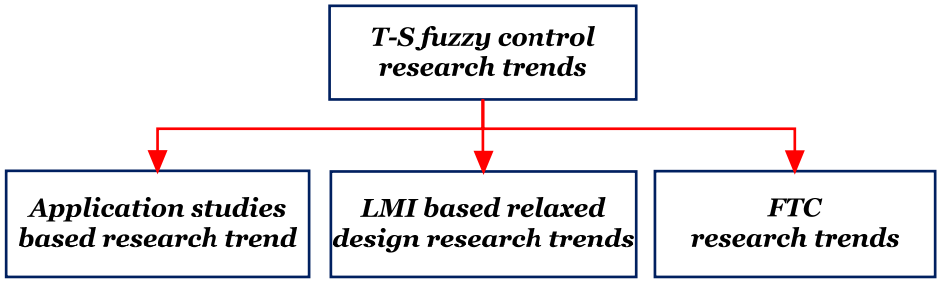

Figure 2-8: T-S fuzzy control research trends

2-3-4-1. LMI-based relaxed design constraints

Due to the fact that using T-S approach is always characterised by the trade-off between the control design complexity and nonlinear system T-S model accuracy (Tanaka and Wang, 2001), the earliest research trend has been to completely focus on relaxing the stability proof constraints. In this research field, two main LMI-based fuzzy controllers and/or observer design methods have been developed. (i) Fuzzy controller and/or observer-based on common Lyapunov function design approach (Tanaka, Ikeda and Wang, 1998, Euntai and Heejin, 2000, Tuan, Apkarian, Narikiyo and Yamamoto, 2001, Lin, Wang and Heng Lee, 2005, Mansouri et al., 2009) and (ii) Fuzzy controller and/or observer-based on fuzzy Lyapunov function design approach in which the fuzzy Lyapunov function is defined by fuzzily blending quadratic Lyapunov functions (Tanaka, Hori and Wang, 2003, Guerra and Vermeiren, 2004, Guelton, Bouarar and Manamanni, 2009). Although the fuzzy Lyapunov design has been suggested to relax the constraints on the fuzzy controller imposed by the common Lyapunov approach, this approach require precise information about the membership function time derivative.

2-3-4-2. FTC via T-S fuzzy control

The use of the T-S fuzzy model in FTC for nonlinear systems has its origins in the work of (Lopez-Toribio, Patton and Daley, 2000). However, the last five years have witnessed increasing interest in the T-S fuzzy based FTC framework.

The fuzzy PFTC considered in (Chen and Liu, 2004) represents the first attempt to design an reliable state feedback controller for uncertain T-S fuzzy model. However, actuator fault tolerance is considered as a consequence of the robustness against model uncertainty. Based on the same idea, (Huai-Ning and Hong-Yue, 2006) proposed a reliable state feedback strategy with actuator faults considered explicitly in the fuzzy model. Additionally, the method proposed two different stability conditions to simplify the controller design conservatism. An enhancement of the aforementioned researches has been introduced in (Gassara, El Hajjaji and Chaabane, 2010) in which reliable observer-based fuzzy FTC is proposed to ensure the stability of time delay fuzzy model system in the presence of actuator faults. Hence, the fuzzy PFTC methods are suggested to handle actuator faults. The actuator faults addressed in these approaches are assumed to be bounded and without need for fault detection or estimation.

On the other hand, in the literature, the fuzzy AFTC approach has gained much more attention than the fuzzy PFTC. (Lopez-Toribio, Patton and Daley, 2000) proposed a sensor FTC based on the idea of the generalized observer. The proposed method was applied to regulate the torque and flux of an induction motor in an industry-based collaboration, for which the system was demonstrated on a real application. The system used robust estimation of torque and flux via a d-q axis model. Based on the same FTC concept, (Oudghiri, Chadli and El Hajjaji, 2008) proposed a sensor FTC approach for the lateral dynamics of a vehicle represented by an uncertain Takagi-Sugeno (TS) fuzzy model. The control strategy uses observer-based control with two observers, with each one driven by a single sensor output. The “failure” is detected first, and then the faulty sensor is identified. After that, the state variables are reconstructed from the output of the healthy sensor. Recently, the generalised observer-based FTC within T-S framework has also been used in (Kamal, Aitouche, Ghorbani and Bayart, 2012) for the wind turbine application study to tolerate the effects of the generator rotational speed affected by a scale factor fault. In (Tong, Yang and Zhang, 2011) the T-S fuzzy descriptor observer design proposed in (Gao, Shi and Ding, 2008) is extended to handle

systems with time delay and for use within an observer-based FTC framework. However, the proposed strategy requires open-loop stable local models. Moreover, the results presented show that the state and fault estimation errors require long settling times.

A number of actuator AFTC approaches for T-S fuzzy system via estimation and compensation approach have been described during the last 10 years. In an earlier study (Yixin and Passino, 2001) use an adaptive control approach to actively tolerate the effect of an actuator fault. In (Zhang, Jiang and Shi, 2009) an observer-based actuator FTC design is proposed for fuzzy systems with time delay. In (Zhang, Jiang and Staroswiecki, 2010), in order to avoid the complexity of designing the observer-based FTC, a combination of estimator and dynamic output feedback controller is proposed. The method has been extended to discrete time T-S fuzzy system in (Jiang, Zhang and Shi, 2011). In (Jiang, Gao, Peng and Yufei, 2010), an adaptive actuator fault tolerant state feedback tracking controller consisting of both a normal control law and an adaptive compensation control term is proposed for a near space vehicle attitude dynamics. In (Ichalal, Marx, Ragot and Maquin, 2012), two actuator AFTC methods are suggested. The first method uses observer-based state feedback control in which the fault estimate signal used to compensate the effect of the actuator fault. The second method is model reference tracking control which also uses the fault estimate signal to compensate the effect of actuator fault. Recently, (Aouaouda, Chadli, Khadir and Bouarar, 2012) proposed a model reference tracking controller for T-S fuzzy system with an unmeasurable premise variable, modelling uncertainty, and an actuator fault. The controller design problem is formulated in a bilinear matrix inequality and the performances of the proposed approach have been tested on a model of wastewater treatment plant.

2-3-4-3. T-S fuzzy control for application study

Along with the increasing interest in the use of T-S fuzzy control in FTC for nonlinear systems, application based research trends have attracted the attention of researchers interested in T-S fuzzy control. This research direction has clearly appeared in the last five years for different application studies such as induction machines modelling and control, photovoltaic power control, power system stabilization, wind turbine control, and power electronic systems control etc. (Kuang-Yow, Liou and Chien-Yu, 2006,

Soliman, Elshafei, Bendary and Mansour, 2009, Chian-Song, 2010, Jiang, Gao, Peng and Yufei, 2010, Aouaouda, Chadli, Khadir and Bouarar, 2012, Kamal, Aitouche, Ghorbani and Bayart, 2012).

2-4. Conclusions

This Chapter started by outlining different FTC methods and the mechanisms of achieving fault tolerance, with more focus on FTC for nonlinear systems via T-S fuzzy modelling and control. Generally, AFTC methods fall into two categories, (1) FDD based FTC and (2) FTC without FDD. The main challenges encountered in these methods are summarized by: high dependency on accurate post-fault modelling provided by the FDD unit and/or accurate estimation of fault signals, the time required to reconfigure the control system must be as low as possible. In fact, this is very important in practice where the time windows during which the system remains stabilisable in the presence of a fault are very short. The last challenge is that usually the reconfiguration strategy considers a finite number of anticipated faults. Hence, any attempt to develop an FTC strategy must take into consideration the aforementioned challenges.

On the other hand, from a control system stand point, the current research interest is to develop FTC methods that have the ability to take into account the system nonlinearity. T-S fuzzy modelling and control is preferred over other nonlinear control strategies because the T-S fuzzy control method offers an approach to control of nonlinear systems via the well-developed linear control strategy. Hence T-S fuzzy modelling methods can represent the nonlinear system either globally or semi-globally, through the use of the sector nonlinearity modelling approach. Moreover, for systems that are too difficult to be embodied into analytical models, the fuzzy modelling literature offers an identification approach to derive T-S fuzzy models. Hence, this method gives opportunity to cover a wide range of nonlinear systems.

Although different FTC schemes have been proposed in the last two decades, the literature lacks to any research study that focuses on the relative impacts of actuator and sensor faults within regulator and tracking control problems. Hence, Chapter 3 will give an investigation of the challenges that are embedded in regulator and tracking control problems when subject to separate actuator and sensor faults.

Chapter 3 : Investigation of the FTC challenges embedded in tracking and regulator control problem

3-1. Introduction

Although control design problems are generally classified as either a regulator or a tracking control problem, the FTC literature lacks investigations of the relative impacts of different actuator and sensor fault scenarios on the regulator and tracking control problems. The motivation behind this investigation is to highlight the challenges embedded in these control problems within the FTC framework in order to provide a suitable background for the remaining Chapters of this thesis.

This Chapter uses the design of state feedback model reference fuzzy controllers for both tracking and regulator problems, forming the basis to highlight the hurdles that are associated with these two approaches to control when subject to separate actuator and sensor faults. The locally approximated T-S fuzzy model of an example non-linear system, the nonlinear inverted pendulum (as presented in Chapter 2) is exploited to achieve the following objectives, to investigate:

1. The importance of the model reference framework within the T-S fuzzy control and FTC.
2. The relative impacts of actuator and sensor faults on the tracking control problem.
3. The relative impacts of actuator and sensor faults on the regulator control problem.

3-2. LMI-based design of T-S fuzzy control within model reference framework

In order to facilitate an investigation of the relative impacts of actuator and sensor faults, formal definitions of regulation and tracking problems are given first. (Slotine and Li, 1991) define the regulation problem as:

"Given a nonlinear dynamic system described by:

$$\dot{\mathbf{x}} = \mathbf{f}(\mathbf{x}, \mathbf{u}, t)$$

find a control law $(\mathbf{u})$ *such that, starting from anywhere in a region in* $(\mathbf{\Omega})$*, the state* $(\mathbf{x})$ *tends to* $(\mathbf{0})$ *as* $t \to \infty$*".*

On the other hand, (Slotine and Li, 1991) define the tracking problem as:

"Given a nonlinear dynamic system described by:

$$\dot{\mathbf{x}} = \mathbf{f}(\mathbf{x}, \mathbf{u}, t)$$

$$\mathbf{y} = \mathbf{h}(\mathbf{x})$$

and a desired output trajectory $\mathbf{y_d}$*, find a control law* $(\mathbf{u})$ *such that, starting from anywhere in a region in* $(\mathbf{\Omega})$*, the tracking errors* $(\mathbf{y} - \mathbf{y_d})$ *go to* $(\mathbf{0})$*, while the whole state* $(\mathbf{x})$ *remains bounded".*

A number of approaches to design both regulator and tracking problems have been proposed in the literature (Veillette, 1995, Tanaka, Ikeda and Wang, 1998, Xiaodong and Qingling, 2003, Kuang-Yow and Jeih-Jang, 2006, Chian-Song and Ya-Lun, 2011, Aouaouda, Chadli, Khadir and Bouarar, 2012). This Section introduces the LMI-based design approach for model reference state tracking fuzzy control of nonlinear system described via T-S fuzzy inference modelling. As described in Section 2-3 the T-S fuzzy model of a nonlinear system is represented by the following non-linear state and output equations:

$$\left.\begin{aligned} \dot{x} &= \sum_{i=1}^{r} h_i\big(p(t)\big)\{A_i x(t) + B_i u(t)\} \\ y &= \sum_{i=1}^{r} h_i\,(p(t))\{C_i\, x(t)\} \end{aligned}\right\} \tag{3-1}$$

where $x(t) \in \mathcal{R}^n$ is the state vector, $u(t) \in \mathcal{R}^m$ is the input vector and $y(t) \in \mathcal{R}^l$ is the output vector, $A_i \in \mathcal{R}^{n*n}$, $B_i \in \mathcal{R}^{n*m}$, and $C_i \in \mathcal{R}^{l*n}$ $i = 1, 2, .., r$ are the system matrices, r is the number of fuzzy rules and the term $h_i\,(p(t))$ is the weighting function.

For the LRMFC within a tracking problem the control objective is to force the nonlinear system to follow the state variables of a reference model that has the same order n as the individual local linear model of the T-S fuzzy system itself. The reference model is assumed to have the form:

$$\dot{x}_d = A_d x_d + B_d d \tag{3-2}$$

where $x_d \in \mathcal{R}^n$ is the desired trajectory for x for all $t \geq 0$, $d \in \mathcal{R}^d$ is the bounded reference input, $A_d \in \mathcal{R}^{n*n}$ and $B_d \in \mathcal{R}^{n*d}$ are a stable and controllable state space pair. To achieve the control aim, the following fuzzy controller is proposed:

$$u_c = \sum_{i=1}^{r} h_i(p)\{K_i(x - x_d) + K_{ir}x_d + K_{id}d\} \tag{3-3}$$

where $K_i \in \mathcal{R}^{m*n}$, $K_{ir} \in \mathcal{R}^{m*n}$, $K_{id} \in \mathcal{R}^{m*d}$ are the feedback and feed-forward controller gains. Subtracting (3-2) from (3-1) and substituting for u_c from (3-3), then the tracking error (e_t) dynamics are given by:

$$\begin{aligned} \dot{e}_t = \dot{x} - \dot{x}_d = \sum_{i=1}^{r}\sum_{j=1}^{r} h_i(p)h_j(p)\{(A_i + B_iK_j)e_t + (B_iK_{jr} + A_i - A_d)x_d \\ + (B_iK_{jd} - B_d)d\} \end{aligned} \tag{3-4}$$

Using Eq. (3-2) and (3-4) the augmented system takes the form:

$$\dot{\tilde{x}}_a(t) = \sum_{i=1}^{r}\sum_{j=1}^{r} h_i(p)h_j(p)\{\tilde{A}_{ij}\tilde{x}_a + \tilde{N}_{ij}d\} \tag{3-5}$$

where:

$$\tilde{A}_{ij} = \begin{bmatrix} A_i + B_iK_j & B_iK_{jr} + A_i - A_d \\ 0 & A_d \end{bmatrix}$$

$$\tilde{x}_a = \begin{bmatrix} e_t \\ x_d \end{bmatrix}, \quad \tilde{N}_{ij} = \begin{bmatrix} B_iK_{jd} - B_d \\ B_d \end{bmatrix}$$

The objective here is to minimize the sensitivity of the error dynamics to a bounded tracking input d via computation of the gains $K_{jr}, K_{jd}, and\ K_j$. Hence, it is required to attenuate the error dynamics to a suitable level γ using H_∞ to ensure robust tracking performance. An LMI-based design formulation is derived so that the closed-loop gains are obtained through a one-step solution to the set of LMIs defined in Theorem 3-1:

***Theorem 3-1*:** *for t>0 and $h_i(p)h_j(p) \neq 0$, The closed-loop fuzzy system in (3-5) is asymptotically stable and the H_∞ performance is guaranteed with an attenuation level γ, provided that the signal (d) is bounded, if there exist symmetric positive definite (SPD) matrices P_1, P_2 and the matrices Y_j, and the scalar γ satisfy the following LMI constraints (3-6)&(3-7):*

$Minimise\ \gamma, such\ that$:

$$P_1 > 0, \qquad P_2 > 0 \tag{3-6}$$

$$\begin{bmatrix} \Psi_{11} & B_i K_{jr} + A_i - A_d & B_i K_{jd} - B_d & X_1 \\ * & P_2 A_d + (P_2 A_d)^T & P_2 B_d & 0 \\ * & * & -\gamma I & 0 \\ X_1 & * & * & -\gamma I \end{bmatrix} < 0 \tag{3-7}$$

$where$:

$K_j = Y_j X_1^{-1}$, $X_1 = P_1^{-1}$, $\Psi_{11} = A_i X_1 + (A_i X_1)^T + B_i Y_j + (B_i Y_j)^T$

Proof: From *Theorem 3-1* the tracking performance objective can be presented mathematically as follows:

$$\frac{\|\tilde{x}_a\|_2}{\|d\|_2} \leq \gamma = \frac{1}{\gamma} \int_0^\infty \tilde{x}_a^T \, \tilde{x}_a dt - \gamma \int_0^\infty d^T \, d \, \leq 0 \tag{3-8}$$

Consider the following candidate Lyapunov function for the augmented system (3-5):

$$\upsilon(\tilde{x}_a) = \tilde{x}_a^T \, \bar{P} \, \tilde{x}_a \ , where \ \bar{P} > 0$$

To achieve the performance required by (3-8) and the required closed-loop stability of (3-5) the following inequality must hold (Ding, 2008):

$$\dot{\upsilon}(\tilde{x}_a) + \frac{1}{\gamma} \tilde{x}_a^T \, \tilde{x}_a - \gamma d^T d < 0 \tag{3-9}$$

where $\dot{\upsilon}(\tilde{x}_a)$ is the time derivative of the candidate Lyapunov function. Using Eq. (3-5), this becomes:

$$\dot{\upsilon}(\tilde{x}_a) = \sum_{i=1}^{r} \sum_{j=1}^{r} h_i \, h_j \left\{ \tilde{x}_a^T \left(\tilde{A}_{ij}^T \bar{P} \, + \bar{P} \tilde{A}_{ij} \right) \tilde{x}_a + \, \tilde{x}_a^T \bar{P} \tilde{N}_{ij} d + d^T \tilde{N}_{ij}^T \bar{P} \tilde{x}_a \right\} \tag{3-10}$$

The inequality (3-9) (in matrix form) after substituting $\dot{\upsilon}(\tilde{x}_a)$ from Eq. (3-10) becomes:

$$\sum_{i=1}^{r} \sum_{j=1}^{r} h_i \, h_j \left\{ \begin{bmatrix} \tilde{x}_a \\ d \end{bmatrix}^T \begin{bmatrix} \tilde{A}_{ij}^T \bar{P} \, + \bar{P} \tilde{A}_{ij} + \frac{1}{\gamma} I & \bar{P} \tilde{N}_{ij} \\ \tilde{N}_{ij}^T \bar{P} & -\gamma I \end{bmatrix} \begin{bmatrix} \tilde{x}_a \\ d \end{bmatrix} \right\} < 0 \tag{3-11}$$

Inequality (3-11) implies that the inequality (3-12) must hold:

$$\begin{bmatrix} \tilde{A}_{ij}^T \bar{P} \, + \bar{P} \tilde{A}_{ij} + \frac{1}{\gamma} I & \bar{P} \tilde{N}_{ij} \\ \tilde{N}_{ij}^T \bar{P} & -\gamma I \end{bmatrix} < 0 \tag{3-12}$$

To be consistent with (3-5), $\bar{P}$ is structured as follows:

$$\bar{P} = \begin{bmatrix} P_1 & 0 \\ 0 & P_2 \end{bmatrix} > 0 \tag{3-13}$$

Then after simple manipulation the inequality (3-12) can be re-formulated as:

$$\Pi_{ij} = \begin{bmatrix} \Omega_{11} & P_1(B_iK_{jr} + A_i - A_d) & P_1(B_iK_{jd} - B_d) \\ * & P_2A_d + (P_2A_d)^T & P_2B_d \\ * & * & -\gamma I \end{bmatrix} < 0 \tag{3-14}$$

where:

$$\Omega_{11} = P_1A_i + (P_1A_i)^T + P_1B_iK_j + \left(P_1B_iK_j\right)^T + \frac{1}{\gamma}I$$

Inequality (3-14) contains several nonlinear terms and the next step is to formulate this as an LMI. The single step design formulation of the LMI in (3-14) is proposed to avoid the complexity of separate design steps characterised by repeated iteration to determine the gains required. Hence, to implement a change of variables, the following Lemma is required:

Lemma 1 (Congruence) Consider two matrices P and Q, if P is positive definite and if Q is a full column rank matrix, then the matrix $Q * P * Q^T$ is positive definite. Now, let $Q = \text{diagonal}\ (P_1^{-1}, I, I)$

Then $Q * \Pi_{ij} * Q^T < 0$ is also true and it can be re-written as:

$$\Pi_{ij} = \begin{bmatrix} P_1^{-1}\Omega_{11}P_1^{-1} & P_1^{-1}P_1(B_iK_{jr} + A_i - A_d) & P_1^{-1}P_1(B_iK_{jd} - B_d) \\ * & P_2A_d + (P_2A_d)^T & P_2B_d \\ * & * & -\gamma I \end{bmatrix} < 0 \tag{3-15}$$

Using the Schur complement Theorem, the LMI in (3-7) obtained. This completes the proof.

To investigate the relative impacts of the actuator and sensor faults within tracking and regulation problems, a tutorial example is considered using the non-linear simulation of the inverted pendulum and cart with tracking of a time-varying reference cart position. Various results are generated by considering the cart position sensor and cart actuator to have either additive, parametric, or stuck faults. The results generated from this example are separated into three sections corresponding to an investigation of:

1. The importance of LRMFC within FTC,

2. The separate effects of the actuator and sensor faults on the tracking control problem,
3. The separate effects of the actuator and sensor faults on the regulator problem.

The nonlinear inverted pendulum and cart system model is presented in Chapter 2 Eqs. (2-21). The system parameters are m: Pendulum mass (2kg), $2l$: Pendulum length (1m), M: Cart mass (8kg), $a = \frac{1}{m+M}$. The output matrix is assumed to be the identity so that all the states are available at the output.

Three system operating points are chosen corresponding to the pendulum angular positions $\theta = 0$ and $\pm\pi/4$. Due to symmetry, this results in the choice of *two* fuzzy rules in the T-S model. Details of the fuzzy model are presented in (Teixeira and Zak, 1999) and are omitted here.

3-2-1. Investigation of the importance of model reference framework within T-S fuzzy control and FTC

It has been stated in Chapter 2 that the model reference framework is one of the many ways of achieving control reconfiguration. The popularity of the model reference framework for system control is due to several advantageous features. Many performance specifications are given in the time domain e.g. in terms of rise time, damping ratio etc. These can be represented in terms of an ideal transfer function response, which represents the reference model the closed-loop system must follow for tracking purposes. Clearly, the choice of reference model has to satisfy two requirements. It should reflect the performance specifications in the control task, whilst at the same time take into account some inherent constraints on the structure of the reference model (e.g., the reference model order).

The closed-loop performance specification within a T-S fuzzy framework is a challenging task due to the global stability constraints required for designing T-S fuzzy controllers. The T-S approach to closed-loop performance specification actually requires additional LMI constraints to locate the closed-loop eigenvalues within a specified region in the stable complex plan. This increases the probability of infeasible solutions (Chilali and Gahinet, 1996, Chadli, Maquin and Ragot, 2002, El Messoussi, Pages and El Hajjaji, 2006, Mansouri, Manamanni, Guelton and Djemai, 2008). Moreover, specifying the closed-loop performance via additional LMI constraints (e.g.

via a D-region) can guarantee bounded performance since only a region in the complex plane is defined. The consequence of this is that precise closed-loop eigenvalue locations are not defined (Chilali and Gahinet, 1996). To overcome these challenges, the trend in some research studies has been to focus completely on relaxing the global stability and the performance constraints via an approach based on the use of fuzzy Lyapunov function design (Tanaka, Hori and Wang, 2003, Guerra and Vermeiren, 2004, Rhee and Won, 2006, Guelton, Bouarar and Manamanni, 2009, Ezzeldin, Jokic and van den Bosch, 2010).

Recently the model reference framework has been proposed within T-S fuzzy formulation (Witczak, Dziekan, Puig and Korbicz, 2008, Aouaouda, Chadli, Khadir and Bouarar, 2012, Ichalal, Marx, Ragot and Maquin, 2012). However, the strategies described by these authors do not exploit the use of the reference model as a way of specifying the closed-loop system performance. This is because they use a T-S (and hence non-linear) reference model which is chosen to precisely replicate the fuzzy model of the real closed-loop plant. This is clearly a disadvantage since the performance of the reference model cannot be governed precisely as long as it is based on a multiple-model representation. Chapter 4 describes three model-reference based fuzzy control strategies for overcoming this problem by making use of a linear reference model strategy to specify the closed-loop system performance. Following this Chapter 4 develops the theme further by applying this T-S control strategy within an FTC system.

Figure 3-1 a, b, & c show how the tracking performance of the nonlinear system is controlled via a T-S fuzzy controller when the reference model dynamics are changed.

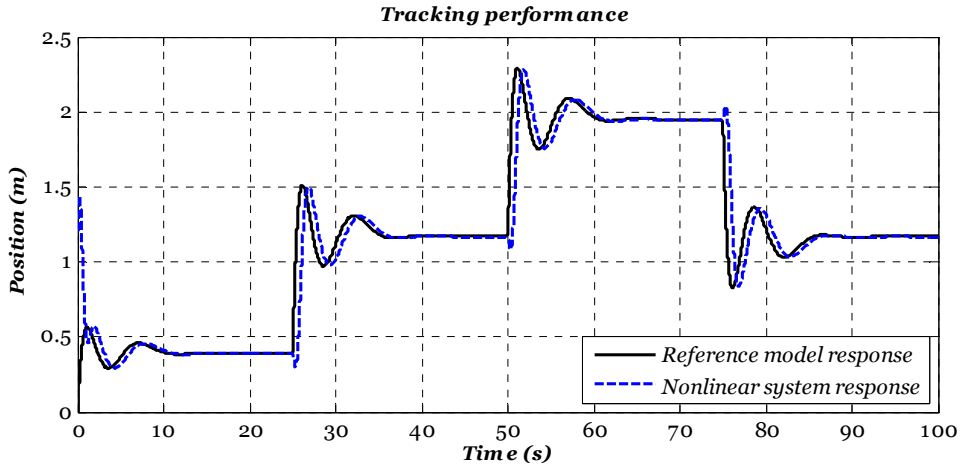

(a)

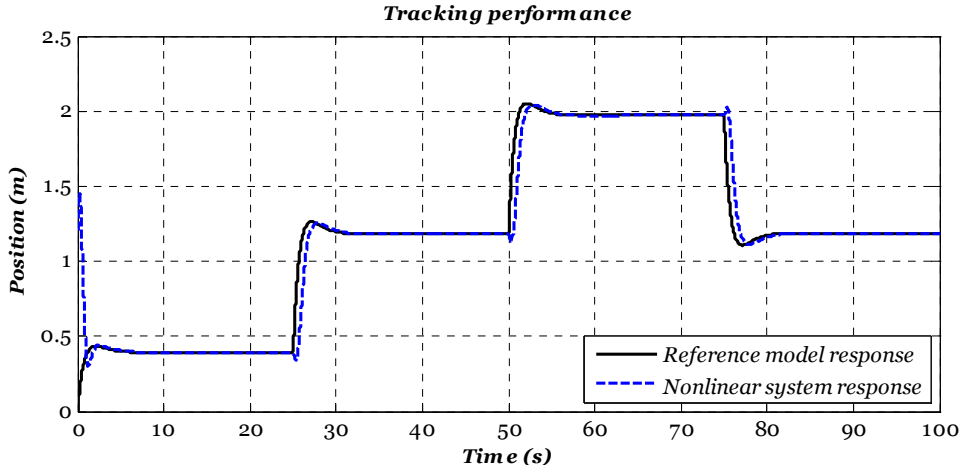

(b)

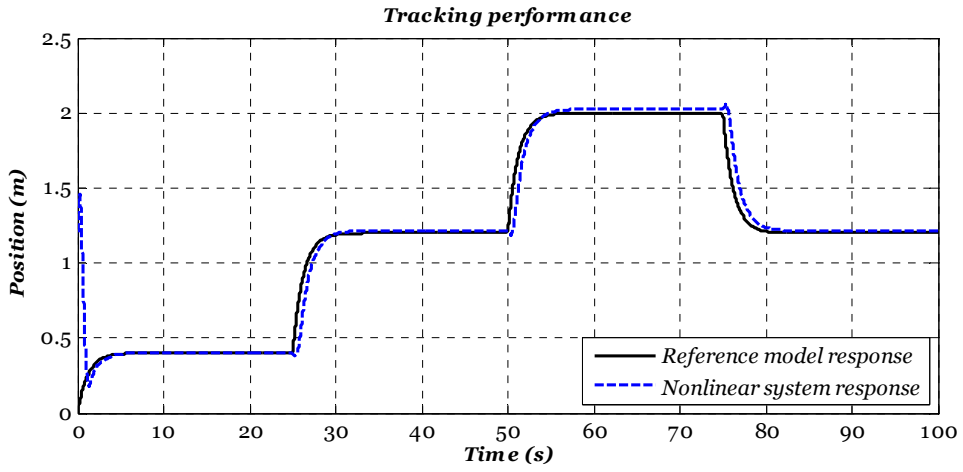

(c)

Figure 3-1: The effect of reference model response on the closed-loop performance. (a) Fast reference model dynamics, (b) & (c) different slow reference model dynamics

Hence, the use of a reference model within the T-S fuzzy control scheme overcomes the design hurdles associated with the use of LMI region constraints. Moreover, in this context the design approach for the model reference system is to assign precise performance whilst the LMI region can only assign performance bounds.

Another advantage of using a model reference framework is that it allows the reference model response to the reference signal to be changed online via either using multiple predesigned reference models or alternatively by adapting the reference model response online to cope with changes in the system operating conditions. This is particularly of value when the control system is also required to be fault tolerant.

The linear model reference strategy used within a T-S fuzzy control system also has an inherent capability to tolerate some actuator faults. For example, in some fault conditions, to reduce the demand on damaged actuators, a ‘slower’ reference model is

desirable (Jin and Youmin, 2006) and this is achieved by changing the reference model response when faults occur. The simulation results in Figure 3-2 show the effect of loss of effectiveness corresponding to an actuator fault modelled as two separate parametric changes in the input matrix B represented as $(0.8B)$ and $(0.75B)$ when fast model-reference dynamics are selected.

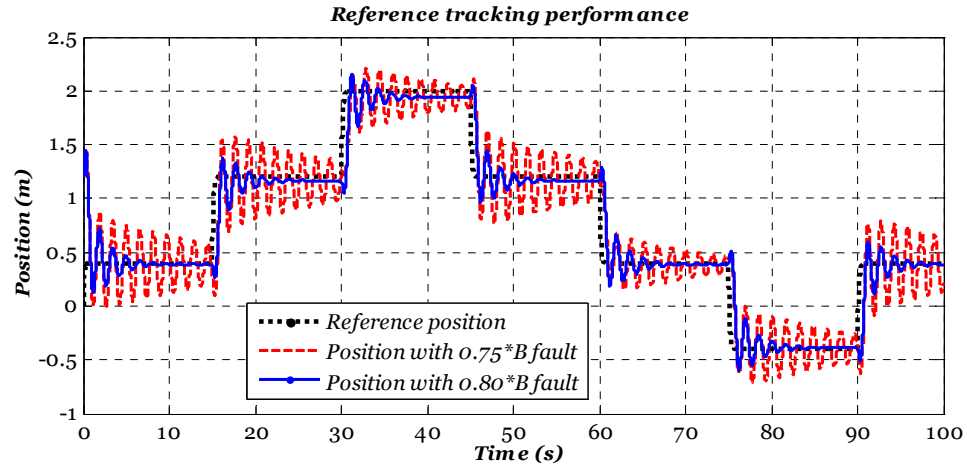

(a)

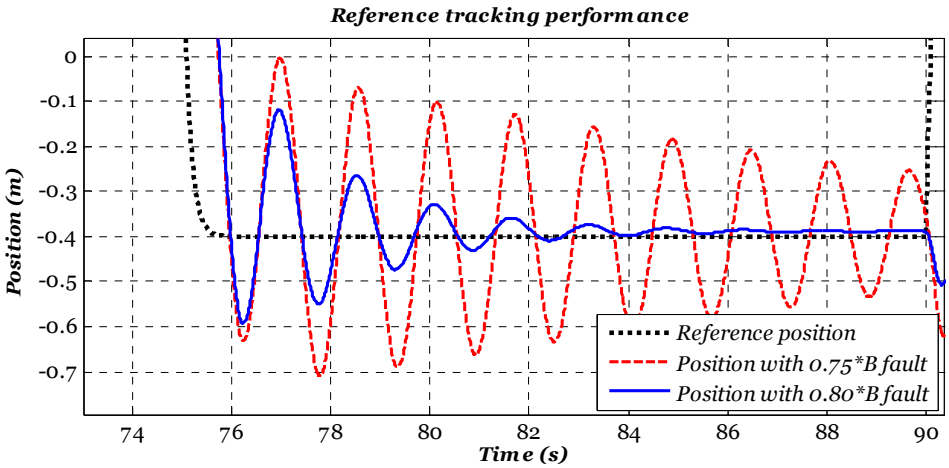

(b)

Figure 3-2: (a) The effect of parametric actuator fault on the tracking performance, and (b) Zoom-in

Figure 3-3 shows that, apart from a transient phase, by changing the reference model response to a slower dynamic acceptable operation in the presence of the two proposed actuator fault scenarios (i.e. $(0.8B)$ and $(0.75B)$) is achieved.

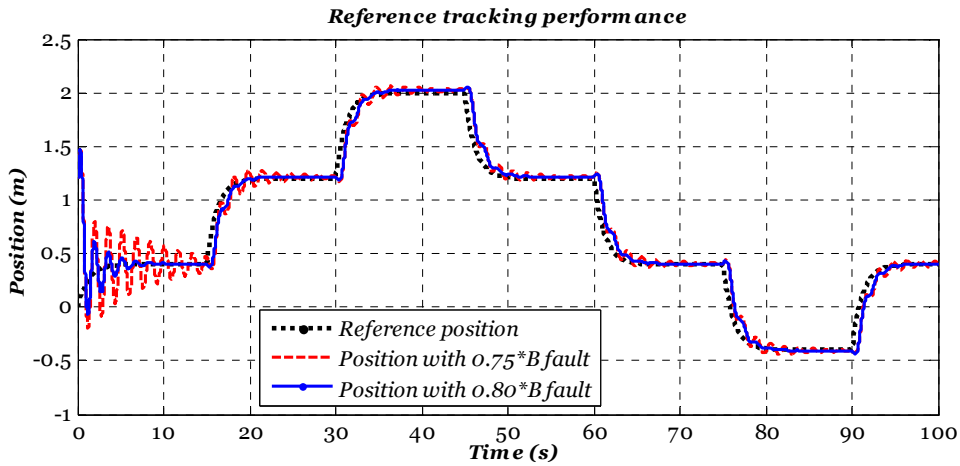

(a)

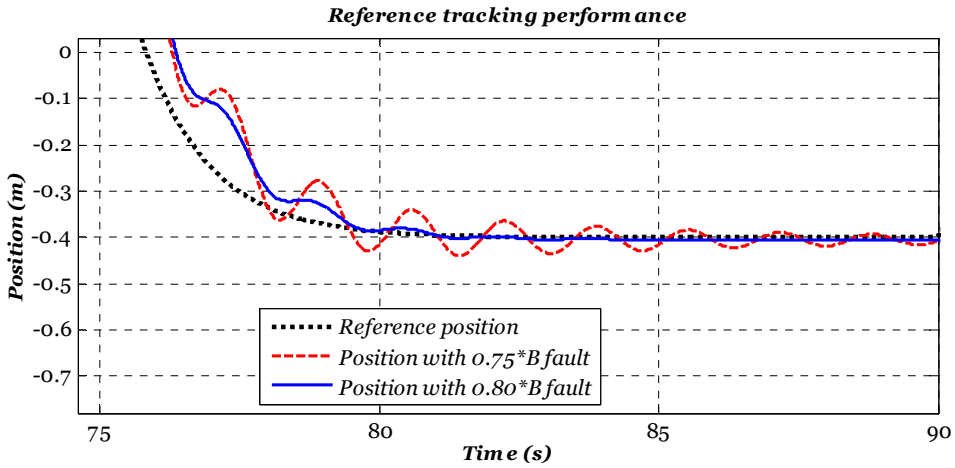

(b)

Figure 3-3: The effect of changing reference model response to minimize fault effects, and (b) Zoom-in

3-2-2. Investigation of the impact of actuator and sensor fault on tracking control problem

Many control problems require a tracking control solution, for example in robotics, missile guidance, unmanned airborne vehicles and wind turbine control systems. It is clear from the literature that there have been no studies covering the impact that actuator and sensor faults have within a *fault-tolerant tracking control* (FTTC) system. This is the case even though the importance of this topic is significant. The non-linear inverted pendulum system has been chosen as a tutorial tracking system example since it is very familiar to the control system community.

Based on the T-S fuzzy state feedback tracking controller introduced in *Theorem 3-1 of* Section 3-2, the simulation results presented in this Section show the effects of different bounded actuator and sensor fault scenarios on the tracking performance without

affecting the closed-loop system stability. The sensor fault is assumed to affect the cart position measurement (x_2) whilst the actuator fault affects the control channel with distribution vector B.

A parametric fault: as presented in Chapter 1, in general this fault is referred to as a multiplicative fault in the literature.

1. An output matrix parametric fault: this fault scenario represents as loss of effectiveness of the sensor so that the faulty measurement becomes:

$$x_{2f} = \alpha x_2 \tag{3-16}$$

where $\alpha \in \mathcal{R}$ represents the fault severity factor. For analysis purposes, consider the tracking error defined in Eq. (3-4) with the assumption that the perfect model matching is achieved (i.e. $\left(B_i K_{jr} + A_i - A_d\right) = 0$ and $\left(B_i K_{jd} - B_d\right) = 0$).

$$\dot{e}_t = [A_i(p) + B_i(p)K_j(p)]e_t \tag{3-17}$$

where $A_i(p) = \sum_{j=1}^{r} h_i\,(p)\,A_i$, $B_i(p) = \sum_{j=1}^{r} h_i\,(p)\,B_i$, and $K_i(p) = \sum_{j=1}^{r} h_i\,(p)\,K_i$. Clearly, the tracking problem becomes a regulation problem in terms of the tracking error (e_t). Specifically, suppose following a transient time that the cart position tracking error (e_{t2}) becomes $\left(e_{t2} = x_{2d} - x_{2f} = 0\right)$, this implies that: $x_2 = x_{2d}/\alpha$. Hence, from a control stand point, for the case of a sensor fault the controller starts to produce a control signal that minimizes the difference between the faulty measurement and the desired cart position. Moreover, as the severity of the sensor fault increases the tracking performance then deeply degrades. Figure 3-4 shows the effect of this sensor fault scenario for $\alpha = 0.9, 0.8, 0.7$.

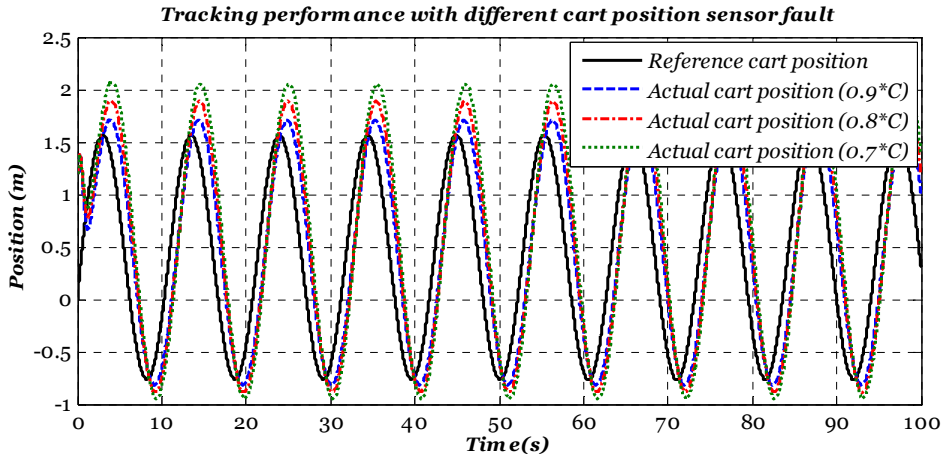

Figure 3-4: The Effect of different sensor parametric faults on tracking performance

2. An input matrix parametric fault: This fault scenario either magnifies or attenuates the control signal (u). The model of this fault usually takes the form:

$$u_f = \alpha u_c \tag{3-18}$$

where u_f is the faulty control signal. Equivalently, this fault can be represented as $(B + \Delta B)$ in which $(\Delta B = \alpha B - B)$ is a scaled version of B. In this case the tracking error dynamics in Eq. (3-17) become:

$$\dot{e}_t = [A_i(p) + \alpha B_i(p) K_j(p)] e_t \tag{3-19}$$

The important difference between the effect if this fault compared with parametric sensor fault is that the controller continues to receive valid measurements whilst the fault affects the closed-loop matrix. Hence, in some bounded fault scenarios for which the tracking dynamics remain stable, the tracking error converges to zero after some transient time. Specifically, suppose the cart position tracking error in this case becomes $(e_{t2} = x_{2d} - x_2 = 0)$, this implies $(x_2 = x_{2d})$.

Clearly, this fault affects the transient performance of the tracking error dynamics since the closed-loop matrix differs from the nominal case. Therefore, the impacts can be passively tolerated by the nominal controller and the effect then becomes the time required to retain the track of reference signal. Figure 3-5 a & b show the effects of a parametric actuator fault on tracking performance for $\alpha = 0.9, 0.8, 0.7$.

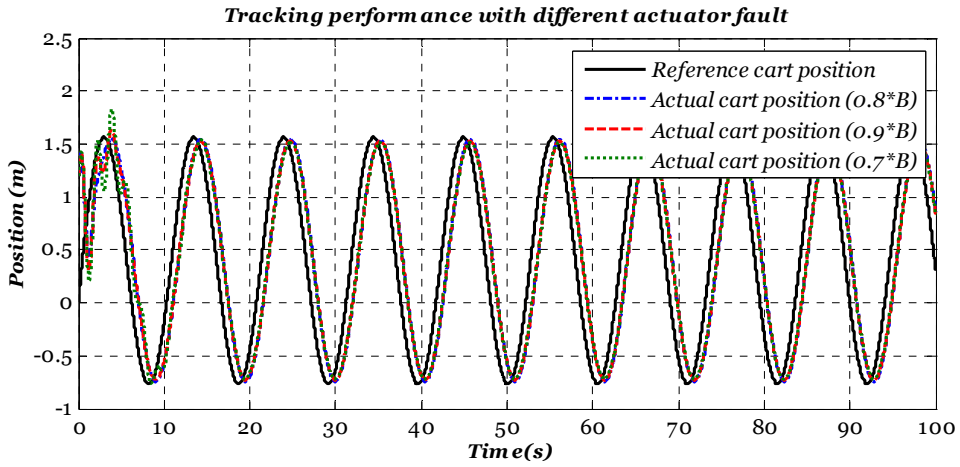

(a)

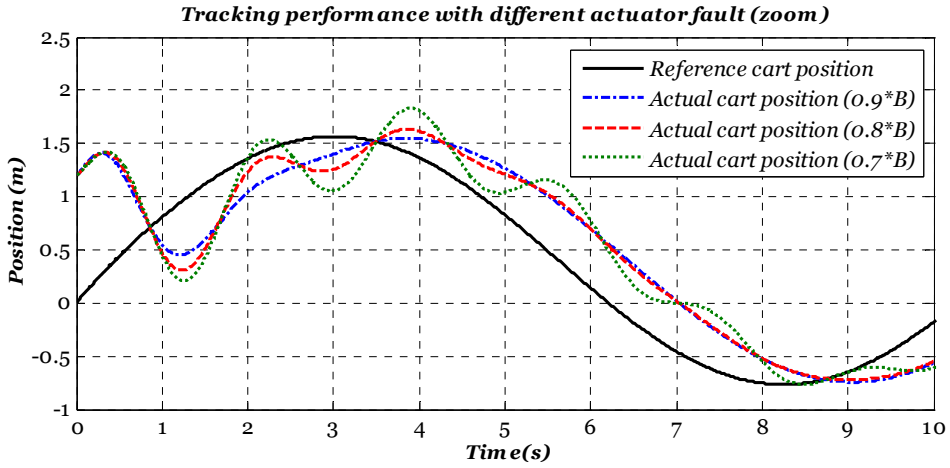

(b)

Figure 3-5 : (a) The effect of different actuator parametric fault on tracking performance, (b) Zoomed-in transient performance with actuator parametric fault

An additive fault: This fault signal is in effect similar to either the measurement noise for the case of a sensor fault or the input disturbance for the case of an actuator fault.

1. A sensor additive fault: The cart position for this fault scenario in this case is represented as:

$$x_{2f} = x_2 + f_s \tag{3-20}$$

where f_s is the fault signal. The effect of the additive sensor fault is similar to the parametric sensor fault case since in this case the tracking error dynamics remain similar to Eq. (3-17), for which if the steady state cart position tracking error is $(e_{t2} = x_{2d} - x_{2f} = 0)$, implies that $(x_2 = x_{2d} + f_s)$. Figure 3-6 shows the effect of an additive sensor fault on the tracking performance with $f_s = 1m$ and $f_s = -1m$.

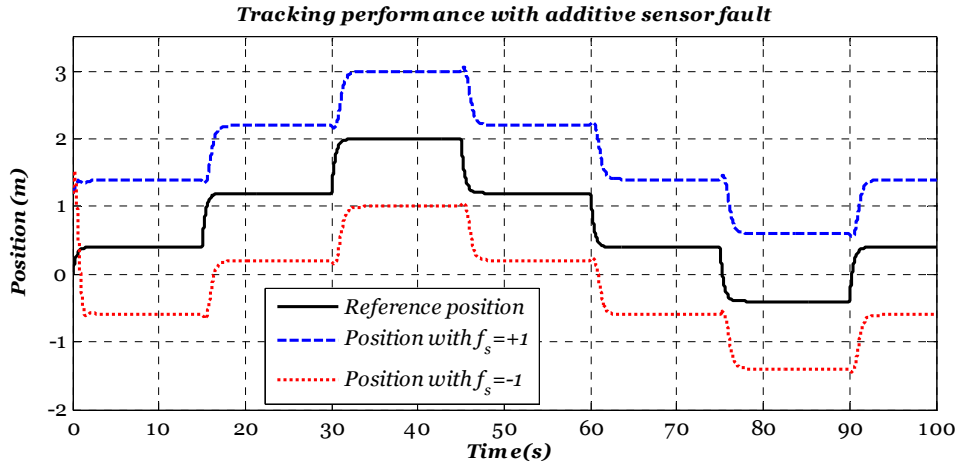

Figure 3-6: Tracking performance with additive sensor fault

2. An actuator additive fault: the fault in this case represent either constant or time varying offset to the control signal. This fault scenario is represented as:

$$u_f = u_c + f_a \tag{3-21}$$

where f_a is the additive actuator fault signal. In this fault scenario the tracking error dynamic given in Eq. (3-17) takes the form:

$$\dot{e}_t = \left[A_i(p) + B_i(p)K_j(p)\right]e_t + B_i(p)f_a \tag{3-22}$$

Clearly, this fault scenario has a different effect from the parametric actuator fault case since the tracking error can only converge to a small region (Ω) in the vicinity of ($e_t = 0$). Moreover, the main difference between this case and the sensor fault case is that by appropriate control design the tracking error can be made as small as possible in the steady state. Hence, the steady state cart position tracking error is approximately. Figure 3-7 a & b show the effect of additive fault on tracking performance with $f_a = 1$ and $f_a = -1$.

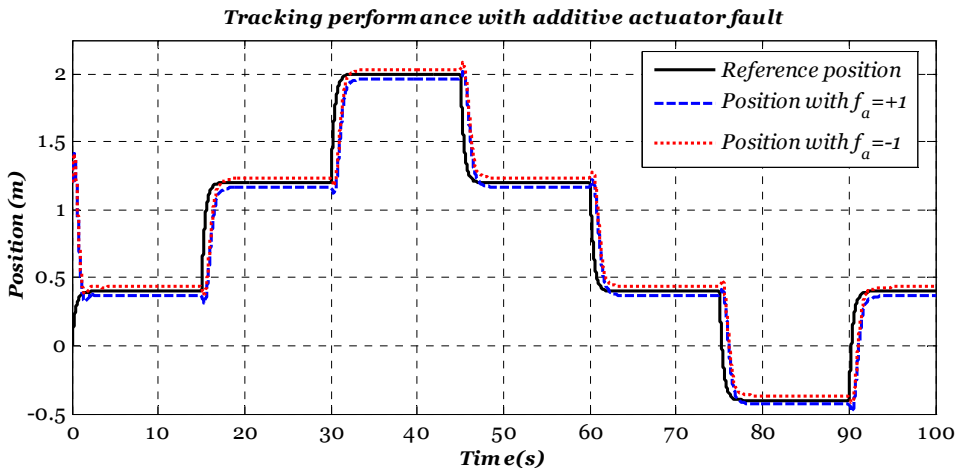

(a)

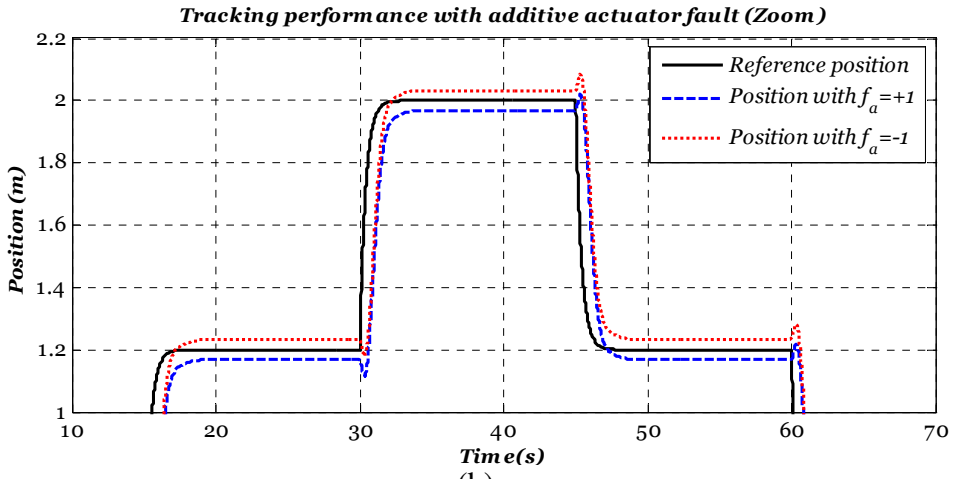

(b)

Figure 3-7 : (a) The tracking performance with additive actuator fault, (b) Zoomed-in tracking performance with additive actuator fault

Based on the simulation results presented in this Section, the following points are now highlighted:

- The relative impacts of actuator and sensor faults on the closed-loop tracking performance are precisely investigated by observing the problem from a controller stand point. In the case of a sensor fault the controller starts to produce the control signal based on measurements that no longer represent the real closed-loop system situation. Hence, as the severity of the sensor fault increases the tracking performance deeply degrades. Conversely, the controller simply reads the actuator fault as form of matched uncertainty.
- Within some bound of actuator faults, the fault impacts can be passively tolerated by the nominal controller. The effect then becomes the time required to retain good tracking of the reference signal for the parametric fault case and minimizing the steady state tracking error for the additive fault case. Moreover, some control strategies can inherently tolerate some actuator faults without the need for an FDD unit. However, same strategies cannot tolerate sensor faults without the FDD function. For example, (1) the PFTC methodology (e.g. robust control) has the ability to tolerate the effects of actuator faults. On the other hand, the sensor fault occurring within tracking control loop cannot be tolerated in a PFTC scheme without an FDD unit. (2) SMC can passively tolerate matched actuator faults and conversely the control performance is significantly degraded if sensors are contaminated by faults. (3) Based on the spirit of adaptive control, actuator faults can be tolerated easily whilst sensor faults cannot be tolerated without compensating their effects via an FDD role (e.g. via fault estimation, or via a redundant sensor).
- For sensor FTTC the design of the estimation and compensation method must take into account the robustness of the sensor fault estimation to (a) the uncertain behaviour of faults, (b) the effects of unknown inputs, and (c) modelling uncertainty. All of these robustness issues are considered in this thesis as follows: the PMIO is used to cover robustness case (a). For case (b) H_∞ performance optimization is used to attenuate the effect of unknown input signals, Modelling uncertainty is tackled in this thesis using multiple-modelling based on T-S fuzzy inference modelling. Conversely, owing to the inherent capability of the nominal controller to tolerate minor actuator faults, some bound on actuator fault estimation error is acceptable.

- The challenging sensor fault scenario within the tracking problem is the sensor fault that affects the objective output, i.e. the output of control interest. Clearly, if the controller aims to force a specific output to follow a desired reference signal, the faulty measurement of the other (non-objective) outputs can be tolerated via PFTC since in this case the fault does not affect the tracking error directly. A similar case is considered in (Wang et al., 2008).

Clearly, this investigation gives the reason why most of the PFTC strategies developed within the tracking control framework consider the actuator rather than the sensor fault problem with the fault affecting the objective output. The literature during the last decade indicates clearly that the community has not clearly highlighted the real issues involved within the tracking control problem. See for example (Fang, Jian Liang and Guang-Hong, 2002, Wang et al., 2008, Zhang, Ye, Li and Wang, 2011, Hu, Yue, Du and Liu, 2012).

3-2-3. Investigation of impact of actuator and sensor faults on the regulator control problem

The investigation of the relative impacts of actuator and sensor faults on the regulator control problem is given here. Clearly, the effects of actuator faults within the regulator problem are similar to their effects within the tracking problem since from a controller stand point these faults emulate the effects of matched uncertainty. Conversely, two factors affect the impact of sensor faults on the closed-loop regulation performance; these are (i) sensor fault type and (ii) time of occurrence of the sensor fault. The following simulation results consider three sensor fault scenarios these are parameter change, additive, and stuck sensor faults.

1. Parameter change sensor fault: Suppose that a dynamical system is at an equilibrium state so that $\mathrm{x}_{\mathrm{steady\ state}} = 0$. As a result, the system state $\mathrm{x(t)}$ will hide the effect of the fault from the controller since pre-fault $C_i x(t) = 0,\ for\ i = 1,2,3,4$. Also, for the post-fault case $C_{if} x(t) = 0$. However, if the system is in its transient phase or just perturbed in the vicinity of its equilibrium, the transient time will be significantly affected by this fault scenario. Consequently, the output matrix for the parametric fault simulates the effect of the initial condition on the transient response, since from the controller stand point the effective initial condition appears to differ

from the actual initial condition and hence the control action is also affected by this difference causing (according to the parameter change), either an increase or a decrease in the transient time. Figure 3-8 illustrates the effects of the parametric change sensor fault on the stabilizing performance of the pendulum system.

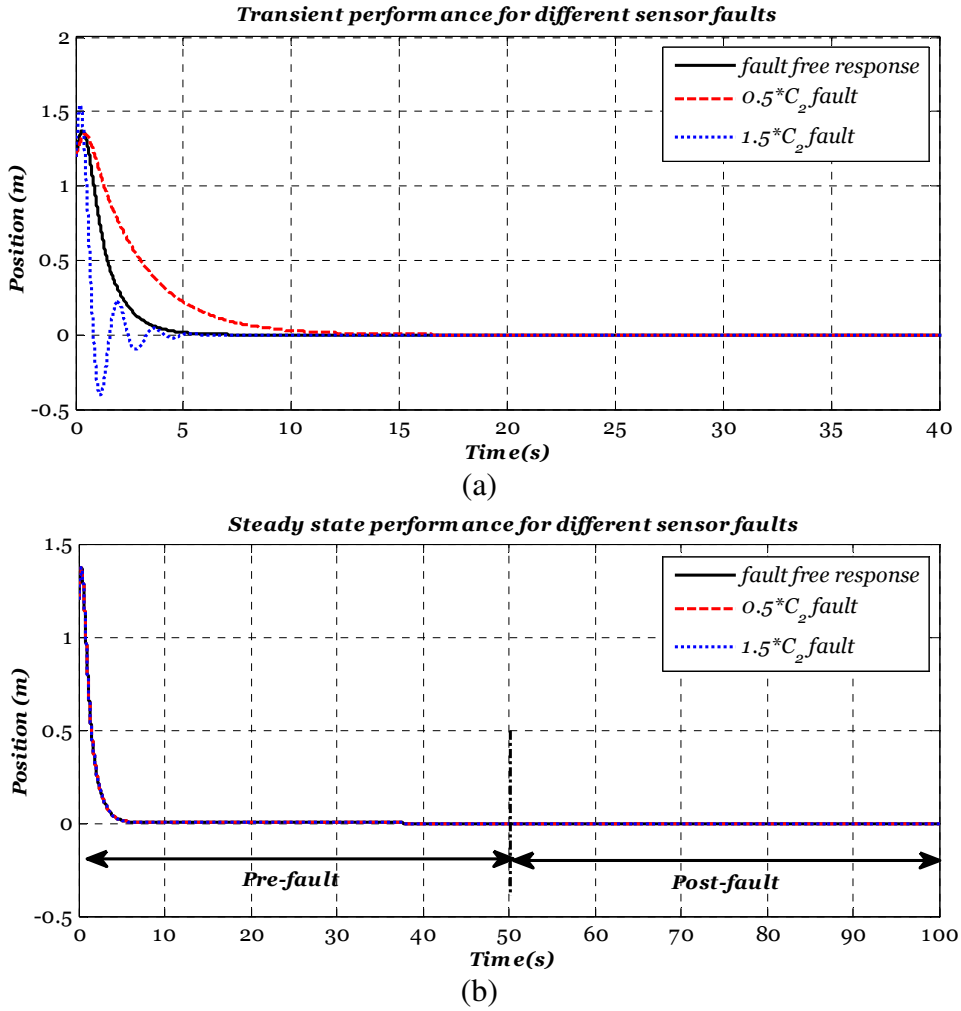

Figure 3-8: Effects of sensor fault on regulation performance. (a) fault started at t=0, (b) fault started at t=50.

2. External additive sensor fault: This fault scenario affects the system both in the transient and in the steady state operating regions. The key difference with the parameter change fault is now that the fault no longer completely depends on the system states. Therefore, even when the system is in its steady state and $C_i x(t) = 0$, the controller receives the state independent measurement $C_i x(t) + f_s(t)$. In fact, the controller starts to direct the system in such a way as to make $C_i x(t) + f_s(t) = 0$. Clearly, the solution to this is to drive the faulty measured state to be equal to $-f_s(t)$. The controller continuously tracks the sensor fault signal (see Figure 3-9).

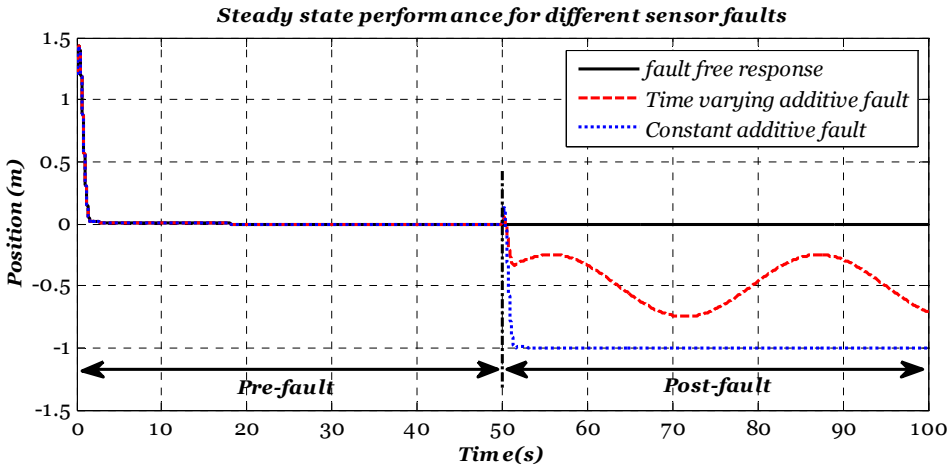

Figure 3-9: Effects of additive sensor fault on stabilizing control problem

3. Stuck measurement sensor fault: $(C_i x(t) = constant)$ This fault scenario represents the worst sensor fault case since the controller receives measurements that are completely independent of the system states. In fact, this fault eventually leads the controller to destabilise the closed-loop system since whatever control signal is delivered, the measurements are fixed at $C_i x(t) = constant$ (see Figure 3-10).

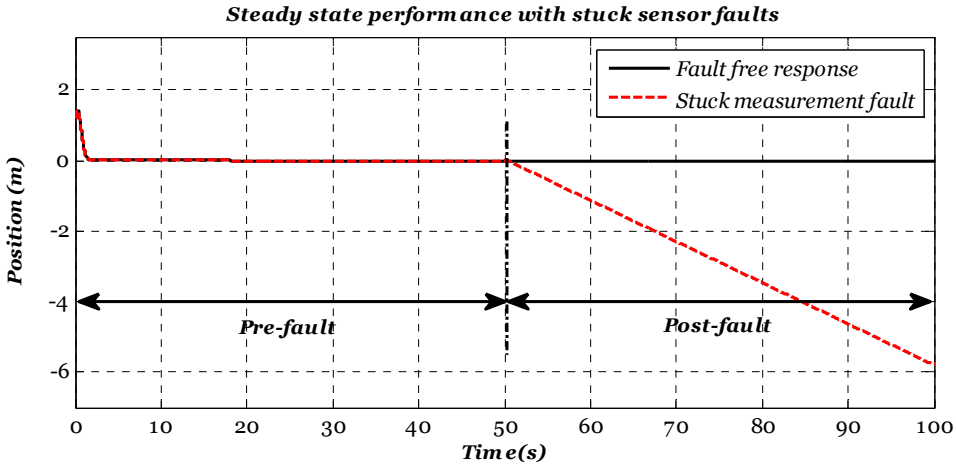

Figure 3-10: Effects of fixed measurement fault on stabilizing control problem

From the controller stand point, parameter changes and additive faults of the input matrix have the same effects in both regulator and tracking control problems. Figure 3-11a below shows the effect of the input matrix parameter change on the performance of the closed-loop system whilst Figure 3-11b shows the effect of the additive actuator fault.

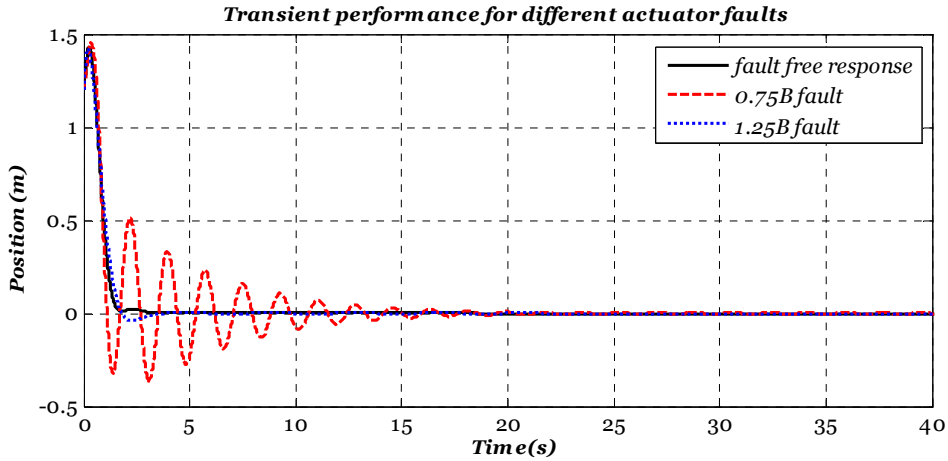

(a)

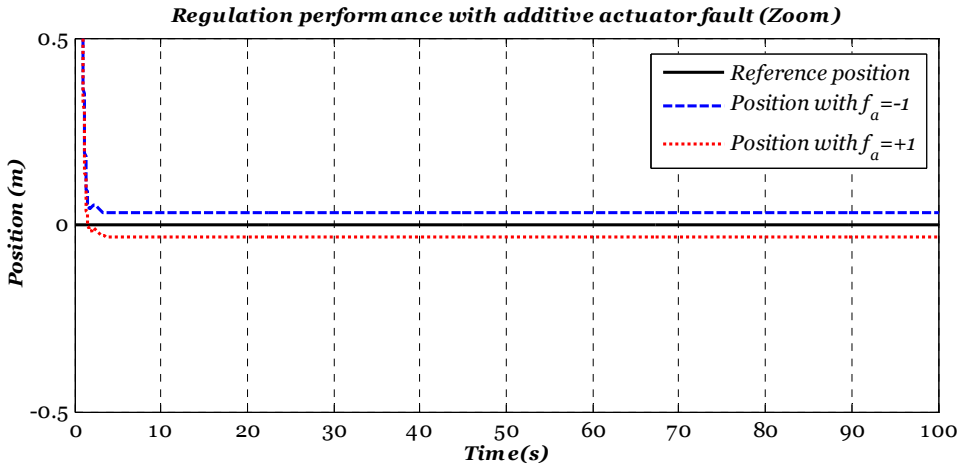

(b)

Figure 3-11 : (a) Effects of parametric actuator fault on regulator control problem, (b) Effects of additive actuator fault on regulator control problem

The main concepts arising from this Section are:

1. In contrast to the tracking control problem, the regulator control problem has greater immunity against output matrix parameter faults and can passively tolerate their effects, i.e. the steady-state value ($x_{steady\ state} = 0$) "hides" the parametric faults.
2. Although the parametric sensor fault does not affect the steady state response in the regulation problem, this fault scenario gives rise to a new challenge within the FDD framework since the steady-state hides the effect of this fault and hence it becomes undetectable in this situation.
3. The FTTC problem involves more design challenges compared with the regulator control problem since within the tracking problem the reference signal and the fault are both considered as dynamic uncertainties that affect the closed-loop performance. Moreover, within the T-S fuzzy based FTC the tracking problem

increases the design challenges from both control and estimation stand points due to the fact that the reference signal can force the system dynamics to fluctuate between the operating points corresponding to the local models and hence the fault affects the whole range of system operation, i.e. the FTC has global behaviour across the range of system operation. Figure 3-12 a & b show the effect of the reference signal on the fuzzy model of the nonlinear inverted pendulum system.

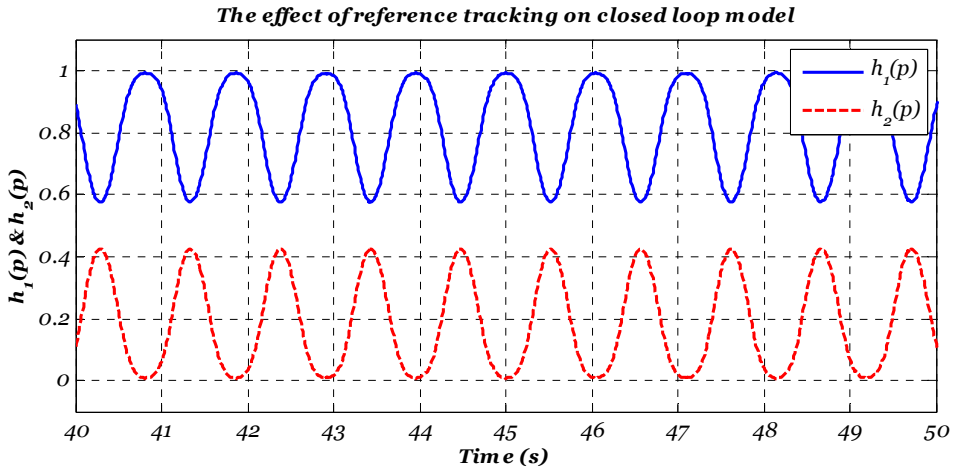

(a)

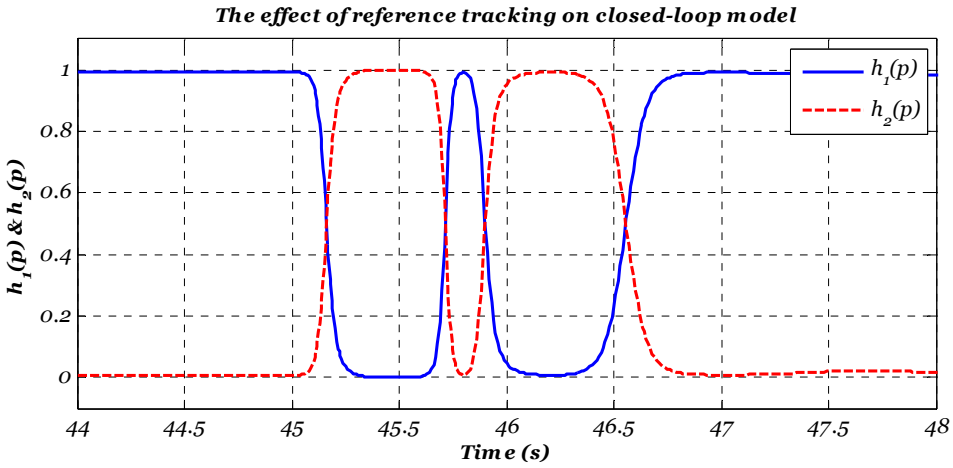

(b)

Figure 3-12: (a) Effect of tracking error on fuzzy model using the sinusoidal reference, (b) Effect of the tracking error on fuzzy model using the multi-step reference.

It is clear from that the presence of reference signal (the sinusoidal in Figure 3-12a and the multi-step in Figure 3-12b signals) forces the inverted pendulum dynamics to continuously hover over the two local models (see the membership functions $h_1(p)$ & $h_2(p)$).

3-3. Fault modelling for FTC framework

It has been already stated in Section 1-2 that some literature classifies the fault as either additive or multiplicative fault. On the other hand, Sections 3-2-2 & 3-2-3 have investigate the separate effects of both the additive and the multiplicative faults on tracking and regulator control problems. Clearly, any remedial action taken to tolerate the effects of any fault depends on the appearance of the fault in system model. For example, the augmented state observer based FTC proposed in (Klinkhieo, 2009) is suitable for additive faults whilst adaptive control based FTC has the capability to tolerate additive or multiplicative actuator faults (Yang and Ye, 2011).

While the main trend of the work presented in this thesis is following the estimation and compensation based AFTC scheme, the use of an additive representation of a fault is proposed as a generalized fault model in the following chapters. This is because the proposed strategies perform online fault estimation and compensation. Hence, there is no restriction even if the faults become state dependent. The following subsections investigate this issue for different sensor fault scenarios:

Suppose the measured output is given by:

$$y = Cx = \begin{bmatrix} 1 & 0 \\ 0 & 1 \end{bmatrix} \begin{bmatrix} x_1 \\ x_2 \end{bmatrix} \tag{3-23}$$

<u>An output matrix parametric fault</u>:

$$y_f = C_f x = \begin{bmatrix} 1 & 0 \\ 0 & 0.3 \end{bmatrix} \begin{bmatrix} x_1 \\ x_2 \end{bmatrix} \tag{3-24}$$

This fault scenario can be represented as an *additive fault* in which the fault signal depends on the measured state, as illustrated below:

$$y_f = Cx + Df_s = Cx + \begin{bmatrix} 0 \\ 1 \end{bmatrix} (-0.7 * x_2) \tag{3-25}$$

Hence, parameter changes in the output matrix C can be considered as a special case in which the faults signal (f_s) is a scaled version of the measured state.

<u>Loss of measurement fault</u>: This fault is a special case of the parametric fault and can also be represented as an additive fault in which the additive fault signal is equal to the negative of the corresponding state:

$$y_f = C_f x = \begin{bmatrix} 1 & 0 \\ 0 & 0 \end{bmatrix} \begin{bmatrix} x_1 \\ x_2 \end{bmatrix} = Cx + \begin{bmatrix} 0 \\ 1 \end{bmatrix} (-x_2) \tag{3-26}$$

Time varying parameter fault: This fault can also be represented as an additive fault as follows:

$$y_f = C_f x = \begin{bmatrix} 1 & 0 \\ 0 & f(t) \end{bmatrix} \begin{bmatrix} x_1 \\ x_2 \end{bmatrix} = Cx + \begin{bmatrix} 0 \\ 1 \end{bmatrix} ((f(t) - 1)x_2) \tag{3-27}$$

Hence, even a time-varying parametric fault can be represented as a special case of an additive fault.

Stuck sensor reading: A given measurement is fixed or "stuck" at a constant value k. This fault can also be considered as an additive fault as follows:

$$y_f = C_f x = \begin{bmatrix} 1 & 0 \\ 0 & \frac{k}{x_2} \end{bmatrix} \begin{bmatrix} x_1 \\ x_2 \end{bmatrix} = Cx + \begin{bmatrix} 0 \\ 1 \end{bmatrix} (k - x_2) \tag{3-28}$$

Thus, parametric faults, multiplicative faults, and stuck faults are special cases of additive faults in which the fault signal is a function of the corresponding measured state. Moreover, an additive fault can be used to represent a fault scenario in which the fault is independent of system state as follows:

$$y_f = Cx + Df_s \tag{3-29}$$

where f_s could be any external signal. As a result, additive faults can be considered via a generalized fault representation. Thus, an additive fault representation is considered appropriate throughout this thesis to cover the different fault scenarios.

3-4. Conclusion

This Chapter presents an investigation of the importance of the LRMFC framework in an approach to FTC using T-S fuzzy multiple-modelling, as well as the relative impacts of actuator and sensor faults for both tracking and regulator control problem. It has been shown that the sensor fault has a direct effect on the performance of the tracking control problem. The importance of the sensor FTTC is attributed to the fact that, when a fault occur, the controller starts to direct the system according to measurements that no longer represent the real system situation. As a result, if the sensor fault severity increases the controller drives the system strongly away from the required reference value.

Based on the investigation presented in this Chapter, the most challenging case within the framework of FTC is to consider either sensor faults or severe actuator faults within

the FTTC problem. On the other hand, designing the FTTC within model reference framework offers several advantageous features that enhance the overall FTTC performance. The combination of FTTC within a model reference framework is the topic of Chapter 4.

Chapter 4 : Design of model reference FTTC of nonlinear systems via T-S fuzzy approach[1]

4-1. Introduction

This Chapter proposes three new FTTC strategies for nonlinear systems described via T-S fuzzy inference form, employing the advantages of LRMFC. The proposed strategies are: (i) Control reconfiguration based sensor FTTC via VS, (ii) Estimation and hiding based sensor FTTC via T-S fuzzy PMIO. (iii) Estimation and compensation based actuator FTTC via T-S fuzzy PPIO. The main contributions in this chapter are:

1. The proposal of an LMI-based design of a T-S fuzzy VS based FTTC. The advantageous feature of the LRMFC is employed in this strategy. Moreover, investigation of the main limitations encountered by this method within the T-S fuzzy framework has also been inspected.
2. The proposal of an LMI-based design of a T-S fuzzy PMIO for simultaneous estimation of system states and sensor faults, as well as the use of the T-S fuzzy PMIO within an LMI design of sensor fault tolerant model reference state tracking fuzzy control.
3. The proposal of an LMI-based design of a T-S fuzzy PPIO for simultaneous estimation of system states and actuator faults, as well as the use of the T-S fuzzy PPIO within an LMI design of actuator fault tolerant model reference state tracking fuzzy control.

Although T-S fuzzy FTTC within a model reference framework has recently been proposed (Aouaouda, Chadli, Khadir and Bouarar, 2012, Ichalal, Marx, Ragot and Maquin, 2012), the strategies presented in this Chapter introduce significant contributions via:

[1] Section 4-4 has been published in the 20th Mediterranean Conference on Control & Automation. Sami, M. & Patton, R. J. 2012f. A multiple-model approach to fault tolerant tracking control for non-linear systems. 20th Mediterranean Conference on Control & Automation, Barcelona, 498-503. 3-6 July.

a) Exploiting the advantages of LRMFC. In fact this is not the case in the aforementioned references since they use a T-S (non-linear) reference model which is chosen to precisely replicate the fuzzy model of the real closed-loop plant.
b) Considering the design of sensor fault within the tracking control problem.
c) Introducing the LMI-based design of LRMFC-based T-S fuzzy PMIO and T-S fuzzy PPIO to enhance the closed-loop fault tolerance capability since the two observers have the ability to provide accurate estimation of a variety of fault scenarios.
d) Considering the use of control reconfiguration (i.e. the VS) for sensor FTTC.
e) The addition of feed-forward control signals to handle the robustness problem is made as a consequence of the use of a linear reference model that does not in any way replicate the T-S model.

The remaining Sections of this Chapter are organized as follows: Section 4-2 presents the main concept of the VS based AFTC as well as the necessary conditions for the existence for both the static and dynamic VS cases. Section 4-2-1 presents the derivation of the LMI-based design of a T-S fuzzy VS to tolerate the effect of sensor faults in the LRMFC loop. The LMI-based approach for sensor fault hiding incorporating the use of T-S fuzzy PMIO and LRMFC is presented in Section 4-3. Section 4-4 presents the LMI-based design of T-S fuzzy PPIO based FTTC within the model reference framework. A concluding discussion and a statement of the motivations behind the work proposed in Chapters 5 and 6 are presented in Section 4-5.

4-2. Sensor fault hiding via VS approach

This Section provides a suitable background for the design of sensor FTTC incorporating the use of T-S fuzzy VS and the LRMFC, focusing on a comparison between different AFTC approaches (specifically the control reconfiguration and the estimation and compensation).

Details about the VS concept and design approaches are given in (Steffen, 2005, Blanke, Kinnaert, Lunze and Staroswiecki, 2006, Richter, Heemels, van de Wouw and Lunze, 2008, de Oca and Puig, 2010, Ponsart, Theilliol and Aubrun, 2010, Richter, 2011, Richter, Heemels, van de Wouw and Lunze, 2011). In summary, the concept of VS based fault hiding is to recover the pre-fault closed-loop system behaviour without changing the nominal controller. On the other hand, static and dynamic VS based FTC is presented in the literature. The choice of a static or dynamic approach depends on the

available number of measurements and the expected fault scenarios. The schematics of the two approaches are shown in Figure 4-1 a&b.

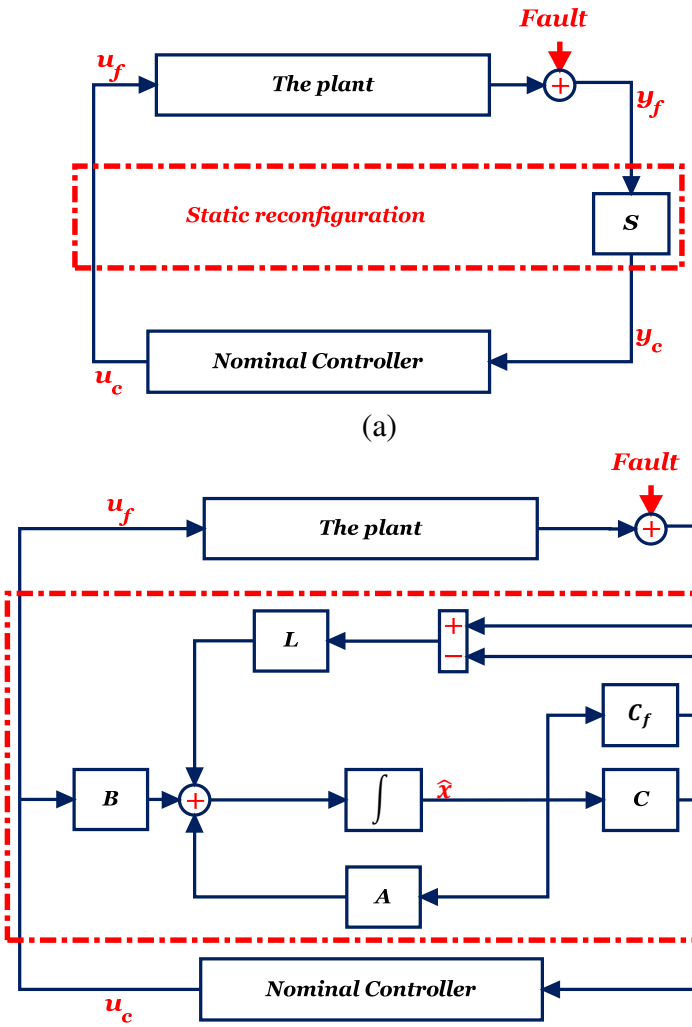

Figure 4-1: VS (a) static, (b) dynamic

Both the static and the dynamic VS require an accurate post-fault plant model. Hence, this method is significantly affected by the robustness of the FDD unit.

Basically, the static VS approach is applied for systems that are equipped with redundant measurements or at least the faulty measurement can be reconfigured from other measurements. The reconfiguration process requires two steps. The first is to detect and isolate the faulty sensor. Secondly, based on the fault isolation, the parameter of the static block (S) is determined so that the faulty measurement is recovered by the redundant one. The following rank condition must hold to successfully reconfigure the faulty measurements:

$$rank\left(C_f\right) = rank\left(\begin{bmatrix} C_f \\ C \end{bmatrix}\right) \tag{4-1}$$

where C and C_f are the pre and post-fault output matrices, respectively. It is clear from the rank condition that if a complete sensor fault occurs that rank condition no longer holds unless there is a redundant measurement to recover the rank. On the other hand, a dynamic VS can cover a variety of sensor fault scenarios. For example, covering the sensor fault cases that destruct the rank condition in Eq. (4-1) provided that the system remains observable via the faulty measurements, see for more details (Steffen, 2005).

In reality, the dynamic VS design problem emulates the observer design problem. Therefore, by combining the post-fault plant and the model of the nominal plant, the dynamical equation of the augmented system can be written as follows:

$$\left.\begin{aligned} \dot{x} &= Ax + Bu_c \\ \dot{x}_f &= Ax_f + Bu_c \\ y_c &= C\hat{x} \\ y_f &= C_f x_f \end{aligned}\right\} \tag{4-2}$$

The aim of the dynamic VS is basically to ensure continuous delivery of the feedback signals that reflect the actual system behaviour during both faulty and fault-free sensor measurements. This requires that the dynamic VS states ($\hat{x}$) continue to converge towards the actual system states (x_f) even if a sensor fault occurs. By achieving the convergence, the controller input (y_c) continuously reflects the actual system states in both the pre- and post-sensor fault cases.

Clearly, the presence of a sensor fault will affect the system states. However, it is assumed that other system parameters (i.e. A and B) are not affected. Under the assumption that C_f is accurately identified via the FDD unit (Steffen, 2005), the dynamical VS is an observer expressed as:

$$\dot{\hat{x}} = A\hat{x} + Bu_c + L_f(y_f - C_f\hat{x}) \tag{4-3}$$

designed to stabilize the error signal:

$$e = y_f - C_f\hat{x} = C_f x_f - C_f\hat{x} \tag{4-4}$$

Obviously, when $e \to 0$ then $\hat{x} \to x_f$ and hence the VS provides "state estimates" that represent the actual system states. Therefore, when a fault occurs, the overall

reconfiguration strategy is completed in *four* steps. Firstly, the faulty output matrix C_f is accurately identified by the FDD unit. Secondly, a check for the observability of the pair (A, C_f) is made. Thirdly, compute the gain L_f so that the dynamic VS is stable. The fourth step is to insert the new dynamic system (based on the VS) and hence the result is a stable reconfigured closed-loop system. Clearly, the necessary condition for the existence of the VS is the observability or at least the detectability of the pair (A, C_f). Furthermore, other constraints could be added to the reconfiguration steps. For example, the gain L_f is required to stabilise the dynamic system by locating the closed-loop eigenvalues in a specific region of the stable complex plane. However, the overall reconfiguration strategy must take due care to minimise the time consumed to reconfigure the closed-loop system, which in turn may limit the design freedom of L_f.

4-2-1. T-S fuzzy VS based model reference FTTC

In this Section a new sensor FTTC scheme is proposed for a nonlinear system that can be described via T-S fuzzy inference modelling. The strategy incorporates the use of T-S fuzzy VS and the LRMFC. The scheme is illustrated in Figure 4-2 in which $A(p) = \sum_{j=1}^{r} h_i(p) A_i$, $B(p) = \sum_{j=1}^{r} h_i(p) B_i$ are the system matrices. $L(p) = \sum_{j=1}^{r} h_i(p) L_i$ and $L_f(p) = \sum_{j=1}^{r} h_i(p) L_{fi}$ are the nominal and the VS gains. C and C_f are the nominal and the faulty output matrices.

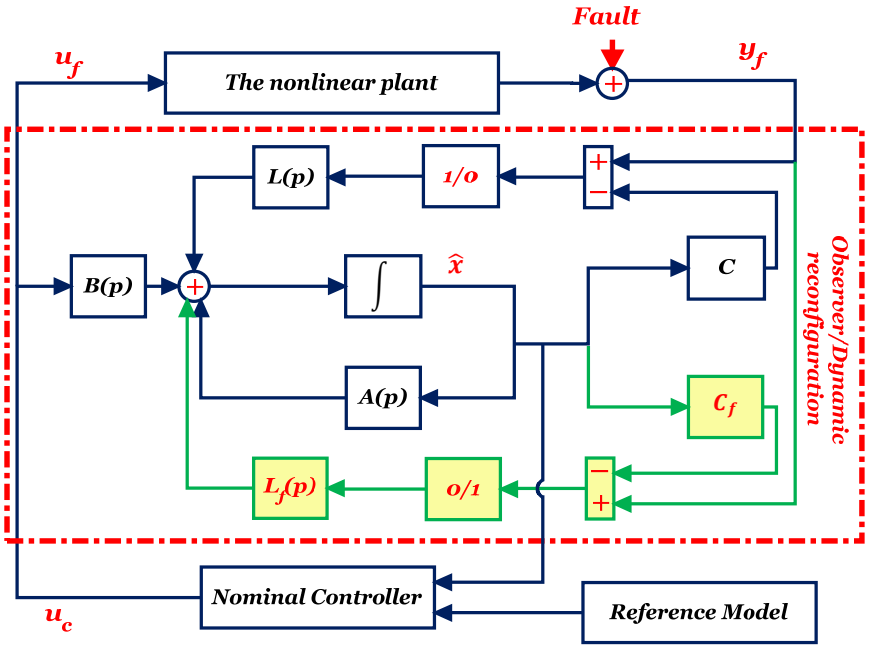

Figure 4-2: Schematic of the proposed sensor FTC strategy

The main contributions in this Section are to: (i) Consider the extension of the VS based FTC method to nonlinear systems via the T-S fuzzy inference modelling approach. (ii) Consider the design of the T-S VS within the tracking control problem. (iii) Exploit the advantageous features of the LRMFC framework.

The T-S fuzzy model of the nonlinear system with sensor faults considered as embedded in the output matrix (via the matrix C_f) can be mathematically represented by the following equation:

$$\left.\begin{aligned} \dot{x} &= \sum_{i=1}^{r} h_i\left(p(t)\right)\{A_i x(t) + B_i u(t)\} \\ y &= \sum_{i=1}^{r} h_i\left(p(t)\right)\{C_{fi}\, x(t)\} \end{aligned}\right\} \tag{4-5}$$

where $x(t) \in \mathcal{R}^n$ is the state vector, $u(t) \in \mathcal{R}^m$ is the input vector and $y(t) \in \mathcal{R}^l$ is the output vector, $A_i \in \mathcal{R}^{n*n}$, $B_i \in \mathcal{R}^{n*m}$, and $C_{fi} \in \mathcal{R}^{l*n}$ $i = 1, 2, .., r$ are the system matrices, r is the number of fuzzy rules and the term $h_i\left(p(t)\right)$ is the weighting function.

The first control objective is to force the states of the actual nonlinear system to follow the states of the reference model, which has the same order n, via the design of the T-S fuzzy observer-based T-S fuzzy control scheme. Maintenance of good tracking performance is expected for both the fault-free and faulty measurement cases. The required reference model is assumed to have the following form:

$$\dot{x}_d = A_d x_d + B_d d \tag{4-6}$$

where $x_d \in \mathcal{R}^n$ is the desired trajectory for x for all $t \geq 0$, $d \in \mathcal{R}^d$ is the bounded reference input, $A_d \in \mathcal{R}^{n*n}$ and $B_d \in \mathcal{R}^{n*d}$ are a stable state space pair chosen to reflect the required closed-loop performance.

To achieve the tracking performance objective, as well as to give due care to the mismatch between the fuzzy model and the reference model a combination of feedback and feed foreword control signals is proposed yielding a T-S fuzzy controller of the following form:

$$u_c = \sum_{i=1}^{r} h_i\left(p\right)\{K_i(\,\hat{x} - x_d) + K_{ir} x_d + K_{id} d\} \tag{4-7}$$

where $\hat{x}$ is the estimate of the system state, $K_i \in \mathcal{R}^{m*n}$ is the feedback gain,, $K_{ir} \in \mathcal{R}^{m*n}$ and $K_{id} \in \mathcal{R}^{m*d}$ are the feed-forward gains. Clearly, from Eq. (4-7) the proposed fuzzy controller tolerates the effect of the sensor fault if the state estimate signal ($\hat{x}$) reflects the actual behaviour of the nonlinear system, i.e. as required to hide the effect of the C_f matrix. Hence, for the sensor fault-free case, by subtracting (4-6) from (4-5) and substituting for u_c from (4-7), then the tracking error (e_t) dynamics are given by:

$$\begin{aligned}\dot{e}_t = \dot{x} - \dot{x}_d = \sum_{i=1}^{r}\sum_{j=1}^{r} h_i(p)h_j(p)\{(A_i + B_iK_j)e_t - B_iK_j\mathrm{e_x} \\ + (B_iK_{jr} + A_i - A_d)x_d + (B_iK_{jd} - B_d)d\}\end{aligned} \tag{4-8}$$

The state estimate signal in the fault-free case is then obtained via the design of a T-S fuzzy observer which is given by:

$$\dot{\hat{x}} = \sum_{i=1}^{r} h_i(p)\{A_i\hat{x} + B_iu_c + L_i(y - C\hat{x})\} \tag{4-9}$$

where $\hat{x} \in \mathcal{R}^n$ is the estimate of the state vector x, $L_i \in \mathcal{R}^{n\times l}$ is the observer gain to be designed, and e_x is the state estimation error defined as:

$$e_x = x - \hat{x} \tag{4-10}$$

Therefore, if the pairs (A_i, C) are observable, then there may exist an observer in the form of Eq. (4-9) providing system state estimation. The state estimation error dynamics are given by:

$$\dot{e}_x = \sum_{i=1}^{r} h_i(p)\{(A_i - L_iC)e_x\} \tag{4-11}$$

The dependence of the estimation error dynamics on the measured output signals is clear from Eq. (4-11) . However, when there is a sensor fault both the estimation error and hence also the control signal are directly affected so that the controller produces a control signal based on the faulty measurements tending to drive the system away from the reference model. Therefore, it is important to reconfigure the estimation process so that when a sensor fault occurs the observer dynamics are reconfigured to ensure the continuity of the accurate estimation of the system states. For this reason, in this

strategy the observer subsystem has been accompanied by an FDD controlled feedback path activated once a sensor fault arises.

Following the idea of the dynamic VS, suppose that the post-fault output matrix has been identified by the FDD unit. The new feedback path of the estimator given in Eq. (4-9) is fed by the estimated faulty output $\hat{y}_f$ $(C_f\hat{x})$. Hence, the new estimator (VS) becomes:

$$\dot{\hat{x}} = \sum_{i=1}^{r} h_i(p)\{A_i\hat{x} + B_i u_c + L_{fi}(y_f - C_f\hat{x})\} \tag{4-12}$$

This clearly shows that the observer starts to minimise the error between y_f and $\hat{y}_f$ through new observer gain L_{fi} which is computed on-line. Off-line computation of L_{fi} could also be carried out based on the information provided by the FDD unit.

Obviously, the whole observer reconfiguration process and so the sensor fault tolerance is governed by the delectability of the post-fault pairs (A_i, C_f). If this necessary condition is satisfied, then there may exist observer gain L_{fi} to stabilise the error between y_f and $\hat{y}_f$ or equivalently between $C_f x$ and $C_f\,\hat{x}$.

Using Eqs. (4-6), (4-8), and (4-11) the augmented system takes the form:

$$\dot{\tilde{x}}_a(t) = \sum_{i=1}^{r}\sum_{j=1}^{r} h_i(p)h_j(p)\{\tilde{A}_{ij}\tilde{x}_a + \tilde{N}_{ij}d\} \tag{4-13}$$

where:

$$\tilde{A}_{ij} = \begin{bmatrix} A_i + B_iK_j & -B_iK_j & B_iK_{jr} + A_i - A_d \\ 0 & A_i - L_iC & 0 \\ 0 & 0 & A_r \end{bmatrix}$$

$$\tilde{x}_a = \begin{bmatrix} e_t \\ e_x \\ x_d \end{bmatrix}, \quad \tilde{N}_{ij} = \begin{bmatrix} B_iK_{jd} - B_d \\ 0 \\ B_d \end{bmatrix}$$

The objective here is to compute the gains $L_i, K_{jr}, K_{jd}, and\ K_j$ such that based on Eq. (4-13) the effect of the bounded input d on the tracking error dynamics is attenuated below the desired level γ to ensure robust tracking performance.

Clearly, a stability proof is required when considering the closed-loop behaviour of the overall augmented system. This stability requirement becomes more complicated for multiple-model systems since the local controllers must stabilize the local linear model

as well as satisfying the global stability constraints. Moreover, the number of design constraints increase as the number of local models is increased. Hence, a "trial and error" design methodology is a time-consuming approach. Therefore, an LMI-based design formulation is derived so that the closed-loop gains are obtained through a one-step solution to the appropriate set of LMIs.

Theorem 4-1**:** *for t>0 and* $h_i(p)h_j(p) \neq 0$*, The closed-loop fuzzy system in (4-13) is asymptotically stable and the* H_∞ *performance is guaranteed with an attenuation level* γ*, provided that the signal* (d) *is bounded, and the pair* (A_i, C) *is observable, if there exist SPD matrices* P_1, P_2, P_3*, and matrices* H_i, Y_j*, and scalars* γ *and* μ *satisfying the following the LMI constraints (4-14)&(4-15):*

$Minimise\ \gamma, such\ that$:

$$P_1 > 0, \qquad P_2 > 0, \qquad P_3 > 0 \tag{4-14}$$

$$\begin{bmatrix} \Psi_{11} & -B_iY_j & \Psi_{13} & B_iK_{jd} - B_d & 0 & 0 & 0 & X_1 \\ * & -2\mu X_1 & 0 & 0 & \mu I & 0 & 0 & 0 \\ * & * & -2\mu I & 0 & 0 & \mu I & 0 & 0 \\ * & * & * & -2\mu I & 0 & 0 & \mu I & 0 \\ * & * & * & * & \Psi_{55} & 0 & 0 & 0 \\ * & * & * & * & * & \Psi_{66} & P_3 * B_d & 0 \\ * & * & * & * & * & * & -\gamma I & 0 \\ X_1 & * & * & * & * & * & * & -\gamma I \end{bmatrix} < 0 \tag{4-15}$$

where $K_j = Y_j X_1^{-1}$, $\bar{L}_i = P_2^{-1}H_i$, $X_1 = P_1^{-1}$,
$\Psi_{11} = A_iX_1 + (A_iX_1)^T + B_iY_j + (B_iY_j)^T$; $\Psi_{13} = B_iK_{jr} + A_i - A_d$
$\Psi_{55} = P_2A_i + (P_2A_i)^T - H_iC - (H_iC)^T$, $\Psi_{66} = P_3A_d + (P_3A_d)^T$

Proof: From *Theorem 4-1* the tracking performance objective can be presented mathematically as follows:

$$\frac{\|\tilde{x}_a\|_2}{\|d\|_2} \leq \gamma = \frac{1}{\gamma}\int_0^\infty \tilde{x}_a^T\, \tilde{x}_a dt - \gamma \int_0^\infty d^T\, d\ \leq 0 \tag{4-16}$$

Consider the following candidate Lyapunov function for the augmented system (4-13):

$$\upsilon(\tilde{x}_a) = \tilde{x}_a^T\, \bar{P}\, \tilde{x}_a\ \ , where\ \bar{P} > 0$$

To achieve the performance required by (4-16) and the required closed-loop stability of (4-13) the following inequality must then hold (Ding, 2008):

$$\dot{v}(\tilde{x}_a) + \frac{1}{\gamma}\tilde{x}_a^T\,\tilde{x}_a - \gamma d^T d < 0 \tag{4-17}$$

where $\dot{v}(\tilde{x}_a)$ is the time derivative of the candidate Lyapunov function. Using Eq. (4-13), this becomes:

$$\dot{v}(\tilde{x}_a) = \sum_{i=1}^{r}\sum_{j=1}^{r} h_i\,h_j\left\{\tilde{x}_a^T\left(\tilde{A}_{ij}^T\bar{P} + \bar{P}\tilde{A}_{ij}\right)\tilde{x}_a + \tilde{x}_a^T\bar{P}\tilde{N}_{ij}d + d^T\tilde{N}_{ij}^T\bar{P}\tilde{x}_a\right\} \tag{4-18}$$

The inequality (4-17) (in matrix form), after substituting $\dot{v}(\tilde{x}_a)$ from Eq. (4-18), becomes:

$$\sum_{i=1}^{r}\sum_{j=1}^{r} h_i\,h_j\left\{\begin{bmatrix}\tilde{x}_a\\ d\end{bmatrix}^T\begin{bmatrix}\tilde{A}_{ij}^T\bar{P} + \bar{P}\tilde{A}_{ij} + \frac{1}{\gamma}I & \bar{P}\tilde{N}_{ij}\\ \tilde{N}_{ij}^T\bar{P} & -\gamma I\end{bmatrix}\begin{bmatrix}\tilde{x}_a\\ d\end{bmatrix}\right\} < 0 \tag{4-19}$$

Inequality (4-19) implies that the inequality (4-20) must hold:

$$\begin{bmatrix}\tilde{A}_{ij}^T\bar{P} + \bar{P}\tilde{A}_{ij} + \frac{1}{\gamma}I & \bar{P}\tilde{N}_{ij}\\ \tilde{N}_{ij}^T\bar{P} & -\gamma I\end{bmatrix} < 0 \tag{4-20}$$

To be consistent with Eq. (4-13) $\bar{P}$ is structured as follows:

$$\bar{P} = \begin{bmatrix}P_1 & 0 & 0\\ 0 & P_2 & 0\\ 0 & 0 & P_3\end{bmatrix} > 0 \tag{4-21}$$

Then after simple manipulation and using variable change ($H_i = P_2L_i$) the inequality (4-20) can be re-formulated as:

$$\Pi_{ij} = \left[\begin{array}{c|ccc}\Omega_{11} & -P_1B_iK_j & P_1\left(B_iK_{jr} + A_i - A_d\right) & P_1\left(B_iK_{jd} - B_d\right)\\ \hline * & \Omega_{22} & 0 & 0\\ * & * & P_3A_d + (P_3A_d)^T & P_3B_d\\ * & * & * & -\gamma I\end{array}\right] < 0 \tag{4-22}$$

where:

$\Omega_{11} = P_1A_i + (P_1A_i)^T + P_1B_iK_j + \left(P_1B_iK_j\right)^T + \frac{1}{\gamma}I$

$\Omega_{22} = P_2A_i + (P_2A_i)^T - H_iC - (H_iC)^T$

Inequality (4-22) contains several nonlinear terms and the next step is to formulate this as an LMI problem. The single step design formulation of the LMI in (4-22) is proposed to avoid the complexity of separate design steps characterised by repeated iteration to

determine the required gains. Hence, after partitioning the matrix inequality shown in (4-22) Π_{ij} becomes:

$$\Pi_{ij} = \begin{bmatrix} \Pi_{11} & \Pi_{12} \\ * & \Pi_{22} \end{bmatrix} \tag{4-23}$$

where $\Pi_{11} = \Omega_{11}$, $\Pi_{12} = [-P_1 B_i K_j \quad P_1(B_i K_{jr} + A_i - A_d) \quad P_1(B_i K_{jd} - B_d)]$, and Π_{22} is the lower right block of inequality (4-22)

To effect the necessary change of variables, the Congruence Lemma presented in Section 3-2 is required. let: $Q = \text{diagonal}\,(P_1^{-1}, X), and\ X = \text{diagonal}(P_1^{-1}, I, I)$

Then $Q * \Pi_{ij} * Q^T < 0$ is also true and it can be re-written as:

$$\begin{bmatrix} P_1^{-1}\Pi_{11}P_1^{-1} & P_1^{-1}\Pi_{12}X \\ * & X\Pi_{22}X \end{bmatrix} < 0 \tag{4-24}$$

The negativity of the inequality (4-24) imposes the negativity of the nonlinear term $(X\Pi_{22}X)$ which can be rewritten using the following approximation (Xie and de Souza Carlos, 1992, Guerra, Kruszewski, Vermeiren and Tirmant, 2006, Mansouri, Manamanni, Guelton and Djemai, 2008):

$$(X + \mu\Pi_{22}^{-1})^T \Pi_{22}(X + \mu\Pi_{22}^{-1}) \leq 0 \Leftrightarrow X\Pi_{22}\text{X} \leq -2\mu X - \mu^2\Pi_{22}^{-1} \tag{4-25}$$

where μ is a scalar.

By substituting (4-25) into (4-24) and using the Schur complement Theorem, then (4-25) holds if the following inequality holds:

$$\begin{bmatrix} P_1^{-1}\Pi_{11}P_1^{-1} & P_1^{-1}\Pi_{12}X & 0 \\ X\Pi_{12}P_1^{-1} & -2\mu X & \mu I \\ 0 & \mu I & \Pi_{22} \end{bmatrix} < 0 \tag{4-26}$$

After substituting for $\Pi_{11}, \Pi_{12}, \Pi_{21}, \Pi_{22}$ from (4-23) and by simple manipulation, the LMI in (4-15) is obtained. This completes the proof.

4-2-2. Reconfiguration steps and constraints

The observer reconfiguration involves *two* steps. The first, is to identify the post-fault output matrix C_f. The second step is to compute a new observer gain L_{if}. However, the reconfiguration process is constrained by several requirements. The satisfaction of these constraints is governed by the fault scenarios and the allowable computation time.

- The pairs (A_i, C_f) must satisfy the observability condition or at least satisfy the detectability condition which in turn implies the stability of any unobservable mode. Clearly, this constraint depends upon the fault itself and hence it is beyond the capability of the designer since the fault is not known *a priori*.
- Stabilisation of the estimation error via the new gain L_{if}. This is the most important reconfiguration task since the overall closed-loop system performance depends on the estimation performance. Consequently, if the reconfiguration process only requires achieving stabilization, then L_{if} can be computed using the following constraints:

$$P_2 A_i + (P_2 A_i)^T - H_i C - (H_i C)^T < 0 \qquad (4\text{-}27)$$

where the variables are defined in Section 4-2-1. However, observer-based control methods always require that fast estimation error dynamics are assured As a result, the assignment of VS eigenvalues in a specific region of the left half of the complex plane is necessary. However, it is not always possible to handle this constraint due to the reconfiguration time limitation. Moreover, if the detectability condition is satisfied, only a subset of the VS eigenvalues can be assigned.

4-2-3. Simulation results

To illustrate the proposed T-S fuzzy VS design, the tutorial example of the non-linear inverted pendulum with a cart is used here. The cart is linked by a transmission belt which is used to drive the wheel via a DC motor to rotate the pendulum into vertical position in the vertical plane by force control $u_c(t)$ on the cart. The nonlinear inverted pendulum and cart system model presented in Chapter 2 Eq. (2-21), the system parameters are m: The pendulum mass (2kg), $2l$: The pendulum length (1m), M: The cart mass (8kg), $a = \frac{1}{m+M}$. The output matrix is:

$$C = \begin{bmatrix} 1 & 0 & 0 & 0 \\ 0 & 1 & 0 & 0 \\ 0 & 0 & 0 & 1 \end{bmatrix}$$

As stated in Chapter 3, three system operating points are chosen corresponding to the pendulum angular positions $\theta = 0\ and \pm \pi/4$. Due to symmetry, this results in the choice of *two* fuzzy rules in the T-S model. By solving the LMI design constraints given in (4-14) & (4-15), the LMI parameters, and the computed controller and nominal observer gains are: $\mu = 10$ and $\gamma = 3.4774$.

$K_1 = [668.4 \quad 75.78 \quad 195.2 \quad 122.8]$; $K_2 = [1167.8 \quad 134.1 \quad 380.04 \quad 229.4]$

$K_{1r} = [-30.58 \quad -7.29]$; $K_{2r} = [-52.63 \quad -17.11]$

$K_{1d} = [241.65 \quad 18.22 \quad 62.31 \quad 36.30]$; $K_{2d} = [375.03 \quad 43.27 \quad 104.29 \quad 79.80]$

$$L_1 = \begin{bmatrix} 12.90 & 0.0003 & -0.0002 \\ -0.0002 & 7.16 & 1 \\ 78.37 & 0.0001 & -0.0007 \\ -1.72 & 0.0002 & 7.16 \end{bmatrix}; L_2 = \begin{bmatrix} 12.90 & 0.0001 & 0.0003 \\ -0.0001 & 7.16 & 1 \\ 70.49 & -0.0005 & 0.0005 \\ 0.1288 & 0.0002 & 7.16 \end{bmatrix}$$

Two fault scenarios are considered in this Section. In the first, two of the output matrix parameters are changed. The result shows that the time allowed to reconfigure the faulty plant is about $20s$. The parameters of the first fault scenario and the VS gains are:

$$C_f = \begin{bmatrix} 1 & 0 & 0 & 0 \\ 0 & 0.6 & 0 & 0 \\ 0 & 0 & 0 & 0.2 \end{bmatrix}$$

$$L_{1f} = \begin{bmatrix} 12.90 & 0.0002 & -0.0004 \\ -0.0008 & 14.32 & 4.99 \\ 78.39 & 0.0001 & -0.0013 \\ -1.72 & 0.0035 & 35.81 \end{bmatrix}; L_{2f} = \begin{bmatrix} 12.90 & -0.0009 & 0.0006 \\ -0.0004 & 14.32 & 4.99 \\ 70.51 & -0.0002 & 0.0010 \\ 0.1288 & 0.0035 & 35.81 \end{bmatrix}$$

Figure 4-3 a, b, &c illustrate the closed-loop performance before, during and after the sensor fault. It is clear how the VS can continuously generate estimates that reflect the real system behaviour.

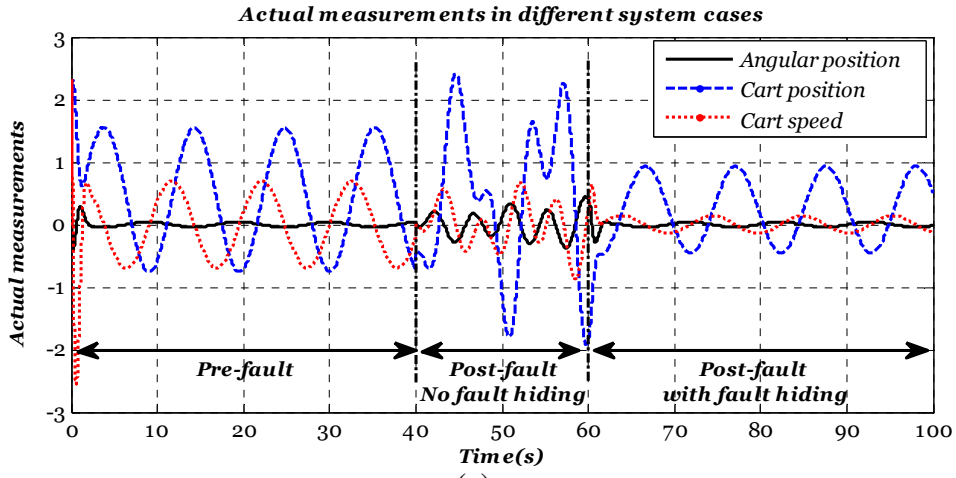

(a)

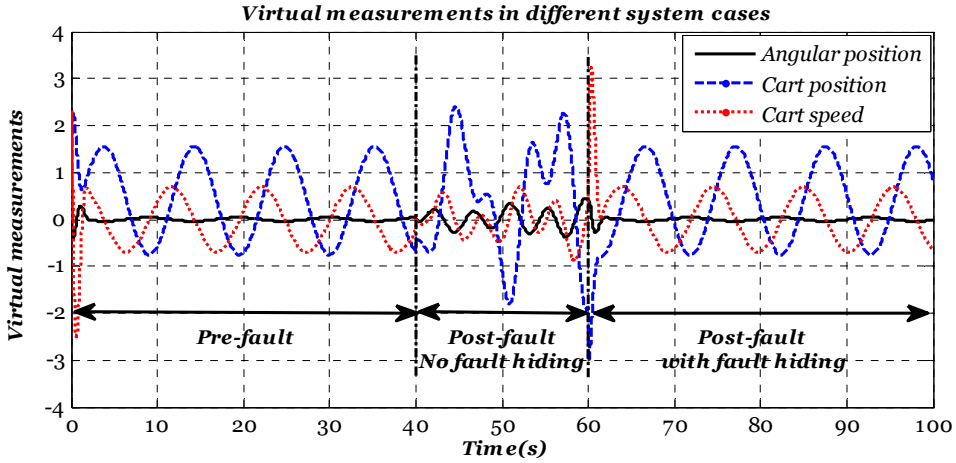

(b)

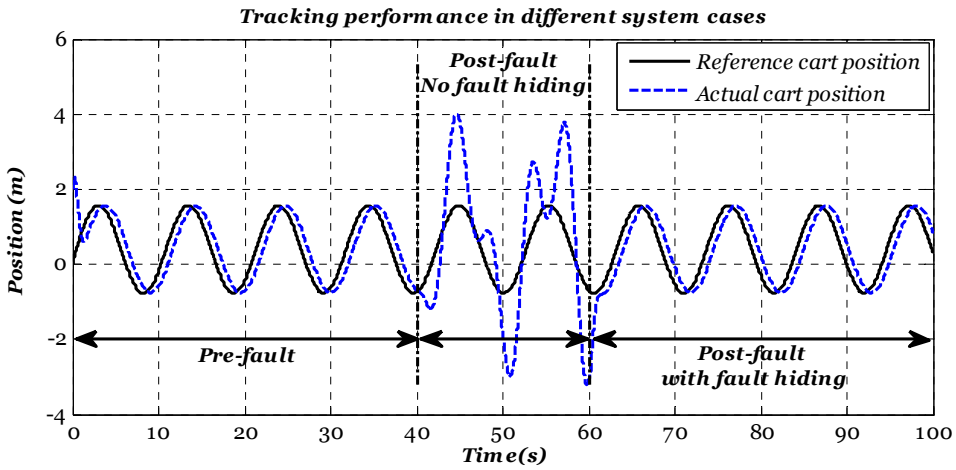

(c)

Figure 4-3: (a) Actual output states, (b) Virtual measurements, and (c) Position tracking performance

The second fault scenario is more severe than the first one. The loss of the cart speed measurement and an attenuation of the cart position measurement are proposed to highlight the fact that the allowable reconfiguring time is a function of the fault scenario. The output matrix and the VS gain in the new fault scenario are computed as:

$$C_f = \begin{bmatrix} 1 & 0 & 0 & 0 \\ 0 & 0.85 & 0 & 0 \\ 0 & 0 & 0 & 0 \end{bmatrix}; L_{1f} = \begin{bmatrix} 12.90 & 0.0006 \\ -0.0007 & 12.90 \\ 78.38 & 0.0003 \\ -1.72 & 61.09 \end{bmatrix}; L_{2f} = \begin{bmatrix} 12.90 & 0.0006 \\ -0.0002 & 12.90 \\ 70.50 & 0.0007 \\ 0.1288 & 61.09 \end{bmatrix}$$

The results for this fault scenario show that the maximum time allowed for reconfiguration is about 5sec.

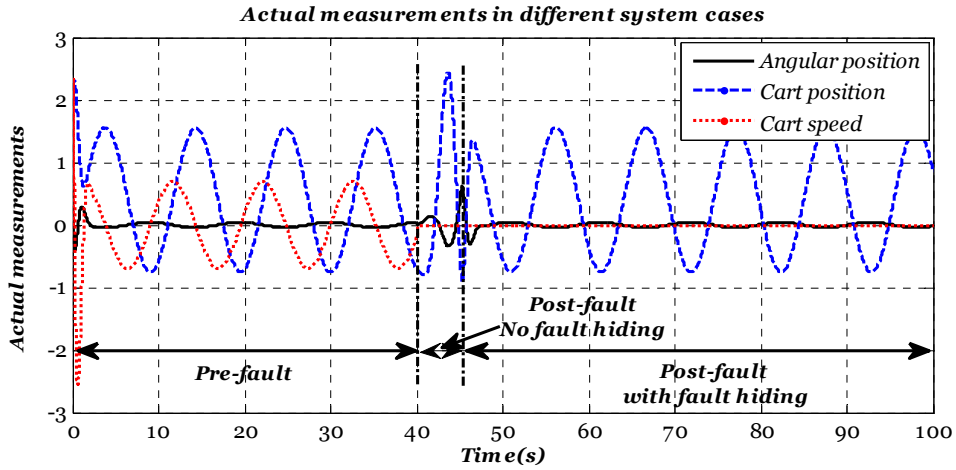

(a)

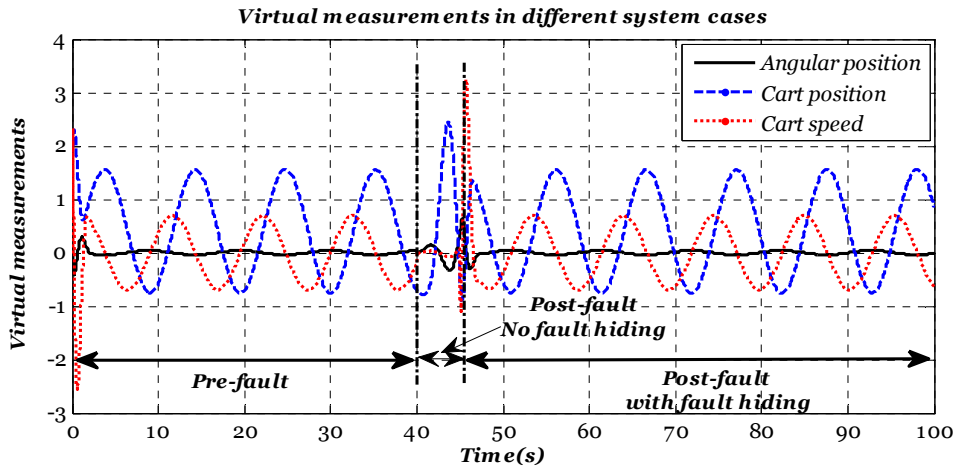

(b)

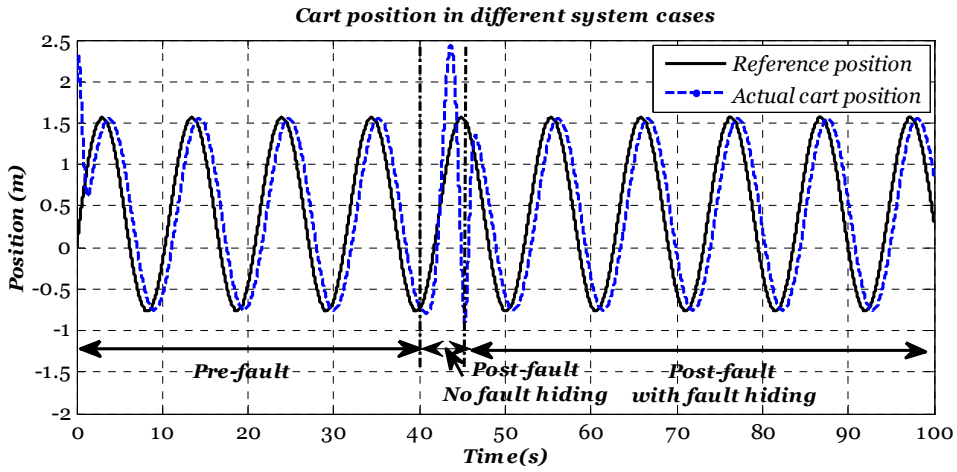

(c)

Figure 4-4: VS simulation results for severe fault. (a) Actual output states, (b) Virtual measurements, and (c) Position tracking performance

From the simulation results the limitations of this method can be summarised as follows:

1. It is clear how the reconfiguration time depends on the fault severity. This fact is highlighted by considering *two* different fault scenarios. In the first instance the time allowed for reconfiguration is $20s$, whereas in the second case severe faults are considered that require very fast reconfiguration times. To avoid a long reconfiguration time, one way to simplify this problem is to pre-compute the VS gains for every probable fault scenario (projection based VS). Hence, following the detection of the fault, a reconfiguration algorithm is used to select the appropriate off-line design.
2. The method relies completely on the robustness of the FDD block. Moreover, a new parameter computation must be performed in an efficient manner to ensure

minimum computation time, especially for critical fault cases (e.g. causing unstable open-loop behaviour after the presence of the fault).

3. The VS approach cannot tolerate the case in which the faulty parameter of the output matrix is continuously varying. However, the only possible solution is to turn the problem into one of a complete loss of measurement provided that the detectability condition is still valid.
4. The use of VS in the T-S fuzzy model framework is limited by the inefficiently handled premise variable sensor fault because the idea of fault hiding is based on the use of estimated signals rather than on actual measurements. In fact this will transfer the control design problem to the unmeasured premise variable case which in turn demands controller robustness against premise variable estimation error. Moreover, during the reconfiguration time required to tolerate the premise variable sensor fault, the T-S model deviates from the model of the system under control and hence the fuzzy blending of the local controllers is no longer suitable for the controlled system.
5. The effect of the initial condition for the VS approach is very significant, especially within the T-S framework since the initial states of the faulty plant cannot be predicted during the insertion of the VS. Hence, the initial estimation error is not guaranteed to satisfy a given bound. This issue is very significant if the T-S fuzzy model is derived based on either local sector nonlinearity or a local approximation approach.

4-3. T-S PMIO based model reference sensor FTTC

AS a consequence of the limitation of the VS approach for sensor FTTC, the PMIO based sensor FTTC is proposed in this Section. Although the proposed strategy simulates the spirit of the VS strategy through maintaining the nominal controller without change, this strategy is an integrated FTC/FDD in which the fault tolerance mechanism is performed online without a reconfiguration time delay. Moreover, the ability of the PMIO to provide simultaneous state and fault estimation signals can be used to gain useful information for fault severity evaluation. Furthermore, the proposed observer takes due care of the unpredictable nature of the fault by augmenting the nominal proportional observer by a multiple integral (PMIO) feedback so that a variety of fault scenarios can be estimated.

Figure 4-5 shows the scheme of the proposed strategy.

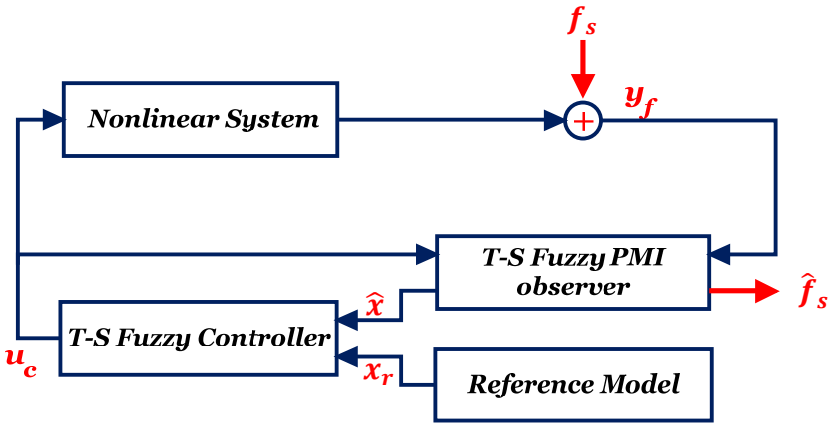

Figure 4-5: PMIO based sensor FTC

4-3-1. The LMI design of the T-S fuzzy PMIO

The aim of this Section is to design a nonlinear observer that has the capability of providing simultaneous state and fault estimates to be used in the advantageous sensor FTTC loop. In the literature, bounded fault signals are typically handled via PIO approaches considering both fault estimation and fault diagnosis (Klinkhieo, 2009). Practically, unbounded fault scenarios are very probable (Gao, Ding and Ma, 2007). However, the combined literature on fault estimation and fault diagnosis rarely deal with the unbounded fault cases.

The work of this Section is motivated by the unpredictable behaviour of the faults affecting a system (e.g. in terms of unknown fault occurrence and unknown fault-induced system time response). The T-S fuzzy PMIO design strategy is presented as a mechanism to provide simultaneous estimation of state and sensor faults to be exploited in an observer-based FTTC system capable of handling cases in which fault signals are unbounded. For this approach to be valid bounds on the q^{th} time derivative of the considered fault must be taken into accounted, where the number of derivatives q is to be chosen by the designer.

In the literature, the PMIO concept is well known for the design of robust observers for linear systems with unknown input disturbances (Guo-Ping, Suo-Ping and Wen-Zhong, 2000, Ibrir, 2004). The development of a PMIO scheme to provide simultaneous state and fault estimates for a linear model of the lateral dynamics of an automobile contaminated by yaw rate and acceleration sensor faults has been proposed by (Gao, Ding and Ma, 2007). An extension of the PMIO design problem applicable to descriptor

systems was proposed by (Koenig, 2005). In this Section a new extension to LMI-based PMIO design is proposed, based on T-S fuzzy inference modelling as follows:

$$\left.\begin{aligned} \dot{x} &= \sum_{i=1}^{r} h_i\big(p(t)\big)\{A_i x(t) + B_i u(t)\} \\ y &= Cx(t) + Df_s \end{aligned}\right\} \tag{4-28}$$

where the variables are already defined below Eq. (4-5), $D \in \mathcal{R}^{l\times k}$ and $f_s \in \mathcal{R}^k$ represents additive sensor faults. Assume that the q^{th} derivative of the sensor fault signal is bounded, then an augmented state system consisting of the original local linear systems state and the q^{th} derivatives of f_s can be constructed.

Let the i^{th} derivate of the sensor fault signal f_s^i be represented by a state variable formulation as follows:

$$\varphi_i = f_s^{q-i} \ \ (i = 1,2,\dots,q) \ ; \ \dot{\varphi}_1 = f_s^q; \dot{\varphi}_2 = \varphi_1; \ \dot{\varphi}_3 = \varphi_2; \dots; \dot{\varphi}_q = \varphi_{q-1}$$

Then the system of Eq. (4-28) when augmented with the sensor fault derivatives becomes:

$$\left.\begin{aligned} \dot{\bar{x}} &= \sum_{i=1}^{r} h_i\big(p(t)\big)\big\{\bar{A}_i\bar{x}(t) + \bar{B}_i u(t) + G f_s^q\big\} \\ y &= \bar{C}\bar{x}(t) \end{aligned}\right\} \tag{4-29}$$

where:

$$\bar{x} = \begin{bmatrix} x^T & \varphi_1^T & \varphi_2^T & \varphi_3^T & \dots. & \varphi_q^T \end{bmatrix}^T \in \mathcal{R}^{\bar{n}} \ ; \bar{A}_i = \begin{bmatrix} A_i & 0 & \dots & 0 & 0 \\ 0 & 0 & \dots & 0 & 0 \\ 0 & I & \dots & 0 & 0 \\ \vdots & \vdots & \ddots & \vdots & \vdots \\ 0 & 0 & \dots & I & 0 \end{bmatrix} \in \mathcal{R}^{\bar{n}\times\bar{n}}$$

$$\bar{B}_i = [B_i^T 0 \ 0 \ \dots 0]^T \quad \in \mathcal{R}^{\bar{n}\times m} \ ; G \ = [0 \ I_k \ 0 \ \dots 0]^T \quad \in \mathcal{R}^{\bar{n}\times k}$$

$$\bar{C} \ = [C \ 0 \ 0 \ \dots D] \quad \in \mathcal{R}^{l*\bar{n}} \ ; \bar{n} = n + kq$$

Hence, the following T-S fuzzy PMIO is proposed to simultaneously estimate the system states and sensor faults:

$$\dot{\hat{\bar{x}}} = \sum_{i=1}^{r} h_i\big(p(t)\big)\{\bar{A}_i\hat{\bar{x}}(t) + \bar{B}_i u(t) + \bar{L}_i(y - \bar{C}\hat{\bar{x}})\} \tag{4-30}$$

where $\hat{\bar{x}} \in \mathcal{R}^{\bar{n}}$ is the estimation of the augmented state vector $\bar{x}$, and $\bar{L}_i = [L_{pi}^T, L_{Ii}^{T1}, .., L_{Ii}^{Tq}]^T \in \mathcal{R}^{\bar{n}*l}$ is the gain to be designed.

Theorem 4-2: *The necessary condition for the T-S fuzzy PMIO given in (4-30) to exist is*

$$rank\begin{bmatrix} A_i & 0 \\ C & D \end{bmatrix} = n + k \tag{4-31}$$

and

$$rank\begin{bmatrix} sI - A_i \\ C \end{bmatrix} = n \quad \forall s \in \mathbb{C} \tag{4-32}$$

Additionally, the PMI observer attenuates the effect of the bounded q^{th} *sensor fault derivative on the augmented estimation error if there exist SPD matrix* $P = P^T > 0$ *and matrices* $\bar{H}_i$ *that minimise* γ_{pmi} *under the following LMI constraints:*

$$\begin{bmatrix} P\bar{A}_i + (P\bar{A}_i)^T - \bar{H}_i\bar{C} - (\bar{H}_i\bar{C})^T & PG & C_p^T \\ G^TP & -\gamma_{pmi} & 0 \\ C_p & 0 & -\gamma_{pmi} \end{bmatrix} \tag{4-33}$$

where the gains of the observer are obtained by:

$$\bar{L}_i = P^{-1}\bar{H}_i \tag{4-34}$$

Proof: Conditions (4-31)&(4-32) follow directly the observability requirements for the states and fault estimates.

The state estimation error dynamic is obtained by subtracting Eq. (4-30) from Eq. (4-28) to yield

$$\dot{e}_x = \sum_{i=1}^{r} h_i\,(p)\{(\bar{A}_i - \bar{L}_i\bar{C})e_x + Gf_s^q\} \tag{4-35}$$

To attenuate the effect of the (f_s^q) on the estimation error and at the same time ensuring system stability, the following inequality must hold (Ding, 2008):

$$\dot{v}(e_x) + \frac{1}{\gamma_{pmi}} e_x^T\, C_p^T C_p e_x - \gamma_{pmi} f_s^{qT} f_s^q < 0 \tag{4-36}$$

where $\dot{v}(e_x)$ is the time derivative of the candidate Lyapunov function ($v(e_x) = e_x^T P e_x$) and C_p matrix is introduced to specify the performance output. Using Eq. (4-35), inequality (4-36) becomes:

$$\begin{aligned} \dot{v}(e_x) = \sum_{i=1}^{r} h_i \Big\{ & e_x^T(\bar{A}_i^T P\ + P\bar{A}_i - P\bar{L}_i\bar{C} - (P\bar{L}_i\bar{C})^T)e_x + \ e_x^T PG f_s^q \\ & + f_s^{qT} G^T P e_x \Big\} \end{aligned} \tag{4-37}$$

The inequality (4-36) (in matrix form) after substituting $\dot{v}(\tilde{x}_a)$ from Eq. (4-37) and using the change of variables $\bar{H}_i = P\bar{L}_i$ becomes:

$$\sum_{i=1}^{r} h_i \left\{ \begin{bmatrix} e_x \\ f_s^q \end{bmatrix}^T \begin{bmatrix} P\bar{A}_i + (P\bar{A}_i)^T - \bar{H}_i\bar{C} - (\bar{H}_i\bar{C})^T + \frac{1}{\gamma_{pmi}} C_p^T C_p & PG \\ G^T P & -\gamma_{pmi} I \end{bmatrix} \begin{bmatrix} e_x \\ f_s^q \end{bmatrix} \right\} \quad (4\text{-}38)$$

< 0

By using the Schur Theorem inequality (4-33) can easily be obtained from inequality (4-38).

4-3-2. The LMI design of T-S PMIO based model reference sensor FTTC

By following the design methodology presented in Section 4-2-1, the augmented system combining the tracking error dynamics, the state estimation error, and the reference model is given by Eq. (4-39) as follows:

$$\dot{\tilde{x}}_a(t) = \sum_{i=1}^{r} \sum_{j=1}^{r} h_i(p) h_j(p) \{ \tilde{A}_{ij} \tilde{x}_a + \tilde{N}_{ij} \tilde{d} \} \quad (4\text{-}39)$$

where:

$$\tilde{A}_{ij} = \begin{bmatrix} A_i + B_i K_j & -B_i [K_j \; 0_{m\times q}] & B_i K_{jr} + A_i - A_d \\ 0 & \bar{A}_i - \bar{L}_i \bar{C} & 0 \\ 0 & 0 & A_r \end{bmatrix}$$

$$\tilde{x}_a = \begin{bmatrix} e_t \\ e_x \\ x_d \end{bmatrix}, \quad \tilde{N}_{ij} = \begin{bmatrix} B_i K_{jd} - B_d & 0 \\ 0 & G \\ B_d & 0 \end{bmatrix}, \tilde{d} = \begin{bmatrix} d \\ f_s^q \end{bmatrix}$$

The objective here is to compute the gains $\bar{L}_i, K_{jr}, K_{jd}, and\ K_j$ such that the effect of the input $\tilde{d}$ in Eq. (4-39) is attenuated below the desired level γ, to ensure robust tracking performance.

Theorem 4-3: *for t>0 and* $h_i(p)h_j(p) \neq 0$, *The closed-loop fuzzy system in (4-39) is asymptotically stable and the* H_∞ *performance is guaranteed with an attenuation level* γ, *provided that the signal* $(\tilde{d})$ *is bounded, if there exist SPD matrices* P_1, P_2, P_3, *and matrices* H_i, Y_j, *and scalar* γ *satisfying the LMI constraints (4-40)&(4-41)* as follows*:*

$Minimise\ \gamma, such\ that$

$$P_1 > 0, \qquad P_2 > 0, \qquad P_3 > 0 \tag{4-40}$$

$$\begin{bmatrix} \Psi_{11} & \Psi_{12} & \Psi_{13} & \Psi_{14} & 0 & 0 & 0 & 0 & 0 & X_1 \\ * & -2\mu\bar{X}_1 & 0 & 0 & 0 & \mu I & 0 & 0 & 0 & 0 \\ * & * & -2\mu I & 0 & 0 & 0 & \mu I & 0 & 0 & 0 \\ * & * & * & -2\mu I & 0 & 0 & 0 & \mu I & 0 & 0 \\ * & * & * & * & -2\mu I & 0 & 0 & 0 & \mu I & 0 \\ * & * & * & * & * & \Psi_{55} & 0 & 0 & P_2 G & 0 \\ * & * & * & * & * & * & \Psi_{66} & P_3 B_d & 0 & 0 \\ * & * & * & * & * & * & * & -\gamma I & 0 & 0 \\ * & * & * & * & * & * & * & * & -\gamma I & 0 \\ X_1 & * & * & * & * & * & * & * & * & -\gamma I \end{bmatrix} < 0 \tag{4-41}$$

where: $K_j = Y_j X_1^{-1}$, $\bar{L}_i = P_2^{-1}\bar{H}_i$, $X_1 = P_1^{-1}$, $\bar{X}_1 = diagonal\ (P_1^{-1}, I_{q\times q})$

$\Psi_{11} = A_i X_1 + (A_i X_1)^T + B_i Y_j + (B_i Y_j)^T$; $\Psi_{12} = [-B_i Y_j \quad 0]$; $\Psi_{13} = B_i K_{jr} + A_i - A_d$

$\Psi_{14} = B_i K_{jd} - B_d$; $\Psi_{55} = P_2\bar{A}_i + (P_2\bar{A}_i)^T - \bar{H}_i\bar{C} - (\bar{H}_i\bar{C})^T$, $\Psi_{66} = P_3 A_d + (P_3 A_d)^T$

Proof: By due care of the augmented fault derivative signals throughout the design formulation, the proof of *Theorem 4-3* follows steps that are similar to those involved in the proof of *Theorem 4-1*. Moreover, the derivation of a more general LMI design of PMIO-based state feedback FTC is presented in Chapter 5 Sections 5-2-1 & 5-2-3. Hence the proof of *Theorem 4-3* is omitted here.

4-3-3. Simulation results

For comparison purposes, the tutorial example of the nonlinear inverted pendulum simulation with a cart (as given in Section 4-2-3) is used once again. It should be noted that the linear local models for this nonlinear system are limited by the rank condition for the PMIO for cart position sensor fault as shown below:

$$A_1 = \begin{bmatrix} 0 & 0 & 1 & 0 \\ 0 & 0 & 0 & 1 \\ 17.29 & 0 & 0 & 0 \\ -1.73 & 0 & 0 & 0 \end{bmatrix} \qquad A_2 = \begin{bmatrix} 0 & 0 & 1 & 0 \\ 0 & 0 & 0 & 1 \\ 9.42 & 0 & 0 & 0 \\ 0.13 & 0 & 0 & 0 \end{bmatrix} \qquad B_1 = \begin{bmatrix} 0 \\ 0 \\ -0.176 \\ 0.117 \end{bmatrix}$$

$$B_2 = \begin{bmatrix} 0 \\ 0 \\ -0.115 \\ 0.108 \end{bmatrix} \qquad C_1 = \begin{bmatrix} 1 & 0 & 0 & 0 \\ 0 & 1 & 0 & 0 \\ 0 & 0 & 0 & 1 \end{bmatrix} \qquad C_2 = \begin{bmatrix} 1 & 0 & 0 & 0 \\ 0 & 1 & 0 & 0 \\ 0 & 0 & 0 & 1 \end{bmatrix}$$

For the cart position sensor fault (2nd measurement), the vector D that appears in (4-28) becomes $[0 \quad 1 \quad 0]^T$ which in turn implies:

$$rank \begin{bmatrix} A_i & 0 \\ C & D \end{bmatrix} < n + k$$

Hence, for this model, the PMIO derived in Section 4-3-1can provide estimates of only the 1st and 3rd sensor faults.

Remark: It is possible to overcome the observability problem of the cart speed sensor fault encountered in this example by transferring the sensor FTC problem to an actuator like fault estimation problem. This can be performed by passing the output signals through a low-pass filter and then defining a new augmented system aggregating the system model and the filter. In doing so, the sensor fault appears as an actuator fault in the augmented model. Section 6-3-1 clearly illustrates this methodology for the sensor fault problem.

Using the inequalities presented in (4-41) and the local system matrices mentioned above, the local controller and observer gains are computed as:

$$\bar{L}_1 = \begin{bmatrix} 6.5130 & -0.0349 & -0.0198 \\ -0.2413 & 1.4891 & -0.0011 \\ 22.4187 & -0.2651 & 0.0180 \\ -1.6845 & 1.0880 & -0.001 \\ 120.223 & -239.734 & 399.969 \\ 13.449 & -108.598 & 28.284 \end{bmatrix} \quad \bar{L}_2 = \begin{bmatrix} 4.8143 & -0.1276 & -0.0015 \\ 0.0417 & 1.4899 & -0.0011 \\ 15.8594 & -0.4966 & 0.0155 \\ -0.6364 & 1.1047 & -0.0010 \\ 42.208 & -240.614 & 399.969 \\ 13.4202 & -108.6 & 28.284 \end{bmatrix}$$

$K_1 = [1295.5 \quad 357.5 \quad 371.1 \quad 309.4]$ $K_2 = [2455 \quad 657.5 \quad 751.4 \quad 586.9]$

$K_{1r} = [129.4 \quad 21.56 \quad 44.89 \quad 9.709]$ $K_{2r} = [506.4 \quad 14.22 \quad 67.34 \quad 100.3]$

$K_{1d} = [-18.498 \quad -8.472]$ $K_{2d} = [-46.974 \quad -5.586]$

$\mu = 20$ and $\gamma = 0.158$.

The results show that the T-S PMIO based approach for FTTC has superior fault tolerance capability compared with the VS approach for FTTC. Furthermore, the argument that the additive fault representation can be considered as a generalised fault representation becomes clear as different sensor fault scenarios are considered.

The results presented are separated into *three* groups considering different sensor fault scenarios. These are: external additive sensor faults, output matrix parameter change faults and loss of measurement faults. The proposed tracking control strategy has the capability to completely tolerate all the sensor fault scenarios efficiently. Moreover, the method can also identify the new parameters of the faulty measurements.

External additive sensor fault: The fault considered is of varying frequency and amplitude and the observer shows the ability to provide excellent simultaneous estimates of system states and the external fault signal. The fault starts at time $t = 10s$, and the fault frequency varies linearly with time. An abrupt amplitude change occurs at $10s$ intervals of simulation time. It should be noted that the VS presented in this

Chapter cannot handle this fault scenario since the identification of the fault is no longer fixed.

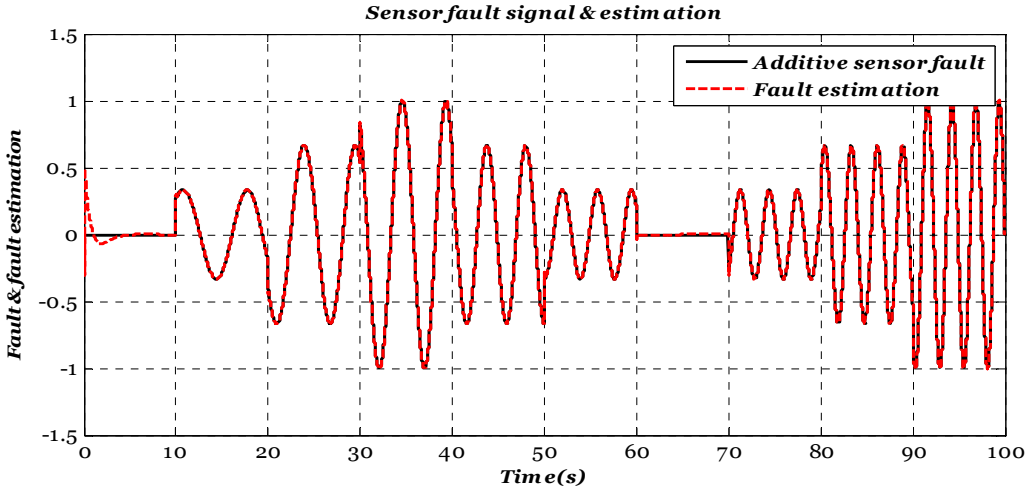

(a)

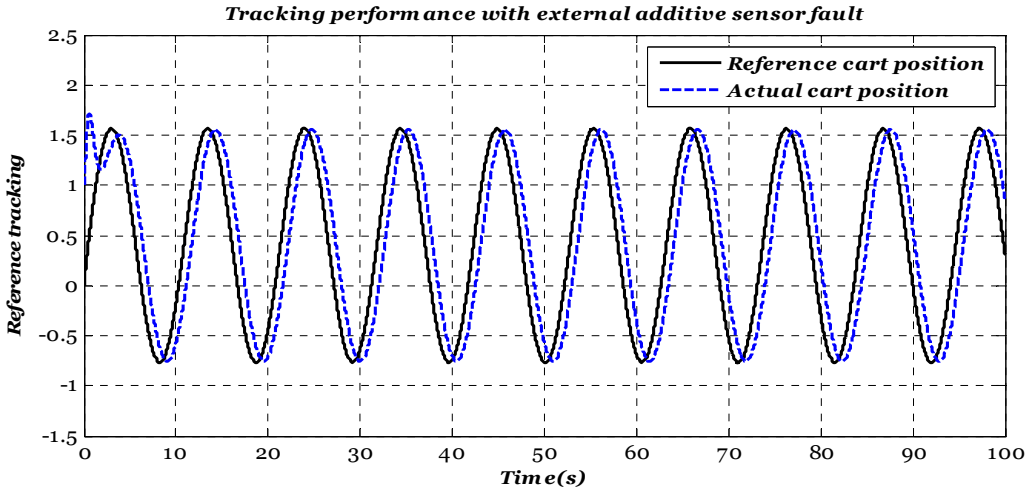

(b)

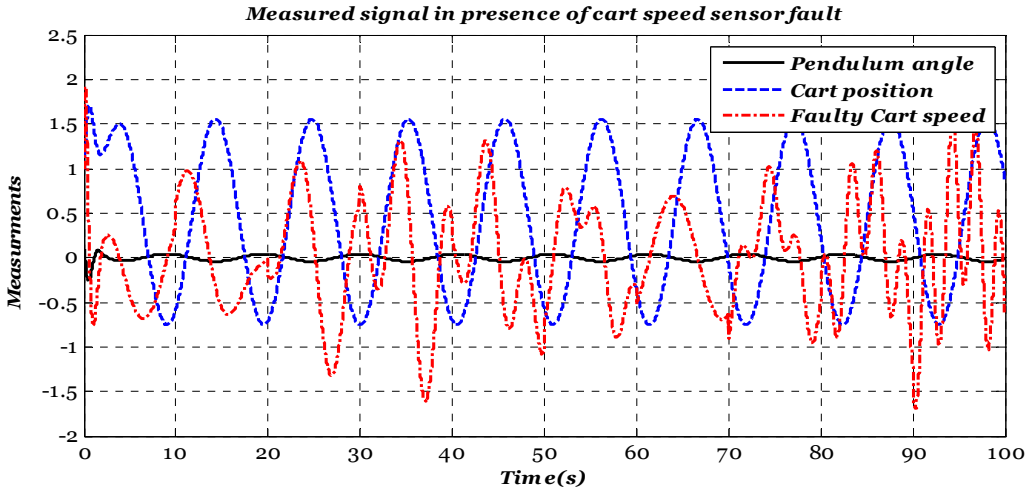

(c)

Figure 4-6: PMIO based additive sensor FTC. (a) Fault estimation, (b) tracking performance, (c) Measurements.

Output matrix parameter change: In this fault scenario the third measurement of the output matrix is changed to (0.3). Hence, the estimated fault in this case represents a scaling of the cart speed (in this case $-0.7 * x_4$) which in turn can be used to identify the new parameter of the faulty measurement as shown in Figure 4-7.

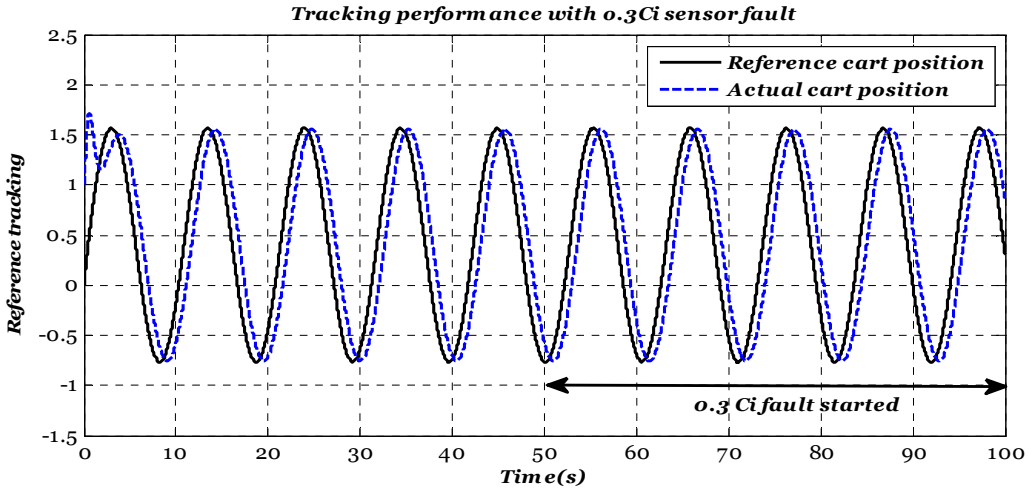

(a)

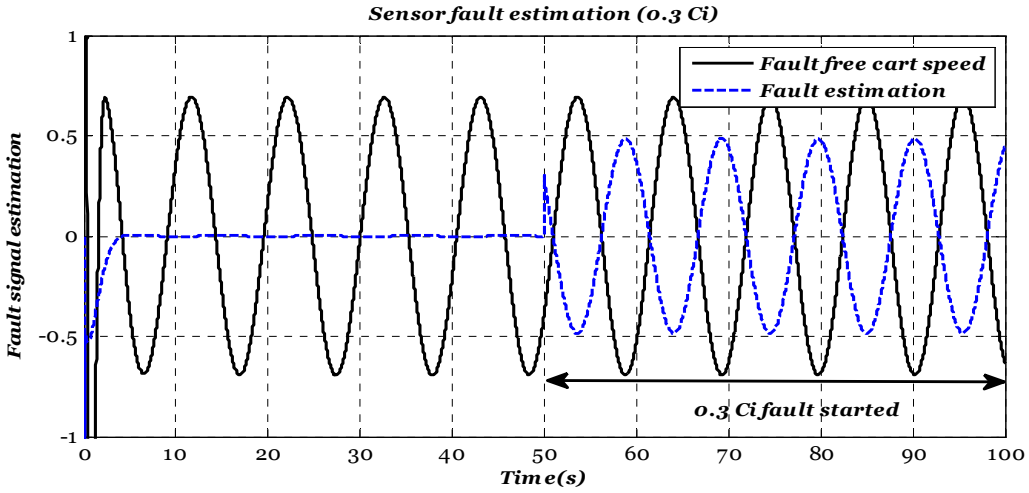

(b)

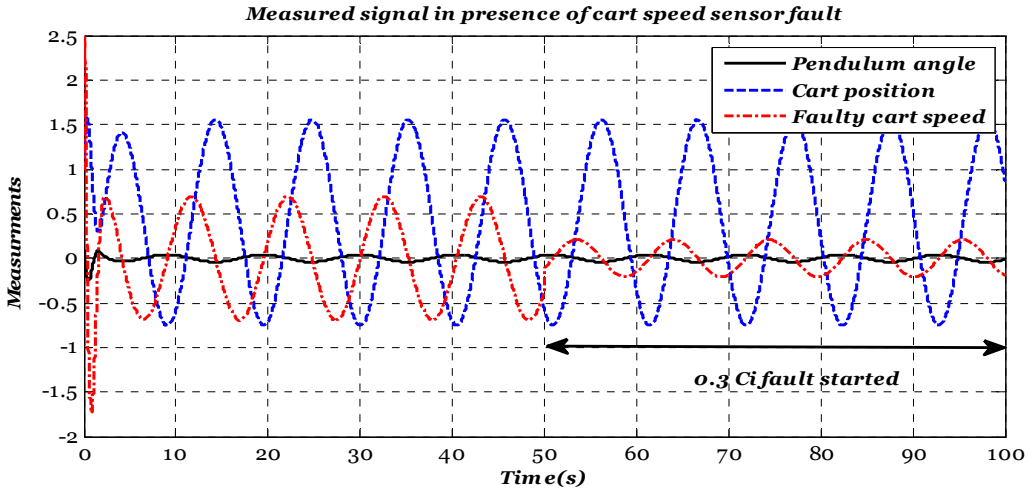

(c)

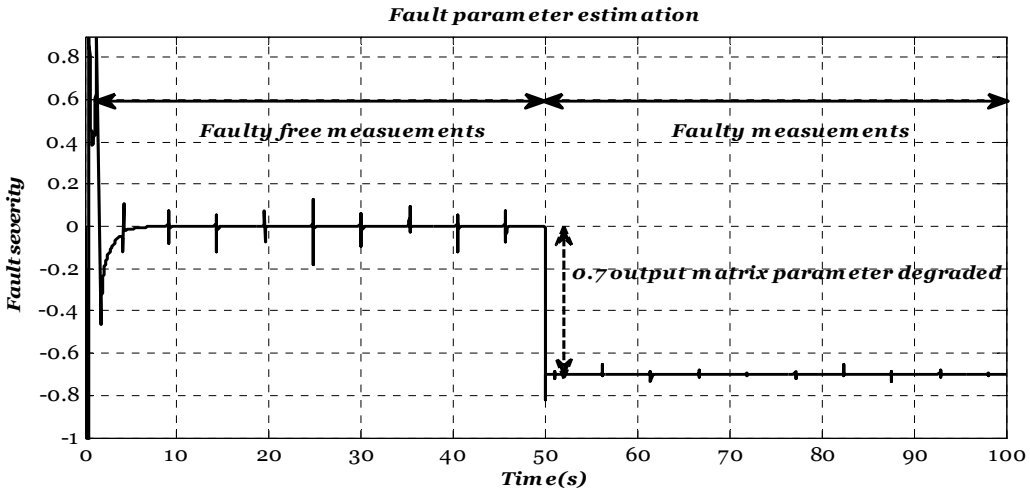

(d)

Figure 4-7: PMIO based output matrix parametric fault FTC. (a) Tracking performance, (b) fault estimation, (c) the measurements, and (d) fault evaluation.

Clearly, the spikes that appear in the fault parameter estimation of Figure 4-7 are due to the zero-crossings since the evaluation is taken directly as a result of division of the fault estimates by the corresponding estimated state. Alternatively, the fault evaluation information can be obtained by tacking the ratio between the measurements and their corresponding state estimates.

Loss of measurements: in this scenario the cart speed measurement is assumed to be completely lost at time $50s$. In this case the estimated fault is equal to ($-x_4$), based on this estimation and the new parameters of the faulty measurement can also be identified as shown below.

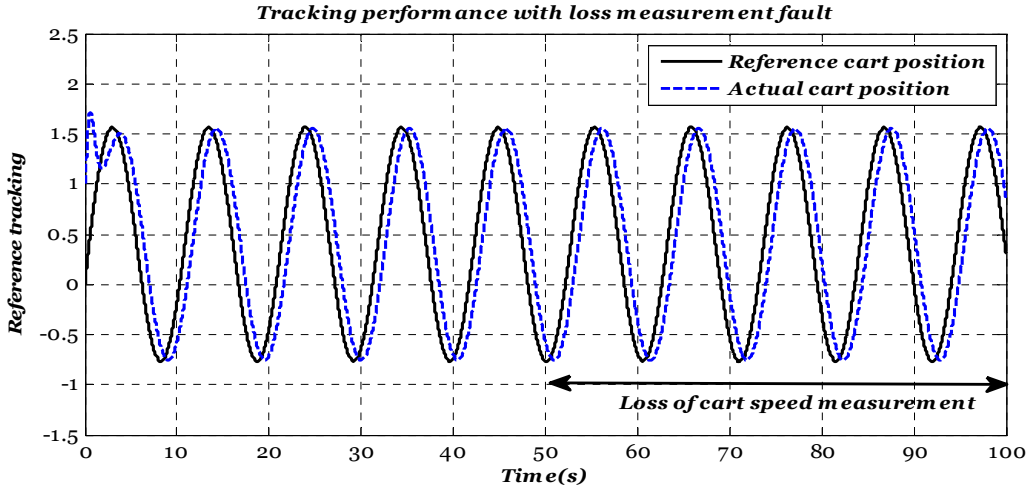

(a)

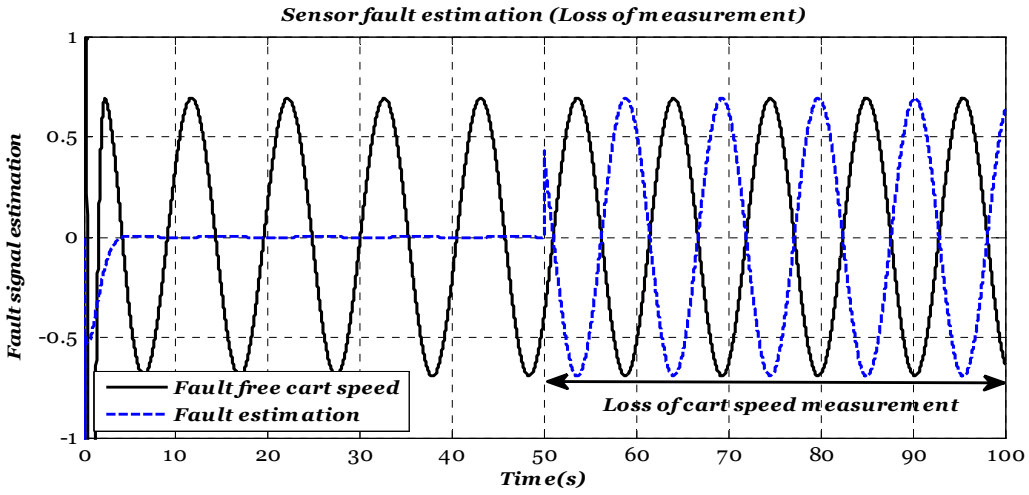

(b)

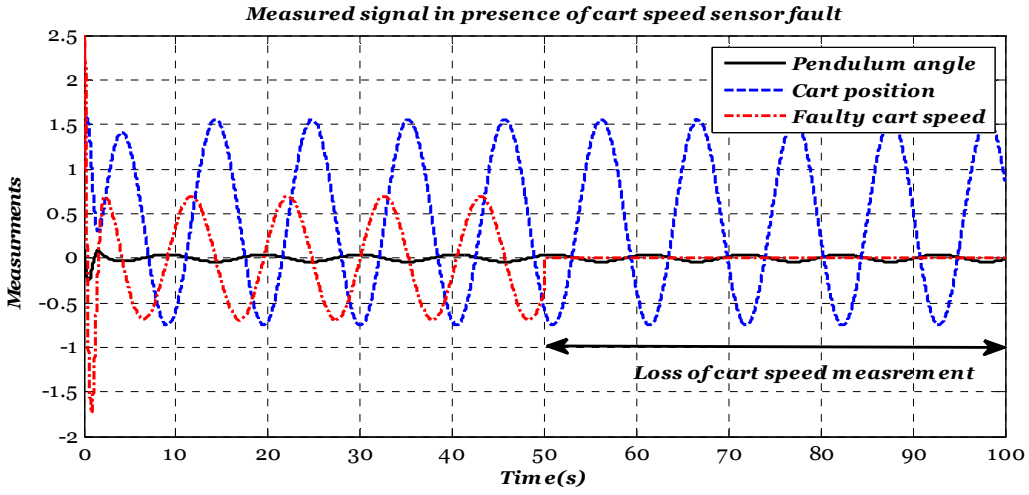

(c)

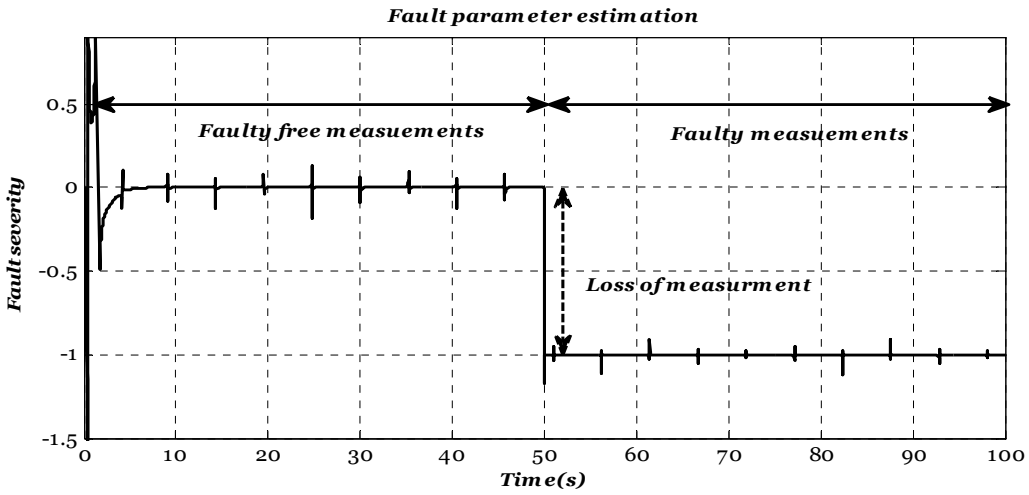

(d)

Figure 4-8: PMIO based loss measurement FTC. (a) Tracking performance, (b) fault estimation, (c) the measurements, and (d) fault evaluation.

It should be noted that:

- The ability to maintain the state estimation without change during the entire range of operation is due to the fact that the PMIO performs *implicit fault estimation and compensation* of sensor fault from the input of the PMIO. This fact is clearly interpreted from the error signal ($y - \bar{C}\hat{\bar{x}}$) which can be rewritten as ($Cx - C\hat{x} - D\hat{f}_s$). Then as long as there is no sensor fault $\hat{f}_s = 0$. Once a sensor fault occurs ($Cx + Df_s - C\hat{x} - D\hat{f}_s$), the fault estimation $\hat{f}_s$ compensates the effect of the fault signal f_s and hence the observer always receives the fault-free error signal.
- The fault evaluation signal can be used to design an integrated static VS based FTC since this information can be utilized to switch between the available redundant measurements. As a result, the proposed strategy provides a superior mechanism for fault tolerance if compared with the static or dynamic VS.
- Although the proposed T-S fuzzy PMIO is designed to be robust against the bounded q^{th} sensor fault time derivative, it is clear that if the system is subjected to an actuator fault alongside the sensor fault this will deteriorate the fault tolerance performance. This is because the proposed T-S PMIO can only passively tolerate the unknown input effects. This in turn needs to assume some constraints on the actuator fault signals (e.g. the actuator fault signal must be bounded).

4-4. T-S PPIO based model reference actuator FTTC

This Section presents a new approach to actuator FTTC for non-linear systems, based on fault estimation and compensation for time-varying faults. The work involves the design of T-S fuzzy PPIO for fault estimation, based on the spirit of the fast *adaptive fault estimation strategy (Zhang, Jiang and Cocquempot, 2008)*, to be used in the framework of T-S fuzzy observer-based FTTC. Although the investigation presented in Chapter 3 states that the nominal controller has some inherent capability to tolerate some bounded actuator faults, the real challenges arise when considering more severe parametric and/or additive actuator fault scenarios. Moreover, the proposed strategy exploits the use of the model reference framework to govern the closed-loop performance.

Suppose the T-S fuzzy model considered in this Chapter, now including the actuator fault f_a, is given as follows:

$$\left.\begin{aligned} \dot{x}_f &= \sum_{i=1}^{r} h_i(p)\{A_i x_f + B_i(u_f + f_a)\} \\ y &= C\, x_f \end{aligned}\right\} \tag{4-42}$$

The control objective is to force the nonlinear plant state in both faulty and healthy cases to follow the states of the reference model given in Eq. (4-6). To achieve this objective the following fuzzy controller is proposed:

$$u_f = \sum_{i=1}^{r} h_i(p)\{K_i(\hat{x}_f - x_d) + K_{i2}x_d + K_{i3}d - \hat{f}_a\} \tag{4-43}$$

where $\hat{x}_f$ is the estimate of the faulty state.

Subtracting the reference model given in Eq. (4-6) from Eq. (4-42) and substituting for u_f from Eq. (4-43) the dynamics of the tracking error ($e_t = x_f - x_d$) are given by:

$$\begin{aligned} \dot{e}_t = \sum_{i=1}^{r}\sum_{j=1}^{r} h_i(p)h_j(p)\{&(A_i + B_iK_j)e_t - B_iK_je_x \\ &+ (B_iK_{j2} + A_i - A_d)x_d + (B_iK_{j3} - B_d)d + B_ie_f\} \end{aligned} \tag{4-44}$$

where e_x and e_f are the state and fault estimation errors. It can clearly be seen from Eq. (4-43) that the performance of the proposed control strategy is highly related to the accuracy of the simultaneous estimation of both the system state and the actuator fault signal. It is also of interest to consider "fast fault" scenario cases for which it can be assumed that the first time derivative of each fault signal is bounded. Therefore, this strategy involves the design of a fuzzy PPIO-based fast fault estimator where the observer is designed to estimate the system state and fault signal.

Assuming that the time derivative of the fault ($\dot{f}_a$) is bounded, then the following fuzzy observer is proposed to simultaneously estimate the system states and actuator fault signal:

$$\left.\begin{aligned} \dot{\hat{x}}_f &= \sum_{i=1}^{r} h_i(p)\{A_i\hat{x}_f + B_i(u_f + \hat{f}_a) + L_i(y - C\hat{x}_f)\} \\ \dot{\hat{f}}_a(t) &= \sum_{i=1}^{r} h_i(p)F_iC(\dot{e}_x + e_x) \end{aligned}\right\} \tag{4-45}$$

where $\hat{x}_f \in \mathcal{R}^n$ is the estimate of the state vector x_f, $L_i \in \mathcal{R}^{n\times l}$ and $F_i \in \mathcal{R}^{m\times l}$ are the observer gains to be designed and e_x is the state estimation error defined as:

$$e_x = x_f - \hat{x}_f \tag{4-46}$$

The state estimation error dynamics are given by:

$$\dot{e}_x = \sum_{i=1}^{r} h_i(p)\{(A_i - L_i C)e_x + B_i e_f\} \tag{4-47}$$

where e_f is the fault estimation error defined as follows:

$$e_f = f_a - \hat{f}_a \tag{4-48}$$

From Eqs. (4-9) & (4-11) the fault estimation error dynamics can be written as:

$$\dot{e}_f = \sum_{i=1}^{r}\sum_{j=1}^{r} h_i(p)h_j(p)\{\dot{f}_a - F_i C(A_j - L_j C + I)e_x - F_i C B_j e_f\} \tag{4-49}$$

In Eq. (4-49) the first time derivative of the fault is considered as a bounded exogenous input signal that affects the estimation dynamics. Using Eq. (4-6), (4-44), (4-47) & (4-49), the augmented system takes the form:

$$\dot{\tilde{x}}_a(t) = \sum_{i=1}^{r}\sum_{j=1}^{r} h_i(p)h_j(p)\{\tilde{A}_{ij}\tilde{x}_a + \widetilde{N}_{ij}\tilde{z}\} \tag{4-50}$$

where:

$$\tilde{A}_{ij} = \begin{bmatrix} A_i + B_i K_j & -B_i K_j & B_i \\ 0 & A_i - L_i C & B_i \\ 0 & -F_i C(A_j - L_j C + I) & -F_i C B_j \end{bmatrix}; \tilde{x}_a = \begin{bmatrix} e_t \\ e_x \\ e_f \end{bmatrix}$$

$$\tilde{z} = \begin{bmatrix} x_d \\ d \\ \dot{f} \end{bmatrix}; \ \widetilde{N}_{ij} = \begin{bmatrix} B_i K_{j2} + A_i - A_d & B_i K_{j3} - B_d & 0 \\ 0 & 0 & 0 \\ 0 & 0 & I \end{bmatrix}$$

The objective here is to compute the gains $L_i, F_i, and\ K_i$ such that the input $\tilde{z}$ in (4-50) is attenuated below the desired level $\bar{\gamma}$, to ensure robust tracking performance. The LMI design formulation is derived so that the design gains are obtained through a one-step solution to the set of LMIs.

Theorem 4-4: *for t>0 and* $h_i(p)h_j(p) \neq 0$, *The closed-loop fuzzy system in (4-50) is asymptotically stable and the* H_∞ *performance is guaranteed with an attenuation level* $\bar{\gamma}$, *Provided that the signal* $(\tilde{z})$ *is bounded, and* $rank(CB_i) = m$, *if there exist SPD matrices* P_1, P_2, *and matrices* H_i, Y_j, F_i, *and a scalar* μ *satisfying the following LMI constraints (4-51), (4-52), and (4-53):*

$Minimise\ (\bar{\gamma} + \tau)\ such\ that$:

$$P_1 > 0, \qquad P_2 > 0 \tag{4-51}$$

$$\begin{bmatrix} \tau I & B_i^T P_2 - F_i C \\ * & \tau I \end{bmatrix} > 0 \tag{4-52}$$

$$\begin{bmatrix}
\Psi_{11} & -B_i Y_j & \Psi_{13} & B_i & \Psi_{14} & 0 \\
* & -2\mu X_1 & 0 & 0 & 0 & 0 \\
* & * & -2\mu I & 0 & 0 & 0 \\
* & * & * & -2\mu I & 0 & 0 \\
* & * & * & * & -2\mu I & 0 \\
* & * & * & * & * & -2\mu I \\
* & * & * & * & * & * \\
* & * & * & * & * & * \\
* & * & * & * & * & * \\
* & * & * & * & * & * \\
* & * & * & * & * & * \\
X_1 & * & * & * & * & *
\end{bmatrix}$$

$$\begin{bmatrix}
0 & 0 & 0 & 0 & 0 & X_1 \\
\mu I & 0 & 0 & 0 & 0 & 0 \\
0 & \mu I & 0 & 0 & 0 & 0 \\
0 & 0 & \mu I & 0 & 0 & 0 \\
0 & 0 & 0 & \mu I & 0 & 0 \\
0 & 0 & 0 & 0 & \mu I & 0 \\
\Psi_{77} & \Psi_{78} & 0 & 0 & 0 & 0 \\
* & \Psi_{88} & 0 & 0 & I & 0 \\
* & * & -\bar{\gamma} I & 0 & 0 & 0 \\
* & * & * & -\bar{\gamma} I & 0 & 0 \\
* & * & * & * & -\bar{\gamma} I & 0 \\
* & * & * & * & * & -w_1^{-1}
\end{bmatrix} < 0 \tag{4-53}$$

$K_j = Y_j X_1^{-1}, L_i = P_2^{-1} H_i, \gamma = \sqrt{\bar{\gamma}}, X_1 = P_1^{-1}, \Psi_{11} = A_i X_1 + (A_i X_1)^T + B_i Y_j + \left(B_i Y_j\right)^T$

$\Psi_{13} = B_i K_{j2} + A_i - A_d, \Psi_{14} = B_i K_{j3} - B_d, \Psi_{77} = P_2 A_i + (P_2 A_i)^T - H_i C - (H_i C)^T$

$\Psi_{88} = -\left(B_i^T P_2 B_j + \left(B_i^T P_2 B_j\right)^T\right) + w_3, \Psi_{78} = (B_i^T H_j C - B_i^T P_2 A_j)^T$

Proof: From *Theorem 4-4* the tracking performance objective can be presented mathematically as follows (Chen, Lee and Chang, 1996, Tseng, Chen and Uang, 2001, Mansouri et al., 2009):

$$\int_0^\infty \tilde{x}_a^T \overline{W}\, \tilde{x}_a \, dt - \gamma^2 \int_0^\infty \tilde{z}^T \tilde{z} \leq 0 \tag{4-54}$$

where $\overline{W} = diagonal\ (w_1, 0, w_3)$.

Consider the following candidate Lyapunov function for the augmented system (4-50):

$$v(\tilde{x}_a) = \tilde{x}_a^T \, \bar{P} \, \tilde{x}_a \;\; , where \; \bar{P} > 0$$

To achieve the performance required by (4-54) and the required closed-loop stability of (4-50) the following inequality must hold:

$$\dot{v}(\tilde{x}_a) + \tilde{x}_a^T \bar{W} \, \tilde{x}_a - \gamma^2 \tilde{z}^T \tilde{z} < 0 \tag{4-55}$$

where $\dot{v}(\tilde{x}_a)$ is the time derivative of the candidate Lyapunov function. Using Eq. (4-50), this becomes:

$$\dot{v}(\tilde{x}_a) = \sum_{i=1}^{r} \sum_{j=1}^{r} h_i \, h_j \left\{ \tilde{x}_a^T \left(\tilde{A}_{ij}^T \bar{P} \; + \bar{P} \tilde{A}_{ij} \right) \tilde{x}_a + \; \tilde{x}_a^T \bar{P} \tilde{N}_{ij} \tilde{z} + \tilde{z}^T \tilde{N}_{ij}^T \bar{P} \tilde{x}_a \right\} \tag{4-56}$$

The inequality (56) (represented in matrix form) after substituting $\dot{v}(\tilde{x}_a)$ from Eq. (4-56) becomes:

$$\sum_{i=1}^{r} \sum_{j=1}^{r} h_i \, h_j \left\{ \begin{bmatrix} \tilde{x}_a \\ \tilde{z} \end{bmatrix}^T \begin{bmatrix} \tilde{A}_{ij}^T \bar{P} \; + \bar{P} \tilde{A}_{ij} + \bar{W} & \bar{P} \tilde{N}_{ij} \\ \tilde{N}_{ij}^T \bar{P} & -\gamma^2 I \end{bmatrix} \begin{bmatrix} \tilde{x}_a \\ \tilde{z} \end{bmatrix} \right\} < 0 \tag{4-57}$$

Inequality (4-57) satisfied if condition (4-58) hold:

$$\begin{bmatrix} \tilde{A}_{ij}^T \bar{P} \; + \bar{P} \tilde{A}_{ij} + \bar{W} & \bar{P} \tilde{N}_{ij} \\ \tilde{N}_{ij}^T \bar{P} & -\gamma^2 I \end{bmatrix} < 0 \tag{4-58}$$

To be consistent with the system model of Eq. (4-50) $\bar{P}$ is structured as follows:

$$\bar{P} = \begin{bmatrix} P_1 & 0 & 0 \\ 0 & P_2 & 0 \\ 0 & 0 & I \end{bmatrix} > 0 \tag{4-59}$$

Then after simple manipulation and using the following equality:

$$F_i C = B_i^T P_2 \tag{4-60}$$

Hence, the inequality (4-58) can be re-formulated as:

$$\Pi_{ij} = \left[\begin{array}{c|cccc} \Omega_{11} & -P_1 B_i K_j & P_1 B_i & \Omega_{14} & P_1 (B_i K_{j3} - B_d) & 0 \\ \hline * & \Omega_{22} & \Omega_{23} & 0 & 0 & 0 \\ * & * & \Omega_{33} & 0 & 0 & I \\ * & * & * & -\gamma^2 I & 0 & 0 \\ * & * & * & * & -\gamma^2 I & 0 \\ * & * & * & * & * & -\gamma^2 I \end{array}\right] < 0 \tag{4-61}$$

where:

$$\Omega_{11} = P_1 A_i + (P_1 A_i)^T + P_1 B_i K_j + \left(P_1 B_i K_j\right)^T + w_1$$
$$\Omega_{22} = P_2 A_i + (P_2 A_i)^T - H_i C - (H_i C)^T,$$
$$\Omega_{33} = -\left(B_i^T P_2 B_j + (B_i^T P_2 B_j)^T\right) + w_3$$
$$\Omega_{23} = (B_i^T H_j C - B_i^T P_2 A_j)^T$$
$$\Omega_{14} = P_1\left(B_i K_{j2} + A_i - A_d\right)$$

The matrix inequality (4-61) contains several nonlinear terms and the next step is to re-formulate this as an LMI. The single step design formulation of the LMI in (4-61) can easily be obtained using the procedure presented in Section 4-2-1.

The equality constraints given in (4-60) add conservatism to the design problem which may be reduced through an approximation via a minimization problem. Using the strategy proposed by (Corless and Tu, 1998, Zhang, Jiang and Cocquempot, 2008):

$$\begin{gathered} Minimise\ \tau \\ \begin{bmatrix} \tau I & B_i^T P_2 - F_i C \\ * & \tau I \end{bmatrix} > 0 \end{gathered} \tag{4-62}$$

This completes the proof.

4-4-1. Simulation results

The nonlinear inverted pendulum model and its local approximation T-S fuzzy model is used here with friction force affecting the system as a type of actuator fault.

By using $\mu = 10$, $w_1 = 10^{-3} * \text{diagonal}\,(37, 11, 1, 1)$, $w_3 = 10$ and solving the optimization design problem in Theorem 1, the minimum attenuation value $\gamma = 2.2361$, the following are computed:

$k_1 = [801.6 \quad 154.1 \quad 231.0 \quad 162.6]$; $k_1 = [950.3 \quad 181.4 \quad 282.3 \quad 194.4]$

$k_{21} = [290.8 \quad 19.6 \quad 46.4 \quad 11.8]$; $k_{22} = [376.1 \quad 29.4 \quad 74.4 \quad 17.8]$

$k_{31} = [-3.8 \quad -15.7]$; $k_{32} = [-5.9 \quad -23.5]$

$F_1 = [34.8 \quad -177.0 \quad 991.3]$; $F_2 = [5.5 \quad -166.3 \quad 914.2]$

$$L_1 = \begin{bmatrix} 65.2 & 5.5 & 0.3 \\ -0.2 & 0.9 & 0.8 \\ 791.0 & 69.8 & 14.5 \\ -2.9 & -0.1 & 1.0 \end{bmatrix}; L_2 = \begin{bmatrix} 58.2 & 5.2 & 0.06 \\ -0.1 & 0.9 & 0.8 \\ 698.7 & 64.7 & 11.3 \\ -1.3 & -0.04 & 0.7 \end{bmatrix}$$

Figure 4-9 shows the simulation signals illustrating the performance of the proposed strategy applied to the system affected by the bearing friction (causing uncertainty). The

observer provides good estimation of the friction force. Moreover, the simulation signals show how the proposed control strategy can also passively tolerate the effect of the friction on the tracking performance.

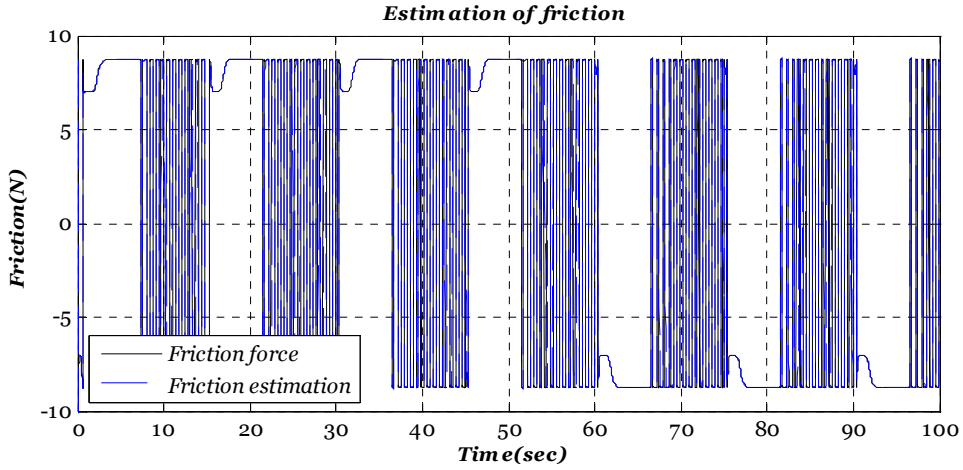

(a)

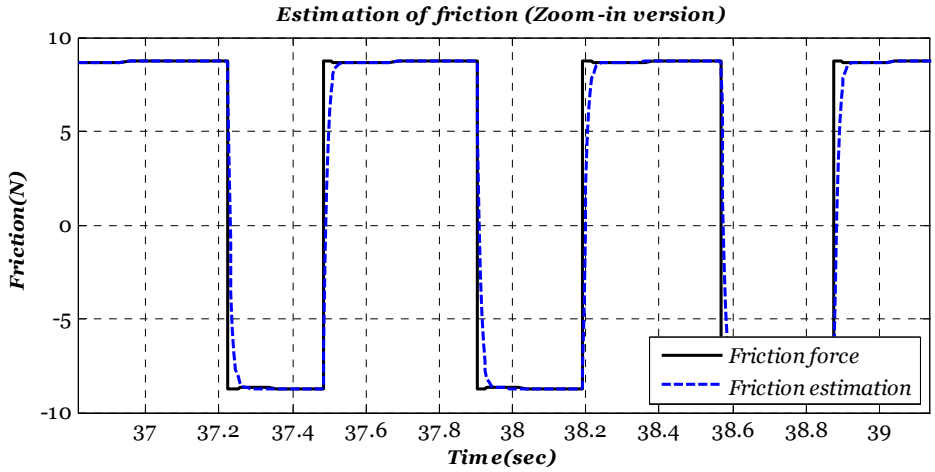

(b)

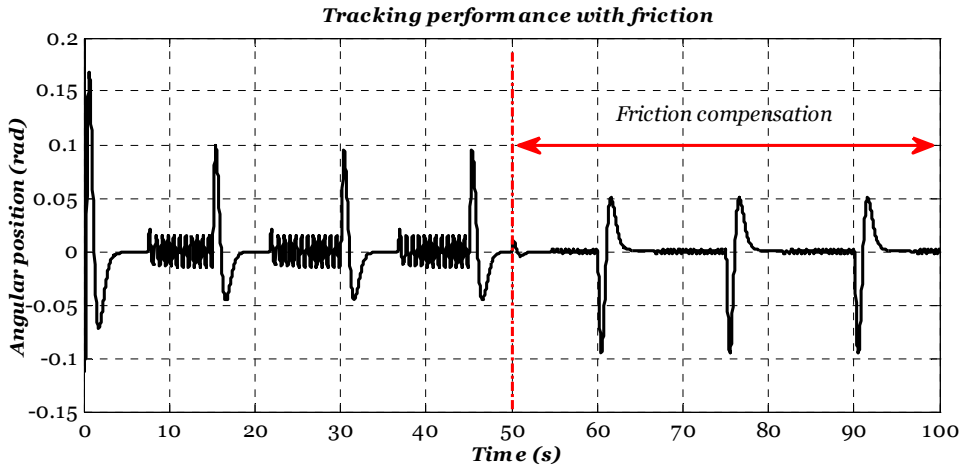

(c)

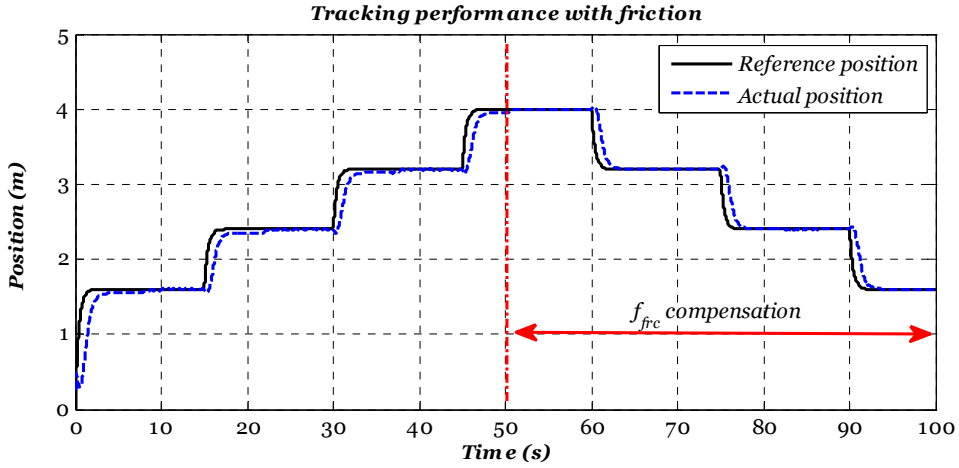

(d)

Figure 4-9: Results for friction tolerant control. (a) Fault estimation, (b) zoomed fault estimation, (c) pendulum angular position, (d) tracking performance.

It should be noted that the estimation accuracy shown in Figure 4-9 a & b is obtained via the proposed T-S PPIO provided that there is no sensor faults that affects the system simultaneously with the actuator fault (the friction). This is because the sensor fault directly affects the error signal that fed to the PPIO input. Hence the actuator fault estimate is vastly deteriorated by any sensor faults (see Eq. (4-45)).

Figure 4-10 shows the case for simulation signals when friction and a parametric fault $(0.25B)$ signal simultaneously affect the system. The results also show how the proposed control strategy can passively tolerate the effects of friction and parametric faults without compensation with performance degradation. However, the use of fault compensation recovers the fault-free tracking performance.

Figure 4-11 shows the simulation signals resulting from simultaneously acting friction, an additive fault, and a parametric fault. Although the system remains stable for this severe fault scenario, the tracking performance is degraded by this fault and hence the estimation of this combined fault has been used to compensate the effect of the fault. Results show how the proposed control strategy can actively tolerate the effects of this combined fault scenario.

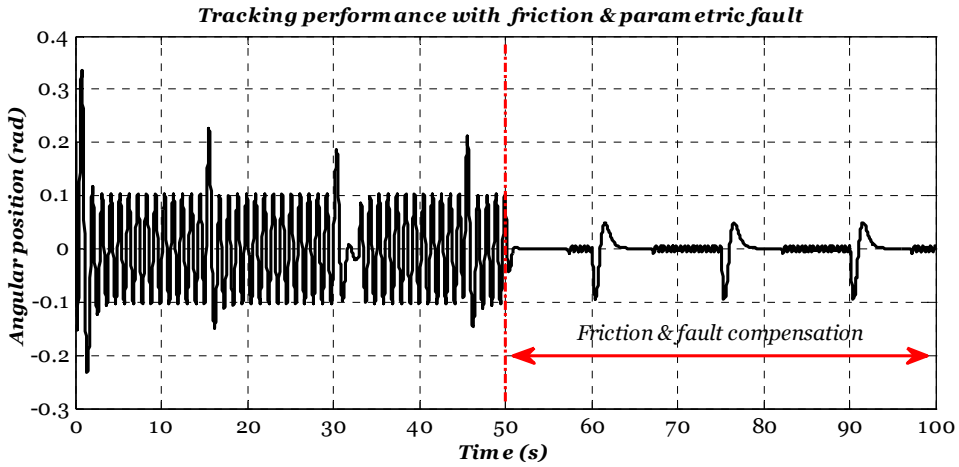

(a)

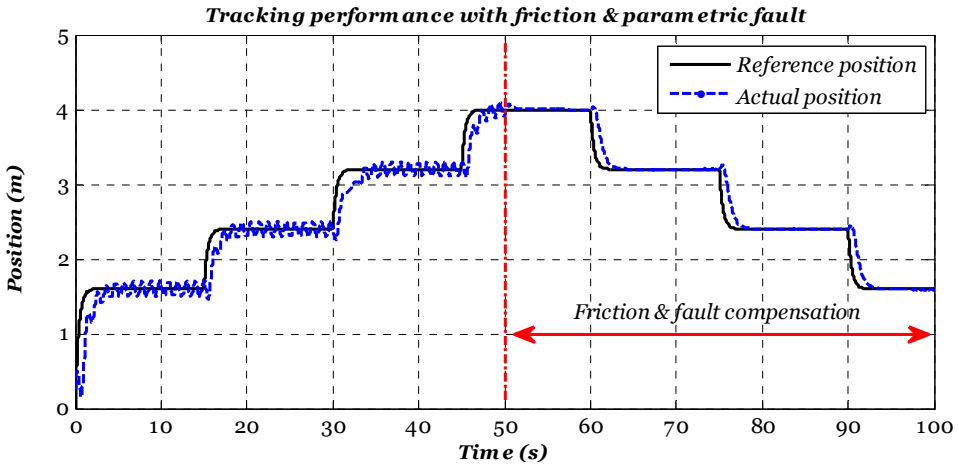

(b)

Figure 4-10: Friction and parametric FTC: (a) Pendulum angular position and (b) tracking performance

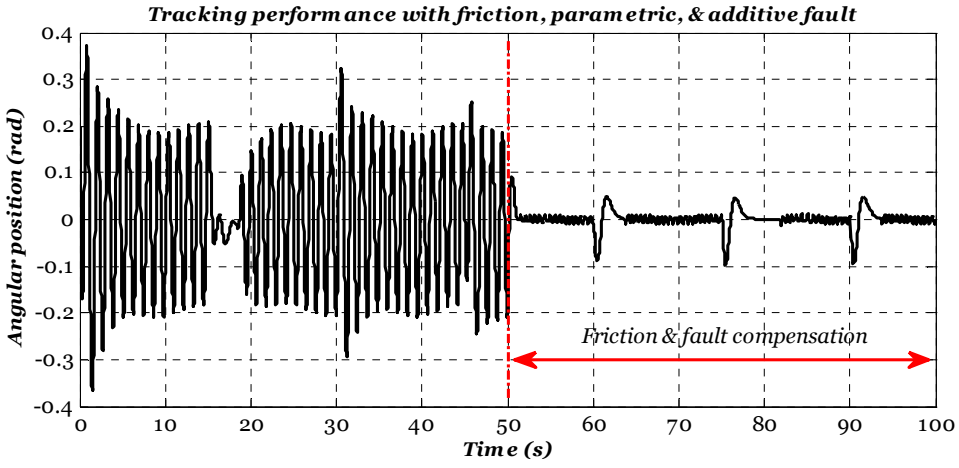

(a)

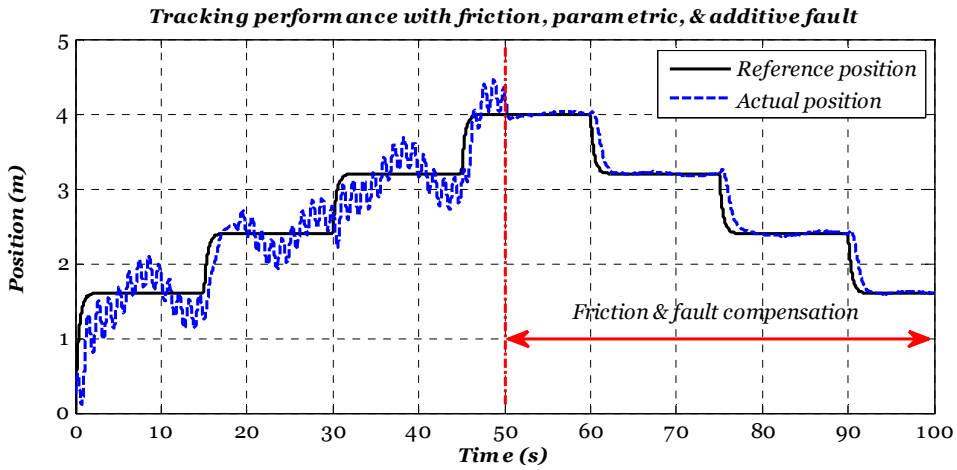

(b)

Figure 4-11: Friction, parametric & additive FTC: (a) Pendulum angular position, and (b) tracking performance.

4-5. Conclusion

In this Chapter, three new FTTC design strategies based on LRMFC are described. These are (i) integrated T-S fuzzy observer/VS based sensor FTTC, (ii) new T-S fuzzy PMIO based sensor FTTC, and (iii) new T-S fuzzy PPIO based actuator FTTC. The proposed methods have the capability to: (a) tolerate the effect of separate actuator and sensor faults within a tracking framework, (b) estimate and compensate for various actuator and sensor fault scenarios, and (c) minimise the reliance on an FDD unit as much as possible.

The common limitation of the proposed strategy is that they lack the ability to tolerate simultaneous actuator and sensor faults. This limitation is clearly highlighted in Sections 4-3-3 & 4-4-1. In fact, the occurrence of simultaneous actuator and sensor faults is practically probable, although this scenario represents a real challenge within the AFTC framework and is the topic of Chapters 5 & 6.

Chapter 5 : Simultaneous actuator and sensor T-S fuzzy FTTC for nonlinear systems

5-1. Introduction

This Chapter focuses on the presentation of *two* novel AFTC architectures for nonlinear systems. The work proposes the use of an estimation and compensation for simultaneous actuator and sensor faults, making use of the T-S fuzzy inference modelling framework. Although simultaneous actuator and sensor fault occurrence is practically probable, this challenging case has not been considered in the FTC literature. This results form a trade-off between estimation accuracy and the effect of simultaneous faults on each other. In the FTC literature, the PFTC approach is usually adopted because this approach does not require the estimation of fault signals (Xuejing and Fen, 2009, Liang, Chang and Wang, 2011). As a consequence of this PFTC limitation (see Section 1-3 for further explanation) an alternative approach is developed in this Chapter using an AFTC strategy incorporating an extension to the PMIO estimation, based on state feedback control. Then extension is developed (within the T-S fuzzy framework) in order to enhance the estimation robustness against the alternative fault, considering the simultaneous actuator and sensor fault scenario. The main contributions of this Chapter can be summarized as:

1. The use of the estimation and compensation concept to enhance the robustness of the T-S fuzzy PMIO against the simultaneous actuator and sensor faults.
2. Proposal of a new FTC architecture for nonlinear systems affected by simultaneous actuator and sensor faults, as well as the development of the LMI-based design of the T-S fuzzy AFTC scheme. The work concentrates on application to nonlinear systems affected by sensor and actuator faults using the concept of estimation and compensation within regulator control framework.
3. Proposal of an extension to Proposal 2 developed within a tracking control framework.

The proposed strategies involve the design of two interacting T-S fuzzy PMIOs for actuator and sensor fault estimates within an observer-based state estimate feedback

control. The strategy can handle the cases in which actuator and sensor faults occur simultaneously. Furthermore, the observers used are capable of estimating a variety of time-varying fault signals. The stability proof with H_∞ performance is formulated as an LMI problem.

The Chapter is organized as follows. Section 5-2 enters into a description of the general architecture of the proposed T-S fuzzy observer-based AFTC approach followed by three Sections illustrating the stability and performance design conditions for (i) T-S fuzzy sensor fault estimate PMIO, (ii) the T-S fuzzy observer-based state feedback regulator control, (iii) the T-S fuzzy actuator fault estimate PMIO, and (iv) the T-S observer-based state feedback tracking control. In Section 5-3, two nonlinear examples are used to illustrate the applicability of the proposed strategies (regulator and tracking). The T-S fuzzy model of the two examples is derived based on local sector nonlinearity. Simulation results have shown the effectiveness of the proposed strategies as well as highlighting the importance of using T-S fuzzy PMIO compared with the T-S proportional integral observer (PIO) fault estimation, when considering FTC performance.

5-2. Observer-based actuator and sensor FTC for nonlinear systems

Simultaneous actuator and sensor faults represent a common challenge for all the AFTC methods. This motivates the proposal of a strategy to ensure system robustness against this challenging and practically probable scenario of simultaneous faults via an estimation and compensation approach. Hence, the goal of this Chapter is to develop a novel FTC strategy for regulator and tracking control problems based on robust fault estimation and compensation of simultaneous actuator faults (f_a) and sensor faults (f_s) whilst maintaining the performance and stability of the nominal control system during both faulty and fault-free cases. An FTC scheme is proposed that is based on the combination of (a) robust control and (b) independent estimates of the each of the actuator faults ($\hat{f}_a$) and sensor faults ($\hat{f}_s$). The controller is required to be robust against expected actuator and sensor fault estimation errors, as well as the bounded reference signal (for the tracking problem). It is clear from the architecture shown in Figure 5-1 that the scheme includes dedicated fault estimation observers in order to ensure accurate estimation and compensation of each of the actuator and sensor faults. Moreover, as the accuracy of the fault estimation is of paramount importance the T-S fuzzy PMIO has

been used in order to cover a variety of fault scenarios. In the sensor fault estimator design the actuator fault signal is considered as an *unknown input* signal that can be compensated directly in the sensor fault estimation.

Conversely, the effect of the sensor fault can be compensated in the estimated actuator fault. Hence, based on the architecture of Figure 5-1 the actuator and sensor fault estimation errors must each be bounded (as well as the q^{th} time derivative of each fault). The controller is driven by the state estimates ($\hat{x}$) from the sensor fault PMIO. On the other hand, the actuator fault PMIO can be considered as an *auxiliary analytical redundancy* to compensate the effects of actuator faults.

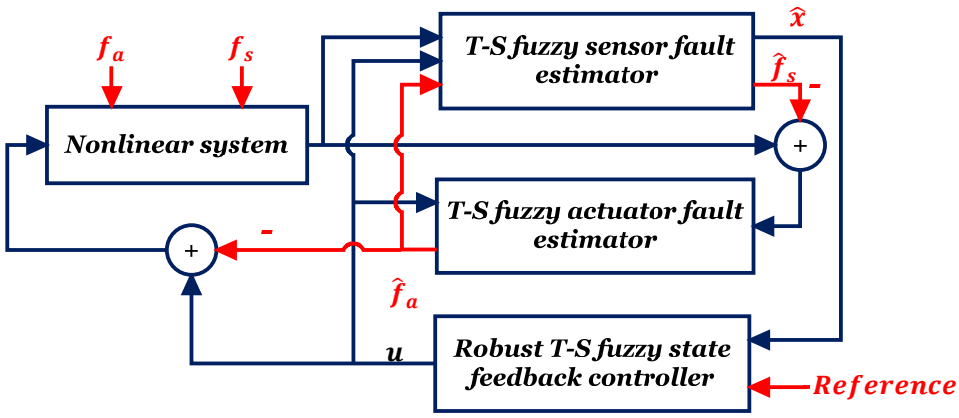

Figure 5-1: Actuator and sensor AFTTC scheme

In fact, the detailed discussion presented in Chapter 4 gives good motivation for the use of the fault estimation and compensation approach. Furthermore, the inability of the adaptive control-based FTC to tolerate sensor faults means that fault estimation and compensation represents the all round most appropriate method for the sensor fault case of FTC.

Section 5-2-1 describes a verification to the application of the proposed strategy for a non-linear system described via T-S fuzzy model.

5-2-1. PMIO based state feedback FTC

This Section presents the LMI-based design for a T-S fuzzy observer-based FTC strategy. The proposed strategy has the ability to tolerate simultaneous actuator and sensor faults online, according to the architecture illustrated in Figure 5-1.

Consider a T-S fuzzy model with actuator and sensor faults signals described as follows:

$$\left.\begin{aligned} \dot{x} &= A(p)x + B(p)u + E(p)f_a \\ y &= Cx + D_f f_s \end{aligned}\right\} \tag{5-1}$$

$A(p) \in \mathcal{R}^{n*n}(= \sum_{i=1}^{r} h_i(p)A_i)$, $B(p) \in \mathcal{R}^{n*m}(= \sum_{i=1}^{r} h_i(p)B_i)$, $E(p) \in \mathcal{R}^{n*f}(= \sum_{i=1}^{r} h_i(p)E_i)$, $C \in \mathcal{R}^{l*n}$, and $D_f \in R^{l*g}$ are the known system matrices. $f_s \in R^g$, and $f_a \in R^f$ are sensor and actuator faults, respectively. r is the number of fuzzy rules and the term $h_i(p)$ is the weighting function that depends on the premise (or scheduling) variable (p).

Firstly, the aim is to tolerate the effects of sensor faults. An estimator is used to estimate the sensor fault signals and implicitly compensate the effects of these faults on the state estimate signals delivered to the controller input. Moreover, the robustness against actuator fault estimation errors effects have also been taken into account during this design stage.

The proposed fuzzy controller has a state feedback structure. The control signal is given by:

$$u = K(p)\hat{x} - K_f(p)\hat{f}_a \tag{5-2}$$

where $K(p) \in \mathcal{R}^{m*n}(= \sum_{i=1}^{r} h_i(p)K_i)$ and $K_f(p) \in \mathcal{R}^{m*f}(= \sum_{i=1}^{r} h_i(p)K_{if})$ are the controller gains, and $\hat{x} \in \mathcal{R}^n$ is the estimated state vector.

Using the design procedure presented in Section 4-3-1, the fuzzy system model in Eq. (5-1) with augmented q^{th} time derivative of the sensor fault (f_s) can be expressed as:

$$\left.\begin{aligned} \dot{x}_a &= A_a(p)x_a + B_a(p)u + E_a(p)f_a + Gf_s^q \\ y_a &= C_a x_a \end{aligned}\right\} \tag{5-3}$$

where

$\varphi_i = f_s^{q-i} \quad (i = 1,2,\dots,q)$; $\dot{\varphi}_1 = f_s^q; \dot{\varphi}_2 = \varphi_1;\ \dot{\varphi}_3 = \varphi_2; \dots; \dot{\varphi}_q = \varphi_{q-1}$

$$x_a = \begin{bmatrix} \bar{x}^T & \varphi_1^T & \varphi_2^T & \varphi_3^T & \dots. & \varphi_q^T \end{bmatrix}^T \in \mathcal{R}^{\bar{n}},\ A_a = \begin{bmatrix} A & 0 & \dots & 0 & 0 \\ 0 & 0 & \dots & 0 & 0 \\ 0 & I & \dots & 0 & 0 \\ \vdots & \vdots & \ddots & \vdots & \vdots \\ 0 & 0 & \dots & I & 0 \end{bmatrix} \in \mathcal{R}^{\bar{n}\times\bar{n}}$$

$$B_a = [\bar{B}^T 0\ 0\ \dots 0]^T \in \mathcal{R}^{\bar{n}\times m},\ E_a = [\bar{E}^T 0\ 0\ \dots 0]^T \in \mathcal{R}^{\bar{n}\times f}$$

$$G = [0\ I\ 0\ \dots 0] \in \mathcal{R}^{\bar{n}*g},\ C_a = \begin{bmatrix} \bar{C} & 0 & 0 & \dots & \bar{D}_f \end{bmatrix} \in \mathcal{R}^{l*\bar{n}},\ \bar{n} = n + gq$$

Hence, the following T-S fuzzy PMIO is proposed to simultaneously estimate the system states and sensor faults:

$$\left.\begin{aligned}\dot{\hat{x}}_a &= A_a(p)\hat{x}_a + B_a(p)u + E_a(p)\hat{f}_a + L_a(p)(y_a - \hat{y}_a)\\ \hat{y}_a &= C_a x_a\end{aligned}\right\} \tag{5-4}$$

where $\hat{f}_a$ in Eq.(5-4) is the actuator fault estimation signal delivered by the auxiliary actuator fault PMIO.

Remark: The PMIO proposed in Section 4-3-1 is modified in this strategy by adding the term $E_a(p)\hat{f}_a$ which is, in turn, responsible for ensuring the robustness of this observer against the expected actuator fault. In fact, this modification offers a considerable advantage since it can ensure observer robustness even for sever actuator fault scenarios whilst the well known H_∞ framework can only deal with bounded faults simultaneously with degraded estimation performance.

Hence, the state estimation error dynamics are obtained by subtracting Eq. (5-4) from Eq. (5-3) to yield:

$$\dot{e}_x = (A_a(p) - L_a(p)C_a)e_x + E_a(p)e_a + Gf_s^q \tag{5-5}$$

The augmented system combining the fuzzy state space system in Eq. (5-1), the controller in Eq. (5-2), and the state estimation error (5-5) is given by:

$$\dot{\tilde{x}}_a(t) = \sum_{i=1}^{r}\sum_{j=1}^{r} h_i(p)h_j(p)\{\tilde{A}_{ij}\tilde{x}_a + \widetilde{N}_{ij}\tilde{d}\} \tag{5-6}$$

where:

$$\tilde{A}_{ij} = \begin{bmatrix} A(p) + B(p)K(p) & [-B(p)K(p) \quad 0] \\ 0 & A_a(p) - L_a(p)C_a \end{bmatrix}, \tilde{x}_a = \begin{bmatrix} \bar{x} \\ e_x \end{bmatrix}, \ \tilde{d} = \begin{bmatrix} \hat{f}_a \\ e_a \\ f_s^q \end{bmatrix}$$

$$\widetilde{N}_{ij} = \begin{bmatrix} E(p) - B(p)K_f(p) & E(p) & 0 \\ 0 & E_a(p) & G \end{bmatrix}$$

The objective here is to compute the gains $L_a(p), K_f(p)\ and\ K(p)$ such that the effect of the input $\tilde{d}$ in Eq. (5-6) is attenuated below the desired level γ_s, to ensure robust stabilization performance.

***Theorem 5-1*:** *For t>0 and* $h_i(p)h_j(p) \neq 0$, *The closed-loop fuzzy system in (5-6) is asymptotically stable and the* H_∞ *performance is guaranteed with an attenuation*

level γ_s, provided that the signal $(\tilde{d})$ is bounded, if there exist SPD matrices P_1, P_2, matrices H_{ai}, Y_j, and scalar γ_s satisfying the following LMI constraints (5-7)&(5-8):

$Minimise\ \gamma_s, such\ that$:

$$P_1 > 0, \qquad P_2 > 0 \tag{5-7}$$

$$\begin{bmatrix} \Psi_{11} & [-B_iY_j \quad 0] & E_i - B_ik_{fj} & E_i & 0 \\ * & -2\mu\bar{X}_1 & 0 & 0 & 0 \\ * & * & -2\mu I & 0 & 0 \\ * & * & * & -2\mu I & 0 \\ * & * & * & * & -2\mu I \\ * & * & * & * & * \\ * & * & * & * & * \\ * & * & * & * & * \\ * & * & * & * & * \\ * & * & * & * & * \end{bmatrix} \tag{5-8}$$

$$\begin{matrix} 0 & 0 & 0 & 0 & P_1^{-1}C_p^T \\ \mu I & 0 & 0 & 0 & 0 \\ 0 & \mu I & 0 & 0 & 0 \\ 0 & 0 & \mu I & 0 & 0 \\ 0 & 0 & 0 & \mu I & 0 \\ \Psi_{77} & 0 & P_2E_{ai} & P_2G & 0 \\ * & -\gamma_s I & * & 0 & 0 \\ * & * & -\gamma_s I & 0 & 0 \\ * & * & * & -\gamma_s I & 0 \\ * & * & * & * & -\gamma_s I \end{matrix} \Bigg] < 0$$

where: $K_j = Y_j X_1^{-1},\ L_{ai} = P_2^{-1}H_{ai}\ ,\ X_1 = P_1^{-1}, \bar{X}_1 = diagonal\ (X_1, I_{q\times q})$

$\Psi_{11} = A_iX_1 + (A_iX_1)^T + BY_j + (BY_j)^T, \Psi_{66} = P_2A_{ai} + (P_2A_{ai})^T - H_{ai}C_a - (H_{ai}C_a)^T.$

Proof: From *Theorem 5-1*, to achieve the performance and required closed-loop stability of Eq. (5-6) the following inequality must hold:

$$\dot{v}(\tilde{x}_a) + \frac{1}{\gamma_s}\tilde{x}_a^T C_p^T C_p \tilde{x}_a - \gamma_s \tilde{d}^T\tilde{d} < 0 \tag{5-9}$$

where $\dot{v}(\tilde{x}_a)$ is the time derivative of the candidate Lyapunov function ($v(\tilde{x}_a) = \tilde{x}_a^T\ \bar{P}\ \tilde{x}_a\ ,where\ \bar{P} > 0$) for the augmented system in Eq. (5-6).

Using Eq. (5-6), the term $\dot{v}(\tilde{x}_a)$ in inequality (5-9) becomes:

$$\dot{v}(\tilde{x}_a) = \sum_{i=1}^{r}\sum_{j=1}^{r} h_i\,(p)h_j(p)\{\tilde{x}_a^T\big(\tilde{A}_{ij}^T\bar{P}\ + \bar{P}\tilde{A}_{ij}\big)\tilde{x}_a + \ \tilde{x}_a^T\bar{P}\tilde{N}_{ij}\tilde{d} + \tilde{d}^T\tilde{N}_{ij}^T\bar{P}\tilde{x}_a\} \tag{5-10}$$

After simple manipulation, inequality (5-9) implies that following inequality (5-11) must hold:

$$\sum_{i=1}^{r}\sum_{j=1}^{r} h_i(p)h_j(p)\left(\begin{bmatrix}\tilde{x}_a\\ \tilde{d}\end{bmatrix}^T\begin{bmatrix}\tilde{A}_{ij}^T\bar{P} + \bar{P}\tilde{A}_{ij} + \frac{1}{\gamma_s}I & \bar{P}\widetilde{N}_{ij}\\ \widetilde{N}_{ij}^T\bar{P} & -\gamma_s I\end{bmatrix}\begin{bmatrix}\tilde{x}_a\\ \tilde{d}\end{bmatrix}\right) < 0 \qquad (5\text{-}11)$$

To be consistent with the augmented system in Eq. (5-6) $\bar{P}$ is structured as follows:

$$\bar{P} = \begin{bmatrix}P_1 & 0\\ 0 & P_2\end{bmatrix} > 0 \qquad (5\text{-}12)$$

after simple manipulation and using the variable change $(H_a(p) = P_2L_a(p))$ the inequality (5-11) can be re-formulated as:

$$\Pi_{ij} = \left[\begin{array}{c|cccc}\Omega_{11} & P_1[-E_iK_j\ 0\ ] & P_1E_i - P_1B_ik_{fj} & P_1E_i & 0\\ \hline * & \Omega_{22} & 0 & P_2E_{ai} & P_2G\\ * & * & -\gamma_s I & 0 & 0\\ * & * & * & -\gamma_s I & 0\\ * & * & * & * & -\gamma_s I\end{array}\right] < 0 \qquad (5\text{-}13)$$

where: $\Omega_{11} = A_iP_1 + (A_iP_1)^T + P_1B_iK_j + (P_1B_iK_j)^T + \frac{1}{\gamma_s}C_p^TC_p$

$\Omega_{22} = P_2A_{ai} + (P_2A_{ai})^T - H_{ai}C_a - (H_{ai}C_a)^T$

The matrix inequality given in (5-13) contains several nonlinear terms. A single step design formulation of the matrix inequality in (5-13) is proposed to avoid the complexity of separate design steps characterised by repeated iteration to determine the required gains. Hence, Π_{ij} as shown in (5-13) becomes:

$$\Pi_{ij} = \begin{bmatrix}\Pi_{11} & \Pi_{12}\\ * & \Pi_{22}\end{bmatrix} \qquad (5\text{-}14)$$

where $\Pi_{11} = \Omega_{11}$, $\Pi_{12} = [-P_1[B_iK_j\ 0]\quad P_1E_i - P_1B_ik_{fj}\quad P_1E_i\quad 0]$, and Π_{22} is the lower right block

To implement a change of variables in an LMI, the Congruence Lemma given in Section 3-2 is required for which the Q matrix has the following form:

$$Q = diagonal\,(P_1^{-1}, X)\ ;\ X = diagonal(\bar{X}_1, I, I, I)\ ;\ \bar{X}_1 = diagonal\,(P_1^{-1}, I_{q\times q})$$

Then $Q * \Pi_{ij} * Q^T < 0$ is also true and can be written as:

$$\begin{bmatrix} P_1^{-1}\Pi_{11}P_1^{-1} & P_1^{-1}\Pi_{12}X \\ * & X\Pi_{22}X \end{bmatrix} < 0 \tag{5-15}$$

Using the approximation given in Eq. (4-25) together with the inequality (5-15) and the Schur complement Theorem, then (5-15) holds if the following inequality holds:

$$\begin{bmatrix} P_1^{-1}\Pi_{11}P_1^{-1} & P_1^{-1}\Pi_{12}X & 0 \\ X\Pi_{12}P_1^{-1} & -2\mu X & \mu I \\ 0 & \mu I & \Pi_{22} \end{bmatrix} < 0 \tag{5-16}$$

After substitution for $\Pi_{11}, \Pi_{12}, \Pi_{12}, \Pi_{22}$ from (5-14) and by simple manipulation, the following LMI is obtained:

$$\begin{bmatrix} \bar{\Psi}_{11} & \bar{\Psi}_{12} & \bar{\Psi}_{13} & E_i & 0 & 0 & 0 & 0 & 0 & P_1^{-1}C_p^T \\ * & -2\mu\bar{X}_1 & 0 & 0 & 0 & \mu I & 0 & 0 & 0 & 0 \\ * & * & -2\mu I & 0 & 0 & 0 & \mu I & 0 & 0 & 0 \\ * & * & * & -2\mu I & 0 & 0 & 0 & \mu I & 0 & 0 \\ * & * & * & * & -2\mu I & 0 & 0 & 0 & \mu I & 0 \\ * & * & * & * & * & \bar{\Psi}_{77} & 0 & P_2E_{ai} & P_2G & 0 \\ * & * & * & * & * & * & -\gamma_s I & * & 0 & 0 \\ * & * & * & * & * & * & * & -\gamma_s I & 0 & 0 \\ * & * & * & * & * & * & * & * & -\gamma_s I & 0 \\ * & * & * & * & * & * & * & * & * & -\gamma_s I \end{bmatrix} < 0 \tag{5-17}$$

where: $\bar{\Psi}_{11} = A_i P_1^{-1} + (A_i P_1^{-1})^T + B_i K_j P_1^{-1} + (B_i K_j P_1^{-1})^T$; $\bar{\Psi}_{12} = \begin{bmatrix} -B_i K_j P_1^{-1} & 0 \end{bmatrix}$

$\bar{\Psi}_{13} = E_i - B_i k_{fj}$; $\bar{\Psi}_{77} = P_2 A_{ai} + (P_2 A_{ai})^T - H_{ai} C_a - (H_{ai} C_a)^T$

using the change of variables ($X_1 = P_1^{-1}, Y_j = K_j P_1^{-1}$), the LMI condition (5-8) can be easily obtained.

5-2-2. T-S fuzzy PMIO based actuator fault estimation

The T-S fuzzy PMIO for the actuator fault estimation case is similar to the estimator derived in Section 5-2-1. However, in this methodology, the estimator must be designed to take good care of the effect of the sensor fault estimation error signal. Therefore, from the actuator fault PMIO stand point, the fuzzy model given in Eq. (5-1) becomes:

$$\left.\begin{aligned} \dot{x} &= A(p)x + B(p)u + E(p)f_a \\ y &= Cx + D_f e_s \end{aligned}\right\} \tag{5-18}$$

where e_s is the sensor fault estimation error. Hence, following the same methodology for the PMIO sensor fault estimator design the system augmented by the q^{th} derivative of the actuator fault f_a, is given as follows:

$$\left.\begin{aligned} \dot{x}_a &= \bar{A}(p)x_a + \bar{B}(p)u + \bar{G}f_a^q \\ y_a &= \bar{C}x_a + D_f e_s \end{aligned}\right\} \tag{5-19}$$

where

$$\varphi_i = f_a^{q-i} \quad (i = 1,2,\dots,q)\ ,\ \dot{\varphi}_1 = f_a^q; \dot{\varphi}_2 = \varphi_1;\ \dot{\varphi}_3 = \varphi_2; \dots; \dot{\varphi}_q = \varphi_{q-1}$$

$$x_a = \begin{bmatrix} \bar{x}^T & \varphi_1^T & \varphi_2^T & \dots. & \varphi_q^T \end{bmatrix}^T \in \mathcal{R}^{\bar{n}}\ ,\ \bar{A} = \begin{bmatrix} A & 0 & \dots & 0 & E(p) \\ 0 & 0 & \dots & 0 & 0 \\ 0 & I & \dots & 0 & 0 \\ \vdots & \vdots & \ddots & \vdots & \vdots \\ 0 & 0 & \dots & I & 0 \end{bmatrix} \in \mathcal{R}^{\bar{n}\times\bar{n}}$$

$$\bar{B} = [B^T 0\ 0\ \dots 0]^T \in \mathcal{R}^{\bar{n}\times m}\ ,\ \bar{G} = [0\ I\ 0\ \dots 0]^T \in \mathcal{R}^{\bar{n}\times w}$$

$$\bar{C} = [C\ 0\ 0\ \dots 0] \quad \in \mathcal{R}^{l*\bar{n}}\ ,\ \bar{n} = (n+w) + mq$$

Hence, the following T-S fuzzy PMIO is proposed to simultaneously estimate the system states and actuator faults:

$$\left.\begin{aligned} \dot{\hat{x}}_a &= \bar{A}(p)\hat{x}_a + \bar{B}(p)u + \bar{L}(p)(y_a - \hat{y}_a) \\ \hat{y}_a &= \bar{C}\hat{x}_a \end{aligned}\right\} \tag{5-20}$$

Remark: Following the idea of the sensor fault fuzzy PMIO designed in Section 5-2-1, the inclusion of the estimation/compensation signal $\hat{f}_s$ into the actuator fault PMIO ensures the robustness against sensor faults. This is clear since the fuzzy PMIO in Eq. (5-21) actually has the following form:

$$\left.\begin{aligned} \dot{\hat{x}}_a &= \bar{A}(p)\hat{x}_a + \bar{B}(p)u + \bar{L}(p)\big(Cx + D_f f_s - C\hat{x} - D_f\hat{f}_s\big) \\ \hat{y}_a &= \bar{C}\hat{x}_a \end{aligned}\right\}$$

The state estimation error dynamics are obtained by subtracting Eq. (5-20) from Eq. (5-19) to yield:

$$\dot{e}_x = (\bar{A}(p) - \bar{L}(p)\bar{C})e_x - \bar{L}(p)D_f e_s + \bar{G}f_a^q \tag{5-21}$$

where e_x is the state estimation error.

Theorem 5-2: *The T-S fuzzy PMIO given in (5-20) exists if*

$$rank\begin{bmatrix} A_i & E_i \\ C & 0 \end{bmatrix} = n + k \tag{5-22}$$

and

$$rank\begin{bmatrix} sI - A_i \\ C \end{bmatrix} = n \quad \forall s \in \mathbb{C} \tag{5-23}$$

Additionally, the PMIO attenuate the effect of the bounded q^{th} actuator fault derivative and sensor fault estimation error on the augmented estimation error if there exist SPD matrix $P = P^T > 0$ and matrices $\bar{H}_i$ that minimise γ_{pmi} under the following LMI constraints:

$$\begin{bmatrix} P\bar{A}_i + (P\bar{A}_i)^T - \bar{H}_i\bar{C} - (\bar{H}_i\bar{C})^T & -\bar{H}_i D_f & P\bar{G} & C_p^T \\ * & -\gamma_{pmi} I & 0 & 0 \\ * & * & -\gamma_{pmi} I & 0 \\ * & * & * & -\gamma_{pmi} I \end{bmatrix} < 0 \tag{5-24}$$

where the observer gains are obtained by:

$$\bar{L}_i = P^{-1}\bar{H}_i \tag{5-25}$$

Proof: Conditions *(5-22)&(5-23)* follow directly the observability requirements for the state and fault estimates.

The state estimation error dynamics can be rewritten from (5-21) as follows:

$$\dot{e}_x = \sum_{i=1}^{r} h_i(p)\{(\bar{A}_i - \bar{L}_i\bar{C})e_x + N_i\bar{d}\} \tag{5-26}$$

where $\bar{d} = \begin{bmatrix} e_s \\ f_a^q \end{bmatrix}$ and $N_i = \begin{bmatrix} -\bar{L}(p)D_f & \bar{G} \end{bmatrix}$

To attenuate the effect simultaneously of $(e_s \& f_a^q)$ on the estimation error whilst also ensuring the system stability, the following inequality must hold:

$$\dot{\upsilon}(e_x) + \frac{1}{\gamma_{pmi}} e_x^T C_p^T C_p e_x - \gamma_{pmi}\bar{d}^T\bar{d} < 0 \tag{5-27}$$

where $\dot{\upsilon}(e_x)$ is the time derivative of the candidate Lyapunov function ($\upsilon(e_x) = e_x^T P e_x$) and C_p matrix is introduced to specify the performance output. Using Eq. (5-21), the inequality (5-27) becomes:

$$\begin{aligned} \dot{\upsilon}(e_x) = \sum_{i=1}^{r} h_i\{ & e_x^T(\bar{A}_i^T P + P\bar{A}_i - P\bar{L}_i\bar{C} - (P\bar{L}_i\bar{C})^T)e_x + e_x^T P N_i\bar{d} \\ & + \bar{d}^T N_i^T P e_x\} \end{aligned} \tag{5-28}$$

The inequality (5-27) (in matrix form) after substituting $\dot{v}(\tilde{x}_a)$ from Eq. (5-28) and using the variable change $\bar{H}_i = P\bar{L}_i$ becomes:

$$\sum_{i=1}^{r} h_i \left\{ \begin{bmatrix} e_x \\ \bar{d} \end{bmatrix}^T \begin{bmatrix} \bar{A}_i^T P + P\bar{A}_i - \bar{H}_i\bar{C} - (\bar{H}_i\bar{C})^T + \frac{1}{\gamma_{pmi}} C_p^T C_p & PN_i \\ N_i^T P & -\gamma_{pmi} I \end{bmatrix} \begin{bmatrix} e_x \\ \bar{d} \end{bmatrix} \right\} < 0 \tag{5-29}$$

Clearly, by using the Schur Theorem inequality (5-24) is easily obtained from inequality (5-29). This completes the proof.

5-2-3. T-S fuzzy PMIO based state feedback within a tracking problem

Owing to the challenges involved in the tracking problem within FTC framework (see the investigation presented in Chapter 3), this Section presents the LMI-based design for T-S fuzzy PMIO based FTTC for nonlinear system subject to simultaneous actuator and sensor faults.

By considering the T-S fuzzy model with actuator and sensor faults signals given in Eq. (5-1), an augmented system consisting of the system in (5-1) and the integral of the tracking error $e_t = \int (y_r - Sy)$ is defined as:

$$\left.\begin{aligned} \dot{\bar{x}} &= A_t(p)\bar{x} + B_t(p)u + E_t(p)f_a + R_t y_r \\ \bar{y} &= C_t\,\bar{x} + D_{ft} f_s \end{aligned}\right\} \tag{5-30}$$

$$A_t(p) = \begin{bmatrix} 0 & -SC \\ 0 & A(p) \end{bmatrix}, \bar{x} = \begin{bmatrix} e_t \\ x \end{bmatrix}, B_t(p) = \begin{bmatrix} 0 \\ B(p) \end{bmatrix}, E_t(p) = \begin{bmatrix} 0 \\ E(p) \end{bmatrix}, R_t = \begin{bmatrix} I \\ 0 \end{bmatrix}$$

$$C_t = \begin{bmatrix} I_w & 0 \\ 0 & C \end{bmatrix}, D_{ft} = \begin{bmatrix} 0 \\ D_f \end{bmatrix}$$

where $S \in \mathcal{R}^{w*l}$ is used to define which output variable is considered to track the reference signal. The integral of the tracking error is used in the control to minimise the steady-state tracking error. The proposed control signal for the state feedback fuzzy control tracking problem is:

$$u = K_t(p)\hat{\bar{x}} - K_{ft}(p)\hat{f}_a \tag{5-31}$$

where $K_t(p) \in \mathcal{R}^{m*(n+w)} (= \sum_{i=1}^{r} h_i\,(p) K_{ti})$ and $K_{ft}(p) \in \mathcal{R}^{m*f} (= \sum_{i=1}^{r} h_i\,(p) K_{ift})$ are the controller gains, and $\hat{\bar{x}} \in \mathcal{R}^{(n+w)}$ is the estimated augmented state vector.

Hence, the system (5-30) with augmented sensor fault derivatives will become:

$$\left.\begin{aligned} \dot{x}_a &= A_{at}(p)x_a + B_{at}(p)u + E_{at}(p)f_a + R_{at}y_r + G_{at}f_s^q \\ y_a &= C_{at}x_a \end{aligned}\right\} \tag{5-32}$$

where the matrix definitions are similar to those given under Eq. (5-3). The T-S fuzzy PMIO for the simultaneous states and sensor fault estimation has the following dynamics:

$$\left.\begin{aligned} \dot{\hat{x}}_a &= A_{at}(p)\hat{x}_a + B_{at}(p)u + E_{at}(p)\hat{f}_a + R_{at}y_r + L_{at}(p)(y_a - \hat{y}_a) \\ \hat{y}_a &= C_{at}x_a \end{aligned}\right\} \tag{5-33}$$

Hence, the state estimation error dynamics are obtained by subtracting Eq. (5-33) from Eq. (5-32) to yield:

$$\dot{e}_x = (A_{at}(p) - L_{at}(p)C_{at})e_x + E_{at}(p)e_a + G_{at}f_s^q \tag{5-34}$$

The augmented system combining the augmented state space system (5-32), the controller (5-31), and the state estimation error (5-34) is given by:

$$\dot{\tilde{x}}_a(t) = \sum_{i=1}^{r}\sum_{j=1}^{r} h_i\,(p)h_j\,(p)\{\tilde{A}_{ijt}\tilde{x}_a + \tilde{N}_{ijt}\tilde{d}\} \tag{5-35}$$

where:

$$\tilde{A}_{ijt} = \begin{bmatrix} A_t(p) + B_t(p)K_t(p) & -B_t(p)[K_t(p) \quad 0_{m\times q}] \\ 0 & A_{at}(p) - L_{at}(p)C_{at} \end{bmatrix}, \tilde{x}_a = \begin{bmatrix} \bar{x} \\ e_x \end{bmatrix},\ \tilde{d} = \begin{bmatrix} \hat{f}_a \\ e_a \\ y_r \\ f_s^q \end{bmatrix}$$

$$\tilde{N}_{ijt} = \begin{bmatrix} E_t(p) - B_t(p)K_{ft}(p) & E_t(p) & R_t & 0 \\ 0 & E_{at}(p) & 0 & G_{at} \end{bmatrix}$$

The objective here is to compute the gains $L_{at}(p), K_t(p)\ and\ K_{ft}(p)$ such that the effect of the input $\tilde{d}$ in Eq. (5-35) is attenuated below the desired level γ_t, to ensure robust stabilization performance.

Theorem 5-3**:** *For t>0 and* $h_i\,(p)h_j\,(p) \neq 0$*, The closed-loop fuzzy system in (5-35) is asymptotically stable and the* H_∞ *performance is guaranteed with an attenuation level* γ_t*, provided that the signal* $(\tilde{d})$ *is bounded, if there exist SPD matrices* P_{t1}, P_{t2}*, and matrices* H_{ati}, Y_{tj}*, and scalar* γ_t *satisfying the following LMI constraints (37&38):*

$Minimise\ \gamma_t, such\ that$:

$$P_{t1} > 0, \qquad P_{t2} > 0 \tag{5-36}$$

$$\begin{bmatrix} \Psi_{11} & [-B_{ti}Y_{tj} \quad 0] & E_{ti}-B_{it}k_{ftj} & E_{ti} & R_t & 0 \\ * & -2\mu\bar{X}_1 & 0 & 0 & 0 & 0 \\ * & * & -2\mu I & 0 & 0 & 0 \\ * & * & * & -2\mu I & 0 & 0 \\ * & * & * & * & -2\mu I & 0 \\ * & * & * & * & * & -2\mu I \\ * & * & * & * & * & * \\ * & * & * & * & * & * \\ * & * & * & * & * & * \\ * & * & * & * & * & * \\ * & * & * & * & * & * \\ * & * & * & * & * & * \end{bmatrix}$$

$$\begin{bmatrix} 0 & 0 & 0 & 0 & 0 & P_{t1}^{-1}C_{pt}^T \\ \mu I & 0 & 0 & 0 & 0 & 0 \\ 0 & \mu I & 0 & 0 & 0 & 0 \\ 0 & 0 & \mu I & 0 & 0 & 0 \\ 0 & 0 & 0 & \mu I & 0 & 0 \\ 0 & 0 & 0 & 0 & \mu I & 0 \\ \Psi_{77} & 0 & P_{t2}E_{ati} & 0 & P_{t2}G_{at} & 0 \\ * & -\gamma_t I & * & 0 & 0 & 0 \\ * & * & -\gamma_t I & 0 & 0 & 0 \\ * & * & * & -\gamma_t I & 0 & 0 \\ * & * & * & * & -\gamma_t I & 0 \\ * & * & * & * & * & -\gamma_t I \end{bmatrix} < 0 \tag{5-37}$$

where: $K_{tj} = Y_{tj}X_{t1}^{-1},\ L_{ati} = P_{t2}^{-1}H_{ati}\ ,\ X_{t1} = P_{t1}^{-1}, \bar{X}_{t1} = diagonal\ (X_{t1}, I_{q\times q})$

$\Psi_{11} = A_{ti}X_1 + (A_{ti}X_1)^T + B_{ti}Y_{tj} + (B_{ti}Y_{tj})^T$

$\Psi_{77} = P_{t2}A_{ati} + (P_{t2}A_{ati})^T - H_{ati}C_{at} - (H_{ati}C_{at})^T.$

Proof: From Theorem 3, to achieve the performance and required closed-loop stability of (5-13) the following inequality must hold:

$$\dot{v}(\tilde{x}_a) + \frac{1}{\gamma_t}\tilde{x}_a^T C_{pt}^T C_{pt}\tilde{x}_a - \gamma_t \tilde{d}^T\tilde{d} < 0 \tag{5-38}$$

By following the steps of proof of Theorem 5-1 introduced in Section 5-2-1 the LMI of Theorem 5-3 can be easily obtained.

Remark: The PMIO proposed in Section 5-2-2 can be used as an auxiliary analytical redundancy to provide estimation of the actuator fault.

Remark: It should be noted that the fuzzy control or observer designer does not have freedom to assign the local system closed-loop poles anywhere in the stable complex plane. This is due to the global stability constraint requirement (*Theorems 5-3 & 5-1*) which may led to infeasible solution for some regions in the stable complex plain. The

consequence of this is that the observer-based T-S state feedback control system suffers a major drawback in that the observer dynamics may not be assigned freely to satisfy closed-loop performance requirements (i.e. it is difficult to recover the *Separation Principle*). A proposal, based on the use of TSDOFC, is developed in Chapter 6 to overcome this limitation.

5-3. Simulation example

PMIO based FTC with simultaneous actuator and sensor fault

The LMI-based fuzzy control proposed in *Theorem 5-1* is applied to the following 4th order nonlinear system adapted from (Tanaka and Wang, 2001):

$$\left.\begin{aligned}\begin{bmatrix}\dot{x}_1\\ \dot{x}_2\\ \dot{x}_3\\ \dot{x}_4\end{bmatrix} &= \begin{bmatrix}0 & 1 & \frac{\sin x_3}{x_3} & 0\\ 1 & 2 & 0 & 0\\ 1 & x_1^2 & 0 & 0\\ 0 & 0 & \frac{\sin x_3}{x_3} & 0\end{bmatrix}\begin{bmatrix}x_1\\ x_3\\ x_3\\ x_4\end{bmatrix} + \begin{bmatrix}x_1^2+1\\ 0\\ 0\\ 0\end{bmatrix}u(t)\\ y &= \begin{bmatrix}x_1\\ x_3\\ x_4\end{bmatrix}\end{aligned}\right\} \tag{5-39}$$

the states x_1 and x_3 are assumed to be bounded according to:

$$x_1 \in [-\delta, \delta],\ \ x_3 \in [-\varepsilon, \varepsilon]$$

where δ and ε are positive values. Based on the concept of local sector nonlinearity (see description in Section 2-3-2), the nonlinear terms can be represented as:

$$\left.\begin{aligned} z_1 &= x_1^2 = M_1 * z_{11} + M_2 * z_{12}\\ z_2 &= \frac{\sin x_3}{x_3} = N_1 * z_{21} + N_2 * z_{22}\end{aligned}\right\} \tag{5-40}$$

where $z_{11} = \delta^2$ and $z_{12} = 0$ are the maximum and minimum values of z_1, and $z_{21} = 1$ and $z_{22} = \frac{\sin \varepsilon}{\varepsilon}$ are the maximum and minimum values of z_2. Since

$$\left.\begin{aligned} M_1 + M_2 &= 1\\ N_1 + N_2 &= 1\end{aligned}\right\} \tag{5-41}$$

By solving Eqs. (5-39)&(5-40), the fuzzy membership functions obtained are as follows:

$$
\left.
\begin{aligned}
M_1 &= \frac{x_1^2}{\delta^2} \\
M_2 &= 1 - \frac{x_1^2}{\delta^2} \\
N_1 &= \begin{cases} \frac{\varepsilon \sin x_3 - x_3 \sin \varepsilon}{x_3(\varepsilon - \sin \varepsilon)}, & x_3 \neq 0 \\ 1, & x_3 = 0 \end{cases} \\
N_2 &= \begin{cases} 1 - \frac{\varepsilon \sin x_3 - x_3 \sin \varepsilon}{x_3(\varepsilon - \sin \varepsilon)}, & x_3 \neq 0 \\ 0, & x_3 = 0 \end{cases}
\end{aligned}
\right\} \tag{5-42}
$$

Hence the overall fuzzy model is given by:

$$
\begin{bmatrix} \dot{x}_1 \\ \dot{x}_2 \\ \dot{x}_3 \\ \dot{x}_4 \end{bmatrix} = \sum_{i=1}^{2} \sum_{j=1}^{2} M_i N_j \left(\begin{bmatrix} 0 & 1 & z_{2j} & 0 \\ 1 & 2 & 0 & 0 \\ 1 & z_{1i} & 0 & 0 \\ 0 & 0 & z_{2j} & 0 \end{bmatrix} \begin{bmatrix} x_1 \\ x_2 \\ x_3 \\ x_4 \end{bmatrix} + \begin{bmatrix} z_{1i} + 1 \\ 0 \\ 0 \\ 0 \end{bmatrix} u(t) \right) \tag{5-43}
$$

In the following simulation results, the parameter values $\delta = 0.8$ and $\varepsilon = 0.6$ have been used. First the importance of using fuzzy PMIOs (two observers for the sensor actuator fault cases) proposed in this strategy in comparison with the single integral observer (PIO) is illustrated in Figure 5-2. It is clear from this simulation result that the fault estimation accuracy is highly degraded whenever the first time derivative of the fault is no longer equal zero. This in turn affects the closed-loop performance since the expected fault tolerance is based on the fault estimation and compensation concept. On the other hand, the fault estimation signals in Figure 5-2 show the advantage of using the PMIOs to obtain accurate estimation even when the first time derivative of the fault signal is not equal to zero.

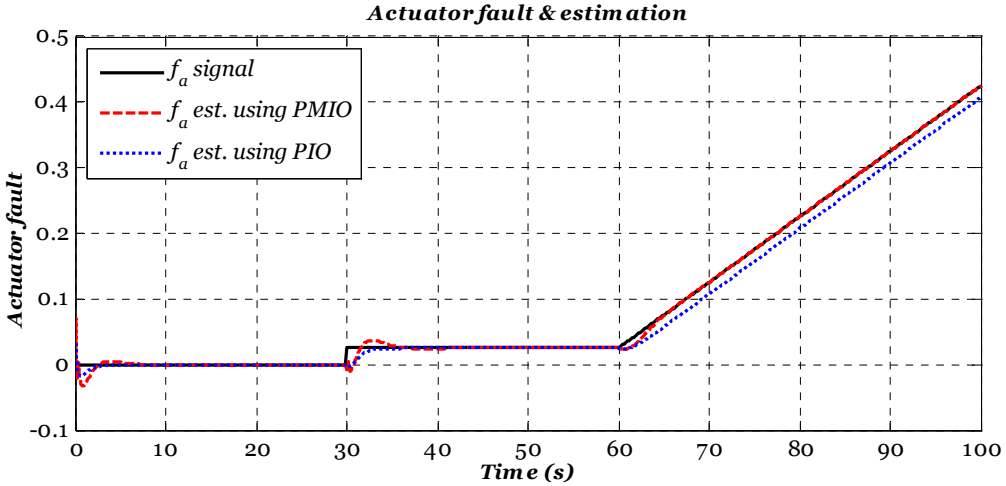

Figure 5-2: Comparison between single integral and multiple integral observers based fault estimation

The initial conditions for the nonlinear system states and the two PMIOs are selected as follows:

$$System\ initial\ states = [0.025 \quad 0 \quad 0.1 \quad 0],$$
$$Actuator\ PMIO = [0.050 \quad 0 \quad 0 \quad 0 \quad 0 \quad 0],$$
$$Sensor\ PMIO = [0.200 \quad 0 \quad 0.2 \quad 0 \quad 0 \quad 0.1],$$

By solving the LMI condition (8), the fuzzy controller gains are

$$K_1 = [-8.3117 \quad -50.7059 \quad 12.8933 \quad 3.5747],$$
$$K_2 = [-8.3132 \quad -50.6807 \quad 12.8833 \quad 3.5648],$$
$$K_3 = [-8.6720 \quad -53.1586 \quad 13.4504 \quad 3.7622],$$
$$K_4 = [-8.6679 \quad -53.1493 \quad 13.4573 \quad 3.7622],$$

actuator fault PMIO gains are

$$L_{a1} = \begin{bmatrix} 19.2301 & 2.3456 & 3.4605 \\ 158.4437 & 64.8806 & 14.4362 \\ 10.6928 & 17.9279 & -2.7191 \\ 0.5607 & 1.3972 & 1.1668 \\ -17.2415 & -7.6481 & -1.7211 \\ -44.3227 & -19.2131 & -4.4765 \end{bmatrix}, \ L_{a2} = \begin{bmatrix} 19.2048 & 2.2658 & 2.9248 \\ 158.4016 & 64.9429 & 12.7304 \\ 10.6065 & 17.8819 & -1.4870 \\ 0.5108 & 1.2745 & 1.2379 \\ -17.2434 & -7.6520 & -1.5006 \\ -44.3227 & -19.2253 & -3.9219 \end{bmatrix},$$

$$L_{a3} = \begin{bmatrix} 20.6456 & 3.2829 & 0.4929 \\ 156.8523 & 62.6973 & -6.6786 \\ 2.2511 & 13.8381 & -2.7192 \\ 0.6295 & 1.3953 & 1.2382 \\ -17.1933 & -7.1979 & 0.5039 \\ -44.0786 & -18.1954 & 1.4195 \end{bmatrix}, L_{a4} = \begin{bmatrix} 20.6340 & 3.1579 & 0.3749 \\ 156.9072 & 62.5444 & -5.5188 \\ 2.2350 & 13.9474 & -1.9162 \\ 0.6051 & 1.3505 & 1.3405 \\ -17.1997 & -7.1870 & 0.3579 \\ -44.0935 & -18.1556 & 1.0647 \end{bmatrix},$$

and sensor fault PMIO gains are

$$\bar{L}_1 = \begin{bmatrix} 7.8949 & 10.0200 & 66.5217 \\ 9.1832 & 77.6580 & 904.2961 \\ 4.2756 & 10.5964 & 181.0095 \\ 0.0105 & 0.9358 & 17.2317 \\ -0.8690 & 5.4975 & -755.4249 \\ -0.0005 & 0.7887 & -163.3622 \end{bmatrix}, \bar{L}_2 = \begin{bmatrix} 7.8579 & 9.9219 & 81.1561 \\ 8.7015 & 7.6053 & 990.1814 \\ 4.2936 & 10.5451 & 185.3293 \\ 0.0098 & 0.8356 & 16.7603 \\ -0.6734 & 5.4707 & -826.1179 \\ 0.0095 & 0.7947 & -168.5356 \end{bmatrix}$$

$$\bar{L}_3 = \begin{bmatrix} 10.5051 & 4.6865 & 93.6955 \\ 33.9894 & 32.9176 & 514.5949 \\ 1.0803 & 6.1056 & 144.8791 \\ 0.0059 & 0.9433 & 17.3032 \\ 0.2912 & 3.5326 & -762.1972 \\ 0.0287 & 0.7481 & -162.4768 \end{bmatrix}, \bar{L}_4 = \begin{bmatrix} 10.5005 & 4.5811 & 97.6094 \\ 33.7719 & 33.4925 & 473.9856 \\ 1.0804 & 6.0868 & 149.1070 \\ 0.0054 & 0.8428 & 16.8098 \\ 0.1886 & 4.0011 & -828.1432 \\ 0.0244 & 0.7747 & -166.8320 \end{bmatrix}.$$

The obtained attenuation coefficients are $\gamma_s = 1.1812$ and $\gamma_{pmi} = 0.832$.

In this simulation, the actuator fault signal affects the nonlinear system in the same direction as the control $u(t)$. The additive sensor fault signal affects the second measurement. The proposed actuator and sensor fault signals and their estimates are given in Figure 5-3.

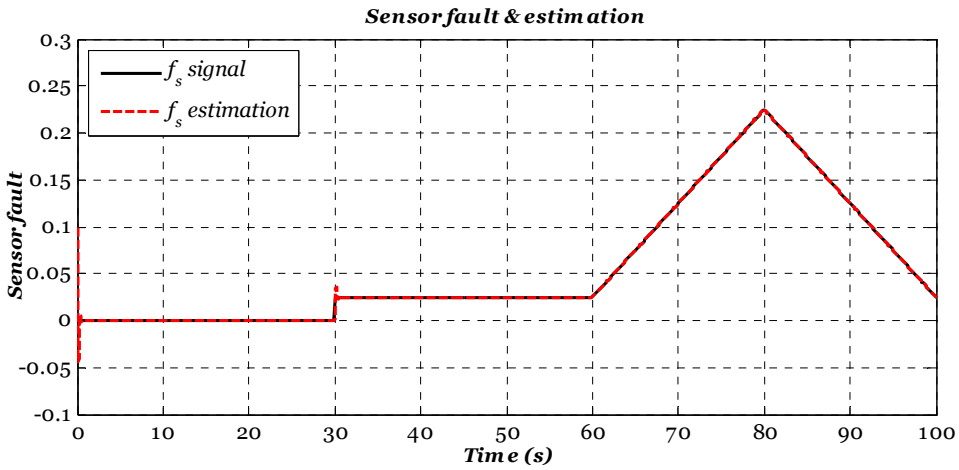

(a)

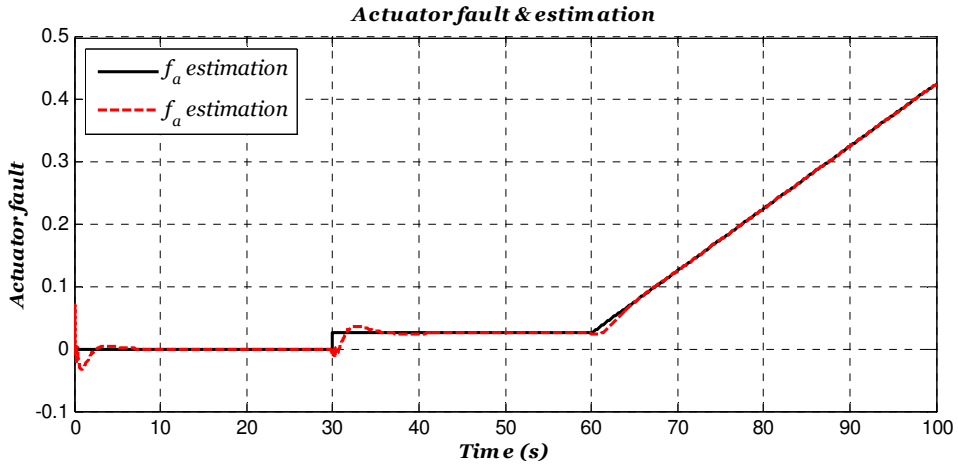

(b)

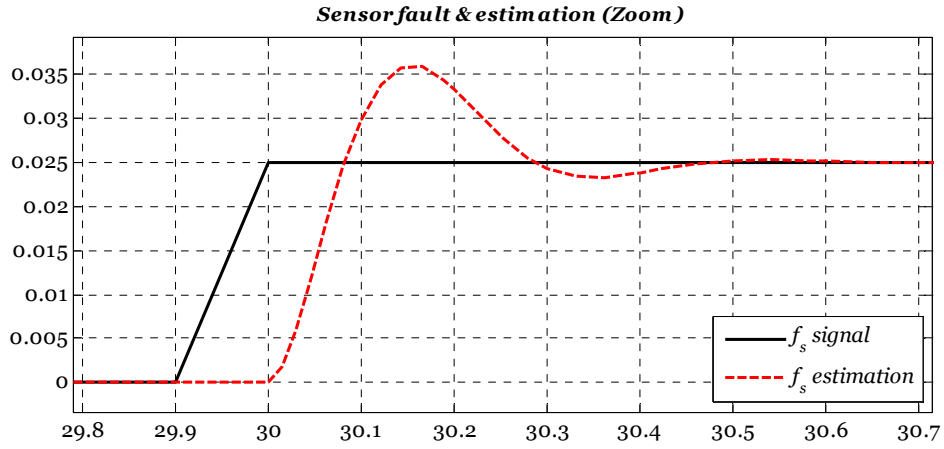

(c)

Figure 5-3: Fault and their estimation (a) sensor fault, (b) Actuator fault, and (c) zoomed sensor fault estimation

However, the estimation accuracy shown in Figure 5-3 is obtained provided that the two simultaneous faults are estimated and compensated online. For example, if the sensor

fault has not been compensated the actuator fault estimation accuracy will degrade as shown in Figure 5-4.

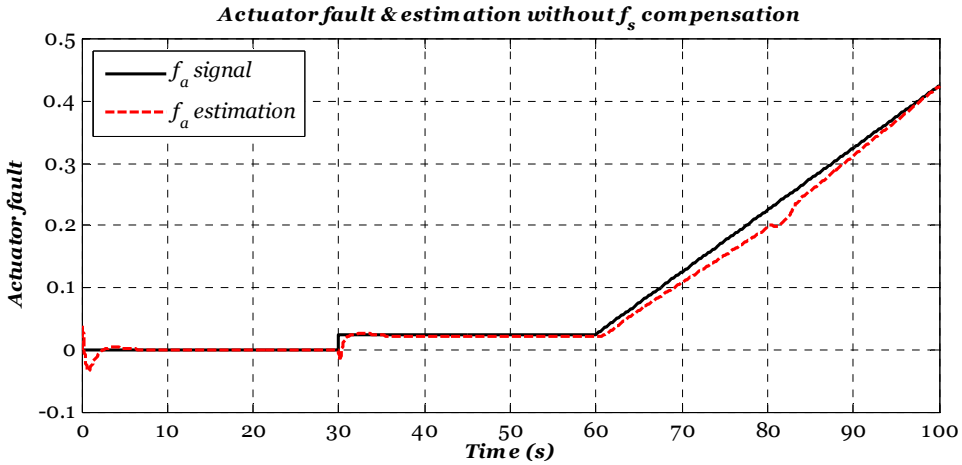

Figure 5-4: Inaccurate actuator fault estimation due to uncompensated sensor fault

Moreover, the effect of the uncompensated simultaneous actuator and sensor fault signals on the system states and the weighting functions are shown in Figure 5-5.

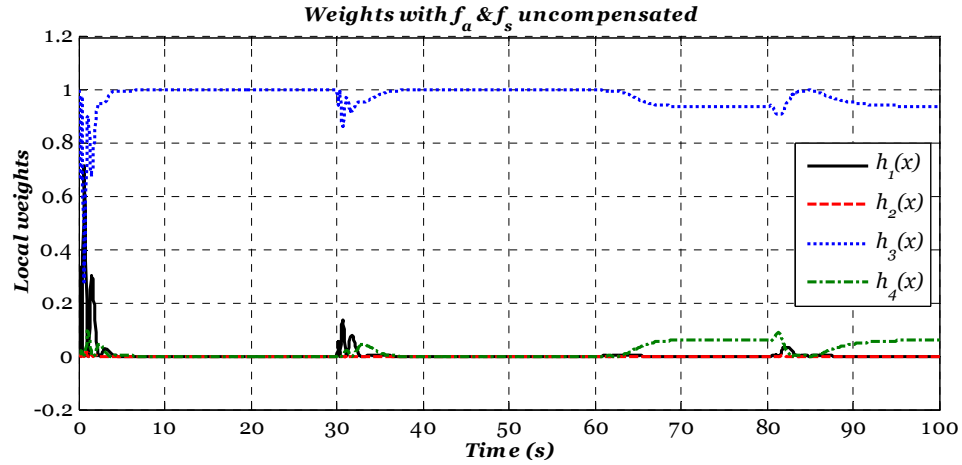

(a)

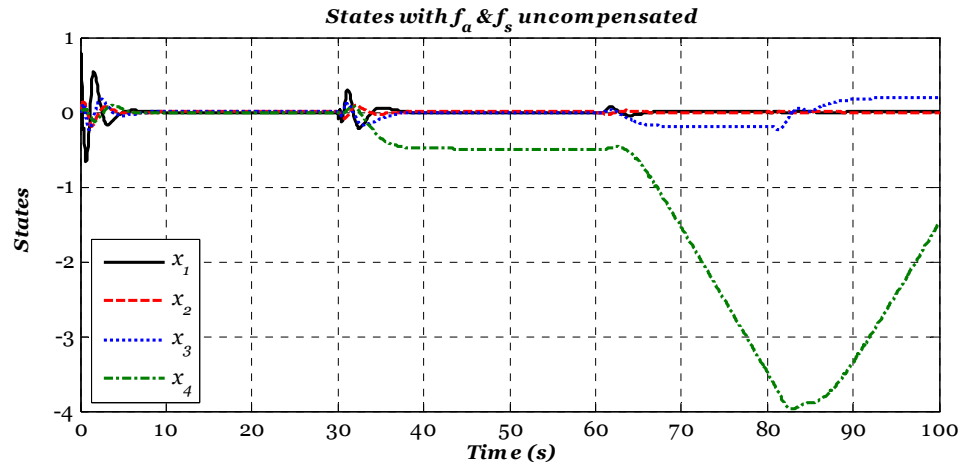

(b)

Figure 5-5: The effect of faults on (a) weighting functions and (b) states.

The uncompensated fault signals cause the fuzzy controller to deviate away from the nominal system behaviour. Hence, the fuzzy control lacks the ability to drive the nonlinear system correctly to the equilibrium. By using the estimation provided by the two PMIOs, the simultaneous faults can be compensated online and the nominal system behaviour is maintained. Figure 5-6 shows weighting functions and system states with online fault compensation.

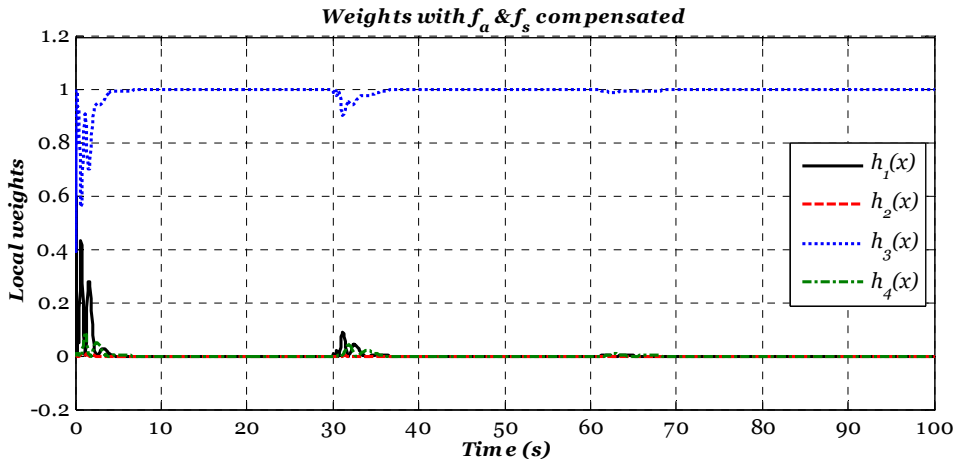

(a)

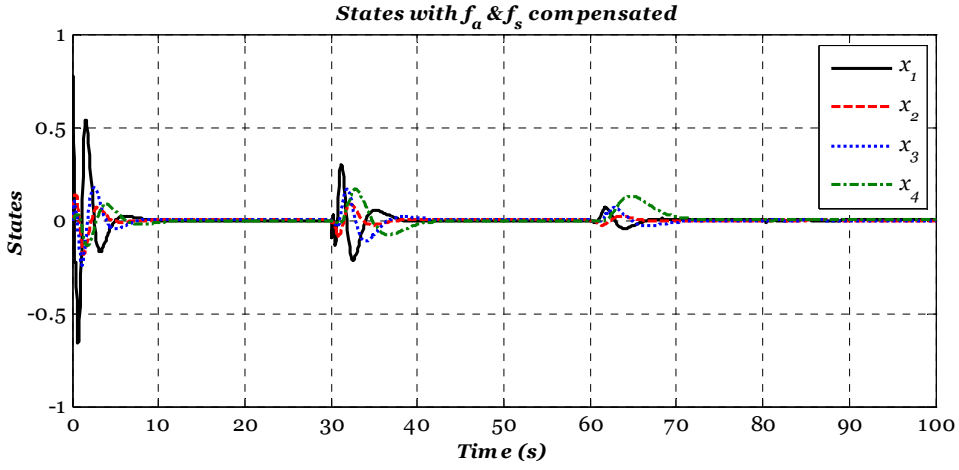

(b)

Figure 5-6: Effects of the fault compensation on (a) weighting functions and (b) states

PMIO based FTTC with simultaneous actuator and sensor faults

In this simulation subsection, the nonlinear inverted pendulum model is used as the case for the LMI-based design procedure for PMIO FTTC given in Theorem 5-3. The T-S fuzzy model of the inverted pendulum derived in Section (2.3.1.2) is used. The fuzzy model represents the nonlinear model exactly in the state intervals $x_1 \in [-\theta, \theta]$ and $x_3 \in [-\beta, \beta]$, where x_1 and x_3 are the pendulum angular position and angular velocity, respectively. Since x_3 is an unmeasurable signal, any fuzzy controller and/or

observer design based on the fuzzy model derived in Section (2.3.1.2) must consider the estimation of the variable x_3. However, to avoid the complexity of the unmeasurable premise variable design problem, an uncertain fuzzy T-S model can be derived so that only x_1 is used as the premise variable.

By rewriting the nonlinear model of inverted pendulum given in Section (2.3.1.2) as follows:

$$\begin{bmatrix}\dot{x}_1\\ \dot{x}_2\\ \dot{x}_3\\ \dot{x}_4\end{bmatrix} = \begin{bmatrix}0 & 0 & 1 & 0\\ 0 & 0 & 0 & 1\\ \frac{g\,sin(x_1)}{4l/3-mla(cos(x_1))^2 x_1}\frac{1}{} & 0 & 0 & 0\\ \frac{-mag\,sin(2x_1)/2\ 1}{4/3-ma(cos(x_1))^2 x_1} & 0 & 0 & 0\end{bmatrix}\begin{bmatrix}x_1\\ x_2\\ x_3\\ x_4\end{bmatrix} + \begin{bmatrix}0\\ 0\\ \frac{-a\,cos(x_1)}{4l/3-mla(cos(x_1))^2}\\ \frac{4a/3}{4/3-ma(cos(x_1))^2}\end{bmatrix}(u + mlx_3^2\,sin(x_1)) \quad (5\text{-}44)$$

The term $(mlx_3^2\,sin(x_1))$ is now considered as the model uncertainty. Hence, the four nonlinear terms defined in Eq. (2-22) are reduced to *three* terms defined as follows:

$$\left.\begin{aligned} z_1 &= 1/(4l/3 - mla(cos(x_1))^2)\\ z_2 &= sin(x_1)/x_1\\ z_3 &= cos(x_1)\end{aligned}\right\} \quad (5\text{-}45)$$

The maximum and minimum values of each nonlinear term within the specified intervals are calculated as shown below:

Max	***Min***
$z_{11} = \frac{1}{4l/3-mla}$	$z_{12} = \frac{1}{4l/3-mla(cos(\theta))^2}$
$z_{21} = 1$	$z_{22} = \frac{sin(\theta)}{\theta}$
$z_{31} = 1$	$z_{32} = cos(\theta)$

From the maximum and minimum values, the nonlinear system can be locally represented in term of membership functions and maximum and minimum values as follows:

$$\left.\begin{aligned} z_1 &= M_1 * z_{11} + M_2 * z_{12}\\ z_2 &= N_1 * z_{21} + N_2 * z_{22}\\ z_3 &= E_1 * z_{31} + E_2 * z_{32}\end{aligned}\right\} \quad (5\text{-}46)$$

Since:

$$\left.\begin{aligned} M_1 + M_2 &= 1\\ N_1 + N_2 &= 1\\ E_1 + E_2 &= 1\end{aligned}\right\} \quad (5\text{-}47)$$

By solving Eqs. (5-46)&(5-47), the membership functions can be obtained as:

$$M_1 = \frac{z_1 - z_{12}}{z_{11} - z_{12}} \qquad M_2 = \frac{z_{11} - z_1}{z_{11} - z_{12}}$$
$$N_1 = \frac{z_2 - z_{22}}{z_{21} - z_{22}} \qquad N_2 = \frac{z_{21} - z_2}{z_{21} - z_{22}}$$
$$E_1 = \frac{z_3 - z_{32}}{z_{31} - z_{32}} \qquad E_2 = \frac{z_{31} - z_3}{z_{31} - z_{32}}$$

Hence, the T-S fuzzy model for the inverted pendulum can be expressed as:

$$\begin{bmatrix} \dot{x}_1 \\ \dot{x}_2 \\ \dot{x}_3 \\ \dot{x}_4 \end{bmatrix} = \sum_{i=1}^{2}\sum_{j=1}^{2}\sum_{k=1}^{2} M_i N_j E_k \left(\begin{bmatrix} 0 & 0 & 1 & 0 \\ 0 & 0 & 0 & 1 \\ g z_{1i} z_{2j} & 0 & 0 & 0 \\ -magl z_{1i} z_{2j} z_{3l} & 0 & 0 & 0 \end{bmatrix} \begin{bmatrix} x_1 \\ x_2 \\ x_3 \\ x_4 \end{bmatrix} + \begin{bmatrix} 0 \\ 0 \\ -a z_{1i} z_{3l} \\ \frac{4}{3} a l z_{1i} \end{bmatrix} (u + mlx_3^2 \sin(x_1)) \right) \tag{5-48}$$

The fuzzy model derived here is an approximation of the fuzzy model given in Section (2.3.1.2). However, the advantages are (1) the model avoids the unmeasurable state variable x_3 and (2) the number of fuzzy models is reduced to 8 (instead of 16).

The initial conditions for the nonlinear inverted pendulum states and the two PMIOs are selected as follows:

$$System\ initial\ states = [0.5 \quad 0.25 \quad 0.1 \quad 0],$$
$$Actuator\ PMIO = [0.1 \quad 0 \quad 0 \quad 0 \quad 0 \quad 0.5],$$
$$Sensor\ PMIO \quad = [0.2 \quad 0 \quad 0 \quad 0 \quad 0 \quad 0.1],$$

By using the LMI conditions given in *Theorem 5-3*, the following controller gains are computed as:

$$K_{t1} = [-153.12 \quad 899.99 \quad 274.72 \quad 234.74 \quad 199.12],$$
$$K_{t2} = [-263.77 \quad 1509.8 \quad 470.11 \quad 393.25 \quad 338.15],$$
$$K_{t3} = [-148.30 \quad 871.03 \quad 266.61 \quad 229.32 \quad 193.82],$$
$$K_{t4} = [-249.64 \quad 1434.1 \quad 446.26 \quad 376.05 \quad 322.04],$$
$$K_{t5} = [-160.34 \quad 939.39 \quad 288.01 \quad 246.96 \quad 209.14],$$
$$K_{t6} = [-261.44 \quad 1499.3 \quad 467.10 \quad 392.91 \quad 336.87],$$
$$K_{t7} = [-151.25 \quad 905.04 \quad 272.96 \quad 239.39 \quad 199.91],$$
$$K_{t8} = [-252.78 \quad 1447.5 \quad 452.19 \quad 381.65 \quad 326.64],$$

The actuator fault PMIO gains are computed as:

$$\bar{L}_1 = \begin{bmatrix} 17.9719 & 1.3713 & 1.9846 \\ 0.4382 & 2.3846 & 2.5626 \\ 76.5690 & 3.2669 & -10.168 \\ -3.1953 & 3.6966 & 21.8061 \\ 13.2098 & 130.8860 & 880.2527 \\ -35.2113 & 96.9756 & 690.5696 \end{bmatrix}, \bar{L}_2 = \begin{bmatrix} 18.1721 & 2.0073 & 2.1116 \\ 0.4201 & 2.4031 & 2.5281 \\ 77.6079 & 6.3168 & -7.2430 \\ -3.0699 & 3.7913 & 21.7448 \\ 14.2634 & 127.9413 & 872.6894 \\ -35.4459 & 96.1540 & 687.1585 \end{bmatrix},$$

$$\bar{L}_3 = \begin{bmatrix} 18.0598 & 1.7171 & 2.2852 \\ 0.4246 & 2.4510 & 2.5621 \\ 76.0742 & 4.5639 & -8.8825 \\ -3.2354 & 3.7396 & 21.7067 \\ 10.4977 & 137.3737 & 879.9821 \\ -37.8209 & 100.2492 & 689.7086 \end{bmatrix}, \bar{L}_4 = \begin{bmatrix} 18.2172 & 1.7894 & 2.0462 \\ 0.4208 & 2.5173 & 2.5462 \\ 76.8136 & 5.0621 & -7.4982 \\ -2.9777 & 4.1167 & 21.7715 \\ 15.0317 & 142.2631 & 871.7578 \\ -34.7599 & 106.1864 & 686.8007 \end{bmatrix},$$

$$\bar{L}_5 = \begin{bmatrix} 17.7729 & 3.4114 & 3.1023 \\ 0.3812 & 2.6481 & 2.6490 \\ 75.3755 & 11.9369 & -4.5554 \\ -3.6183 & 3.3087 & 20.7544 \\ -4.8801 & 154.4795 & 885.1644 \\ -49.5632 & 100.5654 & 686.2338 \end{bmatrix}, \bar{L}_6 = \begin{bmatrix} 18.2538 & 2.4544 & 2.7427 \\ 0.3831 & 2.7310 & 2.6410 \\ 77.3748 & 7.3975 & -4.1088 \\ -3.3913 & 4.0703 & 20.999 \\ 3.0889 & 176.7167 & 885.3523 \\ -44.5795 & 120.5031 & 689.1834 \end{bmatrix},$$

$$\bar{L}_7 = \begin{bmatrix} 16.7756 & 7.2426 & 4.4806 \\ 0.2255 & 3.0719 & 2.7239 \\ 71.1056 & 27.7907 & 1.3567 \\ -4.3688 & 3.5923 & 20.4463 \\ -39.4969 & 186.4794 & 870.6603 \\ -72.6281 & 108.9144 & 673.5661 \end{bmatrix}, \bar{L}_8 = \begin{bmatrix} 18.5032 & 1.7586 & 4.2823 \\ 0.2445 & 2.9285 & 2.7422 \\ 78.2673 & 4.3304 & 2.0990 \\ -4.1622 & 4.3161 & 21.2635 \\ -29.4008 & 183.7983 & 886.4603 \\ -70.0404 & 127.0138 & 683.1295 \end{bmatrix},$$

The sensor fault PMIO gains are computed as:

$$L_{at1} = \begin{bmatrix} 8.8561 & 0.0000 & -1.0000 & 0.0000 \\ 0.0583 & 26.3257 & -17.3989 & -0.8346 \\ 0.0403 & 0.0056 & 38.4432 & 0.6034 \\ 0.0273 & 313.7855 & -472.2179 & -5.4994 \\ 0.7996 & -1.3776 & 624.8847 & 3.7741 \\ -10.5753 & -0.3445 & -7693.710 & 102.9326 \\ -0.9268 & -0.0173 & -669.9160 & 9.2763 \end{bmatrix},$$

$$L_{at2} = \begin{bmatrix} 8.9054 & 0.0000 & -1.0000 & 0.0000 \\ 0.0551 & 26.3548 & -15.6177 & -0.8135 \\ 0.0402 & -0.0058 & 38.4279 & 0.6034 \\ -0.0479 & 315.0935 & -420.8164 & -4.8203 \\ 0.7991 & -1.7791 & 623.9417 & 3.7787 \\ -10.5595 & 0.3876 & -7692.757 & 102.9250 \\ -0.9264 & 0.0186 & -669.8670 & 9.2762 \end{bmatrix},$$

$$L_{at3} = \begin{bmatrix} 8.9569 & 0.0000 & -1.0000 & 0.0000 \\ 0.0592 & 26.3529 & -17.3660 & -0.8349 \\ 0.0401 & 0.0056 & 38.4443 & 0.6035 \\ 0.0451 & 313.4076 & -471.4646 & -5.5172 \\ 0.7969 & -1.2712 & 624.9500 & 3.7821 \\ -10.5696 & -0.3488 & -7693.815 & 102.9202 \\ -0.9268 & -0.0174 & -669.9162 & 9.2763 \end{bmatrix},$$

$$L_{at4} = \begin{bmatrix} 9.0106 & 0.0000 & -1.0000 & 0.0000 \\ 0.0561 & 26.3829 & -15.5830 & -0.8139 \\ 0.0402 & -0.0058 & 38.4290 & 0.6036 \\ -0.0340 & 314.7410 & -420.0204 & -4.8382 \\ 0.8037 & -1.6927 & 624.0101 & 3.7866 \\ -10.5654 & 0.3909 & -7692.857 & 102.9130 \\ -0.9265 & 0.0187 & -669.8669 & 9.2762 \end{bmatrix},$$

$$L_{at5} = \begin{bmatrix} 9.0665 & 0.0000 & -0.9999 & 0.0000 \\ 0.0631 & 26.3867 & -16.2456 & -0.8247 \\ 0.0369 & 0.0017 & 37.9769 & 0.6016 \\ 0.2401 & 314.5361 & -436.8190 & -5.6124 \\ 0.6407 & -1.5188 & 609.2364 & 4.0280 \\ -9.7519 & -0.0293 & -7452.754 & 108.7210 \\ -0.9038 & -0.0058 & -663.3437 & 9.4357 \end{bmatrix},$$

$$L_{at6} = \begin{bmatrix} 9.1249 & 0.0000 & -0.9999 & 0.0000 \\ 0.0629 & 26.4071 & -15.3790 & -0.8194 \\ 0.0368 & -0.0018 & 37.9732 & 0.6018 \\ 0.2401 & 315.2448 & -411.0081 & -5.4271 \\ 0.6404 & -1.4584 & 609.0040 & 4.0392 \\ -9.7425 & 0.0493 & -7452.599 & 108.7191 \\ -0.9037 & 0.0064 & -663.3252 & 9.4358 \end{bmatrix},$$

$$L_{at7} = \begin{bmatrix} 9.1858 & 0.0000 & -0.9999 & 0.0000 \\ 0.0641 & 26.4181 & -16.2051 & -0.8252 \\ 0.0367 & 0.0018 & 37.9796 & 0.6019 \\ 0.2589 & 314.3297 & -435.9555 & -5.6423 \\ 0.6404 & -1.4191 & 609.4206 & 4.0507 \\ -9.7476 & -0.0309 & -7452.672 & 108.7178 \\ -0.9038 & -0.0058 & -663.3404 & 9.4360 \end{bmatrix},$$

$$L_{at8} = \begin{bmatrix} 9.2493 & 0.0000 & -0.9999 & 0.0000 \\ 0.0640 & 26.4398 & -15.3393 & -0.8200 \\ 0.0366 & -0.0018 & 37.9759 & 0.6021 \\ 0.2597 & 315.0702 & -410.1786 & -5.4605 \\ 0.6399 & -1.3767 & 609.1952 & 4.0629 \\ -9.7381 & 0.0514 & -7452.503 & 108.7162 \\ -0.9036 & 0.0065 & -663.3215 & 9.4361 \end{bmatrix},$$

The corresponding attenuation coefficients are $\gamma_t = 1.5812$ and $\gamma_{pmi} = 1.032$.

In this simulation subsection, the additive actuator fault signal affects the nonlinear system in the same direction as $u(t)$ and the additive sensor fault signal affects the measured cart velocity (x_4). The proposed actuator and sensor fault signals and their estimates are given in Figure 5-7. Both signals have been selected so that their slope differs with time in order to clarify the fault estimation accuracy of each PMIO.

In a similar manner to the simulation results given in Figure 5-3, here the estimation accuracy shown in Figure 5-7 is obtained provided that the two simultaneous faults are estimated and compensated online. For example, if the sensor fault has not been compensated or equivalently the PIO is used instead of the proposed PMIO the actuator and sensor fault estimation accuracy will degrade, as shown in Figure 5-8 for different scenarios.

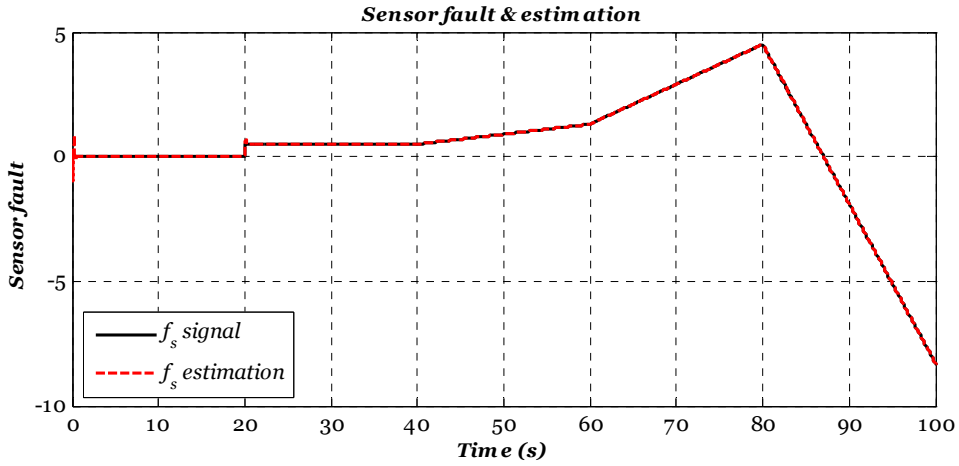

(a)

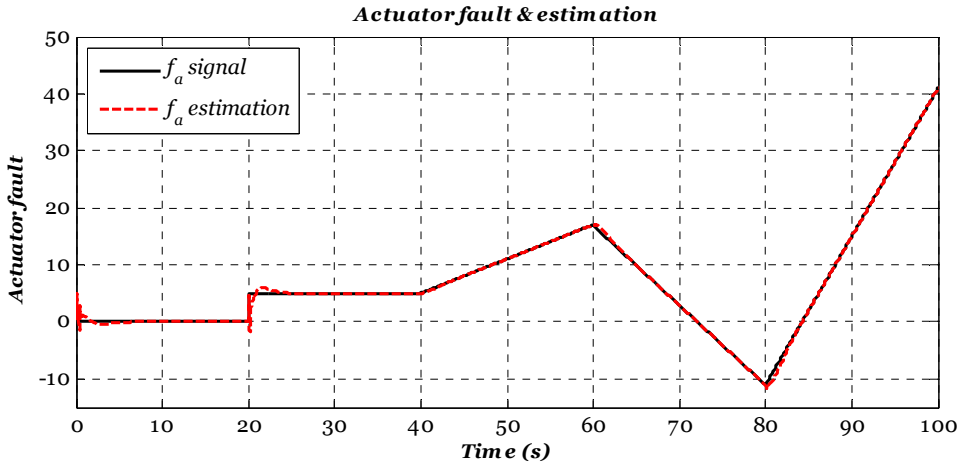

(b)

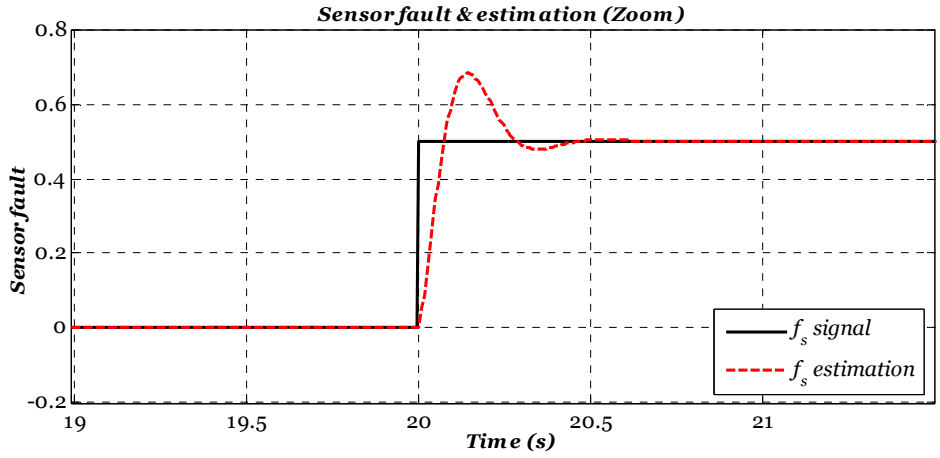

(c)

Figure 5-7: Faults and their estimates: (a) sensor fault, (b) Actuator fault, and (c) zoomed sensor fault estimation

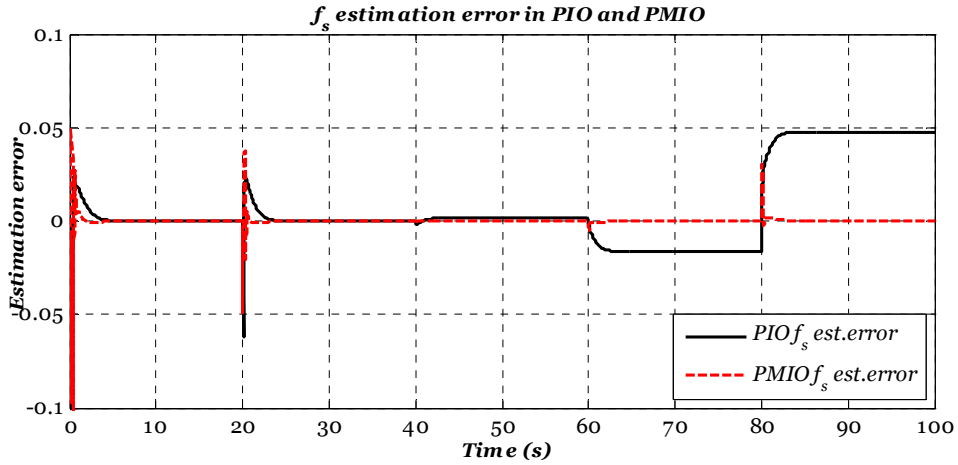

(a)

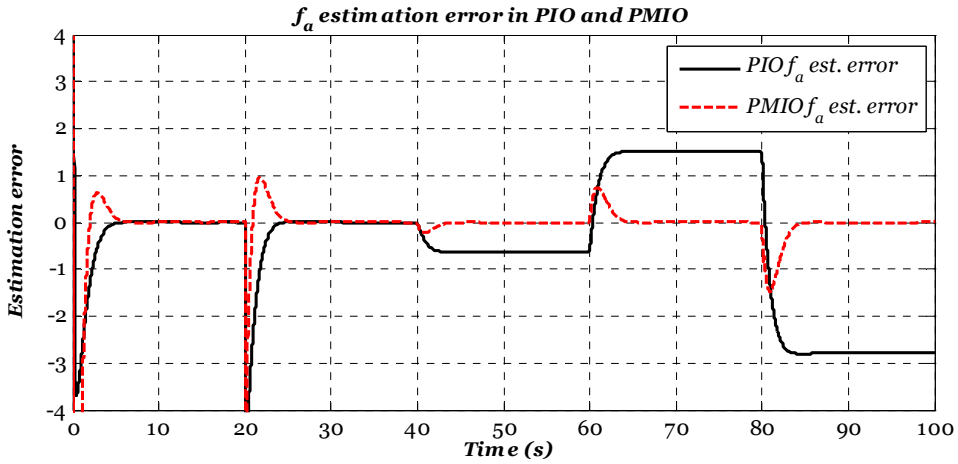

(b)

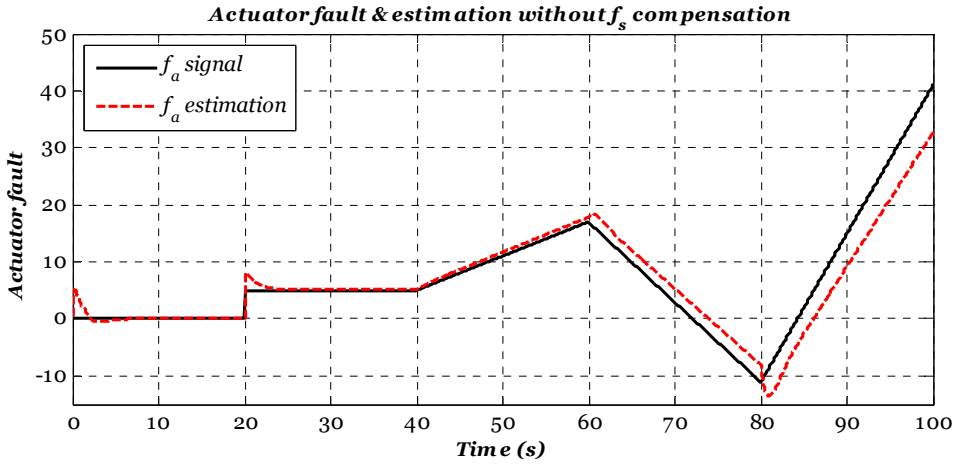

(c)

Figure 5-8: The advantage of PMIO over PIO for (a) actuator fault estimation, (b) sensor fault estimation, and (c) inaccurate actuator fault estimation due to the uncompensated sensor fault.

Moreover, the effect of the uncompensated simultaneous actuator and sensor fault signals on tracking performance is shown in Figure 5-9. The uncompensated fault signals cause the fuzzy controller to deviate away from the nominal system behaviour, so that there is a loss of ability to drive the tracking error to zero.

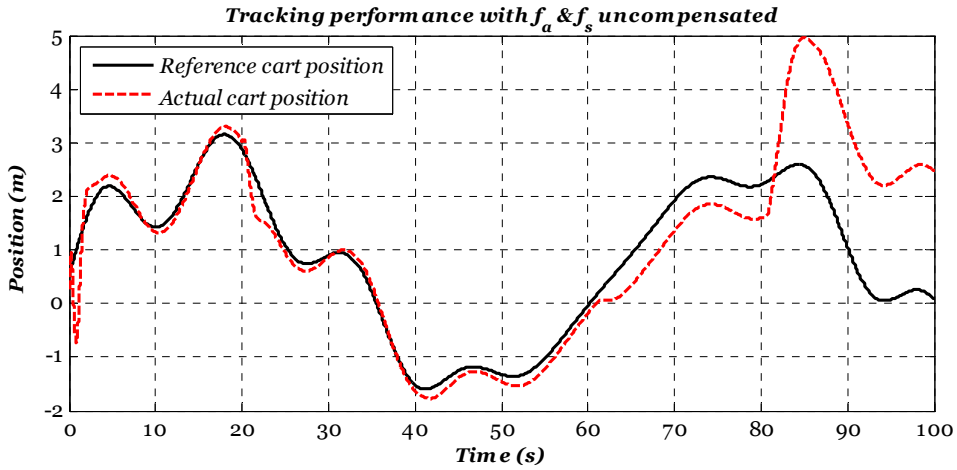

Figure 5-9: The effect of uncompensated actuator and sensor faults on tracking performance

By using the estimation provided by the two PMIOs, simultaneous faults can be compensated online and the nominal system behaviour maintained. Figure 5-10 shows the tracking performance with online fault compensation.

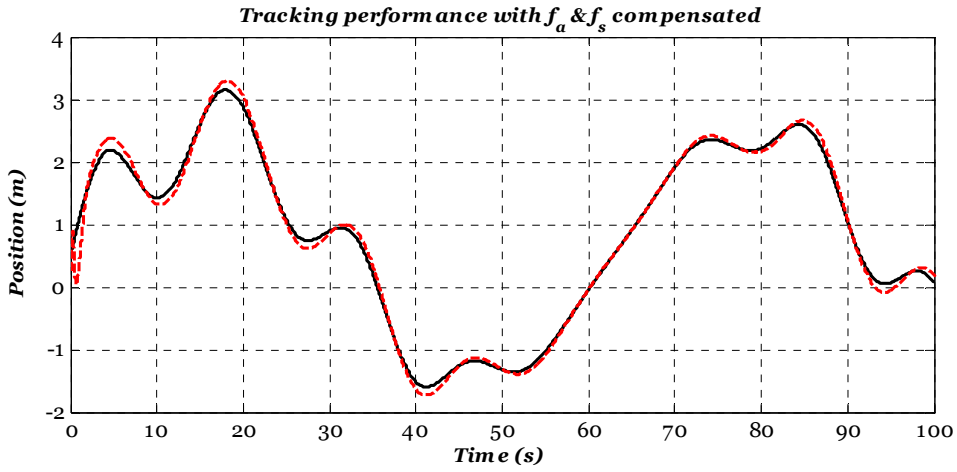

Figure 5-10: Tracking performance with actuator and sensor faults compensated

5-4. Conclusions

In this Chapter, an LMI-based design for simultaneous actuator and sensor AFTC of nonlinear systems has been presented for both tracking and regulator control problem within T-S fuzzy framework.

Results show that the proposed T-S fuzzy simultaneous actuator and sensor AFTC strategy has the capability to take into account some of the most challenging cases of AFTC. (1) It can maintain the closed-loop system performance and keep the nominal controller unchanged even in cases for which the sensor and actuator faults affect the system simultaneously. (2) It can overcome the effects of time-varying actuator and/or sensor faults with bounded q^{th} time derivative using the concept of fault estimation and compensation. (3) The proposed interaction between the dedicated observers enhances the robustness of each of the actuator and sensor fault estimation signals against the alternative fault. Furthermore, the limitation of using an iterative form of static output feedback control design is obviated completely. These factors represent significant contributions to the development of the subject of AFTC.

The main challenge that has arisen in this proposed method is need to recover the *separation principle* (see page 116). Although the model uncertainty has not been considered in this Chapter, the separation principle still represents the main challenge for the use of T-S fuzzy observer-based methods even when the controller and observer can be designed separately. There is no guarantee to ensure that the observer dynamics can be faster than controller dynamics because of the global stability constraints, i.e. the controller and the observer eigenvalues cannot be assigned freely in the stable complex plane. It thus follows that the separation principle cannot be recovered within a T-S fuzzy observer-based state estimate feedback framework. This fact motivates the proposal, in Chapter 6 for a more general way to overcome this limitation in the light of the architecture proposed in this Chapter.

Chapter 6 : Simultaneous actuator and sensor fault tolerant TSDOFC of nonlinear systems[2]

6-1. Introduction

The goal of this Chapter is to describe a novel FTTC strategy based on robust fault estimation and compensation of simultaneous actuator and sensor faults. The strategy provides an enhancement to the fuzzy PMIO based state feedback proposed in Chapter 5. This works by decoupling the dependence of the controller on the state estimates. Based on the investigation introduced in Chapter 3, within the framework of FTC the challenge is to develop an FTTC design strategy for nonlinear systems to tolerate actuator and sensor faults. Hence, only the tracking control problem is considered in this Chapter using the architecture proposed in Chapter 5. The proposed strategy involves the design of (i) a TSDOFC responsible for minimizing the tracking error between the reference and system output signals during nominal operation, and (ii) two T-S fuzzy PPIOs dedicated to provide separate estimates of the actuator and sensor faults for the purpose of fault compensation. The main contributions of this Chapter compared with the literature are:

1. A proposal for an LMI-based design for FTTC of nonlinear systems affected by simultaneous actuator and sensor faults using the estimation and compensation concept.
2. A proposal for an LMI-based design of robust T-S fuzzy PPIO for both the actuator and sensor fault cases. Each of the T-S estimators are available separately with an important consequence on robust L_2 norm fault estimation, as well as on the use of the estimation and compensation concept to enhance the robustness of the T-S fuzzy PPIO against simultaneous actuator and sensor faults.

---

[2]Part of the work (only sensor fault) presented in this chapter has been published in:

Sami, M. & Patton, R. J. 2012c. Fault tolerant output feedback tracking control for nonlinear systems via T-S fuzzy modelling. 8th IFAC Symposium on Fault Detection, Supervision and Safety of Technical Processes, Mexico City, Mexico, 999-1004. 29-31 Aug.

The whole material presented in this Chapter has been submitted to the Int. J. of Adapt. Control and Signal Processing.

The non-linear inverted pendulum example with time-varying cart position reference is used to illustrate the proposed FTTC strategy. Both additive and parametric fault scenarios are considered for simultaneous actuator and sensor faults. The tracking system is introduced (a) to induce significant non-linearity in the inverted pendulum system and (b) to confirm the importance of tolerance to sensor faults in this type of control problem.

The Chapter is organized as follows. In Section 6-2 the problem description and motivation are defined. Section 6-3 presents the LMI-based design of the actuator fault fuzzy PPIO, the sensor fault PPIO, and the TSDOFC. In Section 6-4 the design approach is tested via the nonlinear inverted pendulum example. Finally, Section 6-5 concludes the Chapter.

6-2. Problem description and motivation

The T-S fuzzy controller and T-S fuzzy observer designs are model-based design methods and hence the first design step is the derivation of the fuzzy model via the methods presented in Section 2-3. In the fuzzy control design, each "control rule" is designed from the corresponding rule of a T-S fuzzy model and the fuzzy controller design problem is to determine the local feedback gains within a *parallel distributed compensation* structure (Tanaka and Wang, 2001). Although the fuzzy controller is constructed using the local design structure, the feedback gains should be determined using global design conditions. It is reported in (Tanaka and Wang, 2001) that for the fuzzy state estimate feedback "*the global design conditions are needed to guarantee the global stability and control performance*". Hence, the fuzzy control designer does not have freedom to assign the local system closed-loop poles anywhere in the stable complex plane. Therefore, the observer-based T-S state feedback control system suffers a major drawback in that the observer dynamics may not be assigned freely to satisfy closed-loop performance requirements.

This inherited problem of T-S the fuzzy observer-based state feedback control method motivates us to introduce this Chapter in which the control strategy presented in Chapter 5 has been modified in order to completely decouple the controller design from the redundant observers. The TSDOFC is proposed in this strategy to overcome the limitation of T-S observer-based state feedback control.

6-3. The proposed fuzzy AFTTC strategy

This Section describes the proposed strategy for active actuator and sensor fault tolerant TSDOFC. The TSDOFC is designed to force specific outputs to follow a given reference input (in both faulty and fault-free cases) with robustness against exogenous inputs/outputs (actuator/sensor fault estimation error). The T-S PPIOs are used as a form of analytical redundancy responsible for robustly compensating the effects of actuator and sensor faults from the system inputs and outputs and hence ensure the robustness of the overall closed-loop system. This strategy can be considered as a "fault-hiding" approach to FTTC where the main aim of fault-hiding is to maintain the same controller in both faulty and fault-free system cases.

The design problem is formulated via LMI with the ability to govern the performance of controller and observers separately by assigning their eigenvalues in specific LMI region of the complex plan. Moreover, the observers are capable of sufficiently estimating fast and time varying actuator and/or sensor fault scenarios with bounded first order time derivatives. The schematic diagram shown in Figure 6-1 illustrates the proposed strategy.

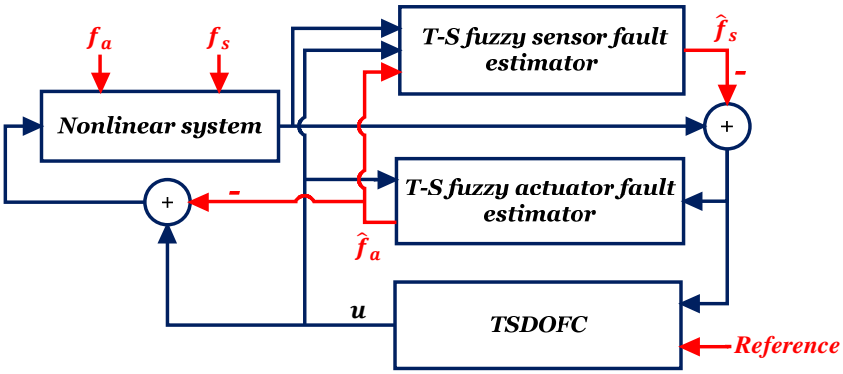

Figure 6-1: Active actuator and sensor FTC scheme

6-3-1. PPIO based sensor fault estimation

Consider a T-S fuzzy model with actuator and sensor fault signals described as follows:

$$\left.\begin{aligned} \dot{x} &= A(p)x + B(p)u + E(p)f_a \\ y &= Cx + D_f f_s \end{aligned}\right\} \qquad (6\text{-}1)$$

$A(p) \in \mathcal{R}^{n*n}(= \sum_{i=1}^{r} h_i(p)A_i)$, $B(p) \in \mathcal{R}^{n*m}(= \sum_{i=1}^{r} h_i(p)B_i)$, $E(p) \in \mathcal{R}^{n*f}(= \sum_{i=1}^{r} h_i(p)E_i)$, $C \in \mathcal{R}^{l*n}$, and $D_f \in R^{l*g}$ are the known system matrices, $f_s \in R^g$, and

$f_a \in R^f$ are sensor and actuator faults, respectively. r is the number of fuzzy rules and the term $h_i(p)$ is the weighting function that depends on the measured premise variable (p).

To avoid the direct multiplication of the sensor and/or noise by the observer gain, an augmented system state with output filter states is constructed (Tan and Edwards, 2003). The filtered output is given as follows:

$$\dot{x}_s = -A_s x_s + A_s C x + A_s D_f f_s \tag{6-2}$$

where $-A_s \in R^{l*l}$ is a stable matrix. The augmented state system is given as:

$$\left.\begin{aligned} \dot{\bar{x}} &= \bar{A}(p)\bar{x} + \bar{B}(p)u + \bar{E}(p)f_a + \bar{D}_f f_s \\ \bar{y} &= \bar{C}\,\bar{x} \end{aligned}\right\} \tag{6-3}$$

$$\bar{A}(p) = \begin{bmatrix} A(p) & 0 \\ A_s C & -A_s \end{bmatrix};\ \bar{x} = \begin{bmatrix} x \\ x_s \end{bmatrix};\ \bar{B}(p) = \begin{bmatrix} B(p) \\ 0 \end{bmatrix}$$

$$\bar{E}(p) = \begin{bmatrix} E(p) \\ 0 \end{bmatrix}\ \bar{D}_f = \begin{bmatrix} 0 \\ A_s D_f \end{bmatrix};\ \bar{C} = [0 \quad I_l]$$

As illustrated in Figure 6-1 the proposed control strategy requires the estimation of the fault effects on the closed-loop system. To ensure the ability to deal with time-varying fault scenarios for which the first time derivative of each fault is assumed bounded, the T-S fuzzy PPIO presented in Section 4-4 is used.

Assume that the signal $(\dot{f}_s)$ is bounded. Then the following fuzzy observer is proposed to simultaneously estimate the system states and the sensor fault:

$$\left.\begin{aligned} \dot{\hat{\bar{x}}} &= \bar{A}(p)\hat{\bar{x}} + \bar{B}(p)u + \bar{E}(p)\hat{f}_a + \bar{D}_f\hat{f}_s + \bar{L}(p)(\bar{C}\bar{x} - \bar{C}\hat{\bar{x}}) \\ \dot{\hat{f}}_s(t) &= F_s(p)\bar{C}(\dot{e}_x + e_x) \end{aligned}\right\} \tag{6-4}$$

where $\hat{\bar{x}} \in \mathcal{R}^{n+l}$ is state estimation vector $\bar{x}$, $\hat{f}_a$ is the actuator fault estimate delivered by another PPIO dedicated for actuator fault estimation, $\bar{L}(p) \in \mathcal{R}^{(n+l)\times l}$ and $F_s(p) \in \mathcal{R}^{g\times l}$ are the observer gains to be designed, and e_x is the state estimation error defined as:

$$e_x = \bar{x} - \hat{\bar{x}} \tag{6-5}$$

Remark: The T-S fuzzy PPIO proposed in Eq. (6-4) introduce an advantageous modification to the T-S fuzzy PPIO given in Section 4-4 by feeding the actuator fault estimation signal into the sensor fault T-S fuzzy PPIO in order to ensure the robustness against actuator faults.

Clearly, the augmented system is observable provided that the original system is observable. This is easily proved from the observability condition:

$$rank\begin{bmatrix} sI - A & 0 \\ A_s C & sI + A_s \\ 0 & I \end{bmatrix} = n + l \quad , \forall s \in \mathbb{C}$$

Additionally, the rank condition ($rank(\bar{C}\bar{D}_f) = g$) is also achieved since $\bar{C}\bar{D}_f = A_s D_f$ and A_s is invertible, then $rank(\bar{C}\bar{D}_f) = rank(A_s D_f) = g$.

The state estimation error dynamics are obtained by subtracting Eq. (6-4) from Eq. (6-3) to yield:

$$\dot{e}_x = (\bar{A}(p) - \bar{L}(p)\bar{C})e_x + \bar{D}_f e_{f_s} + \bar{E}(p)e_{f_a} \tag{6-6}$$

Let $e_{f_s} \in \mathcal{R}^g$ and $e_{f_a} \in \mathcal{R}^f$ are the sensor and actuator faults estimation errors defined as:

$$\left.\begin{aligned} e_{f_s} &= f_s - \hat{f}_s \\ e_{f_a} &= f_a - \hat{f}_a \end{aligned}\right\} \tag{6-7}$$

Using Eqs. (6-4), (6-6), &(6-7) the fault estimation error dynamics are as follows:

$$\dot{e}_{f_s} = \dot{f}_s - F_s(p)\bar{C}(\bar{A}(p) - \bar{L}(p)\bar{C} + I)e_x - F_s(p)\bar{C}\bar{D}_f e_{f_s} - F_s(p)\bar{C}\bar{E}(p)e_{f_a} \tag{6-8}$$

The augmented state estimator will then be of the following form:

$$\dot{\tilde{e}}_a(t) = \tilde{A}(p,p)\tilde{e}_a + \tilde{N}(p,p)\tilde{z} \tag{6-9}$$

where:

$$\tilde{A}(p,p) = \begin{bmatrix} \bar{A}(p) - \bar{L}(p)\bar{C} & \bar{D}_f \\ -F_s(p)\bar{C}(\bar{A}(p) - \bar{L}(p)\bar{C} + I) & -F_s(p)\bar{C}\bar{D}_f \end{bmatrix}, \tilde{e}_a = \begin{bmatrix} e_x \\ e_{f_s} \end{bmatrix}$$

$$\tilde{N}(p,p) = \begin{bmatrix} \bar{E}(p) & 0 \\ -F_s(p)\bar{C}\bar{E}(p) & I \end{bmatrix}, \tilde{z} = \begin{bmatrix} e_{f_a} \\ \dot{f}_s \end{bmatrix}$$

The objective now is to compute the gains $\bar{L}(p)$ and $F_s(p)$ such that the effect of exogenous input $\tilde{z}$ on the estimation error is attenuated below the level γ_s to ensure

robust estimation performance. The location of the closed-loop system poles affects the estimation transient response. Hence, the sensor fault observer can be designed to constrain the estimation error system eigenvalues to lie globally in a complex region. This is defined by merging different eigenvalue constraints to produce a $\mathcal{D}(\rho, \alpha, \beta, \theta)$ LMI region in which the vertical line at ρ bounds the stability region. α and β are the radius and centre of the disc region, and θ is the angle of the sector of the α and β circle. The design requirement for the fuzzy augmented system in Eq. (6-9) is given in the following Theorem.

Theorem 6-1: *The eigenvalues of the estimation error dynamics are located in a LMI region in the complex plane defined by (α, β, ρ, θ), and the error dynamics are stable and the H_∞ performance is guaranteed with an attenuation level γ_s, (provided that the signal ($\tilde{z}$) is bounded), if there exist a SPD matrix P_1, matrices $\bar{H}_i, F_{si}$, and scalar parameters μ, α, β, ρ, and θ satisfying the following LMI constraints:*

Minimize (γ_s) such that:

$$\left.\begin{gathered} \Sigma_i + \Sigma_i^T + 2\rho\bar{P} < 0 \\ \begin{bmatrix} -\alpha\bar{P} & \beta\bar{P} + \Sigma_i \\ (\beta\bar{P} + \Sigma_i)^T & -\alpha\bar{P} \end{bmatrix} < 0 \\ \begin{bmatrix} sin(\theta)\,[\Sigma_i + \Sigma_i^T] & cos(\theta)\,[\Sigma_i + \Sigma_i^T] \\ cos(\theta)\,[\Sigma_i + \Sigma_i^T] & sin(\theta)\,[\Sigma_i + \Sigma_i^T] \end{bmatrix} < 0 \end{gathered}\right\} \tag{6-10}$$

$$\begin{bmatrix} \Psi_{11} & \Psi_{12} & \Psi_{13} & 0 & C_{p1}^T & 0 \\ * & \Psi_{22} & \Psi_{23} & I & 0 & C_{p2}^T \\ * & * & -\gamma_s I & 0 & 0 & 0 \\ * & * & * & -\gamma_s I & 0 & 0 \\ * & * & * & * & -\gamma_s I & 0 \\ * & * & * & * & * & -\gamma_s I \end{bmatrix} < 0 \tag{6-11}$$

$\bar{L}(p) = P_1^{-1}\bar{H}(p)$, $\Psi_{11} = P_1\bar{A}(p) + \left(P_1\bar{A}(p)\right)^T - \bar{H}(p)\bar{C} - (\bar{H}(p)\bar{C})^T$

$\Psi_{12} = -(\bar{A}^T(p)P_1\bar{D}_f - \bar{C}^T\bar{H}^T(p)\bar{D}_f)$

$\Psi_{13} = P_1\bar{E}(p)$, $\Psi_{22} = -2\bar{D}_f{}^T P_1\bar{D}_f$, $\Psi_{23} = -\bar{D}_f{}^T P_1\bar{E}(p)$

$$\Sigma_i = \bar{P}\tilde{A}(p,p) = \begin{bmatrix} P_1\bar{A}(p) - \bar{H}(p)\bar{C} & P_1\bar{D}_f \\ -\left(\bar{A}^T(p)P_1\bar{D}_f - \bar{C}^T\bar{H}^T(p)\bar{D}_f + \bar{D}_f{}^T P_1\right)^T & -\bar{D}_f{}^T P_1\bar{D}_f \end{bmatrix}$$

Proof: Let the performance output be defined as follows:

$$\tilde{e}_p = \bar{C}_p\, \tilde{e}_a \text{ where } \bar{C}_p = \begin{bmatrix} C_{p1} & 0 \\ 0 & C_{p2} \end{bmatrix}$$

$C_{p1} \in \mathcal{R}^{k*n+l}$ and $C_{p2} \in \mathcal{R}^{g*g}$. The estimation performance objective can be presented as:

$$\frac{\|\tilde{e}_p\|_2}{\|\tilde{z}\|_2} \leq \gamma_s = \frac{1}{\gamma_s}\int_0^\infty \tilde{e}_a^T\, \bar{C}_p^T \bar{C}_p \tilde{e}_a dt - \gamma_s \int_0^\infty \tilde{z}^T\, \tilde{z}\, \leq 0 \tag{6-12}$$

To achieve the required performance (6-12) and the stability of the augmented system (6-9) the following inequality should hold:

$$\dot{v}(\tilde{e}_a) + \frac{1}{\gamma_s}\tilde{e}_p^T \bar{C}_p^T \bar{C}_p \tilde{e}_p - \gamma_s \tilde{z}^T \tilde{z} < 0 \tag{6-13}$$

where $\dot{v}(\tilde{e}_a)$ is the derivative of candidate Lyapunov function ($v(\tilde{e}_a) = \tilde{e}_a^T\, \bar{P}\, \tilde{e}_a$) in terms of Eq. (6-9). Inequality (6-13) can now be re-written as:

$$\dot{v}(\tilde{e}_a) = \tilde{e}_a^T \left(\tilde{A}^T(p,p)\bar{P}\, + \bar{P}\tilde{A}(p,p)\right)\tilde{e}_a + \, \tilde{e}_a^T \bar{P}\widetilde{N}(p,p)\tilde{z} + \tilde{z}^T \widetilde{N}^T(p,p)\bar{P}\tilde{e}_a \tag{6-14}$$

By using (6-14), and the Schur Complement Theorem, then the inequality (6-13) implies that the following inequality must hold:

$$\begin{bmatrix} \tilde{A}^T(p,p)\bar{P}\, + \bar{P}\tilde{A}(p,p) & \bar{P}\widetilde{N}(p,p) & \bar{C}_{p1}^T & 0 \\ * & -\gamma_s I & 0 & \bar{C}_{p2}^T \\ * & * & -\gamma_s I & 0 \\ * & * & * & -\gamma_s I \end{bmatrix} < 0 \tag{6-15}$$

To conform to the format of (6-9) $\bar{P}$ is structured as follows:

$$\bar{P} = \begin{bmatrix} P_1 & 0 \\ 0 & I \end{bmatrix} > 0 \tag{6-16}$$

By substituting the corresponding values of $\bar{P}, \tilde{A}(p,p)$, $\widetilde{N}(p,p)$ and using the variable change $\bar{H}(p) = P_1 \bar{L}(p)$, and the equality:

$$F_s(p)\bar{C} = \bar{D}_f{}^T P_1 \tag{6-17}$$

The LMI in (6-11) is obtained.

Remark: Eq. (6-17) can be approximated by the following convex optimization problem (Zhang, Jiang and Cocquempot, 2008):

$minimise\ \mu\ such\ that$

$$\begin{bmatrix} \mu I & \bar{D}_f{}^T P_1 - F_s(p)\bar{C} \\ * & \mu I \end{bmatrix} > 0 \tag{6-18}$$

To prove the validity of the LMI (6-10), the following Lemma is presented first.

Lemma 1 (Chilali and Gahinet, 1996): The matrix $\mathcal{A}$ is $\mathcal{D}(\rho,\alpha,\beta,\theta)$-stable if and only if there exists a symmetric matrix $\mathcal{X} > 0$ such that:

$$\left.\begin{array}{c} \mathcal{A}\mathcal{X} + (\mathcal{A}\mathcal{X})^{\mathrm{T}} + 2\rho\mathcal{X} < 0 \\ \begin{bmatrix} -\alpha\mathcal{X} & \beta\mathcal{X} + \mathcal{A}\mathcal{X} \\ \beta\mathcal{X} + (\mathcal{A}\mathcal{X})^{\mathrm{T}} & -\alpha\mathcal{X} \end{bmatrix} < 0 \\ \begin{bmatrix} \sin(\theta)\,[\mathcal{A}\mathcal{X} + (\mathcal{A}\mathcal{X})^{\mathrm{T}}] & \cos(\theta)\,[\mathcal{A}\mathcal{X} - (\mathcal{A}\mathcal{X})^{\mathrm{T}}] \\ \cos(\theta)\,[\mathcal{A}\mathcal{X} - (\mathcal{A}\mathcal{X})^{\mathrm{T}}] & \sin(\theta)\,[\mathcal{A}\mathcal{X} + (\mathcal{A}\mathcal{X})^{\mathrm{T}}] \end{bmatrix} < 0 \end{array}\right\} \tag{6-19}$$

Hence, via the use of Lemma 1, the estimator gains can be designed to constrain the eigenvalues to lie globally in a complex stable region defined by merging different eigenvalue constraints to produce a $\mathcal{D}(\rho,\alpha,\beta,\theta)$ LMI region (see Figure 6-2).

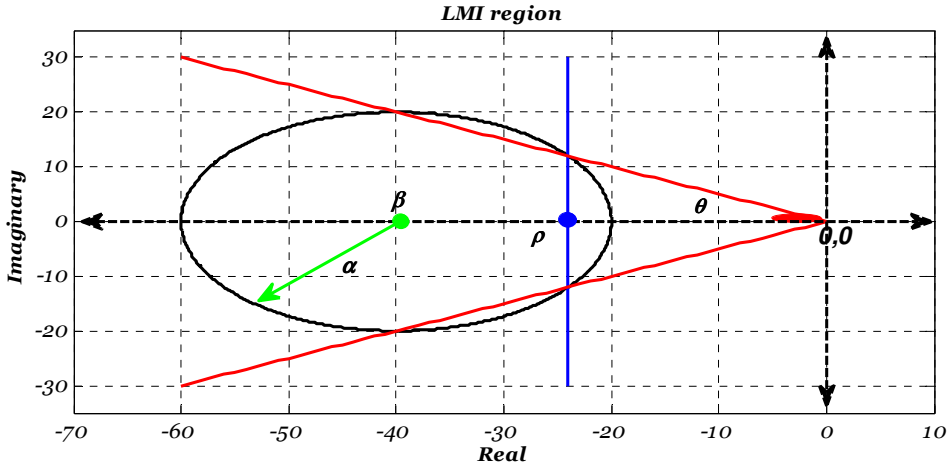

Figure 6-2: An LMI region

To ensure the convenience of the LMI constraints given in Lemma 1 with the constraints given in *Theorem 6-1*, inequalities (6-19) can be rewritten in the following equivalent form:

$$\left.\begin{array}{c} \mathbb{X}\mathcal{A} + (\mathbb{X}\mathcal{A})^{\mathrm{T}} + 2\rho\mathbb{X} < 0 \\ \begin{bmatrix} -\alpha\mathbb{X} & \beta\mathbb{X} + \mathbb{X}\mathcal{A} \\ \beta\mathbb{X} + (\mathbb{X}\mathcal{A})^{\mathrm{T}} & -\alpha\mathbb{X} \end{bmatrix} < 0 \\ \begin{bmatrix} \sin(\theta)\,[\mathbb{X}\mathcal{A} + (\mathbb{X}\mathcal{A})^{\mathrm{T}}] & \cos(\theta)\,[\mathbb{X}\mathcal{A} - (\mathbb{X}\mathcal{A})^{\mathrm{T}}] \\ \cos(\theta)\,[\mathbb{X}\mathcal{A} - (\mathbb{X}\mathcal{A})^{\mathrm{T}}] & \sin(\theta)\,[\mathbb{X}\mathcal{A} + (\mathbb{X}\mathcal{A})^{\mathrm{T}}] \end{bmatrix} < 0 \end{array}\right\} \quad (6\text{-}20)$$

where $\mathbb{X}$ is a SPD matrix.

Proof: By using the Congruence Lemma referred to in Section 3-2, pre and post multiply the first LMI of (6-19) by $\mathcal{X}^{-1}$, pre and post multiply the remaining two constraints by $\mathrm{diagonal}(\mathcal{X}^{-1}, \mathcal{X}^{-1})$. Hence, the LMI constraints (6-20) are obtained after using the variable change $\mathbb{X} = \mathcal{X}^{-1}$. This completes the proof.

The observer eigenvalues are assigned using the matrix inequalities given in (6-20) by using the following change of variables:

$$\mathbb{X} = \bar{P} = \begin{bmatrix} P_1 & 0 \\ 0 & I \end{bmatrix},\ \mathcal{A} = \tilde{A}(p,p)$$

where $\tilde{A}(p,p)$ is defined in Eq. (6-9), the inequalities of (6-10) can be easily obtained. This completes the proof of *Theorem 6-1*.

6-3-2. T-S PPIO based actuator fault estimate

This subsection considers the actuator fault estimator design, the observer delivered by the corrected (sensor fault compensated) output and the corresponding control signals (see Figure 6-1). The system given in Eq. (6-1) becomes:

$$\left.\begin{array}{l} \dot{x} = A(p)x + B(p)u + E(p)f_a \\ y = Cx + D_f e_{f_s} \end{array}\right\} \quad (6\text{-}21)$$

Based on same arguments given in *Section 5-2-3*, the T-S fuzzy PPIO is also used for estimating the actuator fault.

Assume that the first time derivative of the actuator fault ($\dot{f}_a$) and the sensor fault estimation error (e_{f_s}) are bounded. Then the following T-S fuzzy observer is proposed to simultaneously estimate the system states and actuator fault:

$$\left.\begin{aligned}\dot{\hat{x}} &= A(p)\hat{x} + B(p)u + E(p)\hat{f}_a + L_a(p)\big(Cx + D_f e_{f_s} - C\hat{x}\big)\\ \dot{\hat{f}}_a(t) &= F_a(p)C(\dot{e}_x + e_x)\end{aligned}\right\} \tag{6-22}$$

where $\hat{x} \in \mathcal{R}^n$ is the estimation of the state vector x, $L_a(p) \in \mathcal{R}^{n\times l}$, and $F_a(p) \in \mathcal{R}^{m\times l}$ are the observer gains to be designed, and e_x is the state estimation error. The state estimation error dynamics are then:

$$\dot{e}_x = (A(p) - L_a(p)C)e_x + E(p)e_{f_a} - L_a(p)D_f e_{f_s} \tag{6-23}$$

Using (6-21) and (6-22) the actuator fault estimation error dynamics are as follows:

$$\begin{aligned}\dot{e}_{f_a} = \dot{f}_a &- F_a(p)C(A(p) - L_a(p)C + I)e_x - F_a(p)CE(p)e_{f_a}\\ &+ F_a(p)CL_a(p)D_f e_{f_s}\end{aligned} \tag{6-24}$$

The augmented estimator will then be of the following form:

$$\dot{\tilde{e}}_a(t) = \tilde{A}(p,p)\tilde{e}_a + \tilde{N}(p,p)\tilde{z} \tag{6-25}$$

$$\tilde{A}(p,p) = \begin{bmatrix} A(p) - L_a(p)C & E(p) \\ -F_a(p)C(A(p) - L_a(p)C + I) & -F_a(p)CE(p)\end{bmatrix}$$

$$\tilde{e}_a = \begin{bmatrix} \mathrm{e_x} \\ e_{f_a}\end{bmatrix}, \tilde{N}(p,p) = \begin{bmatrix} -L_a(p)D_f & 0 \\ F_a(p)CL_a(p)D_f & I\end{bmatrix}, \tilde{z} = \begin{bmatrix} e_{f_s} \\ \dot{f}_a\end{bmatrix}$$

The objective now is to compute the gains $L_a(p)$ and $F_a(p)$ such that exogenous input $\tilde{z}$ in (6-25) are attenuated below the desired level γ_a to ensure robust estimation performance, in addition to locating the observer poles within a specified LMI region.

Theorem 6-2*: The eigenvalues of the estimation error are located in a disc region in the complex plane defined by (α_a, β_a, ρ_a, θ_a), and the error dynamics are stable and the H_∞ performance is guaranteed with an attenuation level γ_a, (provided that the signal ($\tilde{z}$) is bounded), if there exist SPD matrices P_{a1}, matrices H_{ai},F_{ai}, and scalar parameters μ_a, α_a, ρ_a, θ_a, and β_a satisfying the following LMI constraints:*

Minimize (γ_a) such that:

$$\left.\begin{gathered} \Sigma_{ai} + \Sigma_{ai}^T + 2\rho_a \bar{P}_a < 0 \\ \begin{bmatrix} -\alpha_a \bar{P}_a & \beta_a \bar{P}_a + \Sigma_{ai} \\ (\beta_a \bar{P}_a + \Sigma_{ai})^T & -\alpha_a \bar{P}_a \end{bmatrix} < 0 \\ \begin{bmatrix} sin(\theta_a)\,[\Sigma_{ai} + \Sigma_{ai}^T] & cos(\theta_a)\,[\Sigma_{ai} + \Sigma_{ai}^T] \\ cos(\theta_a)\,[\Sigma_{ai} + \Sigma_{ai}^T] & sin(\theta_a)\,[\Sigma_{ai} + \Sigma_{ai}^T] \end{bmatrix} < 0 \end{gathered}\right\} \quad (6\text{-}26)$$

$$\begin{bmatrix} \Psi_{11} & \Psi_{12} & \Psi_{13} & 0 & C_{p1}^T & 0 \\ * & \Psi_{22} & \Psi_{23} & I & 0 & C_{p2}^T \\ * & * & -\gamma_a I & 0 & 0 & 0 \\ * & * & * & -\gamma_a I & 0 & 0 \\ * & * & * & * & -\gamma_a I & 0 \\ * & * & * & * & * & -\gamma_a I \end{bmatrix} < 0 \quad (6\text{-}27)$$

$$L_a(p) = P_{a1}^{-1} H_a(p)\ ;\ \Psi_{11} = P_{a1}A(p) + \left(P_{a1}A(p)\right)^T - H_a(p)C - (H_a(p)C)^T$$

$$\Psi_{12} = -(A^T(p)P_{a1}E(p) - C^T H_a^T(p)E(p))\ ;\ \Psi_{13} = -H_a(p)D_f$$

$$\Psi_{22} = -\left(E^T(p)P_{a1}E(p) + E(p)P_{a1}E^T(p)\right);\ \Psi_{23} = -E^T(p)H_a(p)D_f$$

$$\Sigma_{ai} = \begin{bmatrix} P_{a1}A(p) - H(p)C & P_{a1}E(p) \\ -(A^T(p)P_{a1}E(p) - C^T H^T(p)E(p) + E^T(p)P_{a1})^T & -E^T(p)P_{a1}E(p) \end{bmatrix}$$

Proof: This proceeds in a similar way to the steps illustrated to prove *Theorem 6-1* and hence the details are omitted here. To overcome the equality constraint $F_a(p)\bar{C} = E^T(p)P_{a1}$ the proof of Theorem 6-2 requires the following optimization:

$$minimise\ \mu_a$$

$$\begin{bmatrix} \mu_a I & E^T(p)P_1 - F_a(p)C \\ * & \mu_a I \end{bmatrix} > 0 \quad (6\text{-}28)$$

6-3-3. LMI base design quadratic parameterized TSDOFC

The control objective here is to design a dynamic output feedback controller capable of forcing the specified output of the nonlinear plant to follow a bounded reference signal in both the faulty and fault-free cases.

An augmented system consisting of Eq. (6-1) and the integral of the tracking error ($e_{ti} = \int y_r - Sy$) are defined below:

$$\left.\begin{aligned}\dot{\bar{x}} &= \bar{A}(p)\bar{x} + \bar{B}(p)u + \bar{E}(p)f_a + Ry_r + D_{in}e_f \\ \bar{y} &= \bar{C}\,\bar{x} + \bar{D}_f e_f\end{aligned}\right\} \tag{6-29}$$

$$\bar{A}(p) = \begin{bmatrix}0 & -SC \\ 0 & A(p)\end{bmatrix}, \bar{x} = \begin{bmatrix}e_{ti} \\ x\end{bmatrix}, \bar{B}(p) = \begin{bmatrix}0 \\ B(p)\end{bmatrix}, \bar{E}(p) = \begin{bmatrix}0 \\ E(p)\end{bmatrix}$$

$$R = \begin{bmatrix}I \\ 0\end{bmatrix}, D_{in} = \begin{bmatrix}-SD_f \\ 0\end{bmatrix}, \bar{C} = \begin{bmatrix}I & 0 \\ 0 & C\end{bmatrix}, \bar{D}_f = \begin{bmatrix}0 \\ D_f\end{bmatrix}$$

where $S \in \mathcal{R}^{q*l}$ is used to define which output variable is considered to track the reference signal. Since the system in (6-29) is of common output matrix (C). The TSDOFC used to stabilize and perform the tracking objective is of quadratic parameterization form and defined below:

$$\left.\begin{aligned}\dot{x}_c &= A_c(p,p)x_c + B_c(p)(S_r y_r - \bar{y}) \\ u &= C_c(p)x_c + D_c(p)(S_r y_r - \bar{y}) - K_f(p)\hat{f}_a\end{aligned}\right\} \tag{6-30}$$

where x_c is the controller state and $A_c(p,p) \in \mathcal{R}^{(n+q)\times(n+q)}$, $B_c(p) \in \mathcal{R}^{(n+q)\times(l+q)}$, $C_c(p) \in \mathcal{R}^{m\times(n+q)}$, $D_c(p) \in \mathcal{R}^{m\times(l+q)}, R \in \mathcal{R}^{(n+q)\times q}, K_f(p) \in \mathcal{R}^{m\times f}, and\ S_r \in \mathcal{R}^{(l+q)\times q}$ is introduced to match the dimensions of $y_r\ and\ \bar{y}$.

Aggregation of Eq. (6-29) and Eq. (6-30) gives the following system:

$$\left.\begin{aligned}\dot{x}_a &= A_a(p,p)x_a + E_a(p,p)\tilde{d} \\ \bar{y} &= C_a x_a + D_a\tilde{d}\end{aligned}\right\} \tag{6-31}$$

$$A_a(p,p) = \begin{bmatrix}\bar{A}(p) - \bar{B}(p)D_c(p)\bar{C} & \bar{B}(p)C_c(p) \\ -B_c(p)\bar{C} & A_c(p,p)\end{bmatrix}, x_a = \begin{bmatrix}\bar{x} \\ x_c\end{bmatrix}$$

$$E_a = \begin{bmatrix}\bar{E}(p) & D_{in} - \bar{B}(p)D_c(p)\bar{D}_f & R + \bar{B}(p)D_c(p)S_r & \bar{E}(p) - \bar{B}(p)K_f(p) \\ 0 & -B_c(p)\bar{D}_f & B_c(p)S_r & 0\end{bmatrix},$$

$$\tilde{d} = \begin{bmatrix}e_{f_a} \\ e_{f_s} \\ y_r \\ \hat{f}_a\end{bmatrix}, C_a = [\bar{C} \quad 0]\ , D_a = \begin{bmatrix}0 & \bar{D}_f & 0\end{bmatrix}$$

Remark: The gain $K_f(p)$ is designed so that the effect of $\hat{f}_a$ is either completely decoupled from the closed-loop system, i.e. when $rank\left(B(p), E(p)\right) = rank\,(B(p))$ which means $Im\,(E(p)) \subseteq Im\,(B(p))$, or attenuates the norm of $\left\|(\bar{E}(p) - \bar{B}(p)K_f(p))\hat{f}_a\right\|_2$ on the closed-loop performance which is in turn achieved by selecting $K_f(p) = B^*(p)E(p)$ (Gao and Antsaklis, 1991) where $B^*(p)$ is the pseudo inverse of $B(p)$. Hence, $K_f(p)$ is considered as a known gain in the derivation of the LMI-based FTC design given below.

***Theorem 6-3**: If the eigenvalues of the closed-loop system Eq.(6-31) are located in a LMI region of the negative complex plane characterised by radius α_c, β_c, ρ_c, θ_c, then the closed-loop system will be stable. Furthermore, the closed-loop system will track the reference signal with guaranteed H_∞ performance with an attenuation level γ_c, (provided that the signal $\tilde{d}$ is bounded), if there exist SPD matrices X, Y, matrices $A_c(p,p)$, $B_c(p)$,$C_c(p)$, $D_c(p)$, and scalars $\gamma_c, \alpha_c, \rho_c$, θ_c, and β_c satisfy the following LMI constraints:*

Minimize γ_c such that

$$\left.\begin{gathered} \mathcal{Q}_{ij} + \mathcal{Q}_{ij}^T + 2\rho_c X < 0 \\ \begin{bmatrix} -\alpha_c X & \beta_c X + \mathcal{Q}_{ij} \\ \beta_c X + \mathcal{Q}_{ij}^T & -\alpha_c X \end{bmatrix} < 0 \\ \begin{bmatrix} sin(\theta_c)\,[\mathcal{Q}_{ij} + \mathcal{Q}_{ij}^T] & cos(\theta_c)\,[\mathcal{Q}_{ij} - \mathcal{Q}_{ij}^T] \\ cos(\theta_c)\,[\mathcal{Q}_{ij} - \mathcal{Q}_{ij}^T] & sin(\theta_c)\,[\mathcal{Q}_{ij} + \mathcal{Q}_{ij}^T] \end{bmatrix} < 0 \end{gathered}\right\} \tag{6-32}$$

$$\begin{bmatrix} \Psi_{11c} & \Psi_{12c} & \bar{E}(p) & \Psi_{13c} & \Psi_{14c} \\ * & \Psi_{22c} & Y\bar{E}(p) & \Psi_{23c} & \Psi_{24c} \\ * & * & -\gamma_c I & 0 & 0 \\ * & * & * & -\gamma_c I & 0 \\ * & * & * & * & -\gamma_c I \\ * & * & * & * & * \\ * & * & * & * & * \\ * & * & * & * & * \\ * & * & * & * & * \\ * & * & * & * & * \end{bmatrix} \tag{6-33}$$

$$\begin{bmatrix} \Psi_{16c} & XC_{p1}^T & 0 & -XC_{p1}^T & 0 \\ \Psi_{26c} & C_{p1}^T & 0 & -C_{p1}^T & 0 \\ 0 & 0 & 0 & 0 & 0 \\ 0 & 0 & 0 & 0 & 0 \\ 0 & 0 & S_r^T & 0 & S_r^T \\ -\gamma_c I & 0 & 0 & 0 & 0 \\ * & -\gamma_c I & 0 & 0 & 0 \\ * & * & -\gamma_c I & 0 & 0 \\ * & * & * & -G^{-1} & 0 \\ * & * & * & * & G \end{bmatrix} < 0$$

where

$$\Psi_{11c} = \bar{A}(p)X + (\bar{A}(p)X)^T + \bar{B}(p)\hat{C}(p) + \left(\bar{B}(p)\hat{C}(p)\right)^T$$

$$\Psi_{12c} = \hat{A}^T(p,p) + \bar{A}(p) - \bar{B}(p)\widehat{D}(p)\bar{C}\ ;\ \Psi_{13c} = D_{in} - \bar{B}(p)\widehat{D}(p)\overline{D}_f$$

$$\Psi_{22c} = Y\bar{A}(p) + \left(Y\bar{A}(p)\right)^T + \hat{B}(p)\bar{C} + \left(\hat{B}(p)\bar{C}\right)^T\ ;\ \Psi_{23c} = YD_{in} + \hat{B}(p)\overline{D}_f$$

$$\Psi_{14c} = R + \bar{B}(p)\widehat{D}(p)S_r\ ;\ \Psi_{24c} = YR - \hat{B}(p)S_r$$

$$\Psi_{15c} = \bar{E}(p) - \bar{B}(p)K_f(p);\ \Psi_{15c} = Y(\bar{E}(p) - \bar{B}(p)K_f(p))$$

$$Q_{ij} = \begin{bmatrix} \bar{A}(p)X + \bar{B}(p)\hat{C}(p) & \bar{A}(p) - \bar{B}(p)\widehat{D}(p)\bar{C} \\ \hat{A}(p,p) & Y\bar{A}(p) + \hat{B}(p)\bar{C}(p) \end{bmatrix}$$

The controller gains are thus calculated as follows:

$$D_c(p) = \widehat{D}(p)$$

$$C_c(p) = \left(\hat{C}(p) + D_c(p)\bar{C}X\right)M^{-T}$$

$$B_c(p) = N^{-1}(-\hat{B}(p) - Y\bar{B}(p)D_c(p))$$

$$A_c(p,p) = N^{-1}(\hat{A}(p,p) - Y\left(\bar{A}(p) - \bar{B}(p)\widehat{D}(p)\bar{C}\right)X - Y\bar{B}(p)C_c(p)M^T + NB_c(p)\bar{C}X)M^{-T}$$

where M and N satisfy $MN^T = I - XY$

Proof: Let the system output performance be defined as follows:

$$y_p = \bar{C}_p\, x_a$$

where $\bar{C}_p$ is selected depending on the design requirements. The robustness of the controller against the augmented input $(\tilde{d})$ can then be represented by minimising the mathematical objective given below:

$$\frac{\|y_p\|_2}{\|\tilde{d}\|_2} \leq \gamma_c = \frac{1}{\gamma_c}\int_0^\infty {x_a}^T \bar{C}_p^T \bar{C}_p x_a dt - \gamma_c \int_0^\infty \tilde{d}^T \tilde{d} \leq 0 \tag{6-34}$$

Consider $v(x_a) = x_a^T \bar{P}\, x_a$, $where\ \bar{P} > 0$ is the candidate Lyapunov function for the augmented system (6-31). Hence, as stated in the observer design, to achieve the required performance (6-34) and stability of augmented system Eq. (6-31) the following inequality should hold:

$$\dot{v}(x_a) + \frac{1}{\gamma_c} y_p^T\, y_p - \gamma_c \tilde{d}^T \tilde{d} < 0 \tag{6-35}$$

where:

$$y_p = (S_r y_r - \bar{y}) \tag{6-36}$$

$$y_p^T\, y_p = (S_r y_r - \bar{y})^T (S_r y_r - \bar{y})$$

$$y_p^T\, y_p = y_r^T S_r^T S_r y_r - \bar{y}^T S_r y_r - \bar{y}_r^T S_r^T \bar{y} + \bar{y}^T \bar{y}$$

Let $E_r = [0\ 0\ I]$ then:

$$y_p^T\, y_p = \tilde{d}^T E_r^T E_r \tilde{d} - \tilde{d}^T E_r^T C_a x_a - x_a^T C_a^T E_r \tilde{d} + x_a^T C_a^T C_a x_a$$

where $\dot{v}(x_a)$ is the derivative of the candidate Lyapunov function, based on the state-space representation of the augmented system Eq. (6-31), inequality (6-35) then becomes:

$$\dot{v}(x_a) = x_a^T \big(A_a^T(p,p)\bar{P} + \bar{P}A_a(p,p)\big)x_a + x_a^T(\bar{P}E_a(p)\tilde{d} + \tilde{d}^T E_a^T(p)\bar{P}x_a \tag{6-37}$$

By using Eq. (6-37) and the Schur Complement Theorem, inequality (6-35) implies that the following inequality must hold:

$$\begin{bmatrix} A_a^T(p,p)\bar{P} + \bar{P}A_a(p,p) & \bar{P}E_a(p) - \frac{1}{\gamma_c} C_a^T E_r & \bar{C}_a^T & 0 \\ * & -\gamma_c I & 0 & E_r^T \\ * & * & -\gamma_c I & 0 \\ * & * & * & -\gamma_c I \end{bmatrix} < 0 \tag{6-38}$$

Inequality (6-38) can be further decomposed as below:

$$\begin{bmatrix} A_a^T(p,p)\bar{P} + \bar{P}A_a(p,p) & \bar{P}E_a(p) & \bar{C}_a^T & 0 \\ * & -\gamma_c I & 0 & E_r^T \\ * & * & -\gamma_c I & 0 \\ * & * & * & -\gamma_c I \end{bmatrix} + \begin{bmatrix} -C_a^T \\ 0 \\ 0 \\ 0 \end{bmatrix} \begin{bmatrix} 0 & \frac{1}{\gamma_c}E_r & 0 & 0 \end{bmatrix} + \begin{bmatrix} 0 \\ \frac{1}{\gamma_c}E_r^T \\ 0 \\ 0 \end{bmatrix} [-C_a \quad 0 \quad 0 \quad 0] < 0 \tag{6-39}$$

Lemma 2: *Given a scalar $\mu > 0$ and the SPD matrix G, the following inequality holds:*

$$X^T R + R^T X \leq \frac{1}{\mu} X^T G X + \mu R^T G^{-1} R \tag{6-40}$$

where *R & X* are any compatibly dimensioned matrices.

Based on Lemma 2 inequality (6-38) implies the following inequality:

$$\begin{bmatrix} A_a^T(p,p)\bar{P} + \bar{P}A_a(p,p) & \bar{P}E_a(p) & \bar{C}_a^T & 0 & -C_a^T & 0 \\ * & -\gamma_c I & 0 & E_r^T & 0 & \frac{1}{\gamma_c}E_r^T \\ * & * & -\gamma_c I & 0 & 0 & 0 \\ * & * & * & -\gamma_c I & 0 & 0 \\ * & * & * & * & -G^{-1} & 0 \\ * & * & * & * & * & -G \end{bmatrix} < 0 \tag{6-41}$$

It can be assumed that $\bar{P}$ and $\bar{P}^{-1}$ is structured as follows:

$$\bar{P} = \begin{bmatrix} Y & N \\ N^T & * \end{bmatrix}, \bar{P}^{-1} = \begin{bmatrix} X & M \\ M^T & * \end{bmatrix}, \text{ since } \bar{P}\bar{P}^{-1} = I$$

we then have that $\bar{P}\begin{bmatrix} X \\ M^T \end{bmatrix} = \begin{bmatrix} I \\ 0 \end{bmatrix} \Rightarrow \bar{P}\begin{bmatrix} X & I \\ M^T & 0 \end{bmatrix} = \begin{bmatrix} I & Y \\ 0 & N^T \end{bmatrix}$

Define $\Pi_1 = \begin{bmatrix} X & I \\ M^T & 0 \end{bmatrix}$; $\Pi_2 = \begin{bmatrix} I & Y \\ 0 & N^T \end{bmatrix}$

Pre- and post-multiplying inequality (6-41) by $[\Pi_1^T \quad I \quad I \quad I \quad I \quad I]$ and its transpose respectively, the following inequality is obtained:

$$\begin{bmatrix} \Pi_1^T A_a^T(p,p)\Pi_2 + \Pi_2^T A_a(p,p)\Pi_1 & \Pi_2^T E_a(p) & \Pi_1^T \bar{C}_a^T & 0 & \Pi_1^T \bar{C}_p^T & 0 \\ * & -\gamma_c I & 0 & E_r^T & 0 & \frac{1}{\gamma_c} E_r \\ * & * & -\gamma_c I & 0 & 0 & 0 \\ * & * & * & -\gamma_c I & 0 & 0 \\ * & * & * & * & -G^{-1} & 0 \\ * & * & * & * & * & -G \end{bmatrix} < 0 \tag{6-42}$$

After simple mathematical computation and using the following change of variables:

$$\hat{A}(p,p) = Y(\bar{A}(p) - \bar{B}(p)D_c(p)\bar{C})X + Y\bar{B}(p)C_c(p)M^T - NB_c(p)\bar{C}X + NA_c(p,p)M^T \tag{6-43}$$

$$\hat{B}(p) = -NB_c(p) - Y\bar{B}(p)D_c(p) \tag{6-44}$$

$$\hat{C}(p) = C_c(p)M^T - D_c(p)\bar{C}X \tag{6-45}$$

$$\hat{D}(p) = D_c(p) \tag{6-46}$$

Then inequality (6-33) can be obtained easily.

By using the change of variables $A = A_a(p,p), X = \bar{P}$, and pre- and post-multiplying the first inequality of (6-19) by Π_1^T, the 2nd and 3rd inequality of (6-19) by $[\Pi_1^T \quad \Pi_1^T]$ and its transpose respectively yields:

$$\left.\begin{array}{c} \Pi_2^T A_a(p,p)\Pi_1 + (\Pi_2^T A_a(p,p)\Pi_1)^T + 2\rho\Pi_1^T\Pi_2 < 0 \\ \begin{bmatrix} -\alpha\Pi_1^T\Pi_2 & \beta\Pi_1^T\Pi_2 + \Pi_2^T A_a(p,p)\Pi_1 \\ \beta\Pi_1^T\Pi_2 + (\Pi_2^T A_a(p,p)\Pi_1)^T & -\alpha\Pi_1^T\Pi_2 \end{bmatrix} < 0 \\ \begin{bmatrix} sin(\theta)\,[\mathscr{g}_+] & cos(\theta)\,[\mathscr{g}_-] \\ cos(\theta)\,[\mathscr{g}_-] & sin(\theta)\,[\mathscr{g}_+] \end{bmatrix} < 0 \end{array}\right\} \tag{6-47}$$

where

$\mathscr{g}_+ = \Pi_2^T A_a(p,p)\Pi_1 + (\Pi_2^T A_a(p,p)\Pi_1)^T$

$\mathscr{g}_- = \Pi_2^T A_a(p,p)\Pi_1 - (\Pi_2^T A_a(p,p)\Pi_1)^T$

then using equality $MN^T = I - XY$ in inequalities (6-47), then inequality (6-32) obtained.

Remark: The matrices M, N^T can be calculated based on the equality $MN^T = I - XY$ using any matrix decomposition techniques e.g. *qr* or *svd*.

- The proposed methodology offers design freedom to combine any estimation strategy for actuator and sensor faults. Moreover, the time response of the two observers as well as the controller can be adjusted separately.
- Due to the fact that T-S fuzzy static output feedback controller (SOFC) has a non convex Lyapunov stability condition (Chun-Hsiung et al., 2006, Ho Jae and Do Wan, 2009), in (Chun-Hsiung et al., 2006) a convex Lyapunov stability condition for SOFC derived through adding a set of linear matrix equalities, However, the proposed design formulation is only feasible in very limited cases (for example, the common B matrix case). Therefore, in this Chapter, the fuzzy DOFC is proposed instead.

6-4. Simulation results

To illustrate the proposed FTC strategy encompassing the possibility of simultaneous actuator and sensor faults, the modified non-linear simulation of the inverted pendulum and cart with tracking of a time-varying reference cart position is considered in this Chapter. The main difference between the T-S model derived in this Chapter and the model derived in Chapter 4 are (a) rewriting the non-linear model so that the term $mlx_3^2\,sin(x_1)$ affects the closed-loop system as a dynamic uncertainty, and (b) the use of the local approximation which is very important to reduce the design complexity specifically in quadratic parameterisation TSDOFC in which the number of controller gains is equal to 2^r (where r is the number of fuzzy rules). For example, the 8 rule fuzzy model of the inverted pendulum system derived in Chapter 5 requires 256 controller gains to be designed and implemented.

The nonlinear inverted pendulum and cart system model is given as follows:

$$\dot{x} = \begin{bmatrix} \dot{x}_1 \\ \dot{x}_2 \\ \dot{x}_3 \\ \dot{x}_4 \end{bmatrix} = \begin{bmatrix} x_3 \\ x_4 \\ \dfrac{g\,sin(x_1)}{4l/3 - mla(cos(x_1))^2} \\ \dfrac{-mag\,sin(2x_1)\ /2}{4/3 - mla(cos(x_1))^2} \end{bmatrix} + \begin{bmatrix} 0 \\ 0 \\ \dfrac{-a\,cos(x_1)}{4l/3 - mla(cos(x_1))^2} \\ \dfrac{4a/3}{4/3 - mla(cos(x_1))^2} \end{bmatrix} (u + (f_a + mlx_3^2\,sin(x_1))) \tag{6-48}$$

where the model parameters are as defined in Chapter 5.

Although, increasing the number of fuzzy rules ensures good approximation of a smooth non-linear system, the design conservatism of the T-S fuzzy controller and

estimator also increase. Therefore, to take into account this trade-off, three system operating points are chosen corresponding to the pendulum angular positions $\theta = 0\ and \pm \pi/4$. Due to symmetry this results in the choice of *two* fuzzy rules in the T-S model. The control objective is to force the cart position to follow a desired cart reference position in the presence of a cart position measurement $C_2 x$ fault and actuator fault.

Various results are generated by considering the cart position sensor and cart actuator to have both additive and parametric faults. It is assumed here that the actuator fault affect the system in the same direction as the control input therefore the controller gain $K_f(p)$ is selected to be $K_f(p) = B^*(p)E(p)$ where $B^*(p)$ is the pseudo-inverse of the input matrix $B(p)$. On the other hand, different sensor fault signals have been considered in the results such as parametric change sensor faults and abrupt and time varying fault scenarios.

The initial conditions for the nonlinear system states and the two PPIOs are selected as follows:

$$\begin{aligned} System\ initial\ states &= [0.25 \quad 0 \quad 0.5 \quad 0], \\ Sensor\ PPIO &= [0 \quad 0 \quad 0 \quad 0 \quad 0 \quad 0.5 \quad 0], \\ Actuator\ PPIO &= [0 \quad 0.2 \quad 0.1 \quad 0], \end{aligned}$$

By solving the LMI conditions given in *Theorems 6-1, 6-2, and 6-3* the fuzzy controller and observers gains are computed as:

$$A_{c(1,1)} = \begin{bmatrix} -1.4900 & 2.0127 & 10.3547 & -29.3842 & 806.9533 \\ -1.1003 & -2.2336 & 7.6739 & -20.9505 & 591.7176 \\ 0.3461 & -0.2708 & -2.5631 & 6.3034 & -187.1907 \\ -0.0990 & 0.1105 & 0.1173 & -2.9509 & 39.9518 \\ 0.0952 & -0.3661 & -0.3899 & 0.7360 & -17.1688 \end{bmatrix},$$

$$A_{c(1,2)} = \begin{bmatrix} -1.9375 & 0.9626 & 17.1862 & -61.8366 & 2748.8609 \\ -1.4309 & -3.0093 & 12.7204 & -44.9284 & 2027.5700 \\ 0.4502 & -0.0264 & -4.1510 & 13.8975 & -637.3877 \\ -0.1202 & 0.0607 & 0.4439 & -4.5116 & 128.9219 \\ 0.1031 & -0.3470 & -0.5143 & 1.3190 & -52.1569 \end{bmatrix},$$

$$A_{c(2,1)} = \begin{bmatrix} -1.4678 & 2.2672 & 10.1970 & -28.0973 & 752.5285 \\ -1.1290 & -2.0149 & 5.2321 & -13.1154 & 333.5020 \\ 0.3343 & -0.3333 & -2.3714 & 5.5003 & -161.4052 \\ -0.0828 & 0.1217 & 0.1182 & -2.9079 & 42.7229 \\ -0.0498 & -0.3434 & -0.2030 & 0.2752 & -2.2480 \end{bmatrix},$$

$$A_{c(2,2)} = \begin{bmatrix} -1.8808 & 1.2985 & 16.4977 & -58.0281 & 2543.0726 \\ -1.3035 & -2.4240 & 7.8920 & -25.7416 & 1086.6248 \\ 0.4218 & -0.1282 & -3.7032 & 11.8800 & -538.6093 \\ -0.1032 & 0.0739 & 0.4315 & -4.4027 & 127.2057 \\ -0.0483 & -0.3406 & -0.2209 & 0.3631 & -8.8193 \end{bmatrix},$$

$$B_{c1} = \begin{bmatrix} 12.2786 & -51.3651 & -334.1074 & -131.4990 \\ 8.6490 & -11.4961 & -251.9183 & 22.2228 \\ 45.0377 & -0.0417 & 49.6370 & 118.8719 \\ 141.6355 & 20.1090 & -111.0111 & -37.8442 \\ 17.2099 & -194.4594 & -4.0767 & 7.9471 \end{bmatrix},$$

$$B_{c1} = \begin{bmatrix} 5.3415 & -27.3864 & -330.1390 & -132.2059 \\ 2.2919 & -8.2930 & -146.2328 & 17.9214 \\ 46.6722 & -5.5339 & 41.8730 & 118.1318 \\ 141.2636 & 21.2783 & -111.5509 & -36.1074 \\ 16.6982 & -182.5085 & -9.5418 & -9.3453 \end{bmatrix},$$

$$C_{c1} = [-0.0121 \quad 0.1798 \quad 0.7541 \quad -2.1933 \quad 59.8626],$$

$$C_{c2} = [-0.0414 \quad 0.1054 \quad 1.2792 \quad -4.5980 \quad 203.3789],$$

$$D_{c1} = [0.74 \quad -2.78 \quad -24.56 \quad -0.07], D_{c2} = [0.26 \quad -1.62 \quad -26.30 \quad -0.02],$$

The sensor fault PPIO proportional gains are computed as:

$$\bar{L}_1 = \begin{bmatrix} 39.3213 & -0.2670 & -8.7955 \\ -1.7163 & 0.0227 & 0.4694 \\ 142.9988 & -1.0278 & -32.1569 \\ -5.9948 & 0.2527 & 1.8612 \\ 33.2835 & -0.2228 & -7.4372 \\ -13.7189 & -17.8893 & 4.1903 \\ -4.6583 & 0.2447 & 1.5577 \end{bmatrix}, \bar{L}_2 = \begin{bmatrix} 40.4585 & -0.2739 & -1.2478 \\ -1.8277 & 0.0230 & 0.1168 \\ 147.1432 & -1.0524 & -4.7097 \\ -6.2352 & 0.2536 & 0.7068 \\ 34.2455 & -0.2287 & -1.0484 \\ -15.2037 & -17.8891 & 1.1314 \\ -4.8602 & 0.2453 & 0.6597 \end{bmatrix},$$

The actuator fault PMIO proportional gains are computed as:

$$L_{1a} = \begin{bmatrix} 522.5073 & -0.0490 & -1.4231 \\ 0.0516 & 1.6186 & 0.9999 \\ 769.4489 & 0.0875 & -3.2869 \\ 0.0137 & 0.0483 & 1.9992 \end{bmatrix}, L_{2a} = \begin{bmatrix} 522.5446 & -0.0613 & -1.1527 \\ 0.0515 & 1.6186 & 0.9999 \\ 768.2967 & 0.0994 & -0.0332 \\ 1.9984 & 0.0884 & 1.7514 \end{bmatrix},$$

The gains for the sensor and actuator fault estimation PPIOs are computed as:

$$F_s = [12.3383 \quad 7.1075 \quad 2.6191], F_a = [-23.4831 \quad -0.0001 \quad 546.3907]$$

The attenuation coefficients are determined as $\gamma_c = 1.3$, $\gamma_s = 0.2722$ and $\gamma_a = 0.1227$.

The controller designed via the LMI D-region is bounded by $\alpha_c = 20$, $\beta_c = 0$, $\rho_c = 0$, $\theta_c = \pi/3$. The sensor fault PPIO LMI region is bounded by $\alpha = 100$, $\beta = 0$, $\rho = -1$, $\theta = \pi/2$, and the fault PPIO LMI region is bounded by $\alpha_a = 100$, $\beta_a = 0$, $\rho_a = -1$, $\theta_a = \pi/2$.

Figure 6-3 shows the tracking performance of the closed-loop system without actuator and/or sensor faults. The FTC objective is to maintain this performance (with acceptable degradation) during different components fault scenarios.

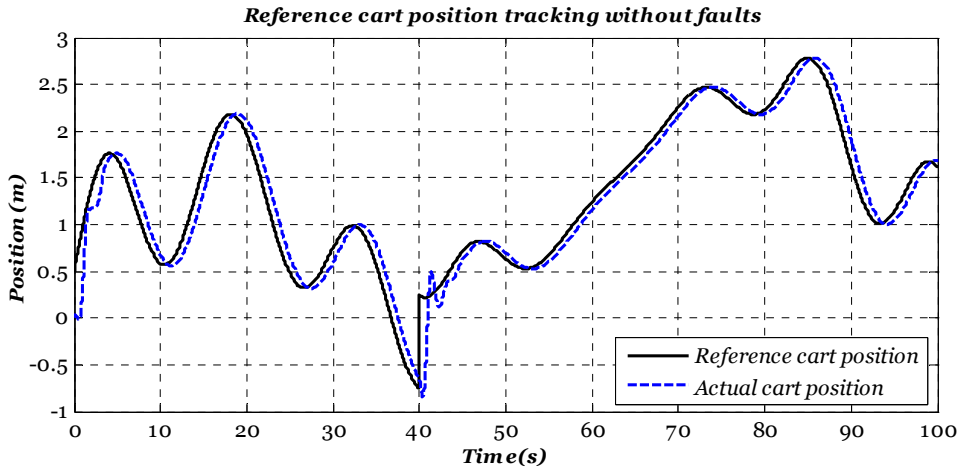

Figure 6-3: Closed-loop tracking performance without component faults

Figure 6-4 shows that the sensor faults of $0.5C_2$, $0.6C_2$ and $0.8C_2$ have a direct impact on the tracking performance since the faulty sensors provide the nominal controller with measurements that no longer represent the actual system variables. As a result, the controller lacks the ability to handle even minor sensor faults ($0.8C_2$). On the other hand, Figure 6-5 shows that the nominal controller can passively tolerate and maintain acceptable tracking performance for up to 40% loss of actuator effectiveness fault (i.e. $0.6B$). However, (50%) actuator faults lead to great tracking degradation and more severe faults with eventual system instability. Figure 6-6 shows that simultaneous actuator and sensor faults further degrade tracking performance.

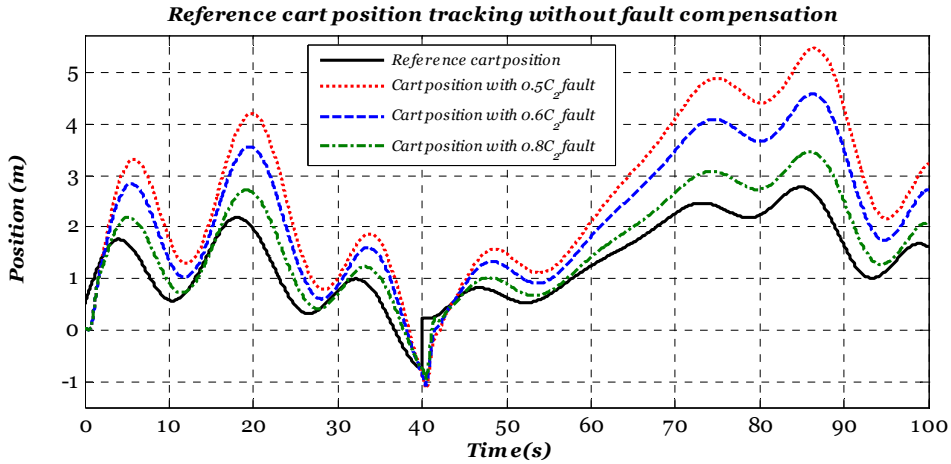

Figure 6-4: Reference position tracking under different position sensor fault

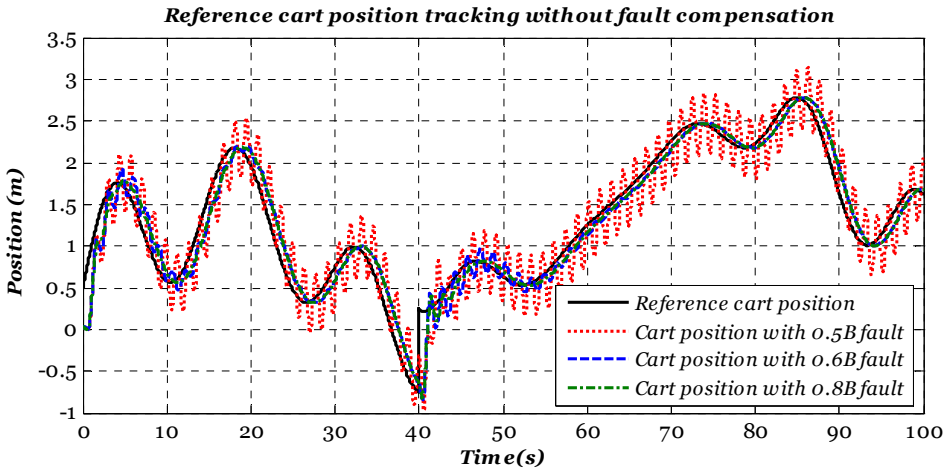

Figure 6-5: Reference position tracking under different actuator fault

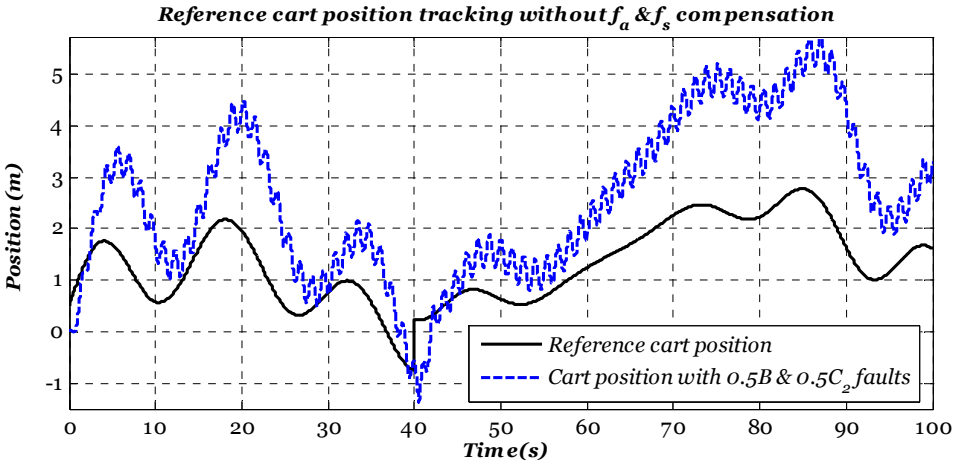

Figure 6-6: Reference position tracking under simultaneous actuator and position sensor loss of effectiveness (50%) fault

Clearly, the results shown in Figure 6-4, Figure 6-5, and Figure 6-6 validate the investigation of the relative impacts of the actuator and sensor faults on the tracking control performance presented in Chapter 3.

The results shown below illustrate how the proposed strategy can maintain the nominal control objectives in different simultaneous actuator and sensor fault cases. To cope with different fault scenarios, the considered actuator fault signal covers several additive fault scenarios of abruptly varying amplitudes and slow to fast (linear time-varying fault frequencies). This fault signal with its estimation via T-S fuzzy PPIO is shown in Figure 6-7.

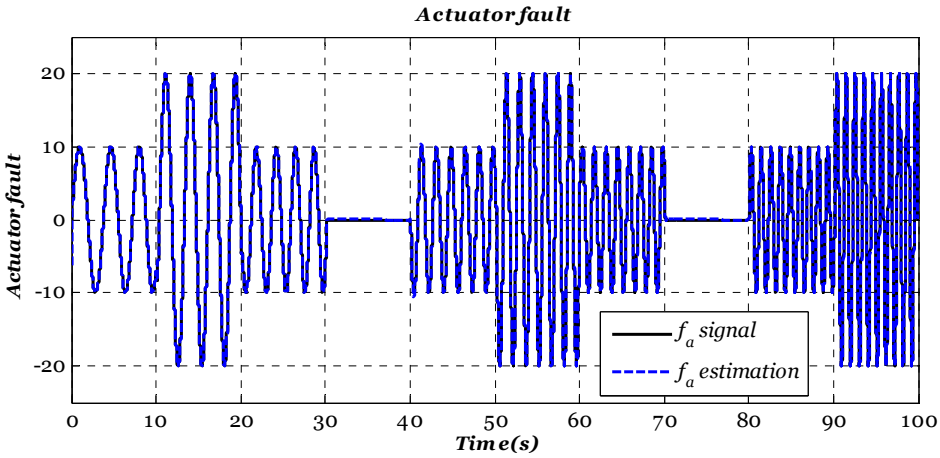

Figure 6-7: Time-varying actuator fault and fault estimation

Figure 6-8 clarifies the trade-off between the fault estimation accuracy on one hand, and the fault magnitude and frequency on the other hand. It is shown in Section 6-3-1 that for the sensor fault estimation observer design problem, due care must be taken for the effect of actuator fault estimation error.

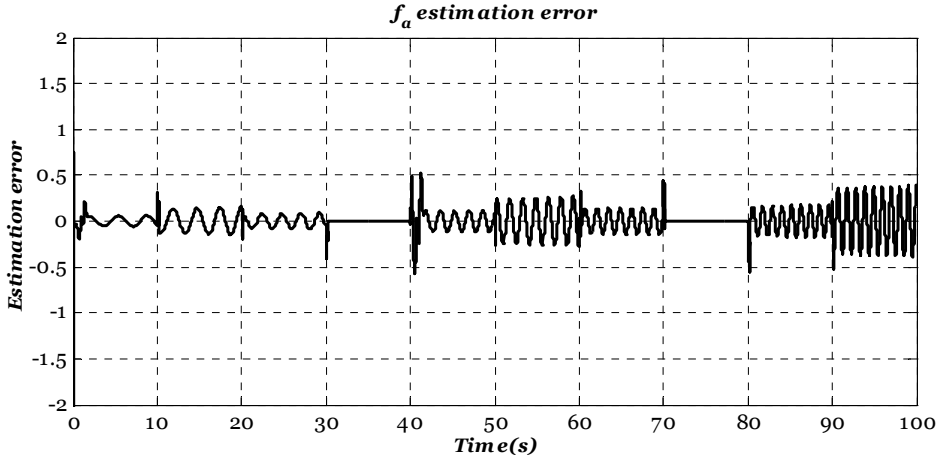

Figure 6-8: Actuator fault estimation error

It is interesting to note that the spikes appear in Figure 6-8 at each $10\ sec$ due to the abrupt change of the actuator fault signal. However, at $40\ sec$ the spike has different behaviour due to abrupt changes in the reference cart position. This highlights the considerable challenge arising from the existence of the reference signal in the tracking problem. This should be compared with the simpler situation of the regulator problem which requires no reference tracking.

Figure 6-9 further demonstrates the effectiveness of the use of the T-S PPIO to provide fast estimation of the fault signal and hence enhance the closed-loop system performance.

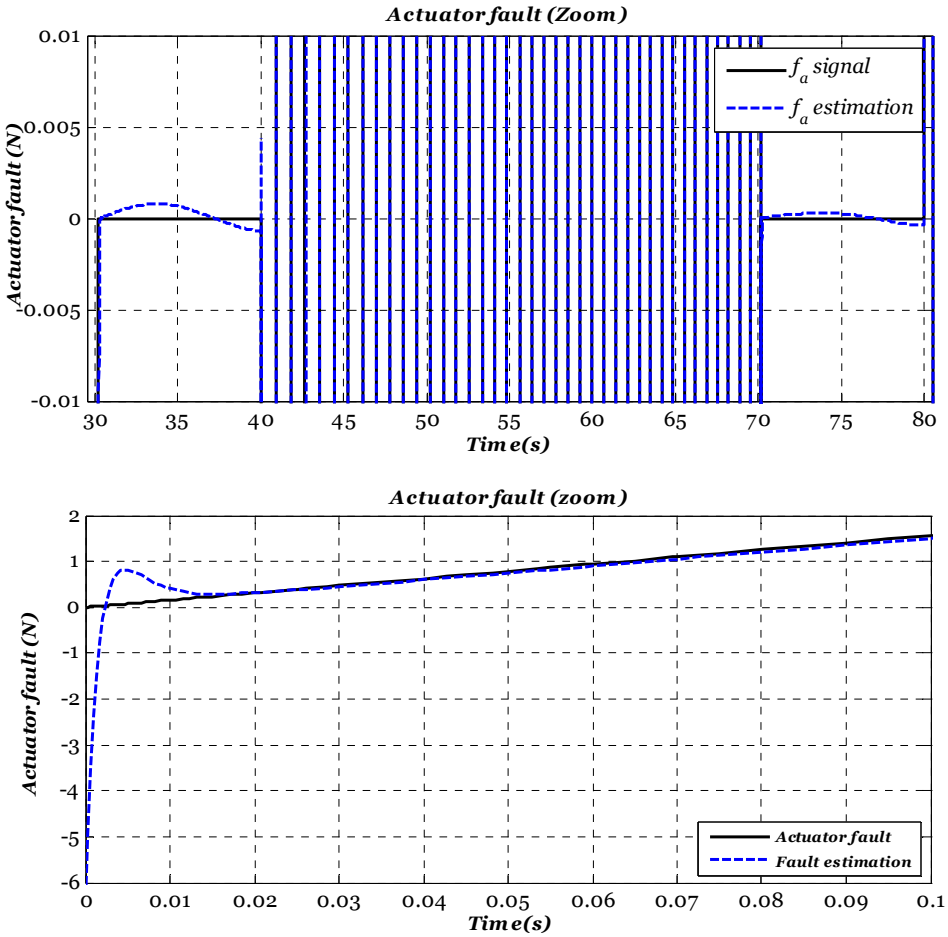

Figure 6-9: T-S PPIO capability to provide fast fault estimation

All the following results consider the effect of the actuator fault given in Figure 6-7 with online estimation (via the actuator T-S PPIO) and compensation. Therefore, more focus is given to different cart position sensor fault scenarios to show the ability of the proposed strategy to handle simultaneous faults.

Additive and parametric cart position sensor fault scenarios have been introduced to show the ability of the proposed strategy to handle simultaneous faults. In Figure 6-10 a parametric change on the cart position sensor fault ($0.3C_2$) is introduced and the proposed FTTC system maintains the tracking performance during the simultaneous fault. The figure shows the effectiveness of actuator and sensor faults compensation, the significant effect of uncompensated sensor fault is also shown. Moreover, the fault estimation in Figure 6-11 indicates that a parameter change fault is a special case of an additive fault in which the fault signal represents the loss of effectiveness multiplied by the corresponding fault-free signal. Consequently, the interpretation of a parameter

change fault as a special case of an additive state-dependent fault signal can be useful for assessing the fault severity, as shown in Figure 6-12.

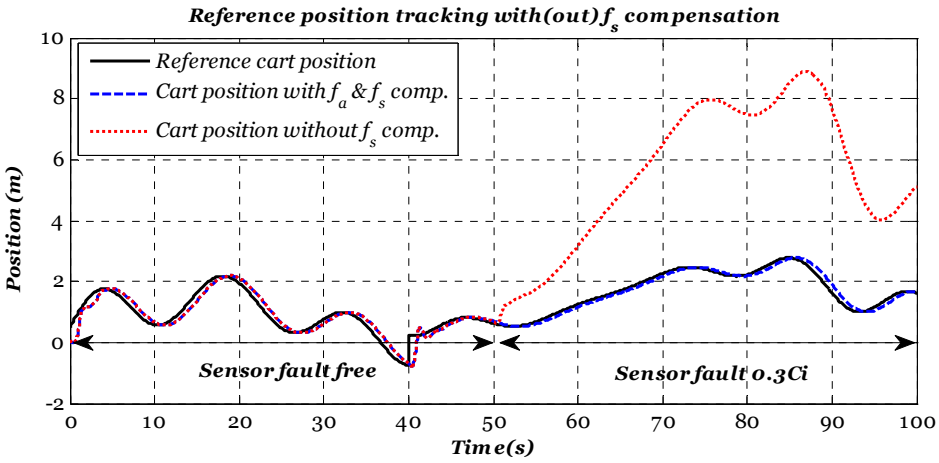

Figure 6-10: Simultaneous actuator and sensor fault compensation with the effect of uncompensated parameter change sensor fault only

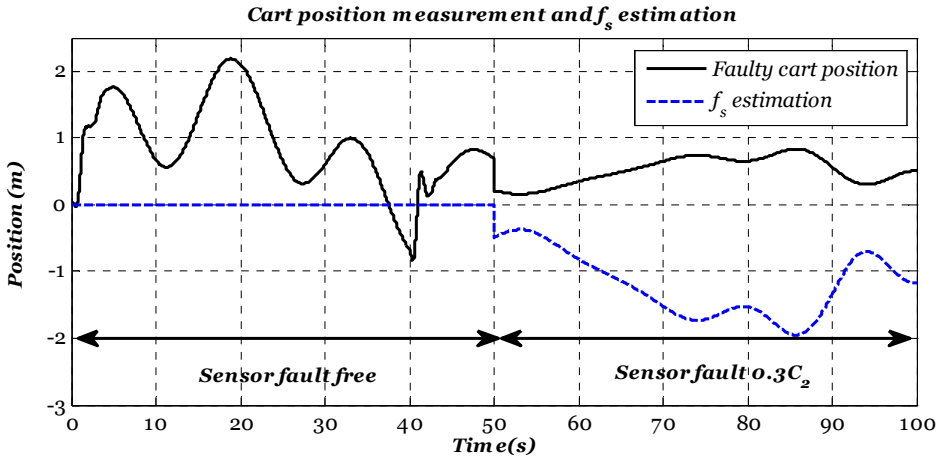

Figure 6-11: Faulty measurement and fault estimation

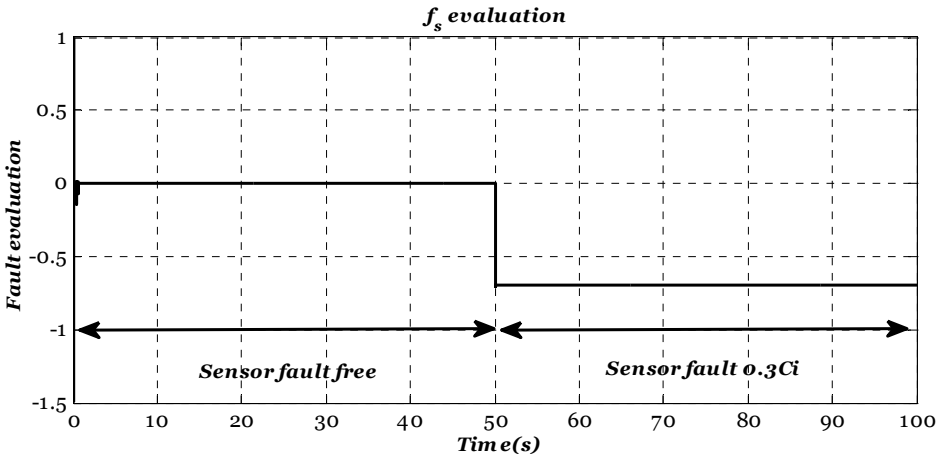

Figure 6-12: Sensor fault evaluation

Figure 6-13 and Figure 6-14 show the result of a further investigation of the proposed FTTC system by considering a time-varying and abruptly changing multi-step sensor fault signal and its T-S PPIO estimate affecting the system at the same time as the actuator fault shown in Figure 6-7.

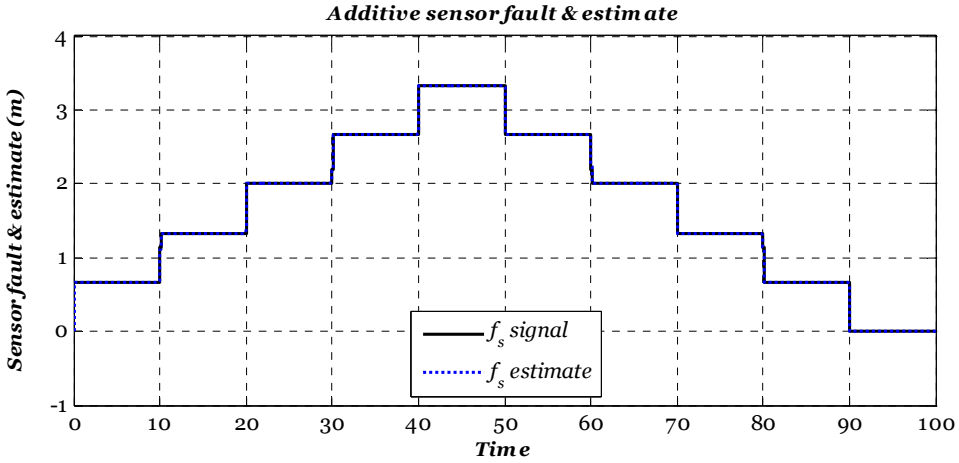

Figure 6-13: Additive sensor fault and estimation

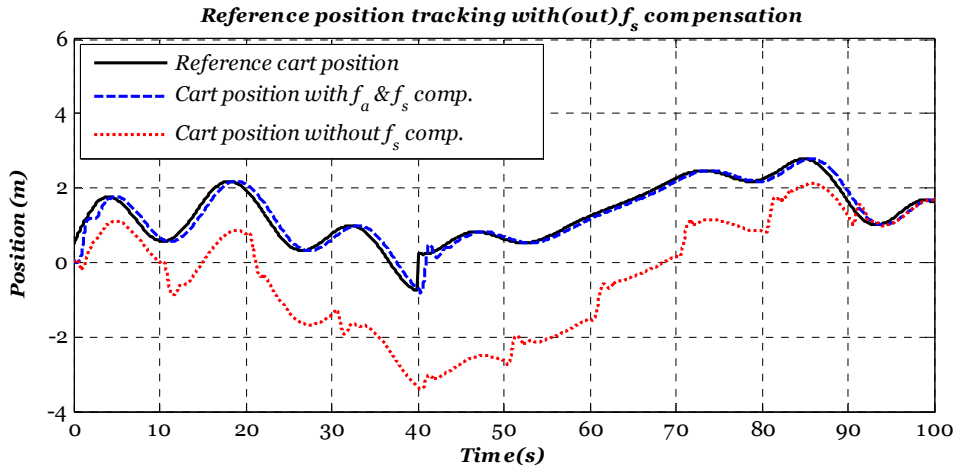

Figure 6-14: Simultaneous actuator and sensor faults compensation with the effect of uncompensated additive sensor fault only

The T-S PPIO fast fault estimation capability is demonstrated via Figure 6-15. Moreover, the zoomed version of the sensor fault estimate signal in Figure 6-16 a & b with separate time windows further demonstrates the effectiveness of the proposed estimation and compensation scheme. Within each window small sinusoidal variations from the actuator fault (with different frequencies and amplitude) are clearly visible showing that the bi-directional interactions between the proposed T-S PPIO are strongly attenuated.

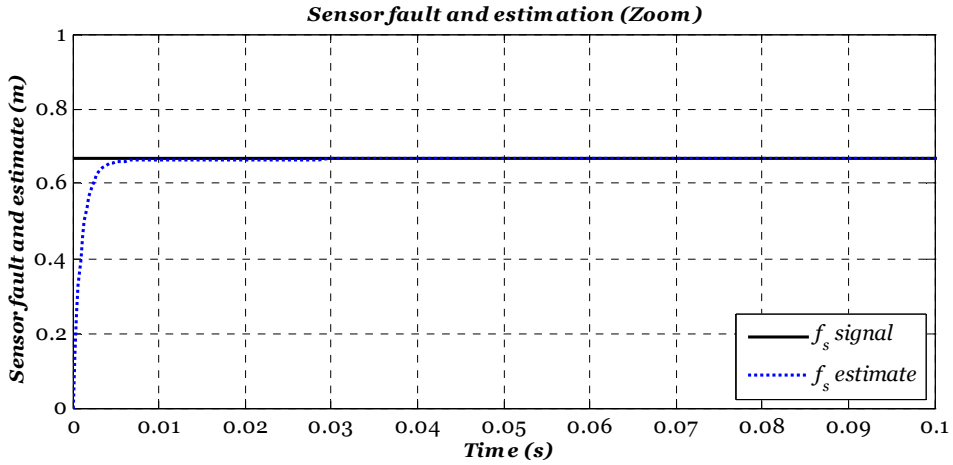

Figure 6-15: T-S PPIO capability to provide fast fault estimation

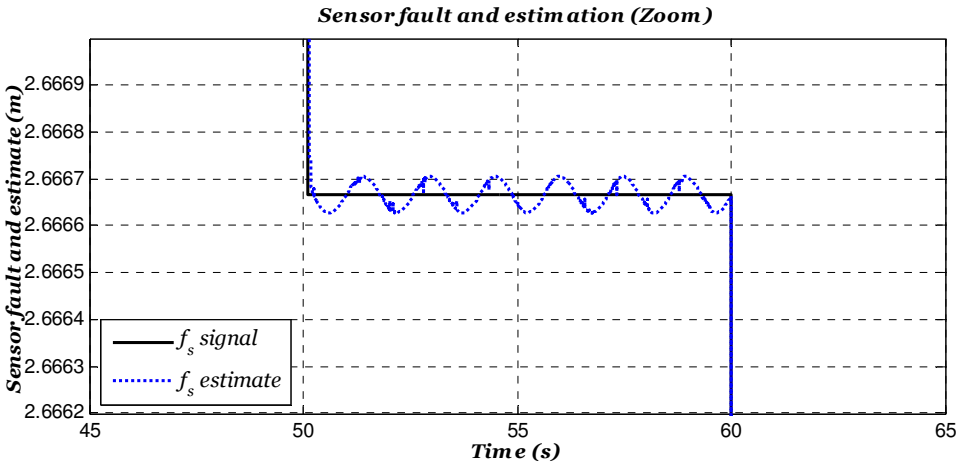

(a)

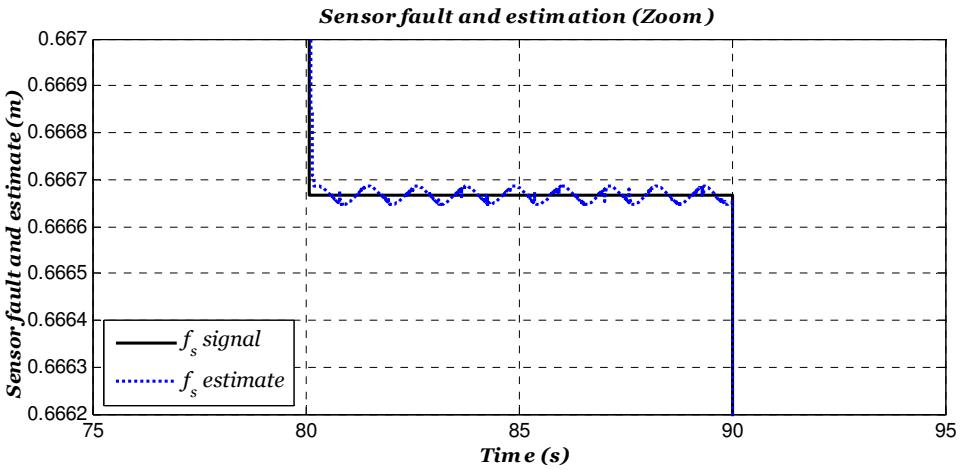

(b)

Figure 6-16 : a & b Zoomed-in view of sensor fault signal/estimation

6-5. Conclusion

The Chapter develops a new FTTC strategy for nonlinear systems with simultaneous actuator and sensor faults based on fault estimation and compensation. The TSDOFC scheme is used as it has a time-varying reference tracking capability and the design of a dual pair of actuator and sensor T-S PPIOs. The controller and fault estimators individually satisfy appropriate L_2 norm robustness conditions guaranteeing minimum tracking error and robust fault estimation. The actuator and sensor fault estimators are developed to have low fault interaction and to provide robust fault compensation in the output feedback controller.

The significant attributes gained by using the proposed FTTC system are. (i) It can handle cases for which the sensor and actuator faults affect the nonlinear system simultaneously. (ii) It can overcome the effects of time-varying actuator and sensor fault signals with bounded first time derivatives using the concept of fault estimation and compensation AFTC, and hence maintaining the controller performance without control system changes. (iii) The use of proportional and integral feedback to estimate the fault signal enhances the fault estimation accuracy. (iv) By combining the two T-S PPIOs and the TSDOFC, the hurdles imposed by the *Separation Principle* in the T-S observer-based state estimate feedback control are removed. Furthermore, the limitation of using an iterative form of SOFC design is obviated completely. The significant impact of a sensor fault on the tracking control problem is also demonstrated. These factors represent significant contributions to the AFTC subject.

Finally, the complexity of the proposed controller depends on the number of fuzzy rules and the input and output matrices. For example, to ensure a high degree of design freedom and to achieve good performance for non-common input and output system matrices cubic parameterization TSDOFC is required. However, the complexity is violated in the case of common input common output fuzzy models since only linear parameterization TSDOFC is required.

Chapter 7 : Investigation of wind turbine operation and control

7-1. Introduction

Owing to inherent limitations in different kinds of the well-known fossil fuel and nuclear energy sources, e.g. carbon footprint, rapidly increasing fuel prices or probability of catastrophic effects of nuclear station malfunction, the last two decades have witnessed a rapid growth in the use of wind energy. Although, it is considered a promising source of energy, depending on naturally generated wind forces, there are several very significant challenges to efficient wind energy conversion for electrical power transformation.

This Chapter focuses on investigations of different aspects of operation and control of wind turbine systems. A typical nonlinear state space model of a wind turbine system is described and a T-S fuzzy model of this system is also presented. The investigations are based on a 5 MW benchmark model proposed by (Odgaard, Stoustrup and Kinnaert, 2009).

7-2. Wind turbine modelling

The principle aim of control in the wind turbine systems operation is to convert wind energy to mechanical energy which in turn is used to produce electricity. These systems are characterized by nonlinear aerodynamic behaviour and depend on a stochastic uncontrollable wind force as a driving signal. To conceptualize the system from analysis and control designs to real application, an accurate overall mathematical model of the turbine dynamics is required. Normally, the model is obtained by combining the constituent subsystem models that together make up the overall wind turbine dynamics. This Section describes the combination of a flexible low speed shaft model together with a two-mass conceptual model of a wind turbine.

The aerodynamic torque (T_a) acting within the rotor represents the principal source of nonlinearity of the wind turbine. T_a depends on the rotor speed ω_r , the blade pitch

angle β and the *effective rotor wind speed* v_{EWS}. The aerodynamic power captured by the rotor is given by:

$$P_{cap} = \frac{1}{2}\rho\pi R^2 C_p(\lambda,\beta)v_{EWS}^3 \tag{7-1}$$

where ρ is the air density, R is the rotor radius, and C_p is the power coefficient that depends on the blade pitch angle (β) and the tip-speed-ratio (λ) (TSR) defined as:

$$\lambda = \frac{\omega_r R}{v_{EWS}} \tag{7-2}$$

The aerodynamic torque is thus:

$$T_a = \frac{1}{2}\rho\pi R^3 C_q(\lambda,\beta)v_{EWS}^2 \tag{7-3}$$

where $C_q = \frac{C_p}{\lambda}$ is the torque coefficient.

The drive train is responsible for gearing up the rotor rotational speed to a higher generator rotational speed. The drive train model includes low and high speed shafts linked together by a gearbox modelled as a gear ratio. The state space model of the wind turbine drive train has the form:

$$\begin{bmatrix}\dot{\omega}_r\\ \dot{\omega}_g\\ \dot{\theta}_\Delta\end{bmatrix} = \begin{bmatrix}a_{11} & a_{12} & a_{13}\\ a_{21} & a_{22} & a_{23}\\ a_{31} & a_{32} & a_{33}\end{bmatrix}\begin{bmatrix}\omega_r\\ \omega_g\\ \theta_\Delta\end{bmatrix} + \begin{bmatrix}b_{11} & 0\\ 0 & b_{22}\\ 0 & 0\end{bmatrix}\begin{bmatrix}T_a\\ T_g\end{bmatrix} \tag{7-4}$$

where:

$a_{11} = -\frac{(B_{dt}+B_r)}{J_r}$ $\quad a_{12} = \frac{B_{dt}}{n_g J_r}$ $\quad a_{13} = -\frac{K_{dt}}{J_r}$ $\quad a_{21} = \frac{B_{dt}}{n_g J_g}$

$a_{22} = -\frac{(B_{dt}+n_g B_g)}{n_g^2 J_g}$ $\quad a_{23} = \frac{K_{dt}}{n_g J_g}$ $\quad a_{31} = 1$ $\quad a_{32} = -\frac{1}{n_g}$

$a_{33} = 0$ $\quad b_{11} = \frac{1}{J_r}$ $\quad b_{22} = -\frac{1}{J_g}$

where J_r is the rotor inertia, B_r is the rotor external damping, J_g is the generator inertia, ω_g and T_g are the generator speed and torque, B_g is the generator external damping, n_g is the gearbox ratio, K_{dt} is the torsion stiffness, B_{dt} is the torsion damping coefficient, and θ_Δ is the torsion angle.

The hydraulic pitch system is modelled as a closed-loop transfer function between the pitch angle β and its reference β_r. In principle it is a piston servo system which can be modelled well by a second order transfer function namely:

$$\beta = \frac{\omega_n^2}{s^2 + 2\zeta\omega_n s + \omega_n^2}\beta_r \tag{7-5}$$

where ζ is the damping factor and ω_n is the natural frequency. A transfer function is associated with each of the three pitch systems. In cases of no fault the damping factors are assumed equal, and the following parameters are used $\zeta = 0.6$ and $\omega_n = 11.11$. In addition, constraints on the pitch actuator are implemented. In particular, the pitch angle is restricted to the interval -2 deg - 90 deg.

Finally, the generator subsystem is given by the following linear relation:

$$\dot{T}_g = -\frac{1}{\tau_g}T_g + \frac{1}{\tau_g}T_{gr} \tag{7-6}$$

Where T_{gr} is the generator torque reference signal and $\tau_g$is the time constant.

7-3. Wind and wind turbine operation

The fact that available wind power is proportional to the wind speed cube, as well as the uncertainty of point measurement of wind speed have given good motivate to include an introductory section to give basic wind characteristics that are exploited to produce electrical power.

The wind varies geographically and temporally. The geographical variation can be understood from both large and local scale points of view. On the large scale, regions around the world differs in their climatic properties and so some of them are windier than others and considered as attractive regions for wind power projects, such geographical variation and illustration of the most world attractive regions are clearly discussed in (Archer and Jacobson, 2005).

Locally, the wind is affected by the local geography such as the proportion of land and sea, the size of land masses, and the presence of mountains. More locally, the wind velocities are reduced by obstacles such as trees and buildings.

The temporal variability of a given local geographical area represents the long term and short term variation of the wind. Long term variation study is concerned with wind

speed variation for intervals of an hour up to several years or decades, whereas, short term variations are considered to operate over a much shorter timescale of minutes down to seconds. Short term variations usually involve turbulence components on the air flow through the turbine rotor. Prediction of long term variations can be a useful aid to determining the most suitable location for developing a wind farm in terms of the amount of power that can be produced for a power generation network. Prediction of long term variations can also assist in the determination or selection of the most suitable wind energy conversion system for a given farm site. Knowledge of the likely extent of the turbulence components will facilitate an understanding of the control design requirements for reducing the effect of turbulence acting on the turbine structure and that also affects the produced power quality (Burton, Sharpe, Jenkins and Bossanyi, 2001).

Currently, wind turbine blades are manufactured to a sweep area with a diameter of up to 120m. With such a large swept area the wind speed differs substantially over the swept area. The modification in the vertical profile of wind speed due to the "surface friction" is called *wind shear*. Wind shear causes the mean wind speed to increase with height, a phenomenon that is one of the contributory factors to aerodynamic loading of the wind turbine. Figure 7-1 shows the wind speed experienced by a sector of the blade a distance r from the rotational axis (Burton, Sharpe, Jenkins and Bossanyi, 2001, Bianchi, de Battista and Mantz, 2007).

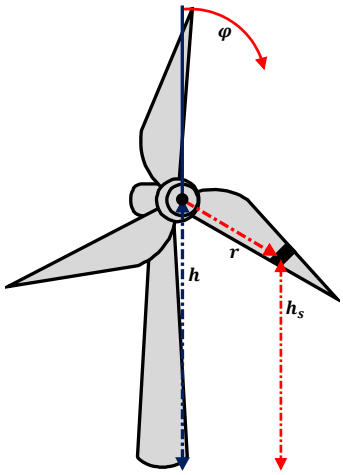

Figure 7-1: Variation of wind speed with vertical profile

Upon rotation the height of this sector (h_s) will vary according to:

$$h_s = h - r\cos\varphi \tag{7-7}$$

Where h is the hub height and φ is the angle the blade makes with respect to upward position. Therefore, the mean wind velocity faced by this blade sector during rotation can be obtained by using the relation between wind speeds at two heights (Bianchi, de Battista and Mantz, 2007):

$$V_m(h_s) = V_m(h)\frac{\ln(\frac{h - r\cos\varphi}{z_o})}{\ln(\frac{h}{z_o})} \tag{7-8}$$

where V_m is the mean wind speed, and z_o is the roughness length that characterizes the terrain. Typical values of z_o for various types of surfaces are given in Table 1.

Table 7-1:Typical values of surface roughness length $\boldsymbol{z_o}$ for various types of terrain (ESDU, 1972)

Type of terrain	$\boldsymbol{z_o}$ **(m)**
Smooth sea	$(2.0 – 3.0) * 10^{-4}$
Sand	$(0.2 – 1.0) * 10^{-3}$
Low grass	$(1.0 – 4.0) * 10^{-2}$
High grass	$(0.4 – 1.0) * 10^{-1}$
Forest	0.1 – 1.0
City	1.0 – 4.0

Figure 7-2 shows the wind shear at different sites. The influence of the wind profile is to cause a thrust force and hence the rotating torque to fluctuate and this clearly has an undesirable effect on both structural loading of the turbine tower and also on the efficiency of energy conversion. The significance of this component is very important in analyzing the effects of blade loads.

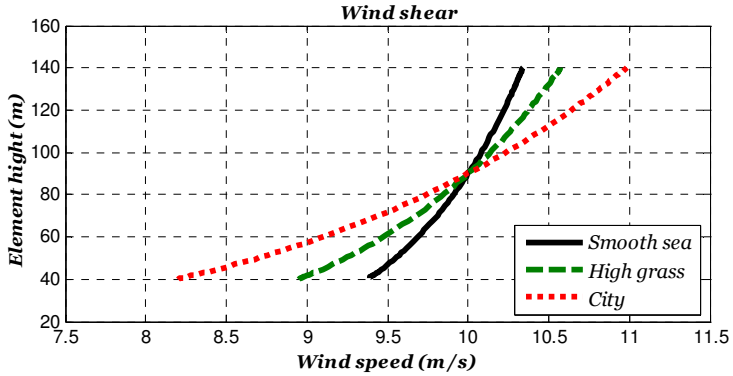

Figure 7-2: The modification in the vertical profile of wind speed (Wind Shear).

Airflow patterns change close to the turbine tower result in what is called *tower shadow*. This is because the tower acts as a periodic obstacle to the airflow through the rotor.. The consequence is a torque reduction at each blade as the blade passes the tower causing periodic pulsations in the overall rotor torque. These pulsations have a significant effect on wind turbine rotors that operate downwind. As a consequence of this wind turbines are usually arranged upwind. More details about the simulation model of wind turbine torque oscillations due to wind shear and tower shadow can be found in (Dolan and Lehn, 2006).

Consequently, wind speed measurements represent a significant challenge in all wind turbine control strategies. This is because the rotor swept area is becoming very large and the wind speed is significantly disturbed in the vicinity of the wind turbine.

7-4. Wind turbine aerodynamic and control

In order to best understand the wind turbine control challenges, the fundamental theory of the wind power extraction process and the upper bound of conversion efficiency $C_{pmax}(\lambda, \beta)$ of the wind power P_{wind} to mechanical power P_{cap} must first be clarified.

Basically, actuator disc theory is used to derive the P_{cap} given in Eq. (7-1) and the maximum $C_p(\lambda, \beta)$. The actuator disc is a generic device that has the ability to extract wind energy when it is immersed in airflow passing through a virtual tube (see Figure 7-3).

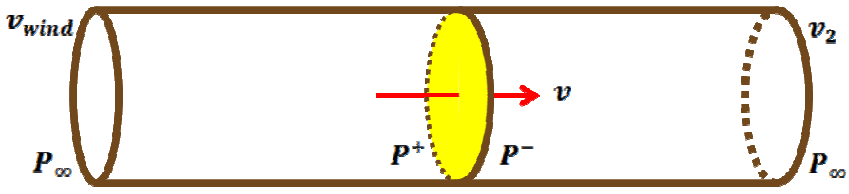

Figure 7-3: Actuator disc

Therefore, due to energy extraction, the downstream wind speed is necessarily slower than the upstream wind speed. However, the mass flow rate must be the same everywhere in the tube. Hence:

$$\rho A_{wind} v_{wind} = \rho A v = \rho A_2 v_2 \tag{7-9}$$

where A_{wind}, A, and A_2 are the upstream, disc, and downstream areas, respectively. The force (F_d) exerted by the wind on the actuator disc is given as:

$$F_d = \rho A v (v_{wind} - v_2) \tag{7-10}$$

Equivalently, F_d can also be defined in term of pressure difference before (P^+) and after (P^-) the disc. Based on Bernoulli's equation, the total energy of the flow remains constant provided no work is done on the fluid. Hence, this equation can be applied upstream and downstream of the actuator disc as follows:

$$\left.\begin{aligned} \tfrac{1}{2}\rho v_{wind}^2 + P_\infty &= \tfrac{1}{2}\rho v^2 + P^+ \\ \tfrac{1}{2}\rho v_2^2 + P_\infty &= \tfrac{1}{2}\rho v^2 + P^- \end{aligned}\right\} \tag{7-11}$$

by taking the difference between expressions in Eq. (7-11), F_d can be rewritten as follows:

$$F_d = A(P^+ - P^-) = \tfrac{1}{2}\rho A (v_{wind}^2 - v_2^2) \tag{7-12}$$

Usually, to represent the P_{cap} in term of P_{wind}, the wind speed at the disc and downstream wind are given in term of upstream wind as follows:

$$\left.\begin{aligned} v &= (1-\alpha) v_{wind} \\ v_2 &= (1-2\alpha) v_{wind} \end{aligned}\right\} \tag{7-13}$$

where α is known as the axial interference factor. Using Eq. (7-12)&(7-13) the power captured by the actuator disc is given by:

$$P_{cap} = \frac{1}{2}\rho A v^3 (4\alpha - 8\alpha^2 + 4\alpha^3) \tag{7-14}$$

the maximum power captured is obtained when $\frac{dP_{cap}}{d\alpha} = 0$, for which $\alpha = \frac{1}{3}$. Hence, by substituting α in Eq. (7-14) the ideal power captured by disc actuator will be:

$$P_{cap} = \frac{1}{2}\rho A v^3 \frac{16}{27} = 0.59 P_{wind} \tag{7-15}$$

Clearly, the three blade variable speed-variable pitch wind turbines are a special case of the actuator disc. In this special structure of actuator disc the blade pitch angles (β), wind speed (v_{EWS})and the rotor rotational speed (ω_r) are the main variables that affect the amount of the power captured. See Figure 7-4.

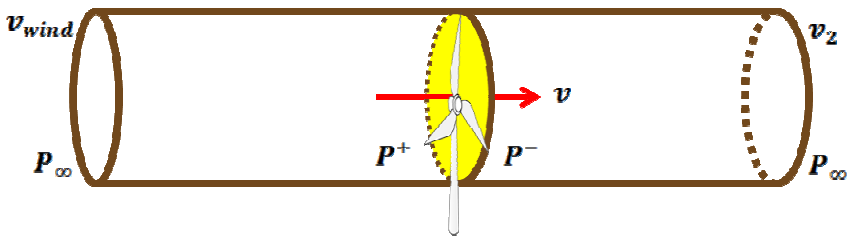

Figure 7-4: Wind turbine power extraction

Usually, wind speed v and rotor rotational speed ω_r are given in terms of the tip speed ratio λ (or TSR). Hence, the variation of power conversion efficiency with respect to λ and β is given either as a mathematical polynomial or as look-up table. Figure 7-5 below shows this relationship for the benchmark wind turbine considered in this thesis.

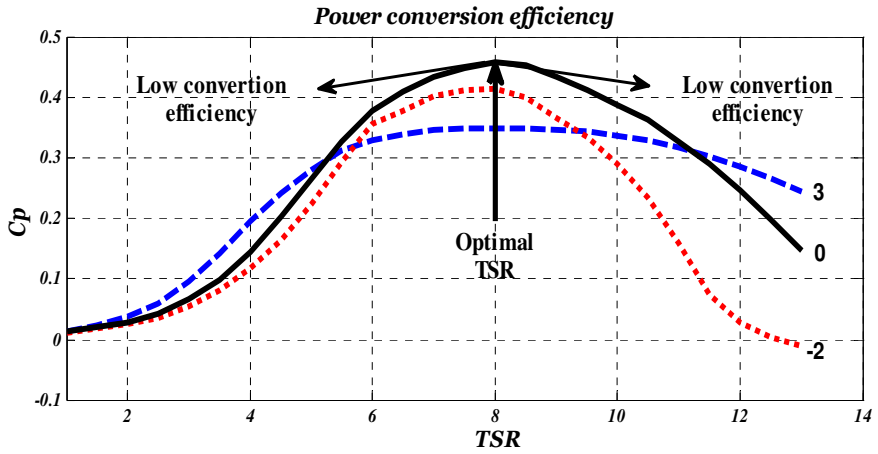

Figure 7-5: Variation of C_p with respect to λ and β

From Figure 7-5 two points must be highlighted:

1. For low wind speeds, to maximize the amount of the captured wind power the blade pitch angle β must be held at a fixed angle corresponding to maximum allowable conversion efficiency curve at which ($\beta = 0$). Additionally, the rotor speed must vary in proportional to the wind speed variation so that λ is kept in the vicinity of it optimal value (λ_{opt}). Specifically, the generator subsystem represents the actuator of the aerodynamic subsystem in the low range of wind speed that decelerates or just releases the aerodynamic subsystem rotation to adjust the variation of rotor speed, so that good tracking of the optimal rotor speed ensured. It should be noted that exact tracking of the optimal rotor speed leads to increasing the load on the drive train shafts and hence minimises the drive train life time. Moreover, exact tracking will also produces a highly fluctuating output power and

produce a varying direction reference torque signals that can lead to abnormal generator operation (Munteanu, Bratcu, Cutululis and Ceanga, 2008).

2. For high wind speeds, it is possible to dissipate some proportion of the available wind power by changing the blade pitch angle to prevent the wind turbine operation from crossing over the rated power. However, to ensure good regulation performance, some control strategies use the generator torque control as a supplementary control signal to overcome the limited rate of change of blade pitch actuator.

The λ_{opt} is determined by relating the blade time t_b and the turbulence time t_w. t_b is the time required by the blade to take the position of the previous one and t_w is the time required to remove the disturbed wind component generated by the movement of the blade. See Figure 7-6.

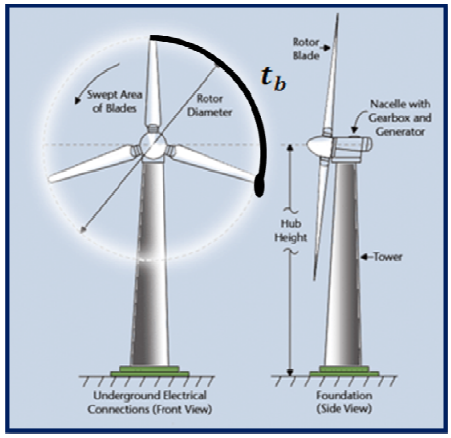

Figure 7-6: The philosophy of λ_{opt}

According to these two times, three operation scenarios can be recognized (Çetin, Yurdusev and Özdemir, 2005, Carriveau, 2011), these are:

1. $t_b > t_w$: This scenario corresponds to slow rotation in which some undisturbed wind passes the area swept by the rotor without harvesting its power content.
2. $t_b < t_w$: This scenario corresponds to fast rotation in which the blade passes through the disturbed wind component generated by the previous blade. In this case the rotor acts as a rigid obstacle and prevents the undisturbed wind from passing through the rotor.
3. $t_b \approx t_w$: This scenario corresponds to the optimal operation in which the blade harvests the power from the re-established wind component.

Suppose the length of the disturbed wind is (S (m)) and (n) is the number of blades, then t_b and t_w are obtained as follows:

$$\left.\begin{aligned} t_b &= \frac{2\pi}{\omega_r n} \\ t_w &= \frac{S}{v} \end{aligned}\right\} \tag{7-16}$$

by setting t_b equal to t_w, the optimal rotational speed thus given as:

$$\omega_{ropt} = \frac{2\pi v}{nS} \tag{7-17}$$

then λ_{opt} can be obtained as follows:

$$\lambda_{opt} = \frac{2\pi R}{nS} \tag{7-18}$$

Hence, wind turbines must be properly controlled to operate at their optimal wind tip speed ratio in order to extract as much wind power as possible. It should be noted that λ_{opt} is determined empirically by the wind turbine manufacturer since it is clear that all the parameters in Eq. (7-18) are dependent on the wind turbine structure. Consequently, the dependence of λ_{opt} on S causes a serious challenge in wind turbine control since S is highly dependent on the blade design. Hence, with turbine aging any deformation in the blade structure causes permanent uncertainty in the value of λ_{opt}.

7-5. Wind turbine development and modes of operation

To be competitive with other energy sources, the main challenges for the deployment of wind turbine systems are to maximize the amount of good quality electrical power extracted from wind energy over a significantly wide range of weather conditions and minimise both manufacturing and maintenance costs (Munteanu, Bratcu, Cutululis and Ceanga, 2008). To maximize the amount of the annual power production and minimize the maintenance times an increase in wind turbine size is suggested (see Figure 7-7). Furthermore, to reduce the effects of obstacles and roughness of terrain (that increases wind force turbulence), offshore wind turbines (OWT) are currently being developed and installed.

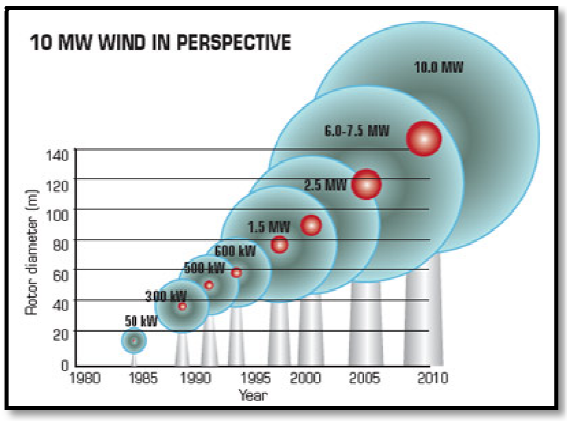

Figure 7-7: Wind turbine sizes and power production (Technology, 2011)

Another opportunity is to change the mode of operation of wind turbines (Bianchi, de Battista and Mantz, 2007, Rahmat Ullah and Thiringer, 2007). There are four modes of wind turbine operation which are:

1. **Fixed speed fixed pitch**: this mode of operation is widely accepted for low capacity wind turbines. the main characteristics of this mode are:
    - The generator is directly connected to the power network and hence the generator speed locked to line frequency.
    - There is no active control to mitigate the loads.
    - Owing to achieve design simplicity, the performance of these wind turbines is poor.
2. **Fixed speed variable pitch**: In this mode of operation, at high wind speed the blade pitch angle is controlled in order to regulate the power generated at the rated one. However, during low wind speed, power maximization is only achieved at single rotational speeds. Hence the main characteristic of this mode are:
    - The generator is directly connected to the power network and hence the generator speed locked to line frequency.
    - At high wind speed the power can be actively regulated via controlling the blade pitch angle.
    - Good regulation at high wind speed and poor power maximization at low wind speed.

    It should be noted that sometimes blade pitch control could be helpful to enhance somewhat the power capture at low wind speed (Hansen et al., 2003, Thiringer and Petersson, 2005).

3. **Variable speed fixed pitch**: In this mode of operation at low wind speed it is possible to control the rotational speed of wind turbine in order to maximize the amount of wind power capture. the main characteristics of this mode are:
    - The generator is not directly connected to the power network and allows changing its rotational speed in proportional to wind speed variation in order to maximize the amount of wind power captured.
    - Passively regulate the power at high wind speed.
4. **Variable speed variable pitch**: This is the recently developed and widely used wind turbine since it can offers superior performance during both low and high wind speed range of operation. the main characteristics of this mode are:
    - The generator speed is allowed to vary according to the wind speed in order to maximize the amount of power captured.
    - Actively regulate the electrical power during high wind speed using blade pitch control.
    - Actively mitigate wind turbine loads.
    - Complex control strategy.

As wind turbines are driven by a naturally generated wind force, in all modes, the operation range is divided into four regions according to wind speed. *Region 1*, this region is also called the *cut-in* region, in which the wind speed is not sufficient to overcome the wind turbine inertia and hence there is no electrical power generated. *Region 2* in which the wind speed is above the cut-in and below the rated wind speed, the wind turbine objective here is to maximize the amount of the power harvested from the wind and transfer it to electrical power. *Region 3* in which the wind speed is high and rotational speed is equal or above the rated speed and below the *cut-out* speed, the objective is to regulate the generated electrical power to be equal to the rate power. *Region 4* in which the wind speed goes above the upper limit of the predefined working range. See Figure 7-8.

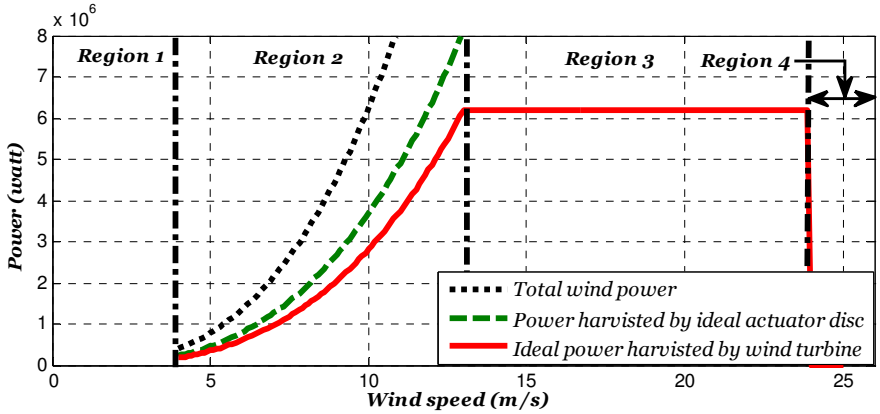

Figure 7-8: Wind turbine region of operation

Whatever the mode of wind turbine operation, the controller designer must consider several facts that characterise the wind turbine systems such as the requirement of different control objective for different ranges of wind speed, the nonlinearity of the aerodynamic subsystem, the lack of accurate measurement of the effective wind speed, and the probability of fault occurrence. Hence, according to the mentioned wind turbine system facts, research concerning wind turbine control can be separated into four parts.

The first part focuses on achieving different control objectives required for each specific range of operating wind speeds. Furthermore, due to reasons of practical implementation simplicity and relative ease of formulating the design objectives, the controllers have been designed based on linearised models of the wind turbine system. Such types of controller can be found in (Burton, Sharpe, Jenkins and Bossanyi, 2001, Wright and Balas, 2004, Esbensen et al., 2008, Munteanu, Bratcu, Cutululis and Ceanga, 2008, Pao and Johnson, 2009, Pao and Johnson, 2011). However, wind turbines have a stochastic and uncontrollable driving force as input in the form of effective wind speed. This, together with overall system nonlinearity, limits the ability of linear control strategies to satisfy the control objectives exactly.

The second part involves strategies to achieve the different control objectives as well as taking into account the system nonlinearity. For example, (Lescher, Zhao and Borne, 2006, Østergaard, Brath and Stoustrup, 2007b, Østergaard, Stoustrup and Brath, 2009, Chadli and El Hajjaji, 2010) uses the multiple-model-based controller design as an approach to cover system nonlinearity.

The third part in which the designers try to consider the control objective, system nonlinearity, and tolerate the effects of probable occurrence of the fault. For example, in

(Kamal, Aitouche, Ghorbani and Bayart, 2012), the suggested methods are observer-based control and the sensor fault tolerant strategy is achieved by switching between two observers directly after the sensor fault being detected by the decision block. The observers are designed based on different sets of output signals that can ensure the observability of the system.

In the fourth part, the designers consider the four requirements of wind turbine control systems. (Sloth, Esbensen and Stoustrup, 2010) proposed a design of active and passive fault tolerant linear parameter varying (LPV) controllers considering the estimation of the effective wind speed. In (Sloth, Esbensen and Stoustrup, 2011) the authors extend their previous work by including the design of the nominal controller and robust controller taking into account the model uncertainty.

7-6. Wind turbine sustainability

Wind turbine systems demand a high degree of reliability and availability (sustainability) and at the same time are characterised by expensive and safety critical maintenance work (van Bussel and Zaaijer, 2001, Verbruggen, 2003, Odgaard and Stoustrup, 2010). The recently developed OWTs are foremost examples since OWT site accessibility and system availability is not always ensured during or soon after malfunctions, primarily due to changing weather conditions. Indeed, maintenance work for OWTs is more expensive than the maintenance of onshore wind turbines by a factor of 5-10 times (van Bussel and Zaaijer, 2001). Hence, to be competitive with other energy sources, the main challenges for the deployment of wind turbine systems are to maximise the amount of good quality electrical power extracted from wind energy over a significantly wide range of weather and operation conditions and minimise both manufacturing and maintenance costs.

The significance of wind turbine control on the overall system behaviour is well investigated in the literature since the control system allows a superior use of the turbine capacity as well as mitigating the effects of mechanical load variation that decrease the useful life of the wind turbine (Burton, Sharpe, Jenkins and Bossanyi, 2001, Bianchi, de Battista and Mantz, 2007, Munteanu, Bratcu, Cutululis and Ceanga, 2008, Bossanyi, Ramtharan and Savini, 2009). However, nominal control systems lack the ability to ensure system sustainability during components and/or system faults. Moreover, since regular and corrective maintenance are among the factors that increase the overall cost

of wind projects, FDD-based preventive maintenance can in some cases capture problems while components are still operational and before other components are damaged, allowing more opportunity to plan the maintenance process whilst reducing system down time. This FDD-based maintenance plays an important role in OWTs project reliability because of site accessibility problem. However, the wind energy technical reports (Verbruggen, 2003) show that some of the currently available signal based monitoring techniques are unreliable and not suitable for wind turbine applications because of the stochastic nature of the wind that affects the fault decision-making.

Consequently, the simultaneous increase of wind turbine accidents with the increase of wind turbine size which are clearly shown in the failure records ,such as the survey of failures in Swedish wind power plant presented in (Ribrant and Bertling, 2007) (see Figure 7-9), as well as the steady increase of the number of OWTs projects have all stimulated research into FTC and FDD in this application area since the ability to detect wind turbine faults and to control turbines in the presence of faults are important aspects of decreasing the cost of wind energy and increasing penetration into electrical grids (Caselitz and Giebhardt, 2005, Andrawus, Watson and Kishk, 2007, Wei and Verhaegen, 2008, Amirat et al., 2009, Hameed et al., 2009, Odgaard, Stoustrup and Kinnaert, 2009, Johnson and Fleming, 2011, Sloth, Esbensen and Stoustrup, 2011, Kamal, Aitouche, Ghorbani and Bayart, 2012).

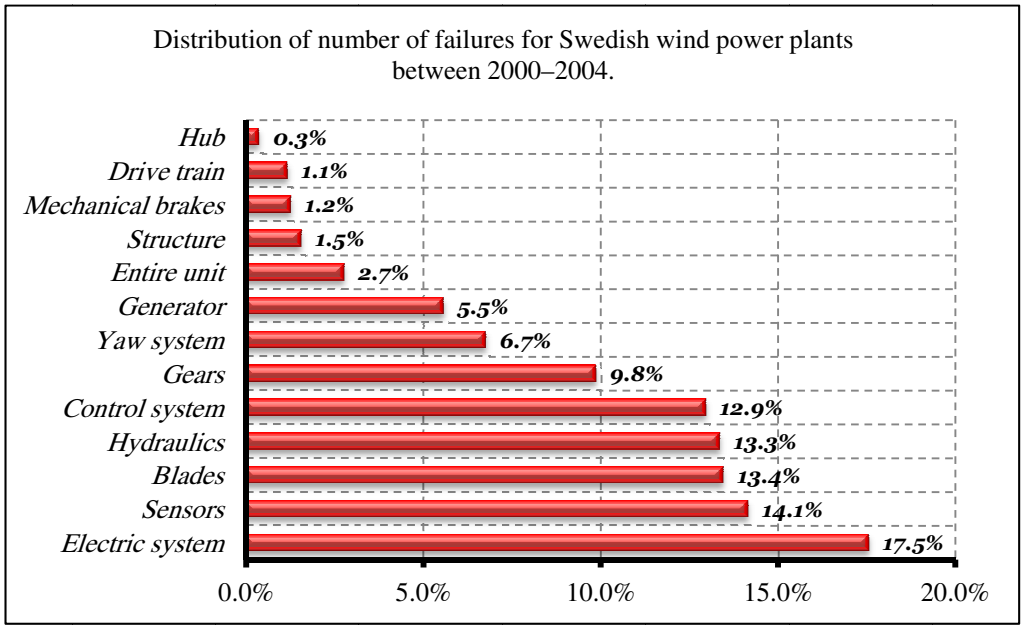

Figure 7-9: Distribution of number of failure for Swedish wind power plants

Clearly, improvements in FDD and FTC can play an important role to ensure the availability of wind turbines during different normal or abnormal operation conditions, minimize the number of unscheduled maintenance operation, and prevent development of minor fault into failure especially for OWTs. For example, the wind turbine benchmark in (Odgaard, Stoustrup and Kinnaert, 2009) involves rotor and generator speed parameter scaling and stuck sensor faults which, from a practical stand point, can be attributed to a smudge on a disc surface of the speed encoder. Clearly, these faults have a direct effect on the reference torque signal provided by the controller. Consequently, the controller will start to drive the wind turbine away from its optimal operation, which in turn leads to lower conversion efficiency or may even prevent the turbine from convert energy (cut-off).

7-7. Wind turbine state space and T-S fuzzy modelling

For controller design purposes the state space model of wind turbine is presented in this Section. The nonlinear model of a wind turbine is established by combining the individual systems given in Section 7-2. However, it is clear that the main source of nonlinearity is the aerodynamic subsystem which is usually linearized in order to predict its effects on all model states. Hence, the state space model of wind turbine is given as:

$$\left.\begin{aligned} \dot{x} &= Ax(t) + Bu + Ev_{EWS} \\ y &= Cx(t) \end{aligned}\right\} \tag{7-19}$$

where

$$A = \begin{bmatrix} -\frac{1}{\tau_g} & 0 & 0 & 0 & 0 & 0 \\ 0 & 0 & I & 0 & 0 & 0 \\ 0 & -\omega_n^2 I & -2\zeta\omega_n I & 0 & 0 & 0 \\ 0 & \frac{1}{J_r}\frac{\partial T_a}{\partial \beta} & 0 & -\frac{(B_{dt}+B_r)}{J_r} + \frac{1}{J_r}\frac{\partial T_a}{\partial \omega_r} & \frac{B_{dt}}{n_g J_r} & -\frac{K_{dt}}{J_r} \\ -\frac{1}{J_g} & 0 & 0 & \frac{B_{dt}}{n_g J_g} & -\frac{(B_{dt}+n_g B_g)}{n_g^2 J_g} & \frac{K_{dt}}{n_g J_g} \\ 0 & 0 & 0 & 1 & -\frac{1}{n_g} & 0 \end{bmatrix}$$

$$B = \begin{bmatrix} \frac{1}{\tau_g} & 0 \\ 0 & 0 \\ 0 & \omega_n^2 I \\ 0 & 0 \\ 0 & 0 \\ 0 & 0 \end{bmatrix}, E = \begin{bmatrix} 0 \\ 0 \\ 0 \\ \frac{1}{J_r}\frac{\partial T_a}{\partial v_{EWS}} \\ 0 \\ 0 \end{bmatrix}, C = \begin{bmatrix} 1 & 0 & 0 & 0 & 0 & 0 \\ 0 & 1 & 0 & 0 & 0 & 0 \\ 0 & 0 & 0 & 1 & 0 & 0 \\ 0 & 0 & 0 & 0 & 1 & 0 \end{bmatrix}, x = \begin{bmatrix} T_g \\ \beta \\ \dot{\beta} \\ \omega_r \\ \omega_g \\ \theta_\Delta \end{bmatrix}, u = \begin{bmatrix} T_{gr} \\ \\ \beta_r \end{bmatrix}$$

$$\frac{\partial T_a}{\partial \beta} = \frac{1}{2\omega_r}\rho A v_{EWS}^3 \frac{\partial C_p}{\partial \beta}$$

$$\frac{\partial T_a}{\partial \omega_r} = \frac{1}{2\omega_r}\rho A v_{EWS}^3 \frac{\partial C_p}{\partial \omega_r} - \frac{1}{2\omega_r^2}\rho A v_{EWS}^3 C_p$$

$$\frac{\partial T_a}{\partial v_{EWS}} = \frac{1}{2\omega_r}\rho A v_{EWS}^3 \frac{\partial C_p}{\partial v_{EWS}} + \frac{3}{2\omega_r}\rho A v_{EWS}^2 C_p$$

where T_g is the generator torque, β is the pitch angle, ω_r and ω_g are the rotor and generator speed respectively, and θ_Δ is the torsional angle. It is clear from the state space model given in Eq. (7-19) that the system matrix A and the disturbance matrix E are not fixed matrices and depend on state variables, the uncontrollable input v_{EWS}, and the partial derivatives of the usually non-analytical function of λ and β, C_p. Hence, to cope with system nonlinearity, a nonlinear control strategy is required to achieve the aim and objectives of wind turbine operation.

Several reasons lead to satisfaction that a T-S fuzzy nonlinear control can cope with wind turbine control requirements, these are:

- The T-S fuzzy control makes use of a linear control strategy locally to produce a nonlinear controller through fuzzy inference modelling, in terms of fuzzy multiple-modelling.
- By increasing the number of premise variables, the T-S fuzzy model can cover a wider range of operation scenarios which cannot be considered with a linear robust controller. For example, a linear robust controller is designed based on the linearized model derived at a specific operation point belong to the ideal operation curve given in Figure 7-8. Hence, all other operating regions are considered as regions with modelling uncertainty, this controller design always degrades the nominal required performance in order to take good care of the modelling uncertainty. On the other hand, by considering the effective wind speed and the rotor speed as premise variables in the low wind speed range (*Region2*), the T-S fuzzy model can approximate the wind turbine model not only during its ideal operation curve but it

can additionally cover the operation scenarios in which the system inputs and outputs deviated from ideal operation trajectory. This scenario usually happens during wind turbine operation, specifically for large inertia wind turbines, since the variation of wind speed is faster than rotor speed variations.

- The structure of the nonlinear state space model given in Eq. (7-19) is characterised by its common input (B) and common output (C) matrices. This fact plays a vital role in simplification and conservatism reduction of T-S fuzzy controller design. For example, the quadratic parameterisation of the dynamic output feedback controller proposed to control the nonlinear inverted pendulum (see description in Chapter 6) can correspondingly be reduced to a linear parameterisation dynamic output feedback controller to control the wind turbine.

As illustrated in Section 7-5 the aim is to develop a controller whose gain varies with wind speed. For example, in the low wind speed range of operation the control aim is to maximise the amount of power extracted from the available wind power through tracking the optimal rotor rotational speed reference signal. Hence, to derive the T-S model with minimum uncertainty, the effective wind speed (v_{EWS}) and the rotor speed (ω_r) are considered as premise variables.

During the low wind speed of operation (*Region 2*) the v_{EWS} varies within the operating range:

$$v_{EWS} \in [v_{min}, v_{max}]\ m\ s^{-1}$$

where in the benchmark wind turbine considered in this thesis $v_{min} = 4\ m\ s^{-1}$ and $v_{max} = 12.5\ m\ s^{-1}$. According to these limits the other premise variable (ω_r) is bounded by:

$$\omega_r \in [\omega_{min}, \omega_{max}]\ rad\ s^{-1}$$

where $\omega_{min} = 0.56\ rad\ s^{-1}$ and $\omega_{max} = 1.74\ rad\ s^{-1}$. The bounds of ω_r are determined using Eq. (7-2) using $\lambda_{opt} = 8$.

The membership function is selected as follows:

$$\left.\begin{aligned} M_1 &= \frac{\omega_r - \omega_{min}}{\omega_{max} - \omega_{min}} \\ M_2 &= 1 - M_1 \\ N_1 &= \frac{v_{EWS} - v_{min}}{v_{max} - v_{min}} \\ N_2 &= 1 - N_1 \end{aligned}\right\} \tag{7-20}$$

Based on these two premise variables four local linear models of the wind turbine can be determined to approximate the nonlinear system at different operating points in the low range of wind speed. Hence, Eq. (7-21) gives the four rule T-S fuzzy model of the nonlinear wind turbine in Eq. (7-19):

$$\left.\begin{aligned} \dot{x} &= \sum_{i=1}^{r} h_i(v_{EWS}, \omega_r)\,[A_i x(t) + Bu + E_i v_{EWS}] \\ y &= Cx(t) \end{aligned}\right\} \tag{7-21}$$

where $h_1 = M_1 * N_1$, $h_2 = M_1 * N_2$, $h_3 = M_2 * N_1$, and $h_4 = M_2 * N_2$.

7-8. Conclusions

In this Chapter the concept of wind turbine operation, the definition of the control problems, modes of operation and the nonlinear and T-S fuzzy model of wind turbine are presented.

Generally, wind turbine control objectives are functions of wind speed. For low wind speeds, the objective is to optimise wind power capture through the tracking of optimal rotor speed signals. Once the wind speed increases above its nominal value the control objective moves to the rated regulating power.

Specifically, in the low wind speed range of operation, the controller optimises power capture through controlling the generator torque so that the wind turbine rotor speed follows the optimal rotor speed.

In fact, from a control stand point, the power optimization problem is a tracking control problem. However, several design constraints must be taken into account in the design of the wind turbine power maximization controller, these are:

a. Wind turbines are characterised by their non-linear aerodynamics and have a stochastic and uncontrollable driving force as input in the form of EWS. This limits

the ability of linear control strategies to maintain acceptable performance over a wide range of wind speed.

b. Due to the common input common output matrices of wind turbine model the conservatism of T-S fuzzy estimation and control is highly reduced.

c. Owing to the direct effect of wind turbine components faults on the wind power conversion efficiency, the designed control strategy must be capable of tolerating different expected fault effects.

d. Accurate computation of optimal rotor speeds (using Eq. 2) depends on the presence of the EWS estimation. Practically, only point wind speed (anemometer based) measurement are available which does not represent the EWS. Therefore, an estimation of EWS based on wind turbine dynamics is preferable since this estimation overcomes the uncertainty in the measured wind speed.

e. Exact tracking leads to increased loading on the two drive train shafts and hence can shorten the drive train life time. This also produces a highly fluctuating output power, and may even produce a varying direction reference torque signal that can lead to abnormal generator operation. It is thus very clear that the multi-objective approach cannot be avoided for robust wind turbine control design.

Chapter 8 : FTC methods for wind turbine operation in *Region 2* [3]

8-1. Introduction

The main challenges for the deployment of wind turbine systems are to maximise the amount of good quality electrical power extracted from wind energy. This must be ensured over a significantly wide range of weather conditions simultaneously with minimising both manufacturing and maintenance costs. In consequence to this, the FTC and FDD research have witnessed a steady increase in interest in this application area as an approach to maintain system sustainability with more focus on OWTs projects.

This Chapter focuses on the presentation of three FTTC strategies for OWTs based on the T-S fuzzy framework. The proposed strategies are: T-S observer-based sensor FTTC, TSDOFC based sensor FTTC, and TSDOFC based sensor FTTC with EWS estimation. The FTTC loops are designed to maintain the power capture optimized even during the generator and rotor rotational speed sensor faults. The simulation results are based on the wind turbine benchmark model presented in (Odgaard, Stoustrup and Kinnaert, 2009).

Recently, T-S fuzzy observer-based sensor AFTC design has been proposed in (Kamal, Aitouche, Ghorbani and Bayart, 2012), see Figure 8-1. The method is based on evaluation of *two* residual signals generated using the *generalized observer* concept of (Patton, Frank and Clark, 1989) to switch the estimation from faulty to healthy observers with the assumption that no simultaneous sensor faults are occur. It is clear that switching between two different observers produces unavoidable spikes that

[3]Part of the work presented in this Chapter was published in:

Sami, M. & Patton, R. J. 2012d. An FTC approach to wind turbine power maximisation via T-S fuzzy modelling and control. 8th IFAC Symposium on Fault Detection, Supervision and Safety of Technical Processes, Mexico City, Mexico, 349-354. 29-31 Aug.

Sami, M. & Patton, R. J. 2012e. Global wind turbine FTC via T-S fuzzy modelling and control. 8th IFAC Symposium on Fault Detection, Supervision and Safety of Technical Processes, Mexico City, Mexico, 325-330. 29-31 Aug.

Sami, M. & Patton, R. J. 2012h. Wind turbine sensor fault tolerant control via a multiple-model approach. The 2012 UKACC International Conference on Control, Cardiff, 3-5 Sep.

specifically affect the drive train torsion of low inertia wind turbines. Also the performance of the proposed FTC strategy is highly affected by the robustness and the computation time of the residual evaluation unit. Moreover, The T-S model in this reference is derived based on measured wind speed which in turn causes clear modelling uncertainty since the wind varies stochastically and faster than wind turbine dynamic and hence it cannot schedule the controller commands appropriately. Furthermore, there is a significant probability of simultaneous occurrence of generator and rotor speed sensor faults.

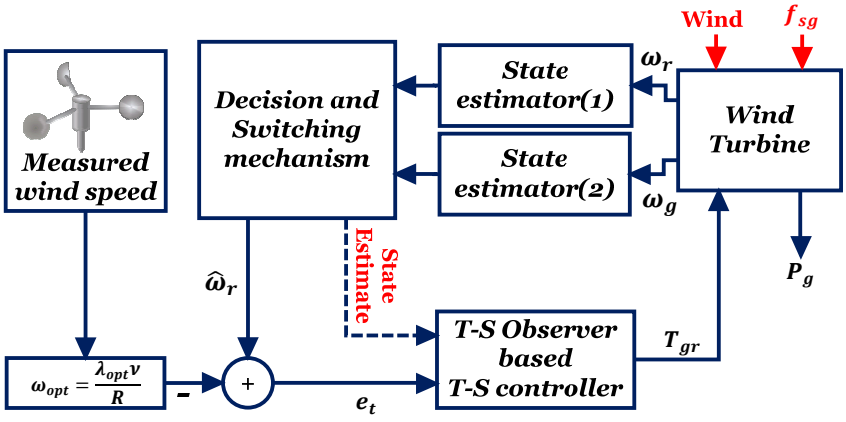

Figure 8-1: Generalized observer-based wind turbine AFTC

Within the framework of the proposed strategies, the use of wind speed and rotor rotational speed as scheduling variables will ensure that the T-S fuzzy model can represents a wide range of operation scenario. Specifically, the model can cover cases in which the system operates away from the ideal power/wind speed characteristic shown in Figure 7-8. In fact, large inertial wind turbines frequently operate away from their ideal power/wind characteristics and hence the use of two scheduling variables is the best approach to handle this challenge.

8-2. Investigation of the effects of some fault scenarios

As stated in Chapter 7, the controller optimises the power captured by controlling the rotor rotational speed by varying the reference generator torque T_{gr} so that the wind turbine rotor speed ω_r follows the optimal rotor speed given by:

$$\omega_{ropt} = \frac{\lambda_{opt} v_{EWS}}{R} \tag{8-1}$$

where ω_{ropt} and λ_{opt} are the optimal rotor speed and the optimal tip speed ratio. In fact, designing a controller for the power optimization problem must achieve the design constraints listed in Section 7-8. One of these constraints is to have capability to tolerate the effects of faults that affect different system components.

The following faults are considered and the proposed control strategies need to tolerate the fault effects so that good tracking performance to ω_{ropt} can be maintained.

- *Rotor speed sensor scaling fault:* the sensor scaling fault (decreasing or increasing) drive the turbine away from the optimal operation. It is very clear that the controller is designed to provide good tracking of ω_{ropt} (i.e. $e_t = \omega_{r-measured} - \omega_{opt} \approx 0$). However, due to the scale factor fault the controller now tries to force the faulty measurement to follow ω_{ropt} (i.e. if the scale faults are $\pm 10\,\%$ then $1.1 * \omega_r - \omega_{opt} \approx 0$ or $0.9 * \omega_r - \omega_{opt} \approx 0$) causing a decelerating or accelerating of the actual rotor speed and hence causing the wind turbine to operate away from the optimal value ω_{opt}. Additionally, more sever sensor scale faults can affect the structure of the wind turbine or guide the wind turbine to the cut-off region. For example, severe scale-down sensor faults cause the turbine to rotate faster according to the available wind speed. Hence, the fast rotation scenario means that the blade passes through the turbulence component of the previous blade before re-establishing the undisturbed wind speed. This induces excessive vibration of the overall structure of the wind turbine. On the other hand, in the scale-up sensor fault the control system slows down the rotor rotational speed. This in turn may lead to the wind turbine entering the cut-off region.
- *Fixed rotor speed sensor fault:* the effect of this fault scenario differs based on the fixed measured rotor speed (magnitude of stuck fault) and ω_{ropt} which in turn depends on wind speed. If ω_{ropt} is lower than the fixed rotor speed measurement then the controller will force the system to slow-down and this in turn may lead to the cut-off rotational speed being reached. On the other hand, if ω_{ropt} is higher than the fixed rotor speed then the controller will simply release the turbine to rotate according to the available wind speed without control.
- *Generator speed sensor bias fault:* the sensor bias fault (decreasing or increasing) affects the closed-loop performance of the wind turbine and hence the wind power conversion efficiency. However, the expected effect of this fault is probably less

than the effect of the rotor speed sensor faults since the generator speed signal is part of the feedback signal and not compared directly with the reference optimal speed (i.e. not the objective signal).

- *Generator torque bias fault:* the effect of torque bias fault is similar to the effect of the rotor speed sensor fault. In this fault scenario the inner-loop generator controller minimises the difference between the T_{gr} and the measured generator torque T_{gm}. In fact, T_{gm} is not directly measured but obtained via soft sensing. Therefore, any bias in this measurement results in driving the system away from optimal operation. This results in a decrease of the wind turbine power conversion efficiency. Fortunately, from a global control stand point this fault appears as a scale actuator fault. This interpretation is considered in Chapter 9.

Figure 8-2 shows the effects of different fault scenarios on the optimal operation of wind turbine.

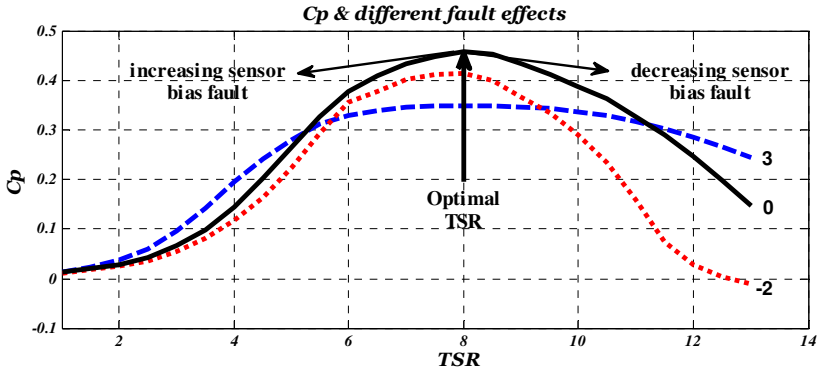

Figure 8-2: The effect of sensor faults on power optimization

Clearly, the generator and rotor speed sensor scaling faults emulate the effect of the λ_{opt} uncertainty problem which arises in part due to wind turbine aging and blade deformation. Hence, even if the scaling fault is minor and does not lead to structural damage, the detection and tolerance of this fault can lead to maintain the harvested power at its optimal value.

Generally, the aim of all proposed FTTC strategies in this Chapter is to maintain the same control law during both faulty and fault-free cases. Estimators are used to simultaneously estimate the sensor fault signals and tolerate their effects on the output signal delivered to the input of the controller.

While the first two proposed strategies make use of measured wind speed, the fault estimator in these strategies is designed to be robust against the expected error between

the measured wind speed and the EWS. This is because the measured wind speed signal does not exactly represent the EWS signal.

8-2-1. T-S fuzzy PMIO based sensor FTC

This Section describes a new T-S fuzzy observer-based sensor FTTC scheme designed to optimise the wind energy captured in the presence of generator and rotor speed sensor faults. To ensure good estimation of a wider than usual range of sensor faults, the FTTC strategy utilises the fuzzy PMIO. The nominal fuzzy controller remains unchanged during faulty and fault-free cases. Although the proposed strategy is dedicated to controlling the wind turbine within the low range of wind speed (below rated wind speed), the proposed controller is useful as a supplementary control to assist the pitch control system as a means of regulating the rotor speed above the rated wind speed.

The main contributions involved in the proposed strategy are: (1) the use of the PMIO to hide or implicitly compensate the effect of drive train sensor faults. This obviates the need for residual evaluation and observer switching (see (Kamal, Aitouche, Ghorbani and Bayart, 2012) for example). (2) The PMIO simultaneously estimates the states and the sensor fault signals. Hence, information about the fault severity can also be provided through the fault estimation signals. (3) The fuzzy PMIO scheme is shown to give good simultaneous state and abrupt sensor fault estimate. Figure 8-3 schematically illustrates the proposed strategy.

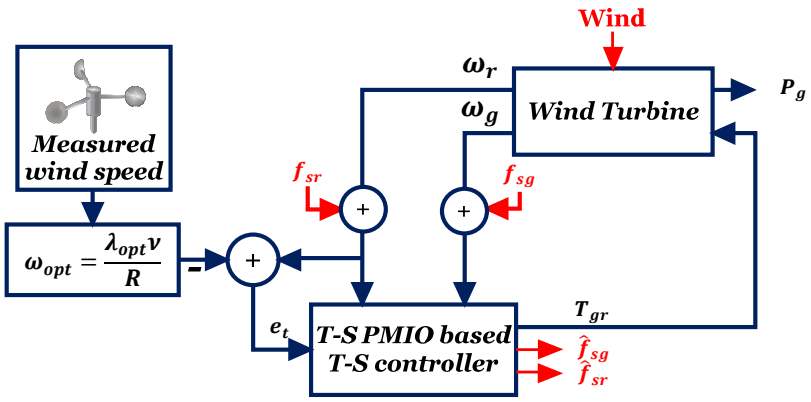

Figure 8-3: Wind turbine PMIO based sensor FTC scheme

In this strategy the controller forces the generator rotational speed to follow the optimal generator speed. Additionally, this strategy makes use of the measured wind speed as an approximation of the EWS.

As derived in Chapter 7 (Section 7-7), the T-S fuzzy model of the nonlinear wind turbine system given in Eq. (7-18) with additive sensor can be expressed as:

$$\left.\begin{aligned} \dot{x} &= A(p)x(t) + Bu + E(p)v_{EWS} \\ y &= Cx(t) + D_f f_s \end{aligned}\right\} \tag{8-2}$$

$A(p) \in \mathcal{R}^{n*n}(= \sum_{i=1}^{r} h_i(p)A_i)$, $B \in \mathcal{R}^{n*m}$, $E(p) \in \mathcal{R}^{n*m_v}(= \sum_{i=1}^{r} h_i(p)E_i)$, $D_f \in \mathcal{R}^{l*g}$ and $C \in \mathcal{R}^{l*n}$ are known system matrices. r is the number of fuzzy rules and the term $h_i(p)$ is the weighting function of the i^{th} fuzzy rule (as defined in Section 7.7) satisfying $\sum_{i=1}^{r} h_i(p) = 1$, and $1 \geq h_i(p) \geq 0$, for all *i*.

An augmented system consisting of the Eq. (8-2) and the tracking error integral ($e_t = \int(y_r - Sy)$) is defined as:

$$\left.\begin{aligned} \dot{\bar{x}} &= \bar{A}(p)\bar{x} + \bar{B}u + \bar{E}(p)v_{EWS} + Ry_r \\ \bar{y} &= \bar{C}\,\bar{x} + \bar{D}_f f_s \end{aligned}\right\} \tag{8-3}$$

$$\bar{A}(p) = \begin{bmatrix} 0 & -SC \\ 0 & A(p) \end{bmatrix}, \bar{x} = \begin{bmatrix} e_t \\ x \end{bmatrix}, \bar{B} = \begin{bmatrix} 0 \\ B \end{bmatrix}, \bar{E}(p) = \begin{bmatrix} 0 \\ E(p) \end{bmatrix}, R = \begin{bmatrix} I \\ 0 \end{bmatrix}$$

$$\bar{C} = \begin{bmatrix} I_q & 0 \\ 0 & C \end{bmatrix}, \bar{D}_f = \begin{bmatrix} 0 \\ D_f \end{bmatrix}$$

where $S \in \mathcal{R}^{w*l}$ is used to define which output variable is considered to track the reference signal. Hence, the tracking problem is transferred to a fuzzy state feedback control, for which the proposed control signal is:

$$u = K(p)\hat{\bar{x}} \tag{8-4}$$

where $K(p) \in \mathcal{R}^{m*(n+w)}(= \sum_{i=1}^{r} h_i(p)K_i)$ is the controller gain and $\hat{\bar{x}} \in \mathcal{R}^{(n+w)}$ is the estimated augmented state vector.

As described in Chapters 4 and 5, if it can be assumed that the q^{th} derivative of the sensor fault signal is bounded, then an augmented state system comprising the states of the original local linear system and the q^{th} derivative of the f_s, is given as follows:

$$\varphi_i = f_s^{q-i} \quad (i = 1,2,\dots,q)\ ,\ \dot{\varphi}_1 = f_s^q; \dot{\varphi}_2 = \varphi_1;\ \dot{\varphi}_3 = \varphi_2; \dots; \dot{\varphi}_q = \varphi_{q-1}$$

Then the system of Eq. (8-2) with the augmented fault derivative states will become:

$$\left.\begin{aligned} \dot{x}_a &= A_a(p)x_a + B_a u + E_a(p)v_{EWS} + R_a y_r + G f_s^q \\ y_a &= C_a x_a \end{aligned}\right\} \tag{8-5}$$

where the augmented matrices are structured as illustrated in Chapters 4 & 5. The following T-S fuzzy PMIO is proposed to simultaneously estimate the system states and sensor faults:

$$\left.\begin{aligned} \dot{\hat{x}}_a &= A_a(p)\hat{x}_a + B_a u + E_a(p)v + R_a y_r + L_a(p)(y_a - \hat{y}_a) \\ \hat{y}_a &= C_a x_a \end{aligned}\right\} \tag{8-6}$$

The state estimation error dynamics are obtained by subtracting Eq. (8-6) from Eq. (8-5) to yield:

$$\dot{e}_x = (A_a(p) - L_a(p)C_a)e_x + G f_s^q + E_a(p)e_v \tag{8-7}$$

where e_v is the difference between the EWS (v_{EWS}) and the measured wind speed (v). The augmented system combining the augmented state space system (8-5), the controller (8-4), and the state estimation error (8-7) is given by:

$$\dot{\tilde{x}}_a(t) = \sum_{i=1}^{r} h_i(p)\{\tilde{A}_i\tilde{x}_a + \tilde{N}_i\tilde{d}\} \tag{8-8}$$

where:

$$\tilde{A}_i = \begin{bmatrix} \bar{A}(p) + \bar{B}K(p) & -\bar{B}[K(p)\ 0_{m\times q}] \\ 0 & A_a(p) - L_a(p)C_a \end{bmatrix}$$

$$\tilde{x}_a = \begin{bmatrix} \bar{x} \\ e_x \end{bmatrix}, \quad \tilde{N}_i = \begin{bmatrix} \bar{E}(p) & 0 & R & 0 \\ 0 & E_a(p) & 0 & G \end{bmatrix}, \tilde{d} = \begin{bmatrix} v_{EWS} \\ e_v \\ y_r \\ f_s^q \end{bmatrix}$$

The objective here is to compute the gains $L_a(p)$ *and* $K(p)$ such that the effect of the input $\tilde{d}$ in Eq. (8-8) is attenuated below the desired level γ, to ensure robust stabilisation performance.

Theorem 8-1**:** *For t>0 and* $h_i(p)h_j(p) \neq 0$, *The closed-loop fuzzy system in (8-8) is asymptotically stable and the* H_∞ *performance is guaranteed with an attenuation level* γ, *provided that the signal* $(\tilde{d})$ *is bounded, if there exist SPD matrices* P_1, P_2, *matrices* H_{ai}, Y_i, *and scalar* γ *satisfying the following LMI constraints (8-9)&(8-10):*

$Minimise\ \gamma, such\ that$:

$$P_1 > 0, \qquad P_2 > 0 \tag{8-9}$$

$$\begin{bmatrix} \Psi_{11} & \Psi_{12} & \bar{E}(p) & 0 & R & 0 & 0 & 0 & 0 & 0 & 0 & X_1 C_p^T \\ * & -2\mu\bar{X}_1 & 0 & 0 & 0 & 0 & \mu I & 0 & 0 & 0 & 0 & 0 \\ * & * & -2\mu I & 0 & 0 & 0 & 0 & \mu I & 0 & 0 & 0 & 0 \\ * & * & * & -2\mu I & 0 & 0 & 0 & 0 & \mu I & 0 & 0 & 0 \\ * & * & * & * & -2\mu I & 0 & 0 & 0 & 0 & \mu I & 0 & 0 \\ * & * & * & * & * & -2\mu I & 0 & 0 & 0 & 0 & \mu I & 0 \\ * & * & * & * & * & * & \Psi_{55} & 0 & E_a(p) & 0 & P_2 G & 0 \\ * & * & * & * & * & * & * & -\gamma I & 0 & 0 & 0 & 0 \\ * & * & * & * & * & * & * & * & -\gamma I & 0 & 0 & 0 \\ * & * & * & * & * & * & * & * & * & -\gamma I & 0 & 0 \\ * & * & * & * & * & * & * & * & * & * & -\gamma I & 0 \\ * & * & * & * & * & * & * & * & * & * & * & -\gamma I \end{bmatrix} < 0 \tag{8-10}$$

where: $K_i = Y_i X_1^{-1},\ L_a = P_2^{-1} H_{ai}\ ,\ X_1 = P_1^{-1}, \bar{X}_1 = diagonal\ (X_1, I_{q\times q})$
$\Psi_{11} = \bar{A}_i X_1 + (\bar{A}_i X_1)^T + \bar{B} Y_i + (\bar{B} Y_i)^T;\ \Psi_{12} = [-\bar{B} Y_i \quad 0];$
$\Psi_{55} = P_2 A_{ai} + (P_2 A_{ai})^T - H_{ai} C_a - (H_{ai} C_a)^T.$

Proof: This proceeds in a similar way to the steps illustrated to prove *Theorem 5-3* and hence the details are omitted here.

8-2-1-1. Simulation results

The rotor and generator sensor faults are represented by two scale errors. The scale factors of 1.1 & 0.9 are multiplied by the simulated real generator and rotor rotational speeds. The expected fault effects represent a deviation of the wind turbine from the optimal operation. Figure 8-4 shows how the wind turbine operation is affected by the two fault scenarios and helps to illustrate the success of the proposed strategy to tolerate the effects of sensor faults and maintain optimal wind turbine operation.

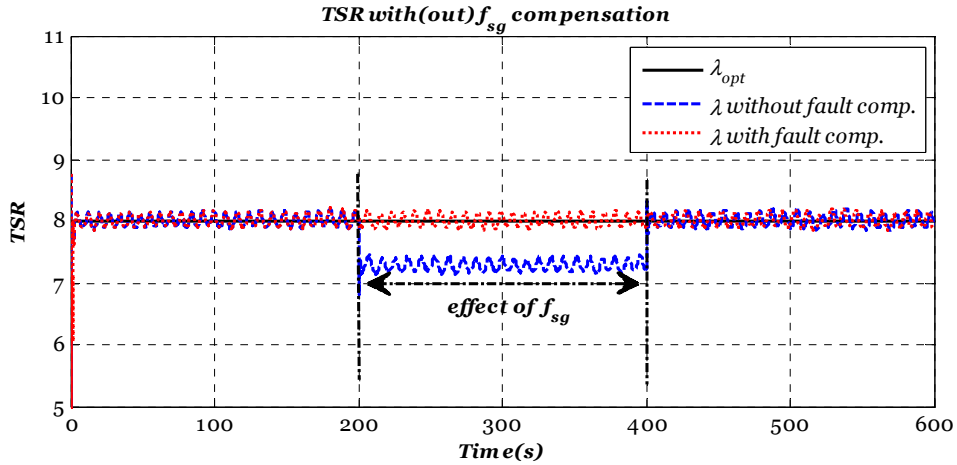

(a)

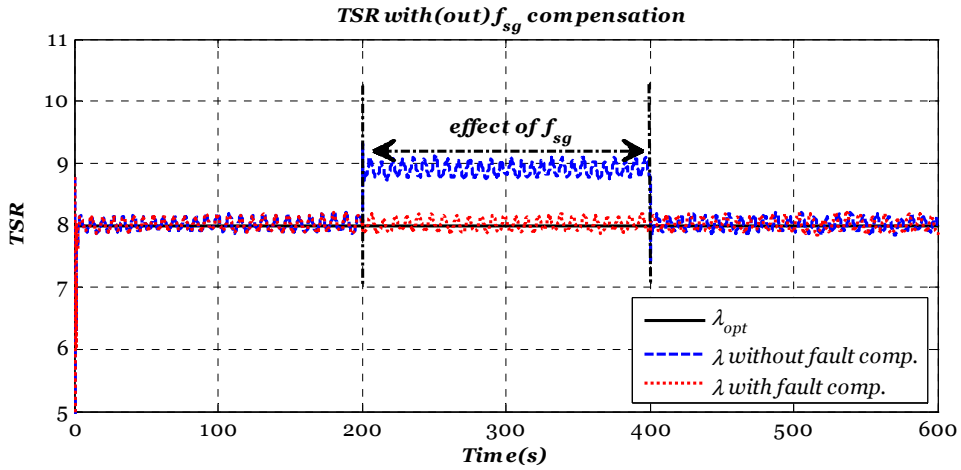

(b)

Figure 8-4: Effect of 1.1 (a) and 0.9 (b) sensor scale faults with(out) fault compensation

It is clear that the 1.1 scale sensor fault causes a deceleration of ω_r & ω_g. Based on the faulty measurement the controller forces the turbine to reduce the rotational speed by increasing the reference generator torque (the generator acts with a breaking torque that can decelerate or release the aerodynamic subsystem) which in turn increases the drive train load. Hence, although the sensor fault is a scale-up fault, the actual rotational speeds of the generator and rotor are decelerated as a result of the dependence of the controller on the faulty measured signal. The effect of this fault scenario is shown in Figure 8-5 without sensor fault compensation. Conversely, the 0.9 scale sensor fault causes acceleration of ω_r & ω_g since, based on faulty measurement; the controller releases the aerodynamic subsystem to rotate according to the available wind speed. Figure 8-6 shows the effect of the 0.9 sensor fault without compensation.

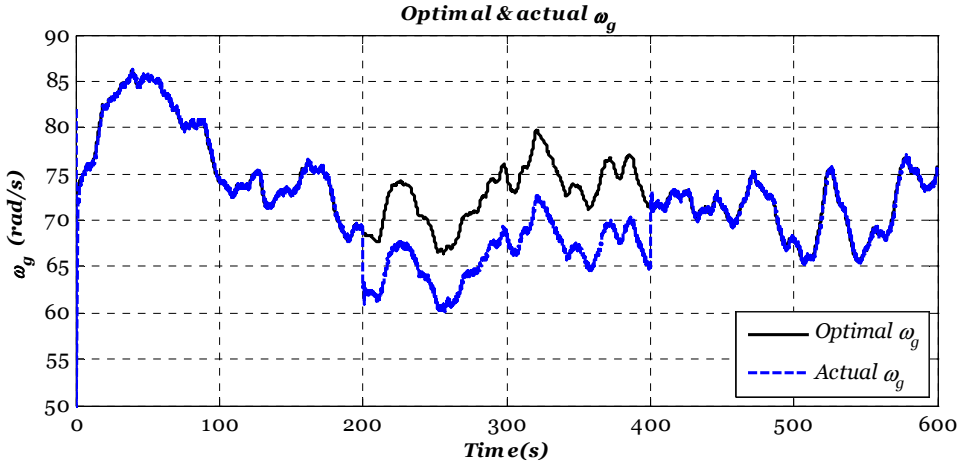

(a)

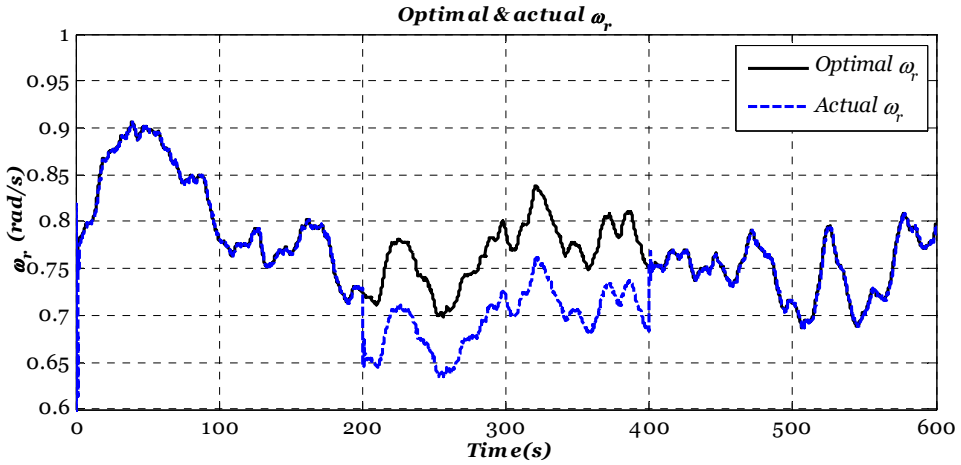

(b)

Figure 8-5: 1.1 sensor scale fault decelerate ω_g(a) & ω_r (b)

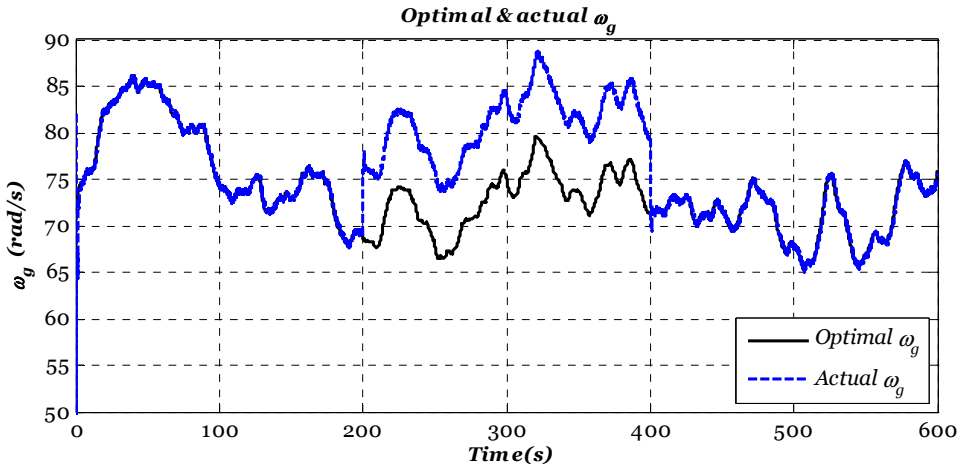

(a)

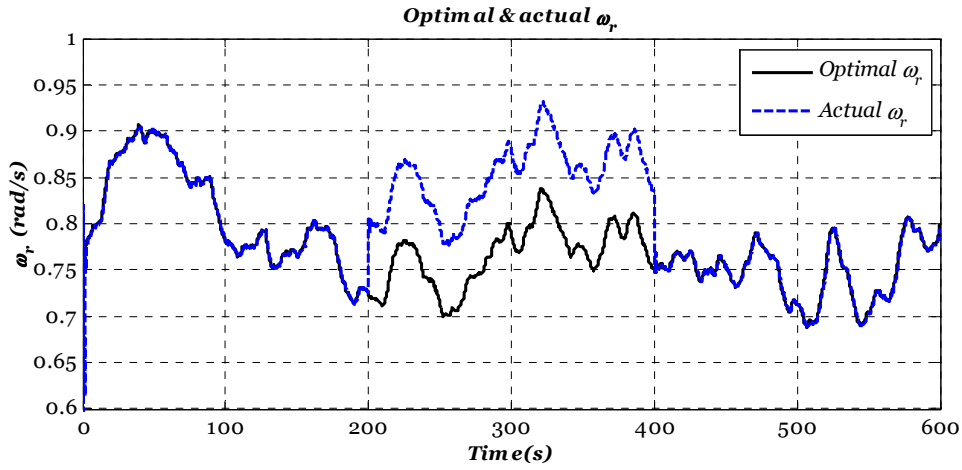

(b)

Figure 8-6: 0.9 sensor bias fault accelerate ω_g(a) & ω_r (b)

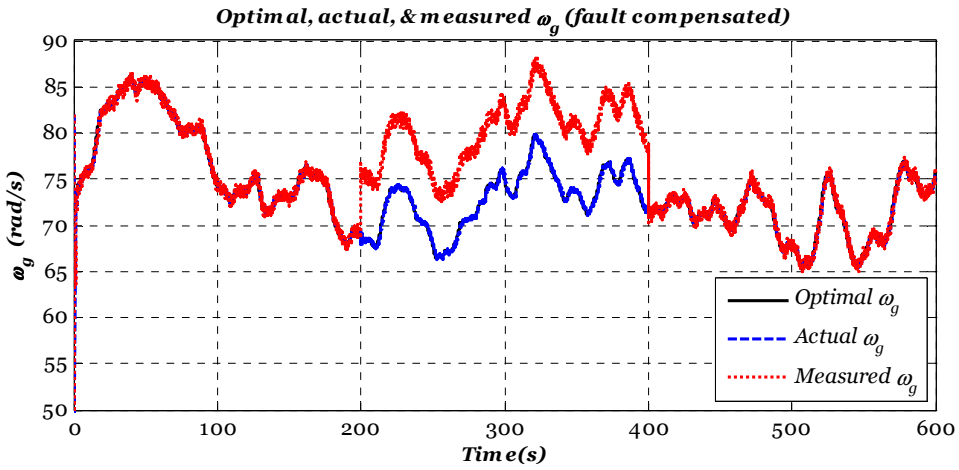

(a)

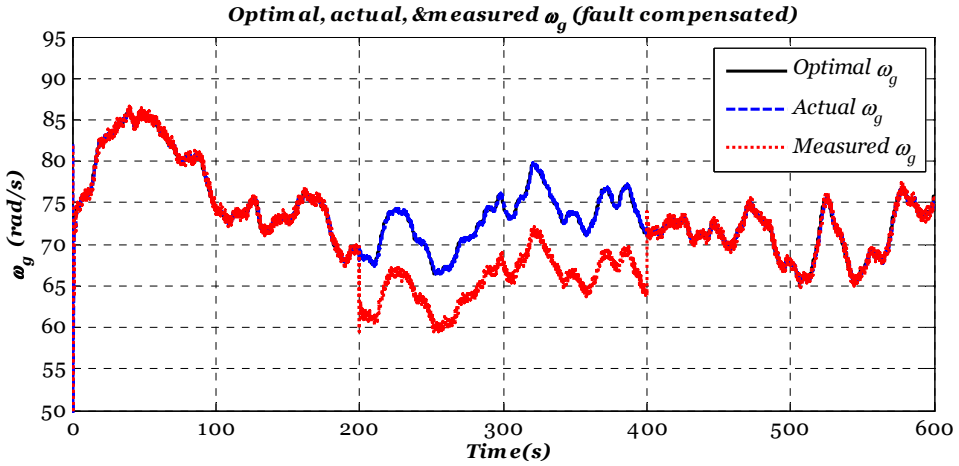

(b)

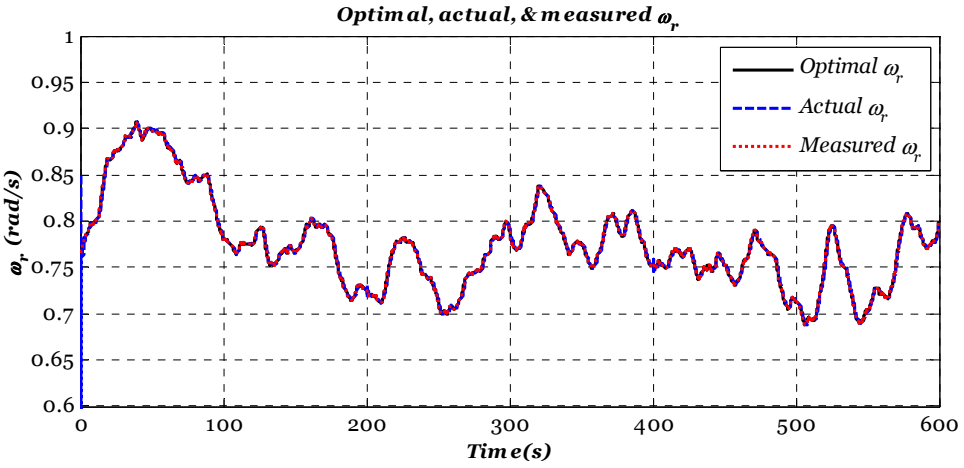

(c)

Figure 8-7: Actual, optimal, and measured ω_g(a &b) & ω_r (c) using the proposed sensor FTC strategy

The generator rotational speed sensor fault estimation signals for both 0.9 and 1.1 scale factor fault scenarios are shown in Figure 8-8.

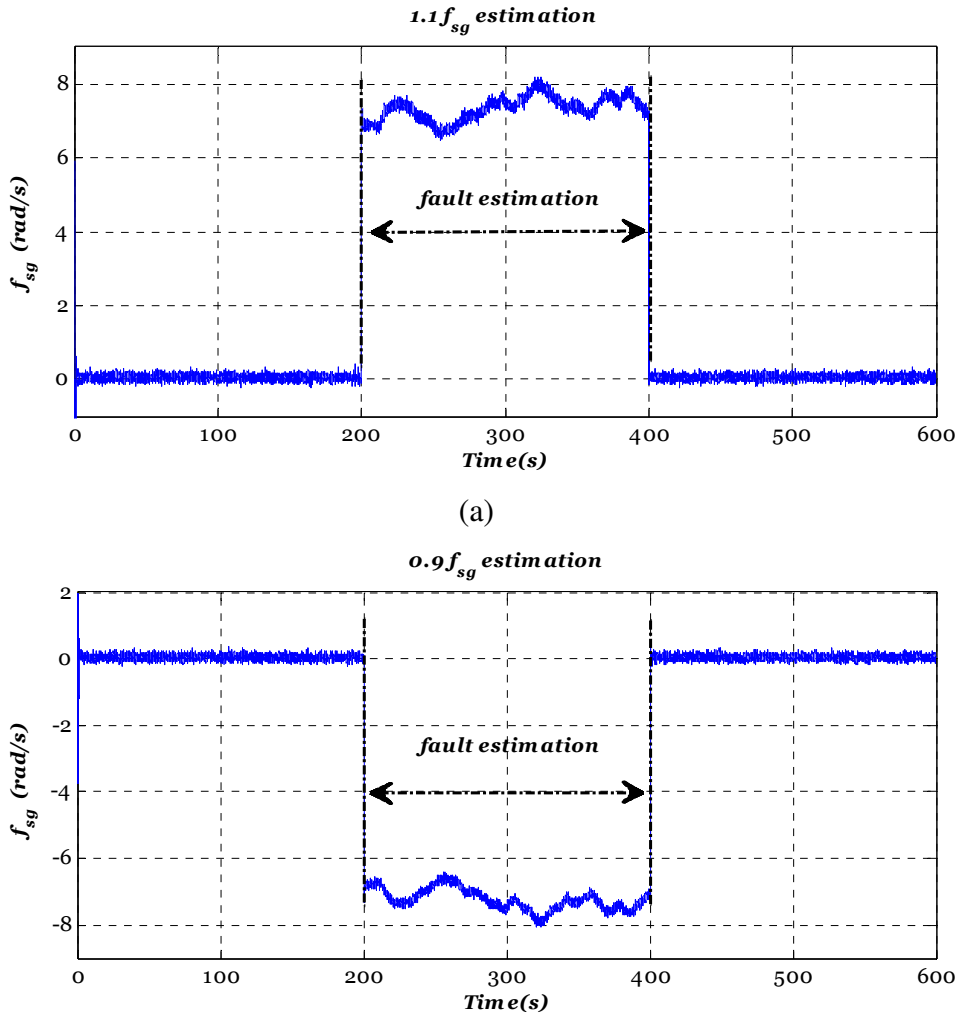

(a)

(b)

Figure 8-8: Estimation of 1.1 (a) and 0.9 (b) sensor bias faults

As discussed in Chapter 4, the T-S PMIO can provide information about the fault severity via the fault estimation signal. This is achieved through taking the ratio between the measured generator speed and the estimated signal. Hence, if there are no faults the ratio should be 1 otherwise any deviation from unity indicates the occurrence of the fault and the magnitude of the deviation represents the fault severity. Figure 8-9 shows the fault evaluation signal for both fault scenarios.

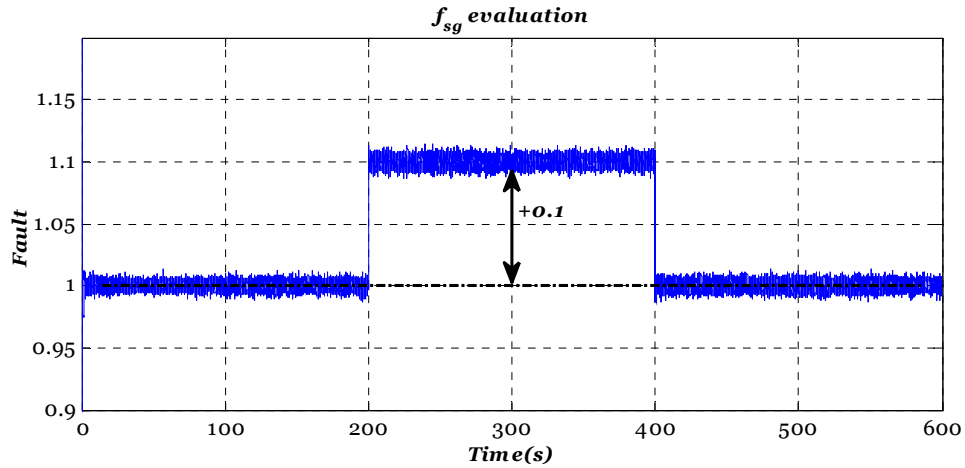

(a)

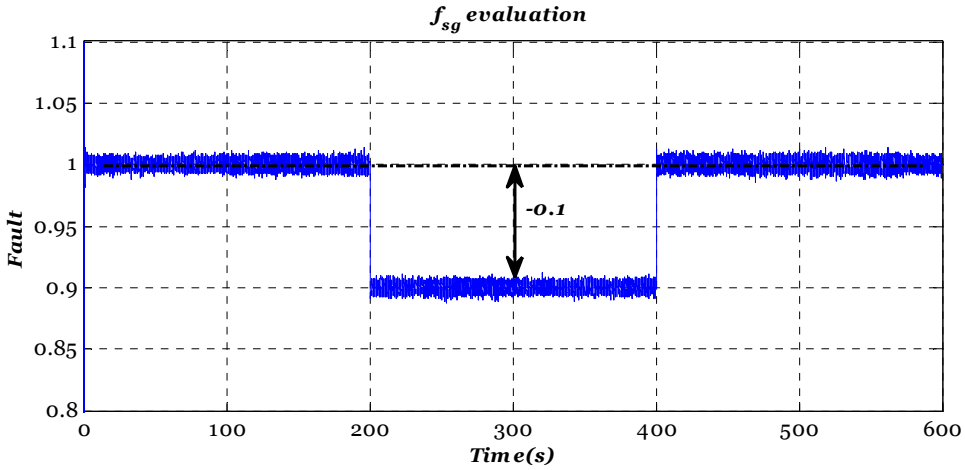

(b)

Figure 8-9: Deviation of 1.1 (a) and 0.9 (b) sensor measurements from unity

It should be noted that maintaining state estimation without changes during the whole range of operation is due to the fact that the fuzzy PMIO performs implicit fault estimation and compensation of sensor faults from the input of PMIO. As discussed in Chapter 4, this fact is clearly interpreted from the error signal ($y_a - C_a\hat{x}_a$) which can be rewritten as ($\bar{C}\bar{x} + \bar{D}f_s - \bar{C}\hat{\bar{x}} - \bar{D}\hat{f}_s$), then as long as there are no sensor faults, $\hat{f}_s = 0$. However, once a sensor fault occurs the fault estimation $\hat{f}_s$ compensates the effect of the fault signal f_s and hence the observer always receives a fault-free error signal.

8-2-2. TSDOFC based active sensor FTTC

Due to a global stability requirement for both of the T-S fuzzy control and the T-S fuzzy observer, the *separation principle* cannot be ensured even when the model uncertainty is not considered (see Section 6-2 for further details). On the other hand, the sensor faults proposed in the benchmark have an abrupt change behaviour for which the use of

fast fault estimation observer is of great advantage. To overcome these challenges this Section focuses on the presentation of a combination of T-S fuzzy PPIO and TSDOFC for wind turbine sensor FTTC. A generic scheme of the proposed strategy is shown in Figure 8-10.

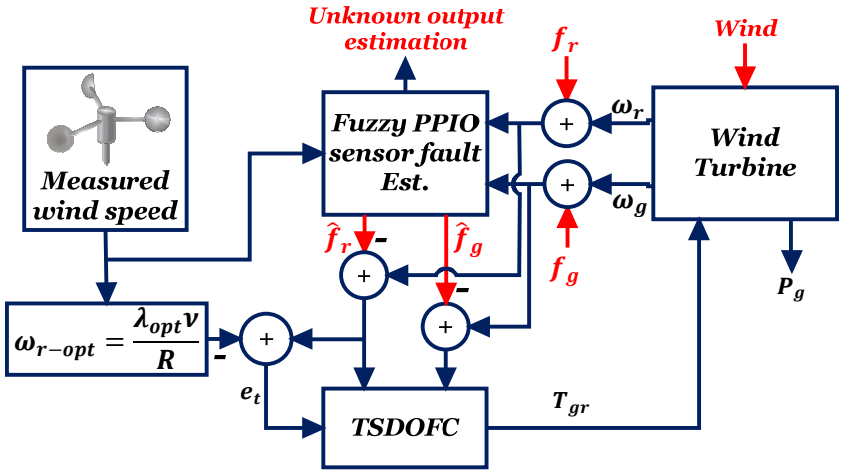

Figure 8-10: Active sensor FTC scheme

8-2-2-1. The T-S fuzzy PPIO design

For the T-S fuzzy model of a wind turbine given in Eq. (8-2), let $e_f \in \mathcal{R}^g$ be the fault estimation error defined as:

$$e_f = f_s - \hat{f}_s \tag{8-11}$$

To avoid the direct multiplication of the sensor and/or noise by the PPIO gains, an augmented system state with output filter states is constructed. The filtered output is given as follows:

$$\dot{x}_s = -A_s x_s + A_s C x + A_s D_f f_s \tag{8-12}$$

where $-A_s \in R^{l*l}$ is a stable matrix. The augmented state system is given as:

$$\left.\begin{aligned} \dot{\bar{x}} &= \bar{A}(p)\bar{x} + \bar{B}u + \bar{E}(p)v_{EWS} + \bar{D}_f f_s \\ \bar{y} &= \bar{C}\,\bar{x} \end{aligned}\right\} \tag{8-13}$$

$$\bar{A}_i = \begin{bmatrix} A(p) & 0 \\ A_s C & -A_s \end{bmatrix}, \bar{x} = \begin{bmatrix} x_f \\ x_s \end{bmatrix}, \bar{B} = \begin{bmatrix} B \\ 0 \end{bmatrix}, \bar{E}(p) = \begin{bmatrix} E(p) \\ 0 \end{bmatrix}, \bar{D}_f = \begin{bmatrix} 0 \\ A_s D_f \end{bmatrix}, \bar{C} = [0 \quad I_l]$$

To deal with time-varying fault scenarios the fuzzy fast fault estimation presented in Chapter 6 is used with assumed bounds on the first derivative of each fault. Hence, the

following fuzzy observer is proposed to simultaneously estimate the system states and sensor fault.

$$\left.\begin{aligned}\dot{\hat{\bar{x}}} &= \bar{A}(p)\hat{\bar{x}} + \bar{B}u + \bar{D}_f\hat{f}_s + \bar{E}(p)v + \bar{L}(p)(\bar{C}\bar{x} - \bar{C}\hat{\bar{x}})\\ \dot{\hat{f}}_s(t) &= F(p)\bar{C}(\dot{e}_x + e_x)\end{aligned}\right\} \tag{8-14}$$

where $\hat{\bar{x}} \in \mathcal{R}^{n+l}$ is the estimate of the state vector $\bar{x}$, v is anemometer measured wind speed, $\bar{L}(p) \in \mathcal{R}^{(n+l)\times l}$, and $F(p) \in \mathcal{R}^{g\times l}$ are the observer gains to be designed, and e_x is the state estimation error defined as:

$$e_x = \bar{x} - \hat{\bar{x}} \tag{8-15}$$

The estimator in Eq. (8-14) provides simultaneous estimation of the system state and fault signals. The state estimation error dynamic are then:

$$\dot{e}_x = (\bar{A}(p) - \bar{L}(p)\bar{C})e_x + \bar{D}_f e_f + \bar{E}(p)e_v \tag{8-16}$$

where e_v is the difference between the EWS and the anemometer measured wind speed. Using (8-14) and (8-16) the fault estimation error dynamics are then as follows:

$$\dot{e}_f = \dot{f}_s - F(p)\bar{C}(\bar{A}(p) - \bar{L}(p)\bar{C} + I)e_x - F(p)\bar{C}\bar{D}_f e_f - F(p)\bar{C}\bar{E}(p)e_v \tag{8-17}$$

The augmented estimator will then be of the following form:

$$\dot{\tilde{e}}_a(t) = \tilde{A}(p,p)\tilde{e}_a + \tilde{N}(p,p)\tilde{z} \tag{8-18}$$

$$\tilde{A}(p,p) = \begin{bmatrix}\bar{A}(p) - \bar{L}(p)\bar{C} & \bar{D}_f\\ -F(p)\bar{C}(\bar{A}(p) - \bar{L}(p)\bar{C} + I) & -F(p)\bar{C}\bar{D}_f\end{bmatrix}$$

$$\tilde{e}_a = \begin{bmatrix}\mathrm{e_x}\\ e_f\end{bmatrix}, \tilde{z} = \begin{bmatrix}e_v\\ \dot{f}_s\end{bmatrix}, \tilde{N}(p,p) = \begin{bmatrix}\bar{E}(p) & 0\\ -F(p)\bar{C}\bar{E}(p) & I\end{bmatrix}$$

The objective is to compute the gains $\bar{L}(p)$ and $F(p)$ such that the exogenous input $\tilde{z}$ in Eq. (8-18) are attenuated below the desired level γ to ensure robust regulation performance in addition to locating the observer poles within a specified disc region characterized by its radius (α) and centre (β).

Theorem 8-2: *The estimation error system eigenvalues are located in a disc region in the complex plane defined by (α, β) so that the error dynamics are stable. Furthermore, the H_∞ performance is guaranteed with an attenuation level γ, (provided that the signal ($\dot{f}_s$) is bounded), if there exist an SPD matrix P_1, matrices $\bar{H}_i, F_i$, and a scalar μ, α, and β satisfying the following LMI constraints:*

$$\begin{bmatrix} -\alpha P_1 & 0 & \phi_1 & \phi_2 \\ 0 & -\alpha I & \phi_3 & \phi_4 \\ * & * & -\alpha P_1 & 0 \\ * & * & 0 & -\alpha I \end{bmatrix} < 0 \tag{8-19}$$

$$\begin{bmatrix} \Psi_{11} & \Psi_{12} & \Psi_{13} & 0 & C_{p1}^T & 0 \\ * & \Psi_{22} & \Psi_{23} & I & 0 & C_{p2}^T \\ * & * & -\gamma I & 0 & 0 & 0 \\ * & * & * & -\gamma I & 0 & 0 \\ * & * & * & * & -\gamma I & 0 \\ * & * & * & * & * & -\gamma I \end{bmatrix} < 0 \tag{8-20}$$

$\bar{L}(p) = P_1^{-1}\bar{H}(p)$, $\Psi_{11} = P_1\bar{A}(p) + \left(P_1\bar{A}(p)\right)^T - \bar{H}(p)\bar{C} - (\bar{H}(p)\bar{C})^T$

$\Psi_{12} = -(\bar{A}^T(p)P_1\bar{D}_f - \bar{C}^T\bar{H}^T(p)\bar{D}_f)$; $\Psi_{13} = P_1\bar{E}(p)$, $\Psi_{22} = -2\bar{D}_f{}^T P_1\bar{D}_f$

$\Psi_{23} = -\bar{D}_f{}^T P_1\bar{E}(p)$; $\phi_1 = P_1\bar{A}(p) - \bar{H}(p)\bar{C} + \beta P_1$, $\phi_2 = P_1\bar{D}_f$

$\phi_3 = -\left(\bar{A}^T(p)P_1\bar{D}_f - \bar{C}^T\bar{H}^T(p)\bar{D}_f + \bar{D}_f{}^T P_1\right)^T$; $\phi_4 = -\bar{D}_f{}^T P_1\bar{D}_f + \beta I$

***Proof*:** Similar to the steps presented in Chapter 6 to prove *Theorem 6-1*, hence details are omitted here.

8-2-2-2. The TSDOFC design

The control objective here is to design a dynamic output feedback controller capable of forcing the wind turbine rotor rotational speed to follow the optimal rotor speed signal in both faulty and fault-free cases.

An augmented system consisting of the system in (8-2) and the integral of the tracking error $e_{ti} = \int(y_r - Sy)$ is defined as:

$$\left.\begin{aligned} \dot{\bar{x}} &= \bar{A}(p)\bar{x} + \bar{B}u + \bar{E}(p)v_{EWS} + Ry_r + D_{in}e_f \\ \bar{y} &= \bar{C}\,\bar{x} + \bar{D}_f e_f \end{aligned}\right\} \tag{8-21}$$

$$\bar{A}(p) = \begin{bmatrix} 0 & -SC \\ 0 & A(p) \end{bmatrix}, \bar{x} = \begin{bmatrix} e_{ti} \\ x \end{bmatrix}, \bar{B} = \begin{bmatrix} 0 \\ B \end{bmatrix}, D_{in} = \begin{bmatrix} -SD_f \\ 0 \end{bmatrix}, \bar{E}(p) = \begin{bmatrix} 0 \\ E(p) \end{bmatrix}, R = \begin{bmatrix} I \\ 0 \end{bmatrix}$$

$$\bar{C} = \begin{bmatrix} I & 0 \\ 0 & C \end{bmatrix}, \bar{D}_f = \begin{bmatrix} 0 \\ D_f \end{bmatrix}$$

where $S \in \mathcal{R}^{q*l}$ is used to define which output variables are considered to track the reference signal. As stated in Chapter 6, since the system in (8-2) has common input and output matrices (*B* & *C*), the linear parameterization dynamic output feedback controller used to stabilize and perform the tracking objective and defined as:

$$\left.\begin{aligned} \dot{x}_c &= A_c(p)x_c + B_c(p)(S_r y_r - \bar{y}) \\ u &= C_c(p)x_c + D_c(p)(S_r y_r - \bar{y}) \end{aligned}\right\} \tag{8-22}$$

where x_c is the state and $A_c(p) \in \mathcal{R}^{(n+q)\times(n+q)}$, $B_c(p) \in \mathcal{R}^{(n+q)\times(l+q)}$, $C_c(p) \in \mathcal{R}^{m\times(n+q)}$, $D_c \in \mathcal{R}^{m\times(l+q)} and\ S_r \in \mathcal{R}^{(l+q)\times q}$ is introduced to match the dimensions of $y_r\ and\ \bar{y}$.

Aggregation of (8-21) and (8-22) gives the following system:

$$\left.\begin{aligned} \dot{x}_a &= A_a(p)x_a + E_a(p)d \\ \bar{y} &= C_a x_a + D_a d \end{aligned}\right\} \tag{8-23}$$

$$A_a(p) = \begin{bmatrix} \bar{A}(p) - \bar{B}D_c(p)\bar{C} & \bar{B}C_c(p) \\ -B_c(p)\bar{C} & A_c(p) \end{bmatrix}, x_a = \begin{bmatrix} \bar{x} \\ x_c \end{bmatrix}, d = \begin{bmatrix} v_{EWS} \\ e_f \\ y_r \end{bmatrix}, C_a = [\bar{C} \quad 0]$$

$$D_a = \begin{bmatrix} 0 & \bar{D}_f & 0 \end{bmatrix}, E_a(p) = \begin{bmatrix} \bar{E}(p) & D_{in} - \bar{B}D_c(p)\bar{D}_f & R + \bar{B}D_c(p)S_r \\ 0 & -B_c(p)\bar{D}_f & B_c(p)S_r \end{bmatrix}$$

Theorem 8-3: *The eigenvalues of the closed-loop system (8-23) are located in the disc region of the negative complex plane characterised by the radius (α) and centre (β), so that the closed-loop is stable and tracks the reference signal with guaranteed H_∞ performance and with an attenuation level γ, (provided that the signals in d is bounded), if there exist SPD matrices X, Y, matrices $A_c(p), B_c(p), C_c(p)$, and $D_c(p)$ satisfying the following LMI constraints:*

$$\begin{bmatrix} -\alpha X & -I & \phi_{1c} & \phi_{2c} \\ -I & -\alpha Y & \phi_{3c} & \phi_{4c} \\ * & * & -\alpha X & 0 \\ * & * & 0 & -\alpha Y \end{bmatrix} < 0 \tag{8-24}$$

$$\begin{bmatrix} \Psi_{11c} & \Psi_{12c} & \bar{E}(p) & \Psi_{13c} & \Psi_{14c} & XC_{p1}^T \\ * & \Psi_{22c} & Y\bar{E}(p) & \Psi_{23c} & \Psi_{24c} & C_{p1}^T \\ * & * & -\gamma I & 0 & 0 & 0 \\ * & * & * & -\gamma I & 0 & 0 \\ * & * & * & * & -\gamma I & 0 \\ * & * & * & * & * & -\gamma I \end{bmatrix} < 0 \quad (8\text{-}25)$$

where

$\Psi_{11c} = \bar{A}(p)X + (\bar{A}(p)X)^T + \bar{B}\hat{C}(p) + \left(\bar{B}\hat{C}(p)\right)^T$; $\Psi_{12c} = \hat{A}^T(p) + \bar{A}(p) - \bar{B}\hat{D}(p)\bar{C}$

$\Psi_{13c} = D_{in} - \bar{B}(p)\hat{D}(p)\bar{D}_f$; $\Psi_{22c} = Y\bar{A}(p) + \left(Y\bar{A}(p)\right)^T + \hat{B}(p)\bar{C} + \left(\hat{B}(p)\bar{C}\right)^T$

$\Psi_{23c} = YD_{in} + \hat{B}(p)\bar{D}_f$; $\Psi_{14c} = R + \bar{B}\hat{D}(p)S_r$; $\Psi_{24c} = YR - \hat{B}(p)S_r$

$\phi_{1c} = \bar{A}(p)X + \bar{B}\hat{C}(p) + \beta X$; $\phi_{2c} = \bar{A}(p) - \bar{B}\hat{D}(p)\bar{C} + \beta I$

$\phi_{3c} = \hat{A}(p) + \beta I$; $\phi_{4c} = Y\bar{A}(p) + \hat{B}(p)\bar{C}(p) + \beta Y$

The controller gains are thus calculated as follows:

$D_c(p) = \widehat{D}(p)$; $C_c(p) = \left(\hat{C}(p) + D_c(p)\bar{C}X\right)M^{-T}$; $B_c(p) = N^{-1}(-\hat{B}(p) - Y\bar{B}D_c(p)$

$A_c(p) = N^{-1}(\hat{A}(p) - Y\left(\bar{A}(p) - \bar{B}\hat{D}(p)\bar{C}\right)X - Y\bar{B}C_c(p)M^T + NB_c(p)\bar{C}X)M^{-T}$

where $M\ and\ N$ satisfy $MN^T = I - XY$

***Proof*:** Similar to the steps presented in Chapter 6 to prove *Theorem 6-3*, hence details are omitted here.

8-2-2-3. Simulation results

This proposed controller is also applied to the benchmark model mentioned previously. Three fault scenarios are considered in this subsection, these are:

1. Generator rotational speed scaling fault (f_{sg}):

The two fault scenarios are 0.9 and 1.1 scale measurements (output matrix parametric changes) of generator rotational speed sensor. As stated in previous Chapters, parameter changes in the output matrix C can be considered as a special case of additive faults in which the fault signals (f_{sg}) is a scaled version of the measured state. Figure 8-11 shows the two fault scenarios and the effectiveness of the proposed strategy to compensate the bias from the scaled measurements. Additionally, via the presented fault estimation signals, the ability of the proposed fuzzy fast fault estimator to accurately estimate abruptly changing fault is also clear.

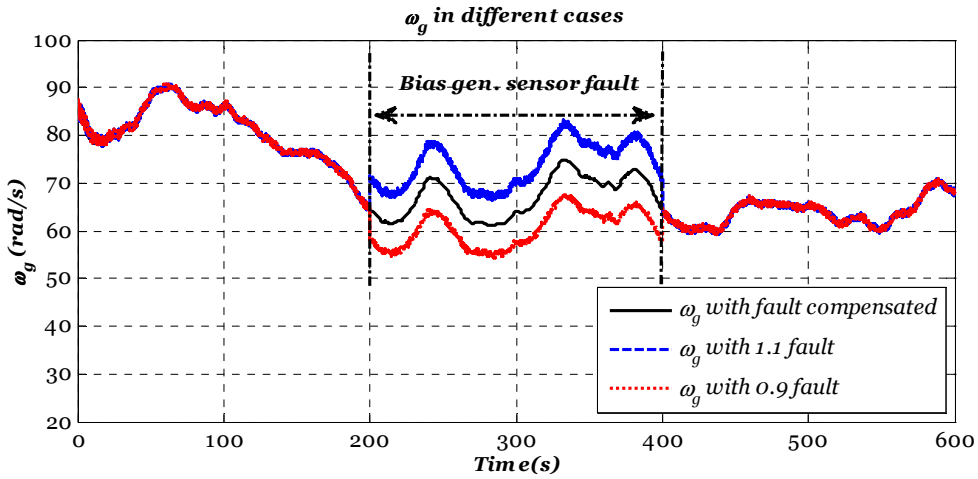

(a)

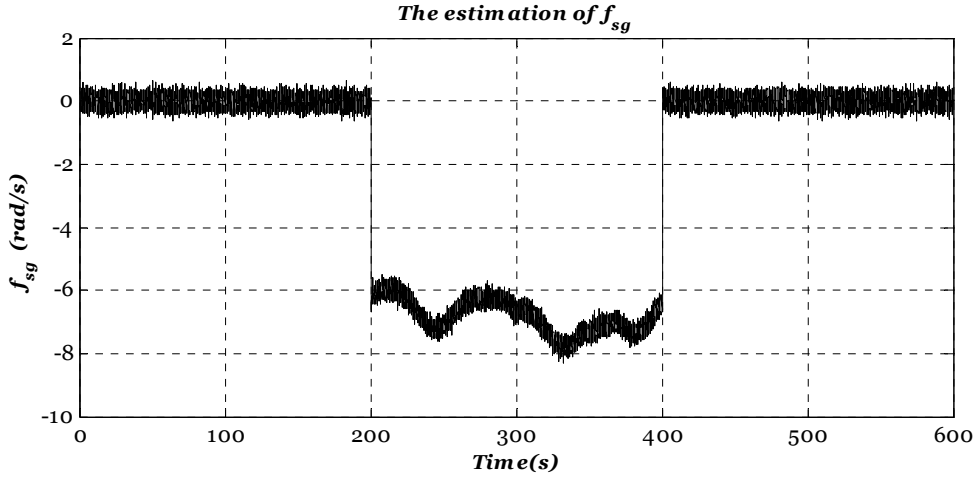

(b)

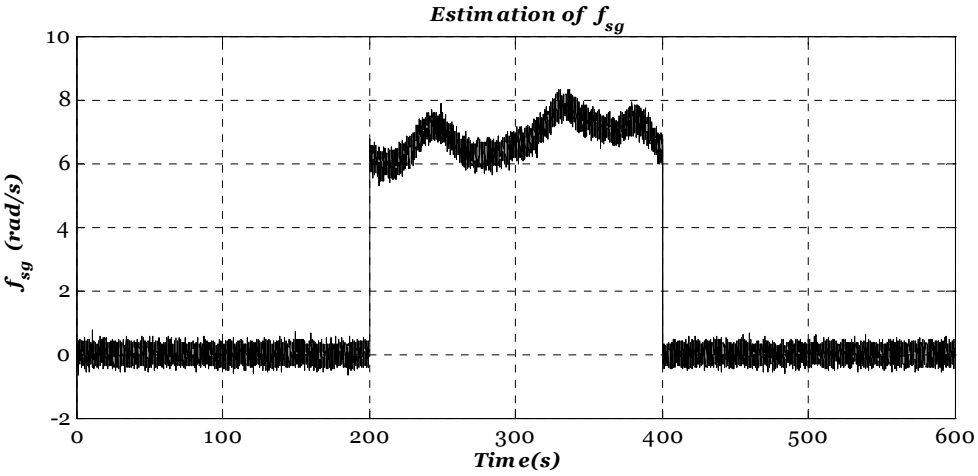

(c)

Figure 8-11: Generator rotational speed sensor faults (b &c) and effectiveness of compensation strategy (a).

Clearly, the two fault scenarios (1.1 or 0.9 scale fault) affect the wind turbine closed-loop performance and hence the wind power conversion efficiency. However, the expected effect of this fault is probably less than the effect of rotor speed sensor fault

since the generator speed signal is part of the feedback signals and not compared directly with the reference optimal speed.

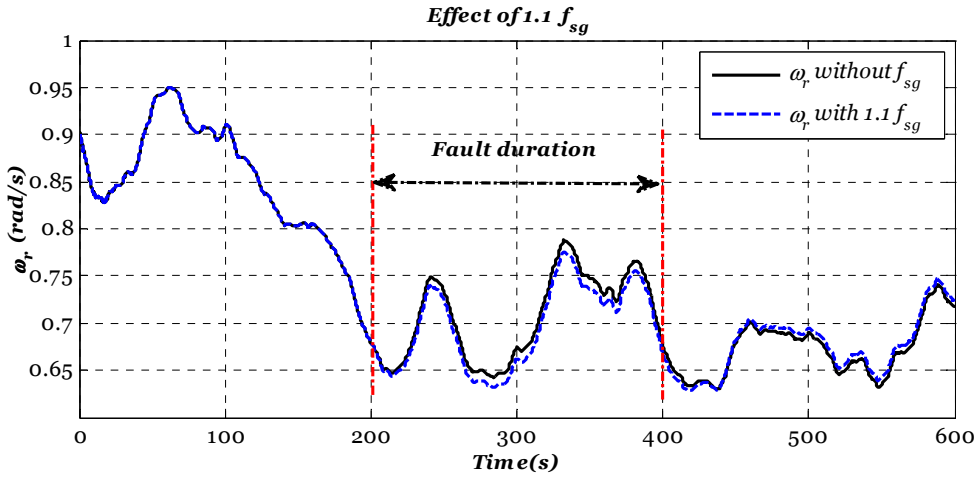

Figure 8-12: The effect of generator speed scale sensor fault

2. Rotor rotational speed stuck sensor fault (f_{sr}) $(\omega_{ropt} < \omega_{r\,measured})$

The second fault scenario is represented by the fixed sensor output of the rotor speed sensor at 1.4 $rad\ sec^{-1}$. As stated in Section 8-2, the effect of this fault scenario varies according to the fixed measurement of rotor speed and ω_{ropt} which in turn depends on the wind speed. In this case ω_{ropt} is lower than the fixed rotor speed measurement and hence the controller starts to force the system to slow-down the rotor speed. Hence, as long as the optimal speed remains below the measured value, the controller keeps increasing the reference generator torque T_{gr} which may lead to the rotaion speed ω_r reaching its cut-off value, i.e. the turbine is shut down due to a rotor rotation speed sensor fault. This fault scenario and the effectiveness of the estimation and compensation strategy to maintain the required system performance in the presence of this severe fault is shown in Figure 8-13. A further investigation of the effect of this severe fault scenario and the ability of the proposed strategy to tolerate the effect of this fault is shown in Figure 8-14. It is clearly shown that this fault scenario can lead to wind turbine shut-down by increasing the breaking action which in turn increases the drive train torsional load.

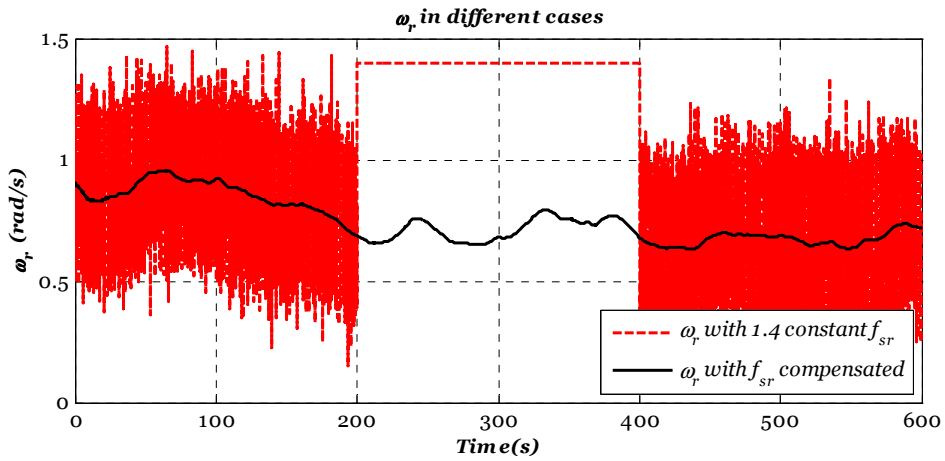

(a)

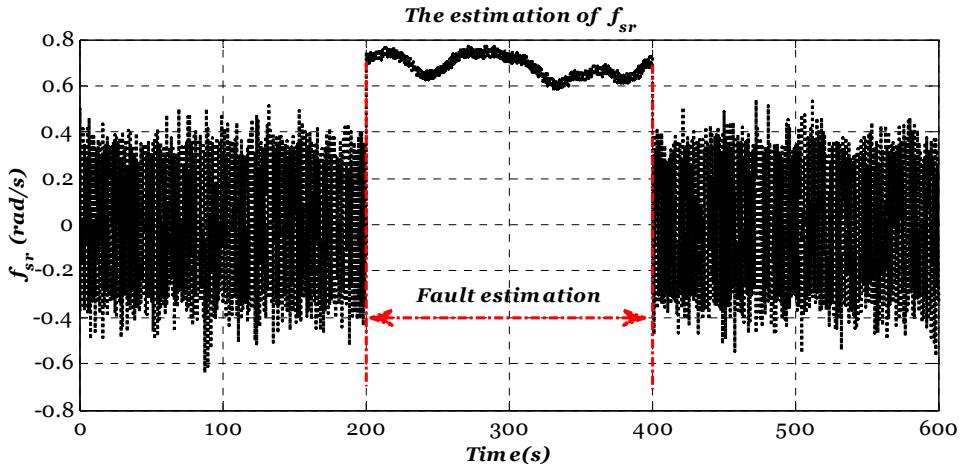

(b)

Figure 8-13: The effectiveness of the proposed strategy to tolerate stuck rotor speed sensor fault (a) and fault estimation (b).

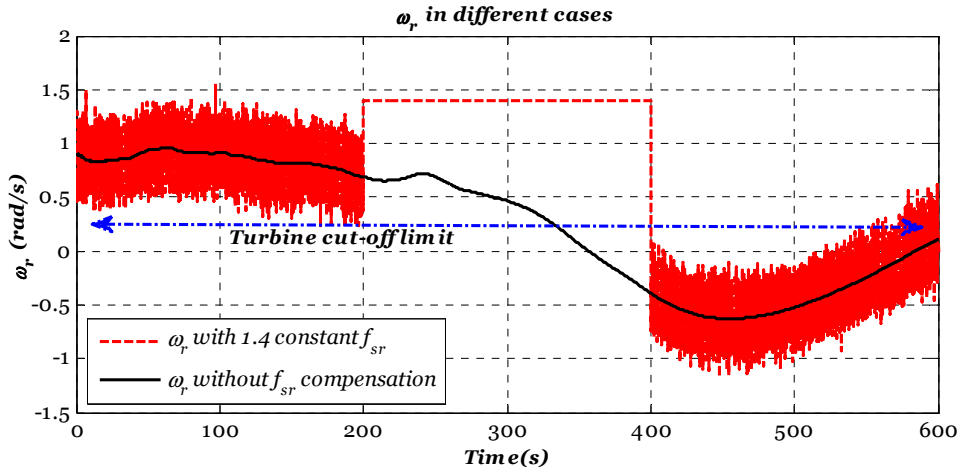

(a)

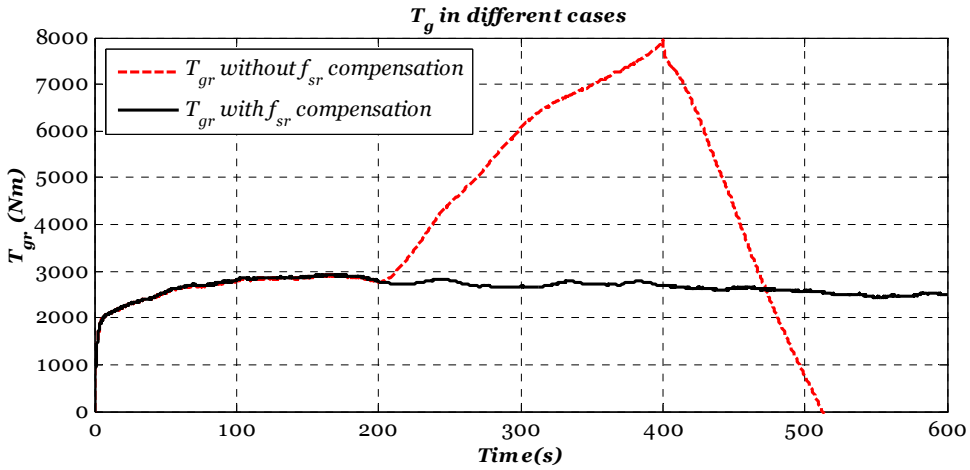

(b)

Figure 8-14: Further investigation of stuck fault effect and the effectiveness of the proposed strategy. (a) Rotor speed and (b) generator torque

3. Rotor rotational speed stuck sensor fault ($\omega_{ropt} > \omega_{r\,measured}$)

In this rotor speed stuck sensor fault scenario ω_{ropt} is higher than the stuck measurement of the rotor speed. Hence, the controller will simply release the turbine to rotate according to the available wind speed without control. The effectiveness of the proposed strategy to tolerate this fault scenario is shown in Figure 8-15. On the other hand, Figure 8-16 shows the effect of stuck fault scenarios from power capture stand point. Additionally, as stated in Section 4-3-3, the fault severity can also be obtained by taking the ratio between the measured generator speed and the estimated signal. Clearly this ratio deviates from unity during a fault and remains at the unity in fault-free case. Figure 8-17.

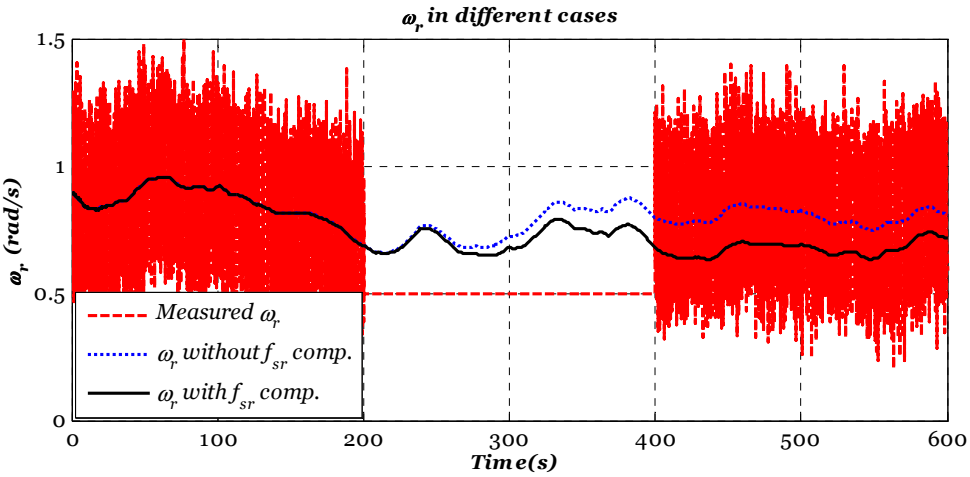

(a)

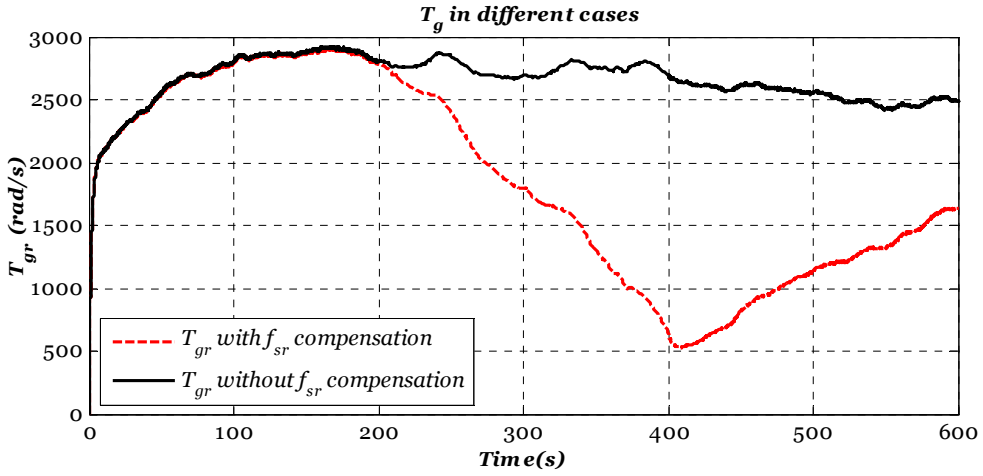

(b)

Figure 8-15: The effectiveness of the proposed strategy to tolerate stuck rotor speed sensor fault. (a) Rotor speed and (b) generator torque

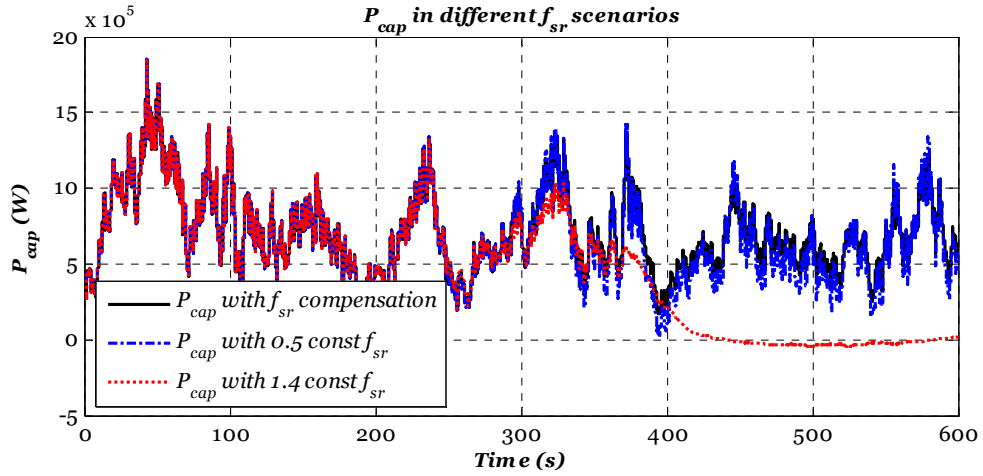

Figure 8-16: The effect of stuck fault scenarios on the power captured

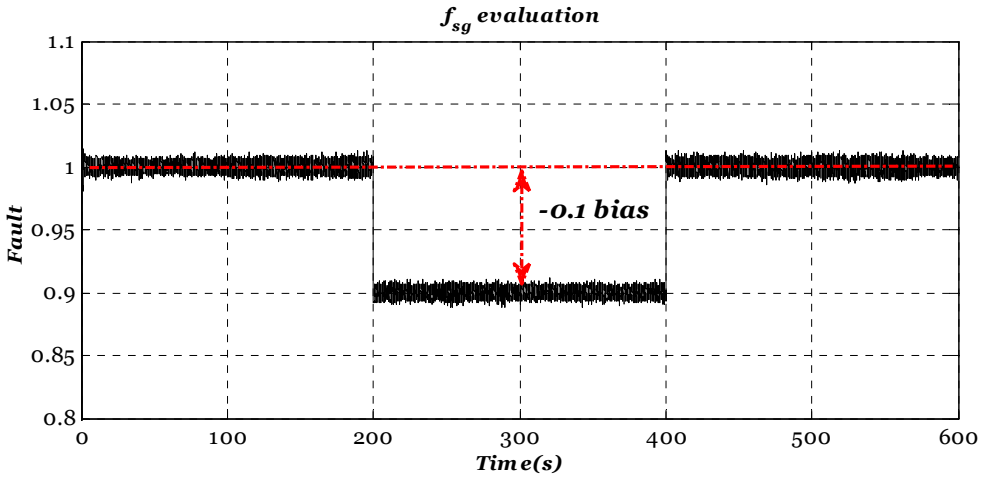

(a)

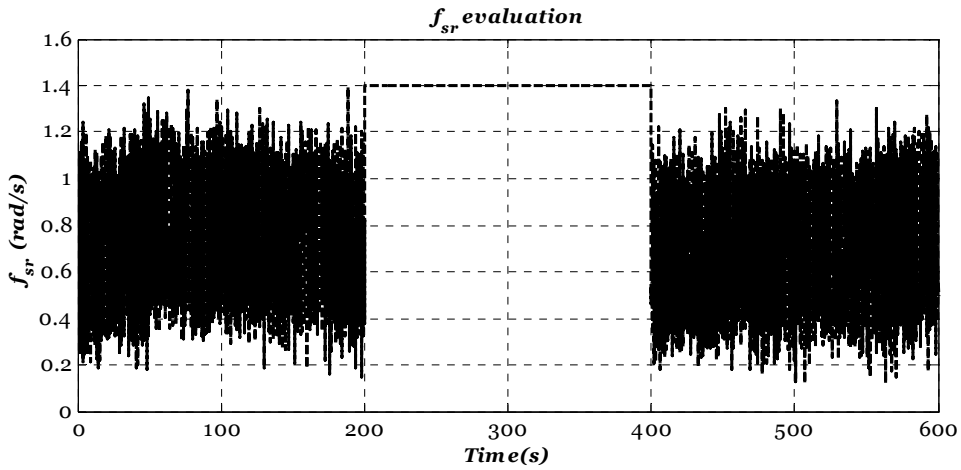

(b)

Figure 8-17: Fault severity evaluation. (a) Scale fault & (b) Additive fault.

8-2-3. TSDOFC based active sensor FTTC with EWS estimation

The proposal in this Section offers further enhancement to the strategies presented in Sections 8-2-1 &8-2-2 for wind turbine FTTC methods. The main advantage compares with the proposals in Sections 8-2-1&8-2-2 is the inclusion of the EWS estimation. In fact, the wind turbine system has an unknown input signal in the form of EWS which should be estimated in order to ensure good wind power transformation efficiency (i.e. to ensure accurate compute of the optimal rotor speed). The effect of this unknown input signal (i.e. the EWS) is actually emulates the effect of generator torque actuator fault on both the control signal (see Sections 8-2 & 7-5) and the sensor fault estimate (see Eqs. (8-7) & (8-16)). Hence, the framework proposed for simultaneous actuator and sensor faults is adopted to design sensor FTTC with EWS estimation for OWT problem. Figure 8-18 illustrates schematically how the wind turbine control problem represents the FTTC strategies proposed in Chapters 5 & 6 (see Sections 5-2 & 6-3).

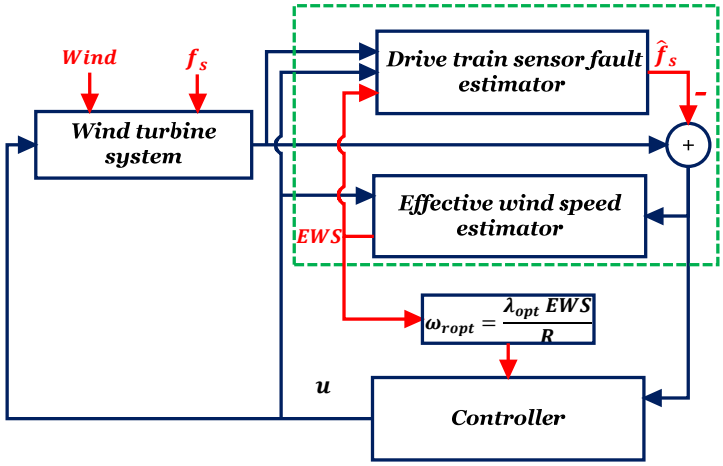

Figure 8-18 : Schematic of the proposed wind turbine AFTC

Remarks:

- It should be noted that the methodology presented in Chapter 6 is used here for simultaneous sensor faults and EWS estimation. In fact, this problem is best coincides with the framework presented in Chapter 6 since both the EWS (the unknown input) and the rotor and generator sensor fault affect the same system simultaneously (i.e. the drive train subsystem). On the other hand, the generator torque fault estimation and compensation can be achieved locally using the generator and converter subsystem (i.e. using Eq. (7-6) only).
- It is already stated in Section 8-2 that although in the wind turbine benchmark the generator torque scale fault is considered as an actuator fault, in reality this fault is attributed to a scale fault in the soft sensing of T_{gm} signal. Hence, owing to the fact that the generator and converter subsystem is approximated using first order dynamic (Eq. (7-6)), the final effect of the soft sensor scale fault appears as generator torque actuator fault.
- To overcome model uncertainty in the generator and converter subsystem, as well as to minimise the number of analytical redundancy layers, Chapter 9 makes use of the robustness of SMC to tolerate the effects of the generator torque scale fault. The use of SMC is attributed to two reasons: (1) The inherent robustness of SMC against model uncertainty. (2) The SMC inherently provides additional layer of analytical redundancy represented by the sliding mode surface and hence obviate the need to increase the number of analytical redundancy layers.

Specifically, the advantages that achieved by this proposal are:

1. Instead of using the uncertain measurements of wind speed, in this strategy a PMIO is used to provide estimation of the aerodynamic torque (as unknown input) based on the drive train subsystem. Specifically, this is achieved by dealing with the torque as an augmented state to the drive train subsystem and then this estimated signal is fed to EWS computation unit to provide estimation of EWS.
2. Since the aerodynamic torque is a resultant of different wind components such as mean, shear, tower shadow, and turbulent wind, the PMIO is selected because it has been already stated in the literature that PMIO can provide good estimation for signals the contain fast and slowly varying components (Gao, Ding and Ma, 2007).

3. Based on the proposed cascade EWS estimation strategy, only the linear PMIO is required since in this strategy the aerodynamic torque, which is the source of nonlinearity, is augmented to the drive train subsystem states.
4. In addition to including the estimation of EWS in this strategy (unknown input), the effects of rotor and generator speed sensor faults are also taken into account.

In this strategy, the TSDOFC is used to achieve the decoupling between the controller on the estimator dynamics. A detailed schematic of this strategy is shown in Figure 8-19.

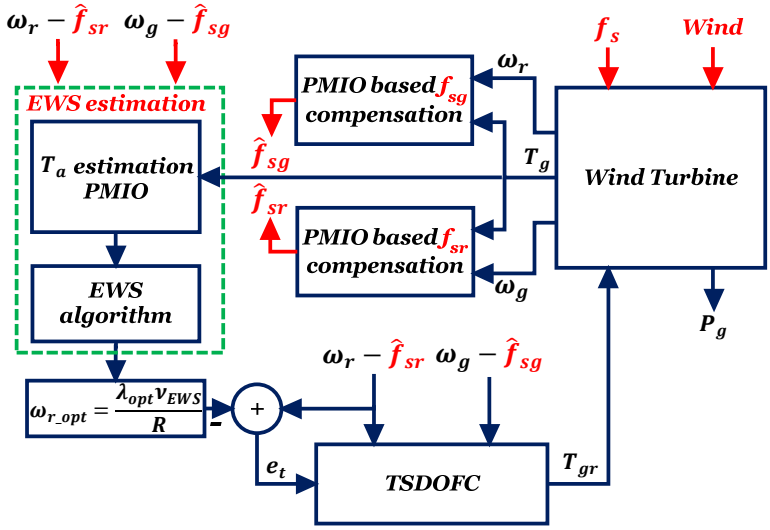

Figure 8-19: Detailed schematic of the proposed strategy

8-2-3-1. The EWS estimation

This Section illustrates the robust strategy for estimating the EWS. This involves *two* steps (1) estimating the aerodynamic torque and (2) computing the EWS. The estimator used here is the robust PMIO.

The drive train state space model in Eq. (7-4) with sensor fault compensated by the estimation taken from the other PMIO can be rewritten as follows:

$$\left.\begin{aligned} \dot{x} &= Ax + B_1 T_a + B_2 T_g \\ y &= Cx + De_{fs} \end{aligned}\right\} \tag{8-26}$$

where $A \in \mathcal{R}^{n*n}$, $B_1 \in \mathcal{R}^{n*1}$, $B_2 \in \mathcal{R}^{n*1}$, $C \in \mathcal{R}^{l*n}$, and $D \in \mathcal{R}^{l*s}$ are known system matrices. Assume that the q^{th} derivative of the signal (T_a) is bounded, then we can

construct an augmented state system consisting from the original drive train states and the q^{th} derivative of the T_a.

Now let:

$$\varphi_i = {T_a}^{q-i} \ (i = 1,2,\dots,q) \ , \ \dot{\varphi}_1 = {T_a}^{q}; \ \dot{\varphi}_2 = \varphi_1; \ \dots; \ \dot{\varphi}_q = \varphi_{q-1}$$

Then the augmented state will be:

$$\bar{x} = \begin{bmatrix} x^T & \varphi_1 & \varphi_2 & \varphi_3 & \dots. & \varphi_q \end{bmatrix}^T \in \mathcal{R}^{\bar{n}}$$

where $\bar{n} = n + kq$ and the augmented drive train model becomes:

$$\left.\begin{aligned} \dot{\bar{x}} &= \bar{A}\bar{x} + \bar{B}_2 T_g + G{T_a}^q \\ y &= \bar{C}\bar{x} + De_{fs} \end{aligned}\right\} \tag{8-27}$$

where the augmented structure is illustrated in Chapters 4 & 5. Hence, the following PMIO is proposed to simultaneously estimate the drive train states and the unknown aerodynamic torque component:

$$\dot{\hat{\bar{x}}} = \bar{A}\hat{\bar{x}} + \bar{B}_2 T_g + \bar{K}\left(y - \bar{C}\hat{\bar{x}} + De_{fs}\right) \tag{8-28}$$

where $\hat{\bar{x}} \in \mathcal{R}^{\bar{n}}$ is the estimation of the augmented state vector $\bar{x}$, and $\bar{K} = [K_p^T, K_I^1, .., K_I^q]^T \in \mathcal{R}^{\bar{n}*l}$ is the gain to be design.

Theorem 8-4: *The PMIO given in (8-28) exists if*

$$rank\begin{bmatrix} A & B_1 \\ C & 0 \end{bmatrix} = n + k \tag{8-29}$$

and

$$rank\begin{bmatrix} sI - A \\ C \end{bmatrix} = n \quad \forall s \in \mathbb{C} \tag{8-30}$$

Additionally, the PMIO attenuates the effect of the bounded ${T_{a2}}^q$ *and* e_{fs} *on the augmented estimation error if there exist SPD matrix* $P = P^T > 0$ *and matrix* $\bar{H}$ *that minimise* γ *under the following LMI constraints:*

$$\begin{bmatrix} P\bar{A} + (P\bar{A})^T - \bar{H}\bar{C} - (\bar{H}\bar{C})^T & PG & -\bar{H}D & I_{\bar{n}\times\bar{n}} \\ (PG)^T & -\gamma I & 0 & 0 \\ -(\bar{H}D)^T & 0 & -\gamma I & 0 \\ I_{\bar{n}\times\bar{n}} & 0 & 0 & -\gamma I \end{bmatrix} \tag{8-31}$$

where the observer gains are obtained by:

$$\bar{K} = P^{-1}\bar{H} \tag{8-32}$$

Proof: Conditions (8-29) & (8-30) follow directly the observability requirements for the states and unknown input estimate.

The state estimation error dynamics are obtained by subtracting Eq. (8-28) from (8-27):

$$\dot{e}_x = (\bar{A} - \bar{K}\bar{C})e_x + G{T_a}^q - \bar{K}De_{fs} \tag{8-33}$$

To attenuate the effect of ${T_a}^q$ and e_{fs} on the estimation error simultaneously whilst also ensuring system stability, the following inequality must hold:

$$\dot{v}(e_x) + \frac{1}{\gamma}e_x^T\, e_x - \gamma({T_a}^{qT}{T_a}^q + {e_{fs}}^T e_{fs}) < 0 \tag{8-34}$$

where $\dot{v}(e_x)$ is the time derivative of the candidate Lyapunov function ($v(e_x) = e_x^T P e_x$). Using Eq. (8-33), inequality (8-34) becomes:

$$\begin{aligned}\dot{v}(e_x) = \Big\{ & e_x^T(\bar{A}^T P + P\bar{A} - P\bar{K}\bar{C} - (P\bar{K}\bar{C})^T)e_x + e_x^T PG{T_a}^q + {T_a}^{qT}G^T Pe_x \\ & - e_x^T P\bar{K}De_{fs} - {e_{fs}}^T(P\bar{K}D)^T e_x\Big\}\end{aligned} \tag{8-35}$$

Inequality (8-34) (in matrix form) after substituting $\dot{v}(\tilde{x}_a)$ from Eq. (8-35) and using the variable change $\bar{H} = P\bar{K}$ becomes:

$$\begin{bmatrix} e_x \\ {T_a}^q \\ e_{fs} \end{bmatrix}^T \begin{bmatrix} P\bar{A} + (P\bar{A})^T - \bar{H}\bar{C} - (\bar{H}\bar{C})^T + \frac{1}{\gamma}I_{\bar{n}\times\bar{n}} & PG & -\bar{H}D \\ G^T P & -\gamma I & 0 \\ -(\bar{H}D)^T & 0 & -\gamma I \end{bmatrix} \begin{bmatrix} e_x \\ {T_a}^q \\ e_{fs} \end{bmatrix} < 0 \tag{8-36}$$

Clearly, by using the Schur Theorem inequality (8-31) can easily be obtained from inequality (8-36).

In the literature there are *two* methods for calculating the EWS based on the estimated aerodynamic torque. The first is based on using the Newton-Raphson method and the second is based on the inversion of the aerodynamic torque equation Eq. (7-3). The aerodynamic inversion method to calculate the EWS is used here. For details see (Østergaard, Brath and Stoustrup, 2007a).

The second PMIO is designed to estimate rotor speed sensor fault. The steps for designing PMIO for sensor fault has been already explained in different Sections in this thesis and hence omitted here. Furthermore, The TSDOFC proposed in this strategy has been already derived previously hence it is also omitted here (see Section 8-2-2-2).

8-2-3-2. Simulation results

Figure 8-21, shows the estimation of the EWS based on the proposed PMIO. This estimated signal is used in Eq.(1) to produce the optimal rotor speed for tracking purposes. In fact, the estimation involves *two* steps. First, the aerodynamic torque estimates (Figure 8-20), and second the EWS computing algorithm.

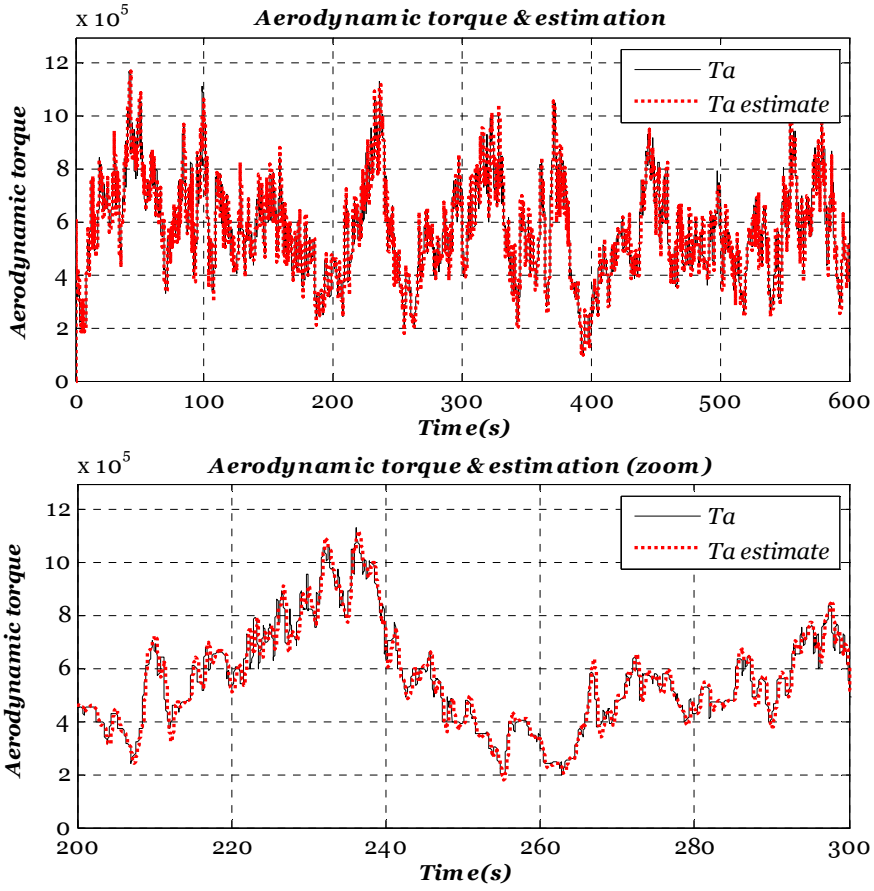

Figure 8-20: Aerodynamic torque estimation

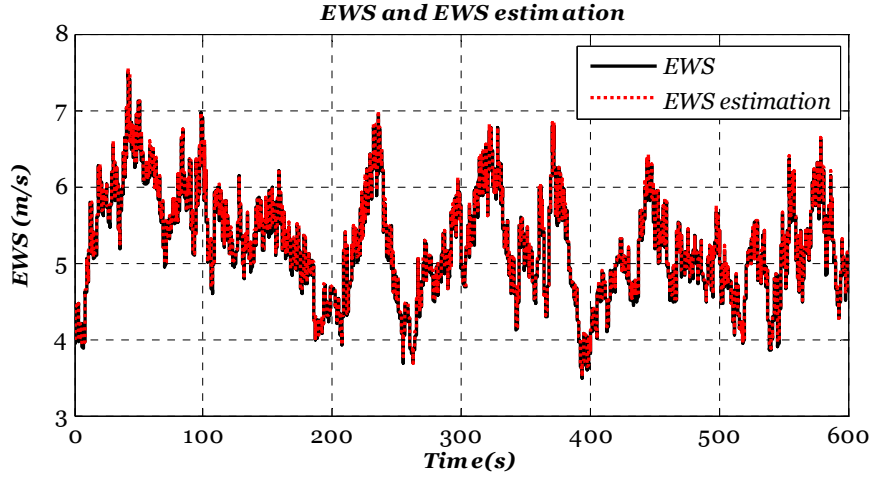

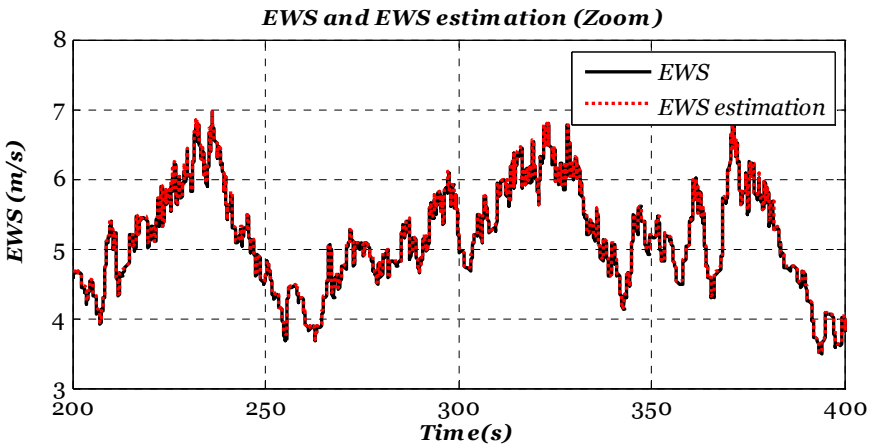

Figure 8-21: EWS estimation

The rotor rotational speed 1.1 scale factor fault is taken as a sample fault to show the ability of the proposed strategy to tolerate the fault and maintain system performance. From Figure 8-22, it is clear that both measurement noise and scale fault are additive signals affecting the measured rotor speed. Therefore, unknown output estimation contain both signals and hence the strategy compensates both fault and measurement noise simultaneously.

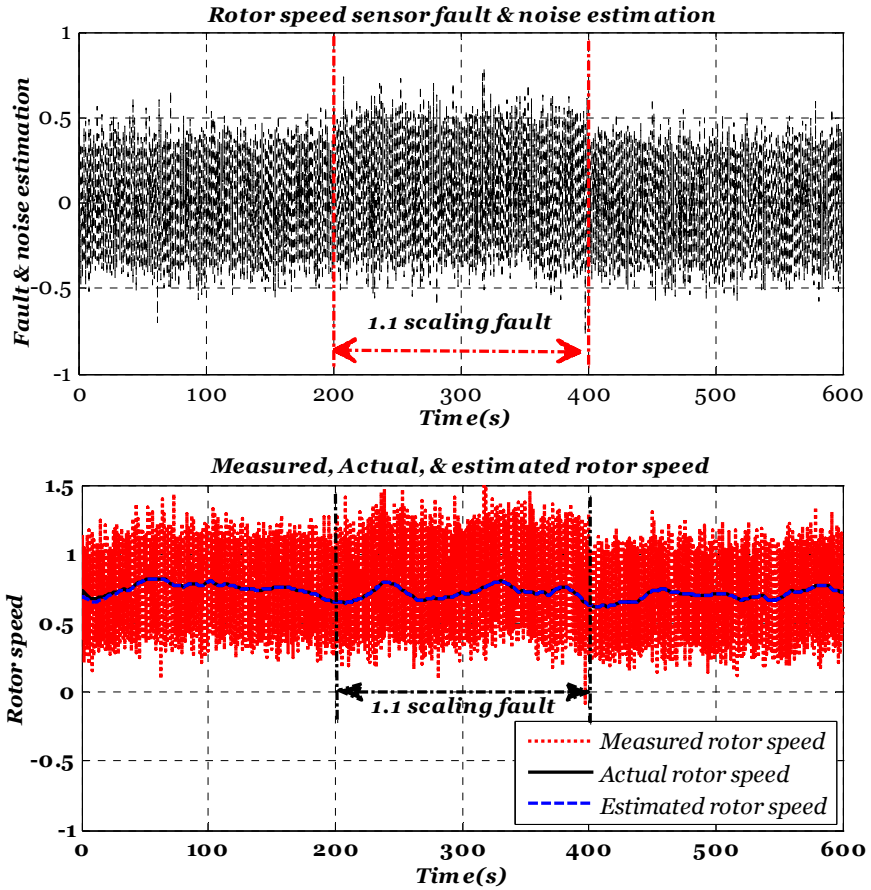

Figure 8-22: Rotor speed scale fault and the ability of the proposed strategy to compensate fault and noise

8-3. Conclusions

The operation of a wind turbine below the rated wind speed is a tracking control problem which aims to force the wind turbine rotor to follow an optimal rotation speed by controlling the generator torque, through a variable reference torque T_{gr}. To ensure good tracking performance, three points must be considered as follows:

1. The inclusion of a nonlinear control strategy to handle system nonlinearity.
2. Robustness against generator and rotor speed sensor faults.
3. Accurate computation of the reference signal.

In addition to an evaluation of the fault effects, this Chapter presents several contributions to the problem of sustainable wind turbine based on FTTC. These can be summarized as follows:

1. The advantages of the use of PMIO based sensor FTTC over the generalized observer-based sensor FTC are clearly given as: (i) Obviate the need for residual evaluation and observer switching, (ii) Ability to tolerate simultaneous generator and rotor rotational speed sensor faults, (iii) The PMIO simultaneously estimates the states and the sensor fault signals. Hence, information about the fault severity can also be obtained through the fault estimation signals, and (v) The new fuzzy PMIO scheme is shown to cover a wide range of sensor fault scenarios.
2. The proposal of an output feedback control strategy that overcomes the dependence of the controller on the observer state estimate and hence overcomes the difficulty of recovering the separation principle in the T-S fuzzy observer-based control due to global stability constraints.
3. The proposal of a TSDOFC-based sensor FTTC with EWS estimation. This new strategy offers great simplification of the estimators. Moreover, it can deal with the cases of simultaneous unknown input (EWS) and unknown output (sensor fault and noise) estimation.
4. The use of the PMIO to estimate the EWS offers a high estimation accuracy since this estimator has the ability to provide good estimation of the unknown signals that contain fast and slow varying components.

Chapter 9 : Sliding mode control based FTTC for wind turbine power maximization[4]

9-1. Introduction

The main challenge for the closed-loop robustness problem against unknown inputs and output signals is highlighted in Chapter 8, namely that the number of unknown input and output signals exceed the number of measurements. Specifically, a worst case operation scenario of a wind turbine is that the system can be simultaneously affected by rotor and generator rotational speed sensor faults and generator torque bias faults. Hence, there is a significant challenge to be able to discriminate between these fault effects robustly whilst at the same time providing a robust method for estimating the EWS. Chapter 8 describes one approach for attempting to overcome this challenge via increasing the level of the analytical redundancy (i.e. increasing the number of redundant fault estimators).

This Chapter focuses on exploiting the inherent robustness of SMC when used within an AFTC framework for power maximization of a wind turbine. In fact, an approach to exploit the SMC to tolerate matched faults without the need for additional analytical redundancy is the main motivation for the work presented in this Chapter.

This Chapter starts from a short explanation of the SMC concepts and an investigation of its robustness against different actuator and sensor faults is illustrated via an academic example. The main contribution is the proposal of three FTTC strategies based on SMC and a combination of SMC with the estimation and compensation concept. The proposed strategies have been applied to the wind turbine benchmark given in Chapter 7.

---

[4] The work presented in this Chapter was published in:

Sami, M. & Patton, R. J. 2012a. Fault tolerant adaptive sliding mode controller for wind turbine power maximisation. 7th IFAC Symposium on Robust Control Design, Aalborg Congress & Culture Centre, Denmark, 499-504. 20-22 Jun.

Sami, M. & Patton, R. J. 2012g. Wind turbine power maximisation based on adaptive sensor fault tolerant sliding mode control. 20th Mediterranean Conference on Control & Automation, Barcelona, 1183-1188. 3-6 July.

Sami, M. & Patton, R. J. 2012b. A fault tolerant approach to sustainable control of offshore wind turbines. 2nd International Symposium On Environment Friendly Energies And Applications, Northumbria University, UK, 25–27 June.

The SMC strategies proposed in this Chapter encapsulate a first attempt to utilize SMC robustness to ensure sustainable control operation of a wind turbine in the presence of control system faults. Moreover, a new approach to SMC design within an FTC framework is outlined. The important notion is that the selection and design of the sliding surface has an important role to play in the development of an FTC scheme. Specifically, by designing a sliding surface with the minimum dimension of the feedback signal, the robustness of the SMC is ensured against more than the usual faults. This is particularly appropriate if a tracking control approach to SMC is chosen. The requirement is to develop a special approach to output feedback within tracking SMC which is appropriate for dealing with a system that is contaminated by different actuator and sensor faults.

9-2. SMC within a tracking framework

The basic concepts of SMC have been illustrated in many books (Utkin, 1992, Edwards and Spurgeon, 1998, Wilfrid and Jean, 2002, Bartolini, Fridman, Pisano and Usai, 2008, Bandyopadhyay, Deepak and Kim, 2009, Bartoszewicz and Nowacka-Leverton, 2009 , Alwi, Edwards and Tan, 2011). Generally, the SMC is characterized by relative simplicity of design and invariance to specific modelling uncertainty and external perturbations. The SMC design steps include: (1) the construction of the sliding surface capable of achieving control goals whenever the system remains into this surface. (2) Designing of a control signal that forces the system toward the sliding surface. (3) The design of the discontinuous control signal around the sliding surface to ensure the remaining of the system dynamics in the sliding surface vicinity. The controller performance depends on a sliding surface design, once the state motion reaches the sliding surface (manifold) the motion remains within or near the manifold in what is effectively a reduced order system with strong insensitivity to parametric variations occurring in the space outside the sliding manifold.

The background material in this Chapter follows closely the tracking control presentation in (Slotine and Li, 1991) since it is well suited to the wind turbine power maximization control problem.

The common approaches for addressing the tracking controller design problem make use of either model reference or state feedback with integral action. Both of these methods are presented in the Chapters 4 and 5, respectively. Although the two

approaches are also used widely within SMC (Edwards and Spurgeon, 1998) and the SMC based FTTC framework (Edwards and Spurgeon, 1998, Edwards, Lombaerts and Smaili, 2010, Alwi, Edwards and Tan, 2011), the main limitation is that the sliding surface is defined based on all of the available feedback signals (i.e. the objective output and other states). As a consequence of this, any sensor fault that affects the objective variable and/or other states will directly affect the sliding surface. In this case the closed-loop performance and stability are directly affected since the SMC lacks the robustness against these faults. Fortunately, by modifying the definition of the sliding surface, for example if the sliding surface depends on the objective variable alone, the closed-loop performance and stability can be maintained even when there are sensor faults that do not affect the sliding surface. This is the main motivation behind the use of the design methodology proposed in (Slotine and Li, 1991), based on the principle that sliding mode tracking control formulation only uses the objective output signal in the sliding surface design. Although these authors did not describe it, the advantageous feature of this approach is that the sensitivity of the sliding surface to faults can be minimised.

Following this concept this Chapter investigates the methodology and benefit of ensuring that the sensitivity of the sliding surface to specific faults is minimized.

According to (Slotine and Li, 1991) the control aim is to force a specific output signal of the single-input dynamic system given in terms of the n^{th} order derivative of the objective variable x, as:

$$x_o^n = a(x) + u \tag{9-1}$$

The specified output signal of interest x_o tracks the time-varying reference signal x_{ro}. u is the scalar input, $x = [x_o \quad \dot{x}_o \quad \cdots \quad x^{n-1}{}_o]^T$, a(x) is a general nonlinear function, and $x_r = [x_{ro} \quad \dot{x}_{ro} \quad \cdots \quad x_{ro}^{n-1}]^T$ is the time-varying reference vector.

Suppose that $e_o = x_o - x_{ro}$ and $e = x - x_r = [e_o \quad \dot{e}_o \quad \cdots \quad e^{n-1}{}_o]^T$ are the tracking error signal and vector, respectively. The first SMC design step is to define a time-varying surface so that the control aim is achieved once the system remains in the vicinity of this surface. Hence, for $n = 2$, the sliding surface can be given as:

$$S = \dot{e}_o + \gamma e_o \tag{9-2}$$

where γ is positive scalar. It is clear that while the system is in the sliding mode ($S = 0$) the unique solution of Eq. (9-2) occurs for $e = 0$ and for zero initial tracking

error $e(0) = x(0) - x_r(0) = 0$ the tracking problem is equivalent to maintaining the error dynamic on the surface S. Hence, the first design step is achieved. Moreover, while the system trajectory is in the sliding manifold the dynamics are reduced to a first order differential equation with time response governed by the positive design parameter (γ).

The second SMC design step proposed by (Slotine and Li, 1991) is to find the control signal that ensures the occurrence of ideal sliding motion, alternatively, find the control signal that makes the sliding surface attractive. This control signal must satisfy the following condition (Slotine and Li, 1991, Edwards and Spurgeon, 1998):

$$\dot{S}S \leq -\eta|S| \tag{9-3}$$

where η is a small positive constant. The condition given in (9-3) is known as *'sliding condition'* or *'reachability condition'* for which the time (t_{reach}) taken to reach $(S = 0)$ satisfies:

$$t_{reach} \leq \frac{|S(0)|}{\eta} \tag{9-4}$$

Clearly, if the control signal guarantees the sliding condition then the sliding motion will take place even if $e(0) = x(0) - x_r(0) \neq 0$ within $t_{reach}s$.

The expression for the control signal (u_{eq}), known as 'equivalent control', can be obtain by solving the dynamics within the sliding motion which can be written as:

$$\dot{S} = 0 \tag{9-5}$$

Hence, for the system given in Eq. (9-1) with $n = 2$ and sliding surface given in Eq. (9-2), the u_{eq} is given as:

$$u_{eq} = -a(x) + \ddot{x}_{r_o} - \gamma\dot{e}_o \tag{9-6}$$

Clearly, u_{eq} would maintain the dynamics in (9-5) provided that there is no modelling uncertainty. To tackle the probable uncertainty on the system model, a discontinuous term across the surface $(S = 0)$ is added to the linear control component u_{eq} so that the final control signal becomes:

$$u = u_{eq} + u_n \tag{9-7}$$

$$u_n = k\ sgn(S) \tag{9-8}$$

where sgn is the sign function:

$$\left.\begin{array}{l} sgn(S) = +1 \quad if \;\; S > 0 \\ sgn(S) = -1 \quad if \;\; S < 0 \end{array}\right\} \tag{9-9}$$

Now, consider the case when the term $a(\mathrm{x})$ is not precisely known. In this situation u_{eq} becomes:

$$u_{eq} = -\hat{a}(x) + \ddot{x}_{r_o} - \gamma \dot{e}_o \tag{9-10}$$

where $\hat{a}(\mathrm{x})$ is an approximation to the actual function $a(\mathrm{x})$. Consequently, based on Eqs.((9-1),(9-7),(9-10)), and the sliding condition given in (9-3), the gain (k) can be determined as follows:

$$\dot{S}S = (a(x) - \hat{a}(x) - k\,\frac{|S|}{S})S$$
$$= (a(x) - \hat{a}(x))S - k|S|$$

suppose the uncertain term $(a(x) - \hat{a}(x))$ is upper bounded by H, i.e.

$$|a(x) - \hat{a}(x)| < H \tag{9-11}$$

Also, by letting:

$$k = H + \eta \tag{9-12}$$

It follows that:

$$\dot{S}S \leq -\eta|S|$$

Therefore, by choosing (k) in (9-8) sufficiently large, the sliding will take place within a specific finite time.

Remark: The discontinuous feedback component induces a particular dynamic in the vicinity of the sliding surface known as *'chattering'*. In general, such a control signal is undesirable and hence an approximation to the *sign* function is considered in the literature to maintain the system close to the surface $(S = 0)$ while avoiding chattering. One approximation is based on the use of saturation function $(sat(y))$ given below (Slotine and Li, 1991):

$$\left.\begin{array}{l} sat\left(\frac{S}{\delta}\right) = \frac{S}{\delta} \qquad if \qquad \frac{|S|}{\delta} \leq 1 \\ sat\left(\frac{S}{\delta}\right) = sgn\left(\frac{S}{\delta}\right) \quad otherwise \end{array}\right\} \tag{9-13}$$

where $\delta > 0$ is the thickness of the boundary layer surrounding the surface $(S = 0)$. A softer approximation is the sigmoid function (Burton and Zinober, 1986, Edwards and Spurgeon, 1998):

$$sgn(S) \cong \frac{|S|}{S + \delta} \tag{9-14}$$

9-3. Investigation of SMC robustness within FTC framework

Although the robustness of the SMC against bounded uncertainty acting in the input channel (*matched uncertainty*) is widely accepted, an investigation of this robustness within the FTTC framework has not been clarified in the SMC literature. Therefore, based on the tracking theory presented in Section 9-2, the separate effects of different actuator and sensor faults on the sliding mode controller performance are investigated in this Section via the following tutorial example taken from (Stefani, Shahian, Savant and Hostetter, 2002):

$$\left.\begin{aligned} \dot{x} &= Ax + Bu \\ y &= Cx \end{aligned}\right\} \tag{9-15}$$

where

$$A = \begin{bmatrix} -4 & -4 \\ 1 & -2 \end{bmatrix}, x = \begin{bmatrix} x_1 \\ x_2 \end{bmatrix}, B = \begin{bmatrix} 0 \\ 2 \end{bmatrix}, C = \begin{bmatrix} 1 & 0 \\ 0 & 1 \end{bmatrix}$$

The controller is designed to force the objective output x_1 to follow the bounded reference signal x_r. Using the sliding surface defined in Eq. (9-2), together with the control signal defined in Eq. (9-7), and the approximation in Eq. (9-14), with the tracking error defined as $e = x_1 - x_r$. The control signal can easily be shown to have the form:

$$u = \frac{-1}{2}[(3-\gamma)x_1 + (6-\gamma)x_2 - \ddot{x}_r - \gamma\dot{x}_r] + k\,\frac{|S|}{S+\delta} \tag{9-16}$$

It is clear that x_2 affects only the linear component of the control signal in (9-19), whilst x_1 affects both the linear component as well as the discontinuous component via the sliding surface S. The consequence of this is that x_1 and x_2 have different effects on the tracking performance from the FTC stand point. This is clarified more fully in Section 9-3-2.

9-3-1. Investigation of SMC robustness to actuator faults

1. **Parametric actuator fault**: This fault represents a scaling (up or down) of the control signal gain matrix B as follows:

$$\left.\begin{aligned} \dot{x} &= Ax + B(u + \epsilon u) \\ y &= Cx \end{aligned}\right\} \tag{9-17}$$

$(1+\epsilon)$ is the scale factor. Clearly, this fault affects the system in the direction of the input channel. Hence, with an appropriate choice of the discontinuous control

component gain (k), the SMC can inherently tolerate the effect of this fault as shown in Figure 9-1 a & b for $\epsilon = -0.7$.

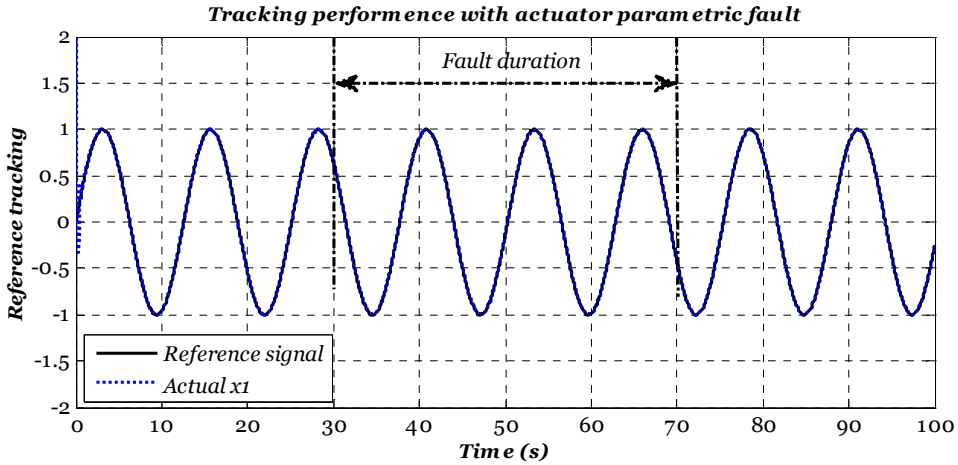

(a)

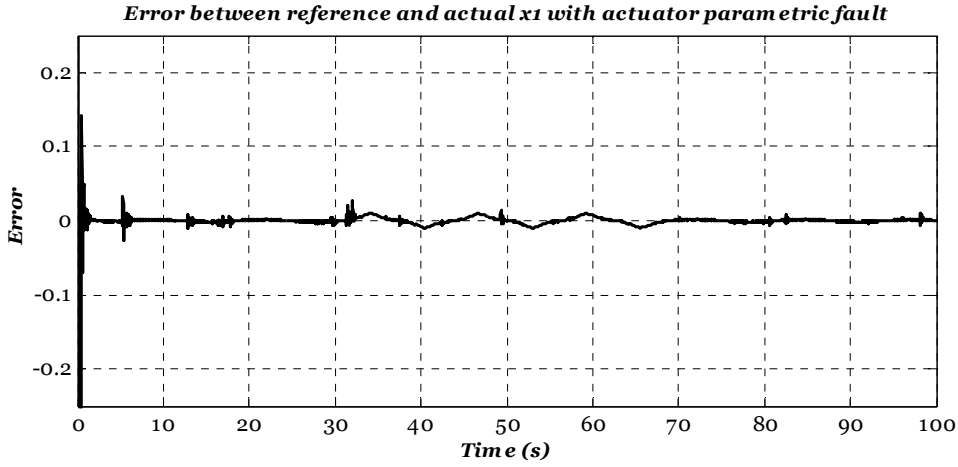

(b)

Figure 9-1: Tracking performance with parametric actuator fault:
(a) State tracking & (b) Tracking error

2. **Additive actuator fault**: This fault scenario is similar to the matched external perturbation effects. The system model in Eq. (9-15) with additive actuator fault become:

$$\left.\begin{aligned} \dot{x} &= Ax + B(u + f_a) \\ y &= Cx \end{aligned}\right\} \tag{9-18}$$

where $f_a = \sin(0.25t)$ is the additive fault signal shown in Figure 9-2b. In a similar manner to the parametric actuator fault, Figure 9-2 a & c shows the ability of the SMC to tolerate the effect of this fault scenario and guarantees the convergence of the tracking error e to the origin.

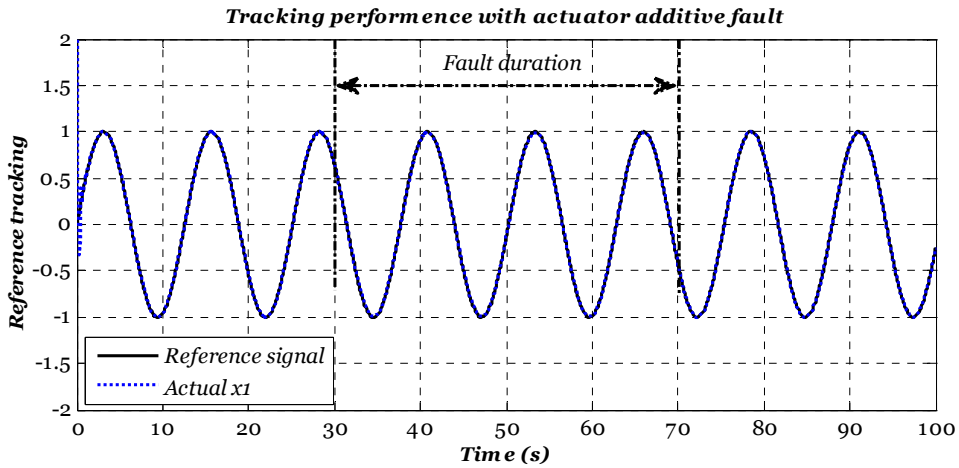

(a)

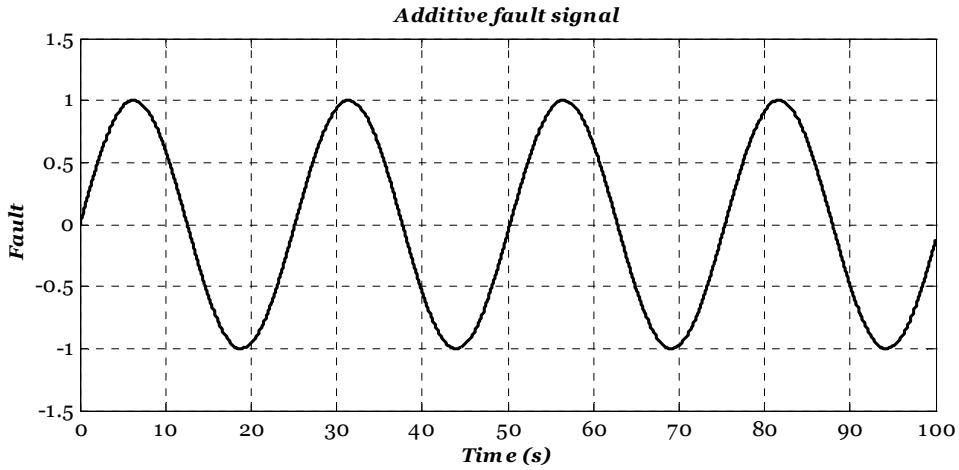

(b)

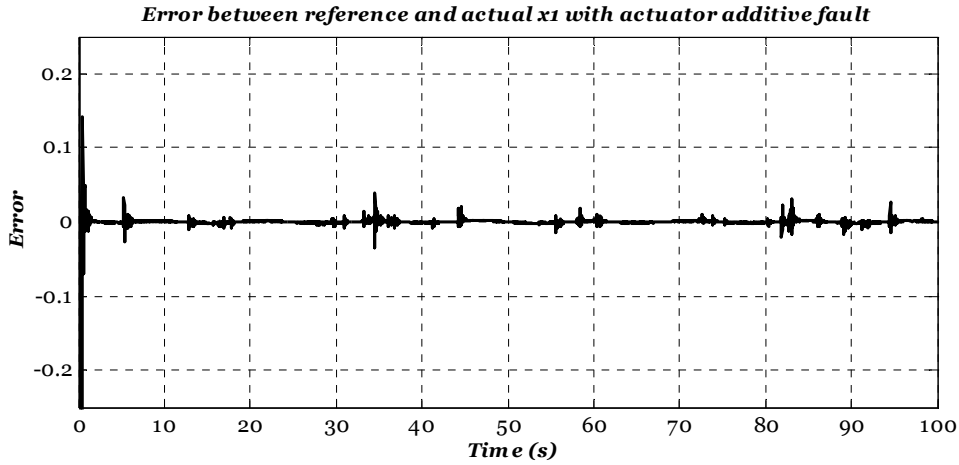

(c)

Figure 9-2: Tracking performance with additive actuator fault. (a) State tracking, (b) fault signal, & (c) tracking error

3. **Stuck actuator fault**: Although the stuck actuator fault affects the system in the direction of the input channel, the actuator lacks the ability to feed the closed-loop system with the SMC signal. Hence, as a result, the closed-loop system cannot

tolerate the effect of this fault unless the SMC is combined with the appropriate control reconfiguration technique to tolerate the fault. The system model in Eq. (9-15) with stuck actuator fault becomes:

$$\left.\begin{aligned} \dot{x} &= Ax + B\mathcal{C} \\ y &= Cx \end{aligned}\right\} \tag{9-19}$$

where $\mathcal{C}$ is fixed value. Figure 9-3 a &b shows the tracking performance and the tracking error with the stuck actuator fault $\mathcal{C} = 0.5$. Clearly, this fault scenario is similar to a complete actuator fault ($\mathcal{C} = 0$) (i.e. actuator failure) in which the faulty actuator hides the SMC signal that direct the operation of the closed-loop system.

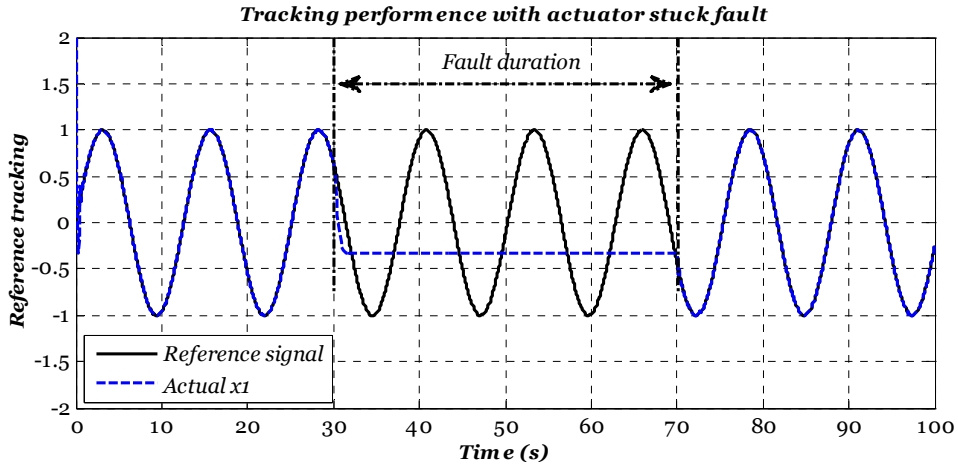

(a)

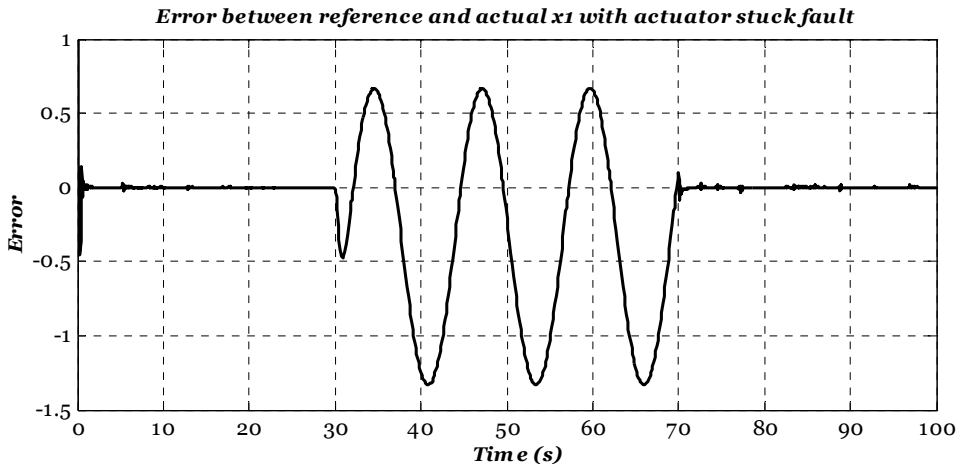

(b)

Figure 9-3: Tracking performance with stuck actuator fault. (a) State tracking & (b) tracking error

9-3-2. An investigation of SMC robustness to sensor faults

This Section introduces a new investigation of the effect of sensor faults on tracking performance within the SMC framework. Sensor faults can be classified based on their function within the control signal u given in Eq. (9-16). So that if the fault affects the linear component u_{eq} (for example the measurement of x_2) then this sensor fault is similar to the additive actuator fault and hence it can be tolerated by the SMC. On the other hand, if the sensor fault affects the sliding surface (i.e. affects u_n, for example the measurement of x_1), the SMC lacks the ability to tolerate this sensor fault since this fault causes deviation in the sliding surface. The effect of separate x_1 and x_2 measurement faults on the tracking performance within the SMC framework is illustrated in the following simulation results.

1. **x_1 parametric sensor fault**: This fault affects the sliding surface given in Eq. (9-2) as follows:

$$S = (\dot{x}_1 + \epsilon\dot{x}_1 - \dot{x}_r) + \gamma(x_1 + \epsilon x_1 - x_r) = \dot{e} + \gamma e + (\epsilon\dot{x}_1 + \gamma\epsilon x_1) \qquad (9\text{-}20)$$

where ϵ is a real scalar depends on fault severity. Hence, the SMC system tries to force the actual x_1 to track the reference signal based on the faulty measurement. This fault cannot be tolerated via the SMC since the sliding surface is contaminated by the fault. Figure 9-4 a & b shows the effect of this fault for $\epsilon = -0.7$.

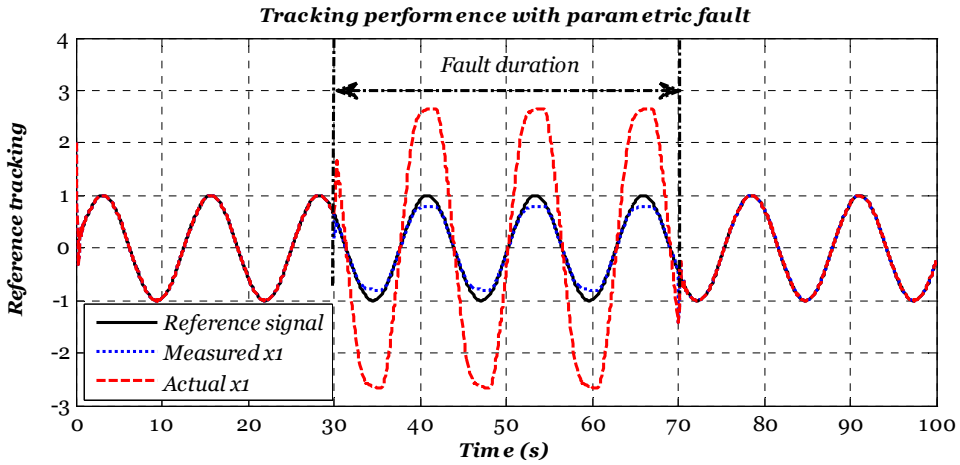

(a)

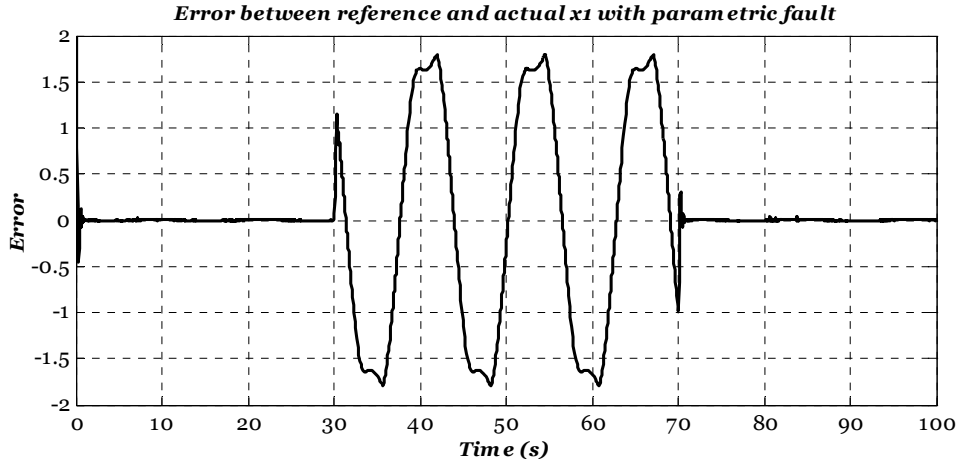

(b)

Figure 9-4: Tracking performance with $\boldsymbol{x_1}$ parametric sensor fault:

(a) State tracking & (b) tracking performance.

2. $\boldsymbol{x_1}$ **additive sensor fault**: This fault affects the sliding surface as follows:

$$S = \left(\dot{x}_1 + \dot{f}_s - \dot{x}_r\right) + \gamma(x_1 + f_s - x_r) = \dot{e} + \gamma e + (\dot{f}_s + \gamma f_s) \tag{9-21}$$

where f_s is the additive fault signal. Similar to the parametric sensor fault, this fault cannot be tolerated via the SMC. Figure 9-5 a & b shows the effect of this fault with $f_s = \sin(0.25t)$.

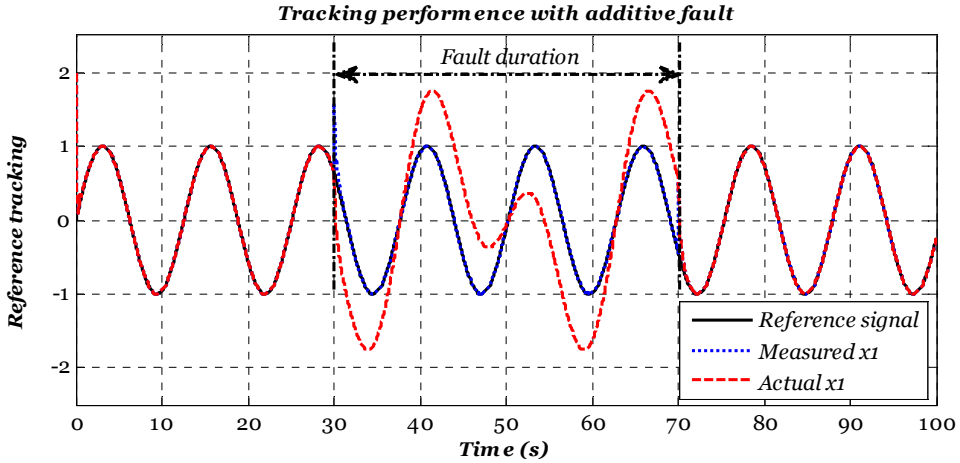

(a)

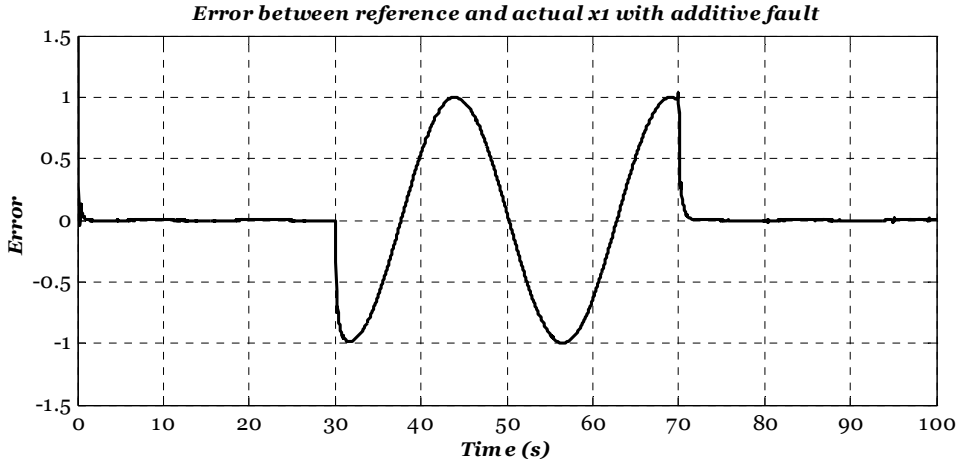

(b)

Figure 9-5 : Tracking performance with the $\boldsymbol{x_1}$ additive sensor fault:

(a) State tracking & (b) tracking performance.

3. **Stuck fault**: This fault affects the sliding surface as follows:

$$S = \left(\dot{x}_1 + \left(\dot{\mathcal{C}} - \dot{x}_1\right) - \dot{x}_r\right) + \gamma(x_1 + (\mathcal{C} - x_1) - x_r) = -\dot{x}_r + \gamma(\mathcal{C} - x_r) \qquad (9\text{-}22)$$

where $\mathcal{C}$ is a constant value at which the measurement sticks. This fault cannot be tolerated via SMC. Figure 9-6 shows the effect of this fault for $\mathcal{C} = 0.5$.

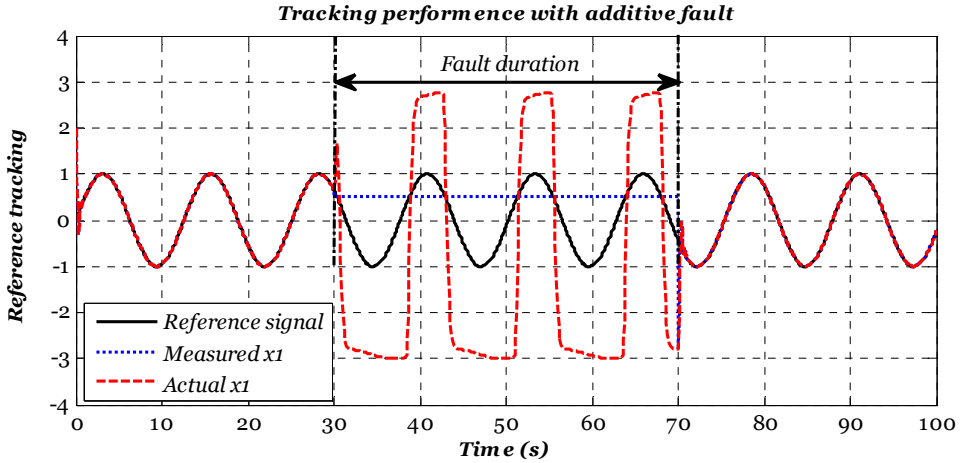

(a)

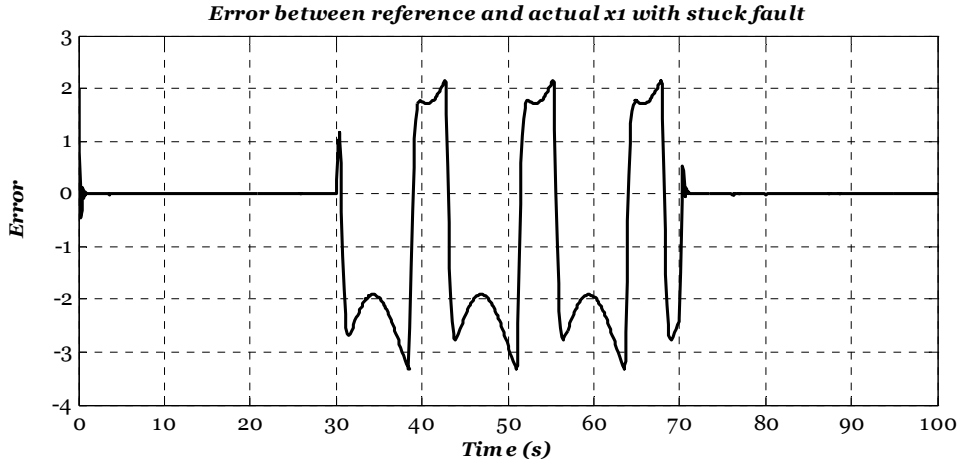

(b)

Figure 9-6 : Tracking performance with $\boldsymbol{x_1}$ stuck sensor fault:

(a) State tracking & (b) tracking performance.

4. $\boldsymbol{x_2}$ **parametric sensor fault**: In this fault scenario the control signal in Eq. (9-16) become as follows:

$$u = \frac{-1}{2}[(3-\gamma)x_1 + (6-\gamma)x_2 - \ddot{x}_r - \gamma\dot{x}_r] + k\,\frac{|S|}{S+\delta} + (\frac{-1}{2}((6-\gamma)\epsilon x_2) \quad (9\text{-}23)$$

It is clear that the effect of this fault is similar to (actually emulates) the additive actuator fault case. Hence, the SMC has the ability to tolerate this fault provided that k is selected sufficiently high. Figure 9-7a & b shows the robustness of the SMC against this fault for $\epsilon = -0.7$.

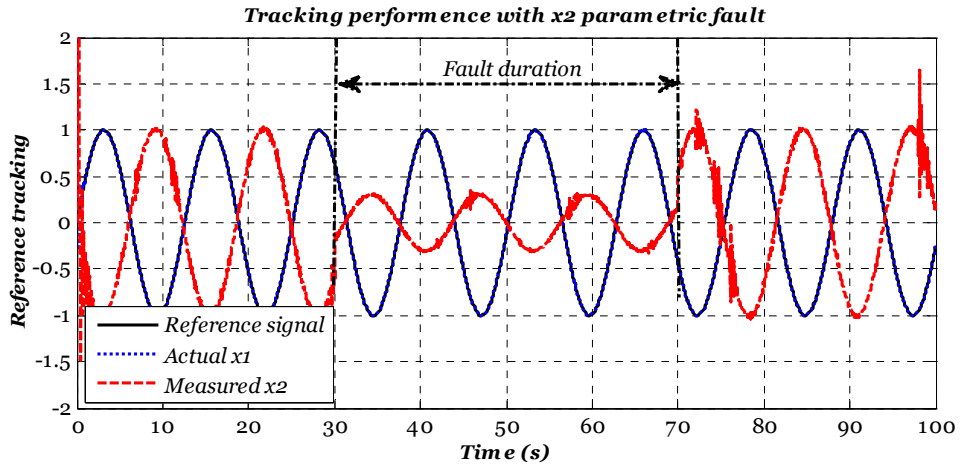

(a)

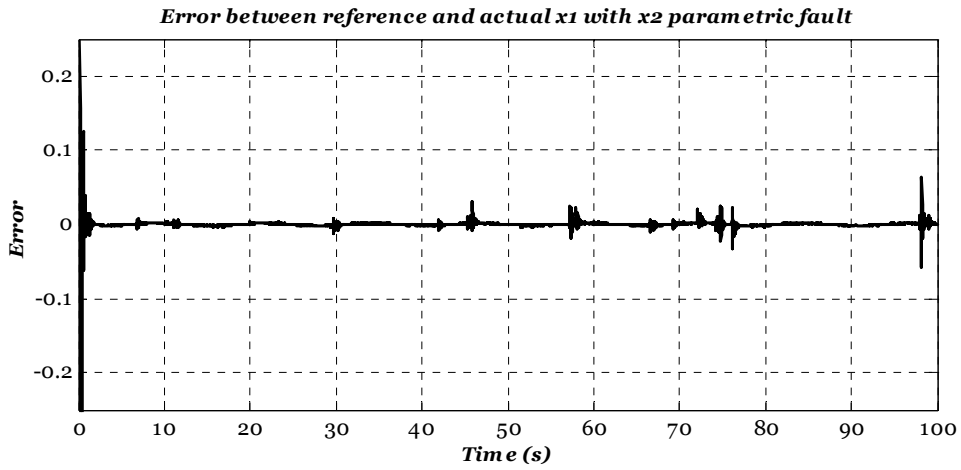

(b)

Figure 9-7 : Tracking performance with $\boldsymbol{x_2}$ parametric sensor fault:

(a) State tracking & (b) tracking performance.

5. $\boldsymbol{x_2}$ **additive sensor fault**: In this fault scenario the control signal is given as:

$$u = \frac{-1}{2}[(3-\gamma)x_1 + (6-\gamma)x_2 - \ddot{x}_r - \gamma\dot{x}_r] + k\,\frac{|S|}{S+\delta} + (\frac{-1}{2}((6-\gamma)f_s) \qquad (9\text{-}24)$$

Clearly, from the SMC stand point, this fault is similar to the x_2 parametric sensor fault. Figure 9-8a, &b shows the robustness of the SMC against this fault for $f_s = \sin(0.25t)$.

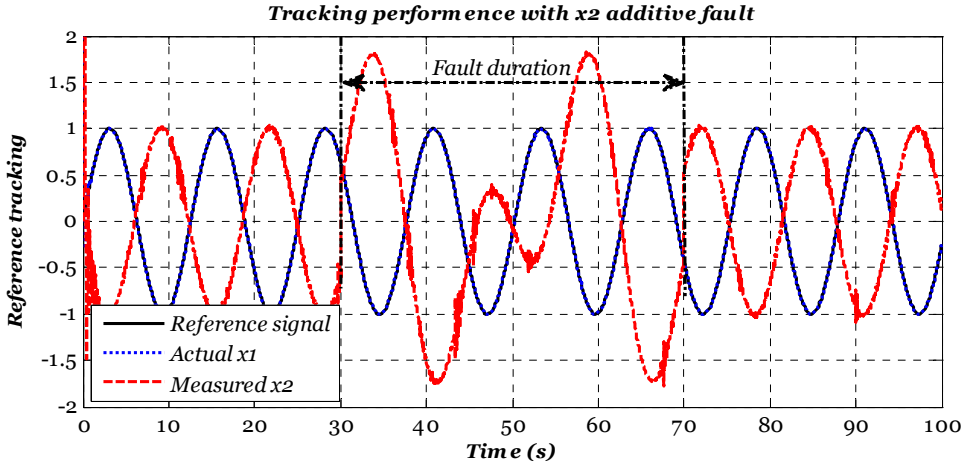

(a)

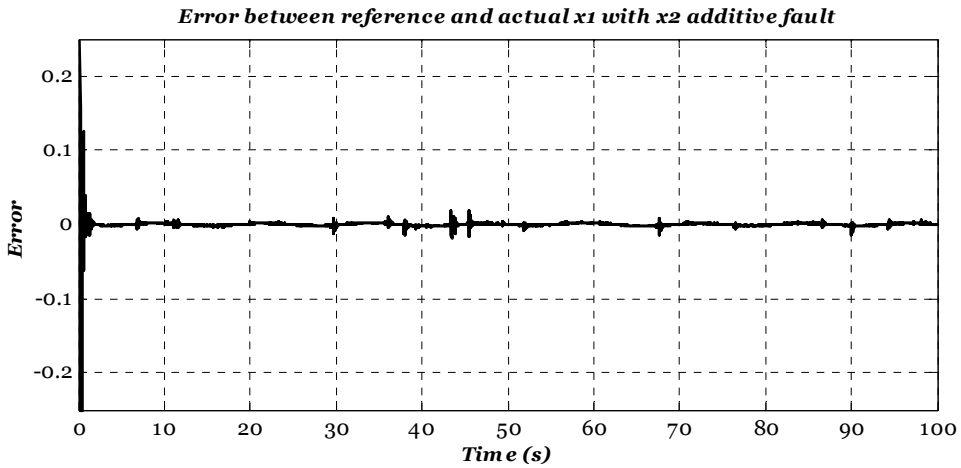

(b)

Figure 9-8 : Tracking performance with $\boldsymbol{x_2}$ additive sensor fault:

(a) State tracking & (b) tracking performance.

6. **Stuck fault**: This fault appear as an additive actuator fault as follows:

$$u = \frac{-1}{2}[(3-\gamma)x_1 + (6-\gamma)x_2 - \ddot{x}_r - \gamma\dot{x}_r] + k\,\frac{|S|}{S+\delta} + \frac{-1}{2}(6-\gamma)(\mathcal{C} - x_2) \tag{9-25}$$

Figure 9-9a, &b shows the robustness of the SMC against this fault for $\mathcal{C} = 0.5$.

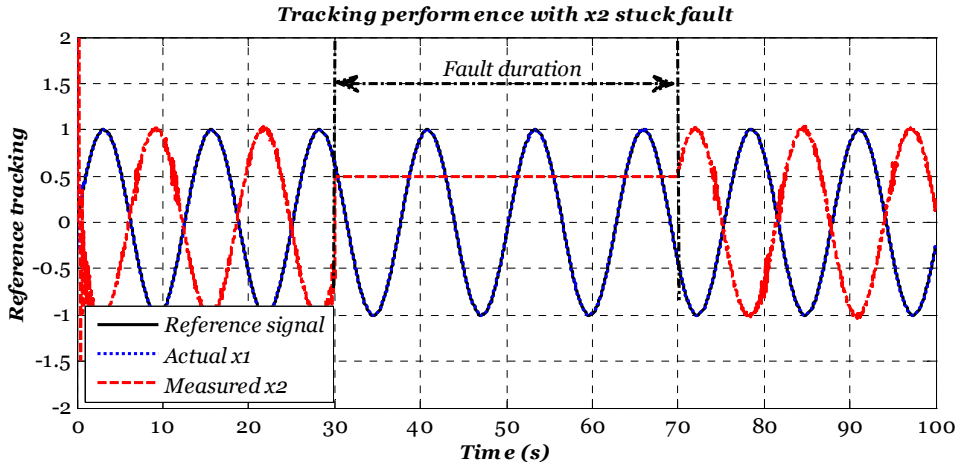

(a)

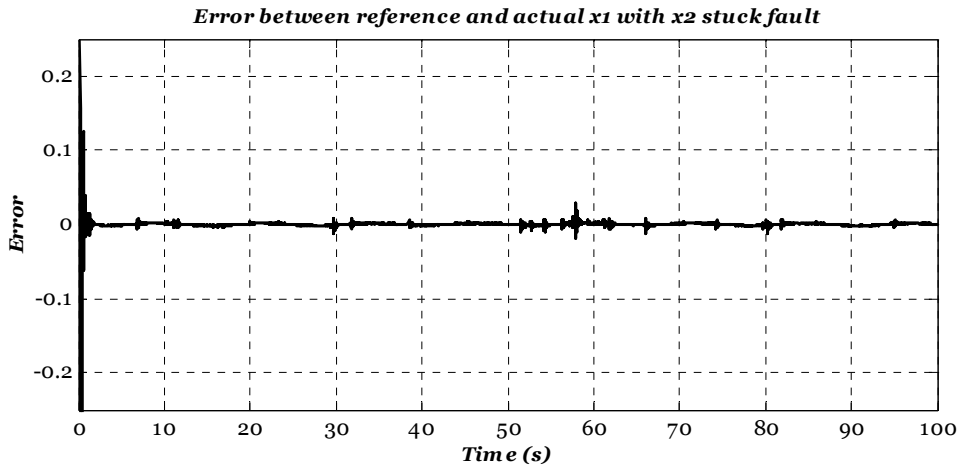

(b)

Figure 9-9 : Tracking performance with $\boldsymbol{x_2}$ stuck sensor fault:
(a) State tracking & (b) tracking performance.

Remarks:

- Although the faults affect x_1 measurement cannot be tolerated by the SMC, within the regulator control problem, as stated in Chapter 3, the state itself hides the effect of the parametric sensor fault. This is clear from the sliding surface equation:

  $$S = (\dot{x}_1 + \epsilon\dot{x}_1 - \dot{x}_r) + \gamma(x_1 + \epsilon x_1 - x_r) = \dot{e} + \gamma e + (\epsilon\dot{x}_1 + \gamma\epsilon x_1)$$

  which clearly shows the fact that if ($x_{1-measured} = 0$) then $S = \dot{e} + \gamma e$. Hence, the robustness in this case is not attributed to SMC but to the state itself.

- The investigation presented in this Section is a function of sliding surface design problem. Hence, for the model reference or state feedback with integral action based tracking control, sensor faults might have different effects if all the states are included in the definition of the sliding surface.
- To enhance the robustness of the SMC against some fault scenarios, a combination of SMC with other fault FTC techniques could enhance the overall robustness of the closed-loop system.

9-4. SMC based sustainable OWTs

Owing to the robustness of the SMC against some actuator and sensor fault scenarios, this Section presents a new strategy for robust FTTC to maintain the optimisation of the wind energy captured by a wind turbine in the presence of generator rotational speed sensor faults and generator torque faults using an adaptive gain SMC. Compared with

the work in (Boukhezzar, Lupu, Siguerdidjane and Hand, 2007, Boukhezzar and Siguerdidjane, 2009, Boukhezzar and Siguerdidjane, 2011), the proposal presents significant contribution to the literature of wind turbine control. This is attributed to the robustness of the proposed strategy against model uncertainty and some fault scenarios.

In fact, the existence of an unexpected component fault and model uncertainty requires the upper bounds on the norm of these uncertainties to be known, to guarantee the stability of the closed-loop system. Unfortunately, sometimes these upper bounds may not be easily obtained. Therefore, a simple adaptive gain is used within the SMC framework presented in Section 9-2 which can guarantees asymptotic stability of the wind turbine system in the presence of bounded norm uncertainties. As stated in Chapter 7, to ensure power maximisation the control strategy must force the wind turbine to operate in the vicinity of the optimal tip-speed-ratio (λ_{opt}). Hence, the power maximisation control problem is summarised as:

- Track the optimal rotor rotational speed ω_{ropt} given in Eq. (8-1).
- Tolerate the effect of faulty measurement signals.
- Tolerate the effect of actuator faults.

The sliding mode surface must be designed so that when the system enters the sliding mode the control objectives are achieved.

For the wind turbine model presented in Chapter 7, the tracking error is defined as follows:

$$e_t = \omega_r - \omega_{opt} \tag{9-26}$$

Then the first, second, and third order differential equations of the tracking error can easily be obtained based on Eq. (9-26) and Eq. (7-4), as:

$$\left.\begin{aligned} \dot{e}_t &= a_{11}\omega_r + a_{12}\omega_g + a_{13}\theta_\Delta + b_{11}T_a - \dot{\omega}_{opt} \\ \ddot{e}_t &= \ddot{\omega}_r - \ddot{\omega}_{opt} \\ \dddot{e}_t &= \dddot{\omega}_r - \dddot{\omega}_{opt} \end{aligned}\right\} \tag{9-27}$$

For the order three tracking error dynamics the proposed sliding surface is:

$$S = \ddot{e}_t + 2\gamma\dot{e}_t + \gamma^2 e_t \tag{9-28}$$

Hence, while the system trajectory is in the sliding manifold ($S = 0$) the dynamics are reduced to a second order differential equation with time response governed by the positive design parameter (γ) which can be considered as a tuning parameter that governs the response of the system during sliding. The most important challenge then is to find the control signal that achieves the sliding condition given in Eq. (9-3) so that the sliding surface starts to attract the system trajectories to reach and remain in the sliding surface vicinity. Hence, when the system reaches the sliding vicinity $S = 0 \Rightarrow \dot{S} = 0$, then the equivalent control signal is:

$$\dot{S} = 0 = \ddot{e}_t + 2\gamma\ddot{e}_t + \gamma^2\dot{e}_t \tag{9-29}$$

$$\begin{aligned}\dot{T}_g = \frac{-1}{b_{22}a_{12}}(&b_{11}a_{11}\dot{T}_a + b_{11}\ddot{T}_a + \tilde{a}_{11}b_{11}T_a + b_{22}\tilde{a}_{12}T_g + \tilde{\tilde{a}}_{11}\omega_r + \tilde{\tilde{a}}_{12}\omega_g \\ &+ \tilde{\tilde{a}}_{13}\theta_\Delta - \dddot{\omega}_{opt} + 2\gamma\ddot{e}_t + \gamma^2\dot{e}_t)\end{aligned} \tag{9-30}$$

where:

$\tilde{a}_{11} = a_{11}a_{11} + a_{12}a_{21} + a_{13}a_{31}$, $\tilde{a}_{12} = a_{11}a_{12} + a_{12}a_{22} + a_{13}a_{32}$

$\tilde{a}_{13} = a_{11}a_{13} + a_{12}a_{23} + a_{13}a_{33}$, $\tilde{\tilde{a}}_{11} = \tilde{a}_{11}a_{11} + \tilde{a}_{12}a_{21} + \tilde{a}_{13}a_{31}$

$\tilde{\tilde{a}}_{12} = \tilde{a}_{11}a_{12} + \tilde{a}_{12}a_{22} + \tilde{a}_{13}a_{32}$, $\tilde{\tilde{a}}_{13} = \tilde{a}_{11}a_{13} + \tilde{a}_{12}a_{23} + \tilde{a}_{13}a_{33}$

Eq. (9-30) represents the actual equivalent control signal required to bring the wind turbine system trajectories to the sliding surface. However, several unknown signals contribute to an expected uncertainty that prevent the control signal given in Eq. (9-30) to achieve this task. For example, the estimation error of the unmeasured signals (i.e. T_a and θ_Δ), the existence of faults, and model parameter uncertainty. Hence, an adaptive gain is proposed to overcome the uncertainty in the control signal. Using this and Eq. (7-6), the generator reference torque (T_{gr}) is given by:

$$\begin{aligned}T_{gr} = \frac{-\tau_g}{b_{22}a_{12}}(&\tilde{\tilde{a}}_{11}(\omega_r + f_{sr}) + \tilde{\tilde{a}}_{12}(\omega_g + f_{sg}) + \tilde{\tilde{a}}_{13}\hat{\theta}_\Delta + 2\gamma\ddot{e}_t + \gamma^2\dot{e}_t \\ &+ \tilde{a}_{11}b_{11}\hat{T}_a + \left(b_{22}\tilde{a}_{12} + \frac{b_{22}a_{12}}{\tau_g}\right)T_g + \frac{b_{22}a_{12}}{\tau_g}f_a + (k(t) + \eta) \\ &* sgn(S))\end{aligned} \tag{9-31}$$

where $k(t)$ is the adaptive gain, f_a is the generator torque bias fault, f_{sr} is the rotor speed sensor fault, f_{sg} is the generator speed sensor fault, and η is a positive constant.

The proposed control signal as shown in Eq. (9-31) consists of *two* components, the linear and discontinuous controls. In this Section the rotor rotational speed measurement is assumed to be fault-free since this fault cannot be tolerated via the inherent robustness of the sliding surface. Hence, only f_{sg} & f_a are considered in this Section.

Substitution of Eq. (9-31) in the expression of $\dot{S}$ yields:

$$\dot{S} = b_{11}\ddot{T}_a - \ddot{\omega}_{opt} + \mathcal{E} - (k(t) + \eta) * sgn(S) \tag{9-32}$$

where $\mathcal{E}$ represents the sum of upper bound of f_a, f_{sr}, f_{sg} and the total error between the original signals and their estimates. Suppose that:

$$h(t) = b_{11}\ddot{T}_a - \ddot{\omega}_{opt} + \mathcal{E} \tag{9-33}$$

The upper bound of $h(t)$satisfies:

$$|h(t)| \leq H \tag{9-34}$$

The assumption on the upper bound of $h(t)$ is not conservative since the operation of the wind turbine is governed within the specific range of wind speed (usually between 4-25 m s^{-1}). Moreover, this controller is dedicated to maximizing the extracted wind power for which the range of operation is further governed in the range (4-12 ms^{-1}). Furthermore, since wind turbine operation starts at specific wind speeds the initial estimation error can be minimized.

To analyze the stability, consider the following Lyapunov function:

$$V(S) = \frac{1}{2}SS + \frac{1}{2}(k(t) - H)^2 \tag{9-35}$$

The time derivative is:

$$\dot{V}(S) = \dot{S}S + (k(t) - H)\dot{k}(t) \tag{9-36}$$

Using (9-31) and (9-32), then Eq. (9-36) becomes:

$$\dot{V}(S) \leq HS - k|S| - \eta|S| + k(t)\dot{k}(t) - H\dot{k}(t) \tag{9-37}$$

To ensure the negativity of (9-37) the adaptive gain is designed to be equal to:

$$\dot{k}(t) = |S| \tag{9-38}$$

Hence, the derivative of the Lyapunov function always satisfies:

$$\dot{V}(S) < -\eta|S| \tag{9-39}$$

Hence, the tracking error converges towards zero. However, to avoid the chattering accompanied with sliding motion the approximation to the function $sgn(S)$ given in Eq. (9-14) is used to ensure smooth sliding motion in the vicinity of the line $(S = 0)$. However, the adaptive gain presented in (9-38) is continuously increasing as long as S is away from $S = 0$. Therefore, a slight modification to (9-38) is introduced below:

$$\dot{k}(t) = \begin{matrix} |S| & S > \delta \\ 0 & S \leq \delta \end{matrix} \Bigg\} \tag{9-40}$$

The fault tolerance performance is to be demonstrated in the simulation results below. It becomes clear that the generator rotational speed sensor fault and the actuator fault can be considered as matched uncertainties. These faults can be tolerated by the proposed control strategy involving the robustness and the adaptive gain of the SMC.

9-4-1. Simulation results

The simulation of proposed adaptive SMC design is based on the wind turbine benchmark system proposed by (Odgaard, Stoustrup and Kinnaert, 2009). The schematic of this strategy is shown in Figure 9-10.

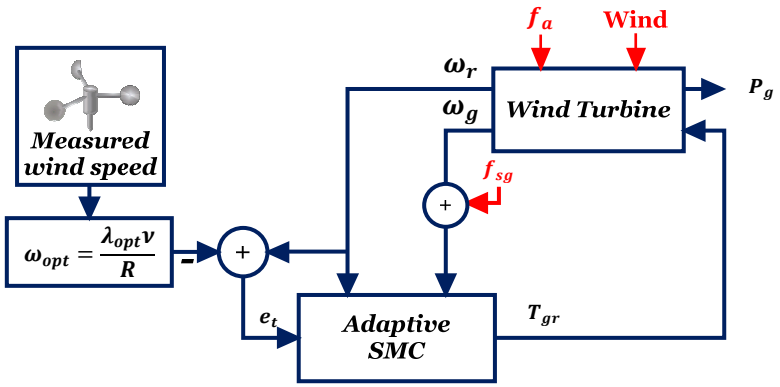

Figure 9-10: Schematic of the proposed strategy

The two generator sensor faults are represented by scaling factor errors. In the first scenario the scaling is 1.1 times the real generator rotational speed, the second fault involves another scaling of 0.9. In both cases the expected fault effects cause the reference generator torque to deviate from the torque required to achieve optimal power conversion.

As shown in Figure 9-10 the computation of the reference signal in Eq. (8-1) is based on the measured wind speed signal. Moreover, as stated in Chapter 7 and 8, exact tracking of the optimal rotor speed leads to increasing the load on the drive train shafts and hence

minimises the drive train life time. This also produces a highly fluctuating output power, and may even produce a varying direction reference torque signal that can lead to abnormal generator operation. Actually, these effects deteriorate for large inertia wind turbines (e.g. of the offshore type). Therefore, the computed optimal rotor rotational speed signal is passed through a low-pass filter so that these effects are minimised. In addition to filtering the reference optimal rotational speed, another degree of freedom for governing the tracking performance during sliding is available by adjusting the design parameter γ.

For comparison purposes, the tracking performance of the proposed strategy compared with the well-known *'standard control'* (SC) ($T_{gr} = k_{opt}\omega_r^2$) proposed in the benchmark model (Burton, Sharpe, Jenkins and Bossanyi, 2001, Johnson, 2004, Pao and Johnson, 2011). Figure 9-11 shows the optimal rotor speed, the actual rotor speed using SMC, and for comparison purposes the rotor speed using SC. These signals show that the proposed SMC can track the tendency of the optimal speed much better than SC. This difference appears to be significant for the benchmark system used because of the large turbine inertia that prevents the tracking of the optimal rotational signal. This is the case as long as the SC depends on the turbine dynamics only, i.e. without taking the wind dynamics into consideration. Table 9-1 gives some statistical data used to analyse the performance of these controllers. The minimum (Min), the maximum (Max), the standard deviation (STD), and the mean values show how far away the rotor rotational speed is from the optimal value, using the SC. The lowest values of STD and mean appear in the SC case which shows the fact that the power conversion efficiency decreased significantly during wind turbulence.

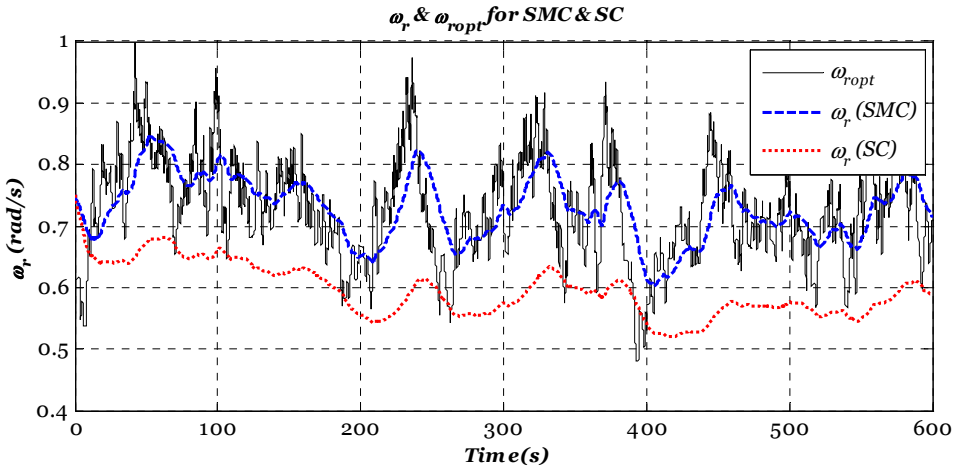

Figure 9-11: Tracking performance using SMC and SC

Table 9-1: Statistics of the turbine rotational speed.

ω_r	Min	Max	STD	Mean
Optimal	0.4803	0.9983	0.0830	0.7256
With SMC	0.6032	0.8457	0.0520	0.7283
With SC	0.5195	0.7500	0.0429	0.5962

Figure 9-12 shows three signals of the generator rotational speed which are the actual speed, and with (1.1 and 0.9) scale sensor faults. Clearly, due to the robustness of the SMC against these faults, the actual generator speed is not affected by any of the proposed fault scenarios.

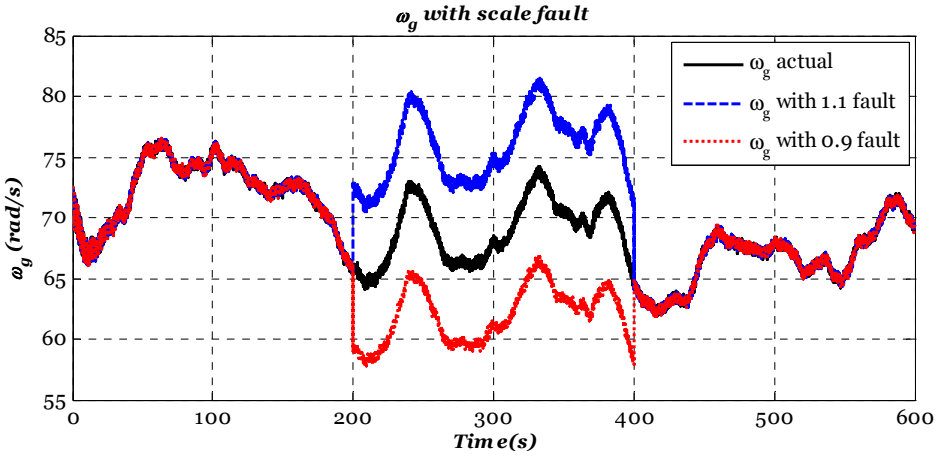

Figure 9-12: Different cases of generator rotational speed

Figure 9-13 firstly shows the reference generator torque (T_{gr}) for the nominal and faulty cases. Secondly, the power generated by the turbine is also shown in different generator rotational speed fault cases. Table 9-2 further clarifies, through statistical measurements, the robustness of the proposed strategy against the generator rotational speed sensor fault.

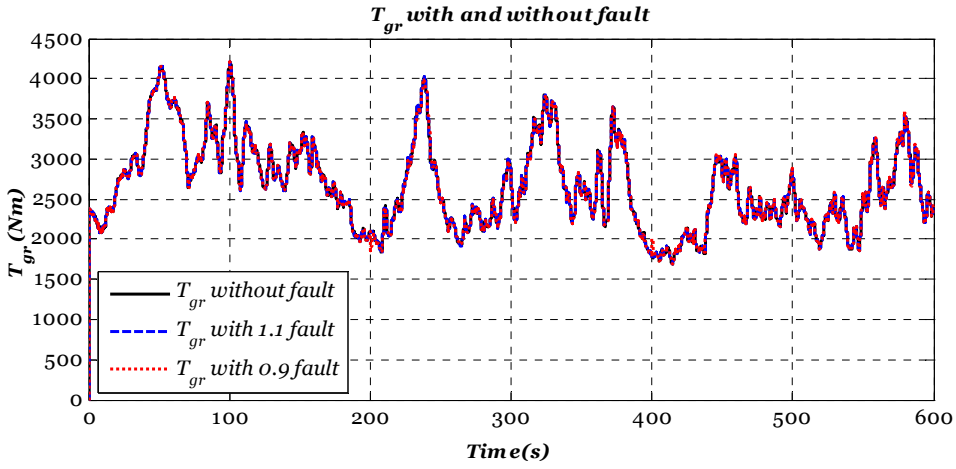

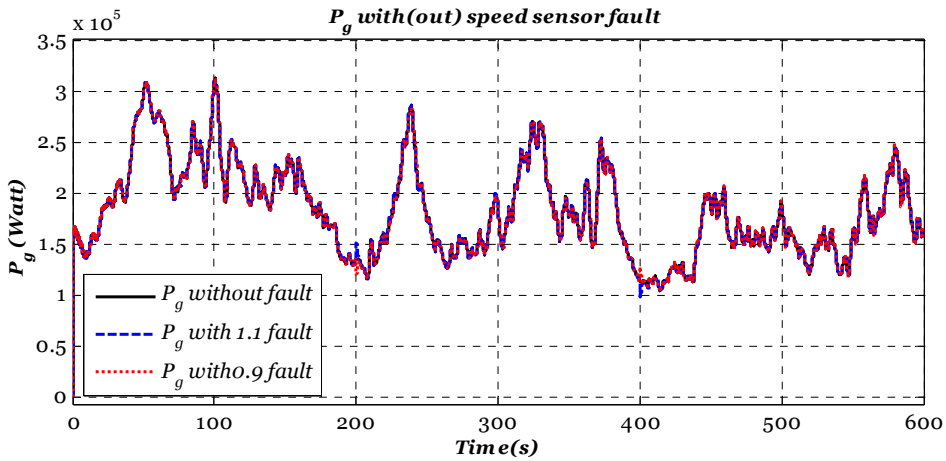

Figure 9-13: Generator reference torque and turbine generated power in different sensor fault scenarios.

Table 9-2: Statistics of the turbine generated power.

P_g	*Min*	*Max*	*Std*	*Mean*
Fault-free	0	$3.1267*10^5$	$4.4633*10^4$	$1.822*10^5$
1.1 fault	0	$3.1222*10^5$	$4.4655*10^4$	$1.823*10^5$
0.9 fault	0	$3.1244*10^5$	$4.4674*10^4$	$1.822*10^5$

Another fault scenario proposed in the benchmark model is the bias of the generator torque "soft sensor". Clearly, this bias will drive the turbine away from the optimal operation and minimise the wind power conversion efficiency. This fault scenario appears in the control signal as given in Eq. (9-31) where $f_a = 500$ [Nm] is the generator torque (T_g) bias fault which appears between $100\ and\ 200\ sec$. Clearly, this fault affects the system in the same direction as the control signal and hence the robustness of the proposed adaptive SMC inherently tolerates this fault as shown in Figure 9-14

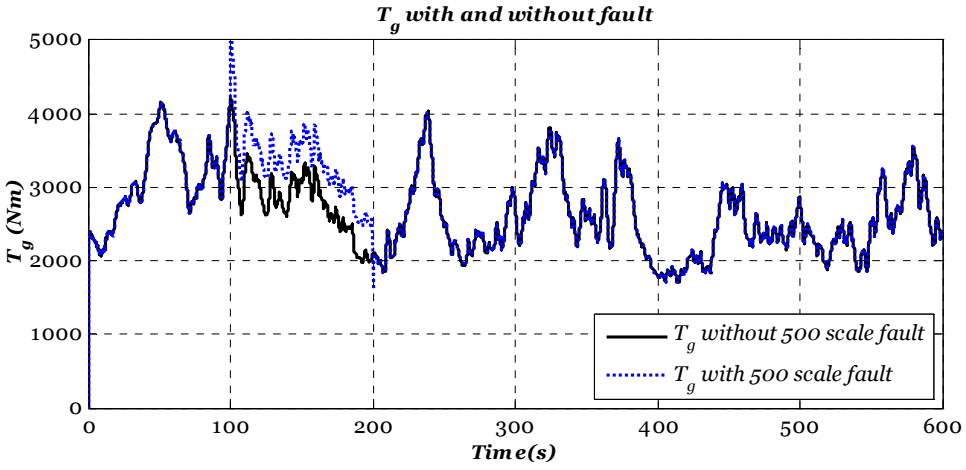

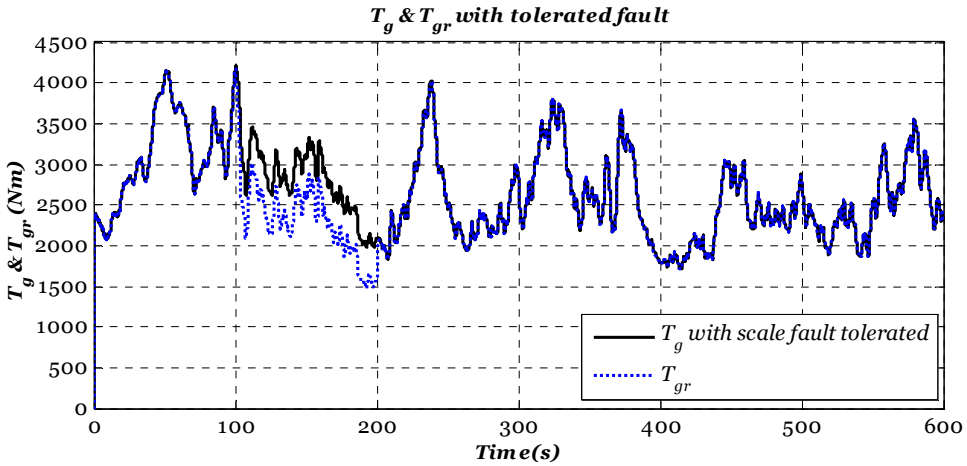

Figure 9-14: Reference and actual generator torque with $\boldsymbol{f_a}$ bias fault in the period (100-200) sec.

Figure 9-14 also shows clearly how the reference generator torque generated by the SMC takes into account the bias fault effect so that the actual torque remains unaffected by f_a.

9-5. SMC based sustainable OWTs within estimation and compensation framework

This Section proposes a new FTTC strategy for sustainable OWTs. Within the SMC based FTTC presented in Section 9-4 the challenge is to develop a SMC based FTTC for OWTs to tolerate the expected rotor speed measurement fault since this fault has a direct effect on the defined sliding surface. Hence, owing to the inherent robustness against model matched parameter uncertainty of SMC, the proposed method can first tolerate the reference generator torque bias fault using the inherent robustness of SMC. In addition, the proposed method involves the design of a robust PMIO that can provide robust simultaneous estimation of states and the "unknown outputs" (sensor faults and/or noise) in order to guarantee the robustness of the sliding surface against unknown output effects. Clearly, the use of SMC within the estimation and compensation framework enhances the overall closed-loop robustness and provides information about the fault via fault estimation which in turn can be used for scheduling of maintenance operations. The schematic of the proposed strategy is shown in Figure 9-15 in which $\hat{\omega}_r = \omega_r - f_{sr}$ and $\hat{\omega}_g = \omega_g - f_{sg}$.

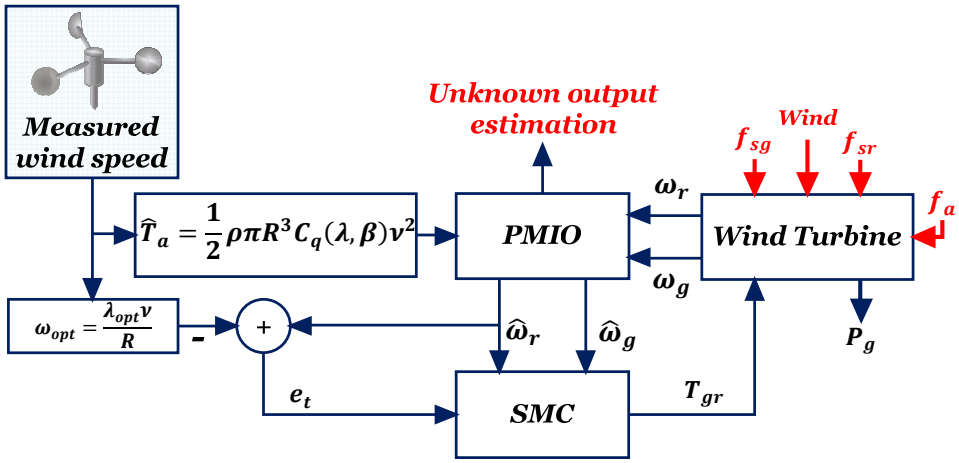

Figure 9-15: Schematic of the proposed strategy

9-5-1. Sensor fault estimation via PMIO

This Section illustrates the robust strategy to estimate the generator and rotor speed sensor faults using the PMIO. The drive train state space model in Eq. (7-4) with sensor fault can be rewritten as follows:

$$\left.\begin{aligned} \dot{x} &= Ax + B_1\hat{T}_a + B_2T_g \\ y &= Cx + D_f f_s \end{aligned}\right\} \tag{9-41}$$

where $x \in \mathcal{R}^n$ and $f_s = [f_{sr} \quad f_{sg}] \in \mathcal{R}^k$ are the state vector and the sensor fault signals. The model matrices are $A \in \mathcal{R}^{n*n}$, $B_1 \in \mathcal{R}^{n*1}$, $B_2 \in \mathcal{R}^{n*1}$, $C \in \mathcal{R}^{l*n}$, $D \in \mathcal{R}^{l*s}$, and $\hat{T}_a$ is the estimation of the unmeasured aerodynamic torque obtained using Eq. (7-3). Under the assumption that the q^{th} derivative of the fault f_s is bounded, an augmented state system comprising the original drive train state equations and the q^{th} derivative of the f_s can be constructed as follows:

$$\left.\begin{aligned} \dot{\bar{x}} &= \bar{A}\bar{x} + \bar{B}_1\hat{T}_a + \bar{B}_2T_g + \bar{D}f_s^q \\ y &= \bar{C}\bar{x} \end{aligned}\right\} \tag{9-42}$$

Hence the following PMIO is proposed to simultaneously estimate the drive train states, the sensor fault, and the unknown aerodynamic torque component:

$$\dot{\hat{\bar{x}}} = \bar{A}\hat{\bar{x}} + \bar{B}_1\hat{T}_a + \bar{B}_2T_g + \bar{K}(y - \bar{C}\hat{\bar{x}}) \tag{9-43}$$

where $\hat{\bar{x}} \in \mathcal{R}^{\bar{n}}$ is the estimation of the augmented state vector $\bar{x}$, and $\bar{K} = [K_p^T, K_I^1, .., K_I^q]^T \in \mathcal{R}^{\bar{n}*l}$ is the gain to be design.

Theorem 9-1: *The PMIO given in Eq. (9-43) exists if:*

$$rank\begin{bmatrix} A & 0 \\ C & D_f \end{bmatrix} = n + k \tag{9-44}$$

and if:

$$rank\begin{bmatrix} sI - A \\ C \end{bmatrix} = n \qquad \forall s \in \mathbb{C} \tag{9-45}$$

Additionally, the PMIO attenuates the effect of the bounded f_s^q *and* e_T *on the augmented estimation error if there exists SPD matrix* $P = P^T > 0$ *and matrices* $\bar{H}$ *that minimise* γ *under the following LMI constraints:*

$$\begin{bmatrix} P\bar{A} + (P\bar{A})^T - \bar{H}\bar{C} - (\bar{H}\bar{C})^T & PG & P\bar{B}_1 & I_{\bar{n}\times\bar{n}} \\ (PG)^T & -\gamma I & 0 & 0 \\ (P\bar{B}_1)^T & 0 & -\gamma I & 0 \\ I_{\bar{n}\times\bar{n}} & 0 & 0 & -\gamma I \end{bmatrix} \tag{9-46}$$

where the observer gains are obtained by:

$$\bar{K} = P^{-1}\bar{H} \tag{9-47}$$

Proof: Conditions (9-44)&(9-45) follow directly the observability requirements for the states and unknown input estimate.

The state estimation error dynamics are obtained by subtracting Eq. (9-43) from (9-42):

$$\dot{e}_x = (\bar{A} - \bar{K}\bar{C})e_x + \bar{D}f_s^q - \bar{B}_1 e_T \tag{9-48}$$

To attenuate the effect of ${T_a}^q$ and e_{fs} on the estimation error simultaneously whilst also ensuring system stability, the following inequality must hold:

$$\dot{v}(e_x) + \frac{1}{\gamma}e_x^T\, e_x - \gamma({f_s^q}^T f_s^q + {e_T}^T e_T) < 0 \tag{9-49}$$

where $\dot{v}(e_x)$ is the time derivative of the candidate Lyapunov function ($v(e_x) = e_x^T P e_x$). Using Eq. (9-48), inequality (9-49) becomes:

$$\begin{aligned} \dot{v}(e_x) = \Big\{ & e_x^T(\bar{A}^T P\ + P\bar{A} - P\bar{K}\bar{C} - (P\bar{K}\bar{C})^T)e_x + \ e_x^T P\bar{D}f_s^q + {f_s^q}^T\bar{D}^T P e_x \\ & - e_x^T P\bar{B}_1 e_T - {e_T}^T(P\bar{B}_1)^T e_x \Big\} \end{aligned} \tag{9-50}$$

The inequality (9-49) (in matrix form) after substituting $\dot{v}(\tilde{x}_a)$ from Eq. (9-50) and using the variable change $\bar{H} = P\bar{K}$ becomes:

$$\begin{bmatrix} e_x \\ f_s^q \\ e_T \end{bmatrix}^T \begin{bmatrix} P\bar{A} + (P\bar{A})^T - \bar{H}\bar{C} - (\bar{H}\bar{C})^T + \frac{1}{\gamma} I_{\bar{n}\times\bar{n}} & PG & P\bar{B}_1 \\ G^T P & -\gamma I & 0 \\ (P\bar{B}_1)^T & 0 & -\gamma I \end{bmatrix} \begin{bmatrix} e_x \\ f_s^q \\ e_T \end{bmatrix} < 0 \qquad (9\text{-}51)$$

Clearly, by using the Schur Theorem inequality (9-46) can easily be obtained from inequality (9-51). This completes the proof.

The controller design has been already developed in Section 9-4. The following Section shows the simulation results of the proposed strategy using the benchmark model presented in Chapter 7.

Remark: To enhance the fault estimation accuracy a separate PMIO for each measurement can be designed since the drive-train subsystem is observable using either ω_r or ω_g.

9-5-2. Simulation results

In the first fault scenario the generator and rotor speed sensor faults are represented by scaling factor errors. The scaling is 1.1 times the real generator and rotor rotational speeds. The expected fault effects cause the reference generator torque to deviate from the torque required to achieve optimal power generation. Figure 9-16 shows the measured, actual and estimated generator and rotor speed signals with scaling fault 1.1. The simulation signals show that the rotor rotational speed is highly affected by noise. However, the proposed PMIO effectively decouples and estimates the unknown outputs.

The fault estimation of both generator and rotor sensors are shown in Figure 9-17.

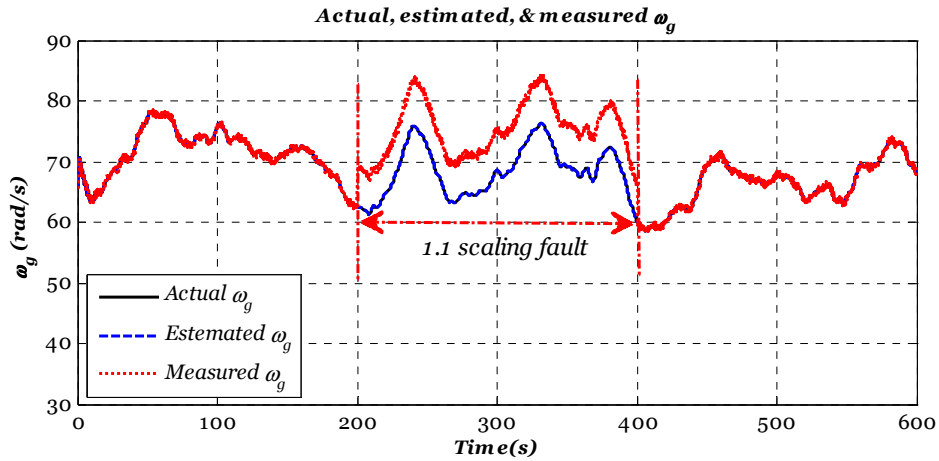

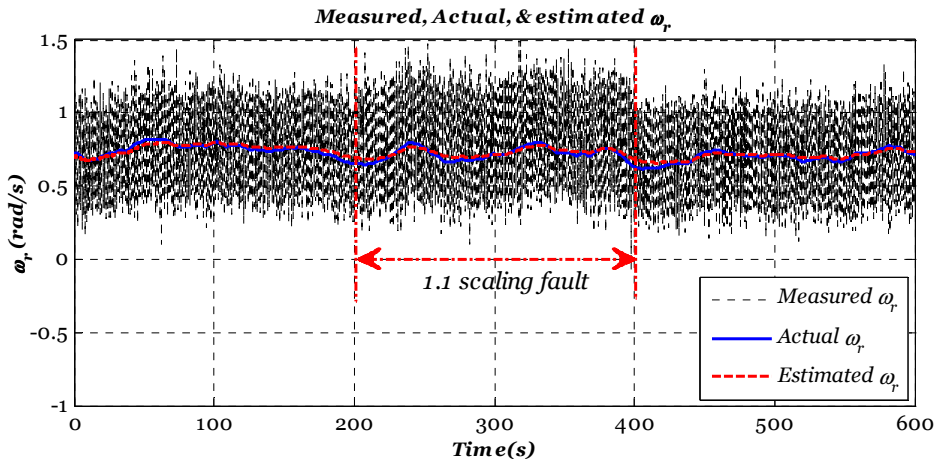

Figure 9-16: Generator & rotor rotational speed

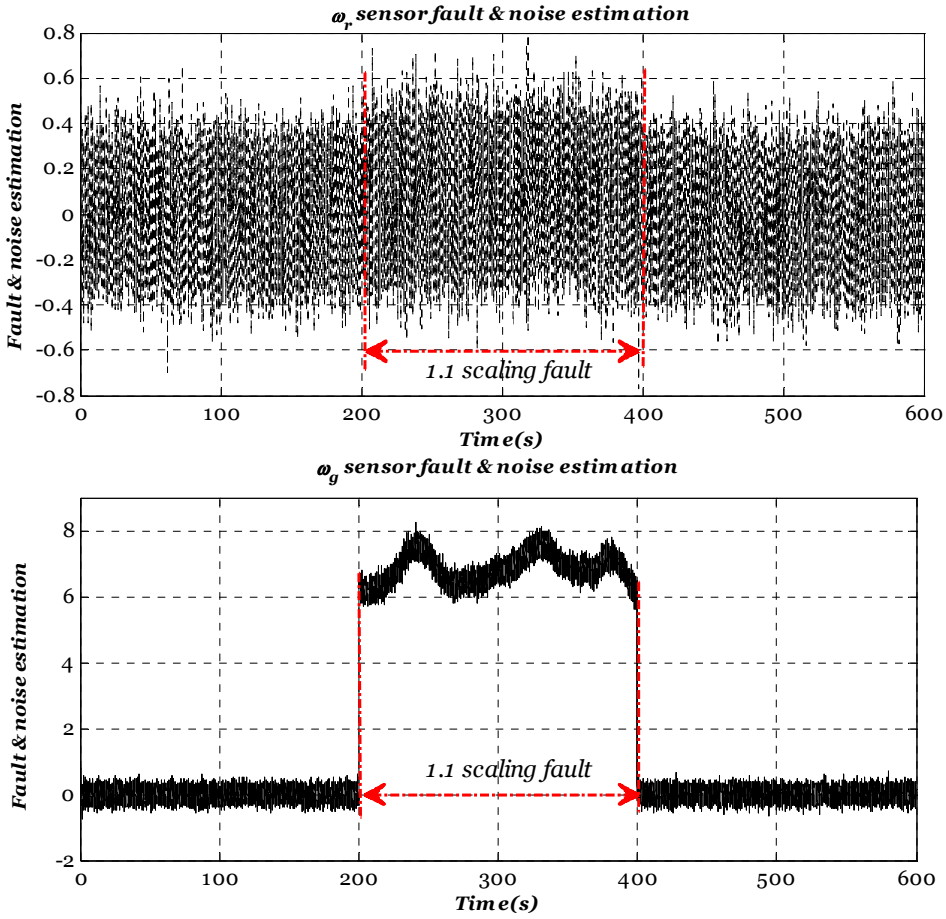

Figure 9-17: Rotor & generator measurement fault

The rotor scale fault forces the wind turbine to operate away from the optimal conversion efficiency as shown in Figure 9-18. Finally, the reference generator torque responds to the rotor scale fault through increasing the torque to break the aerodynamic rotation so the faulty measurement tracks the optimal rotational speed (see Figure 9-19). It should be noted that the spikes appear in the generator torque signal shown in

Figure 9-19 is attributed to the abrupt fault that affect the rotor speed measurement which in turn affect the sliding surface directly. The scale fault in the generator soft sensor can be handled via the inherent robustness of the SMC without the need for the estimation and compensation approach (see Figure 9-20).

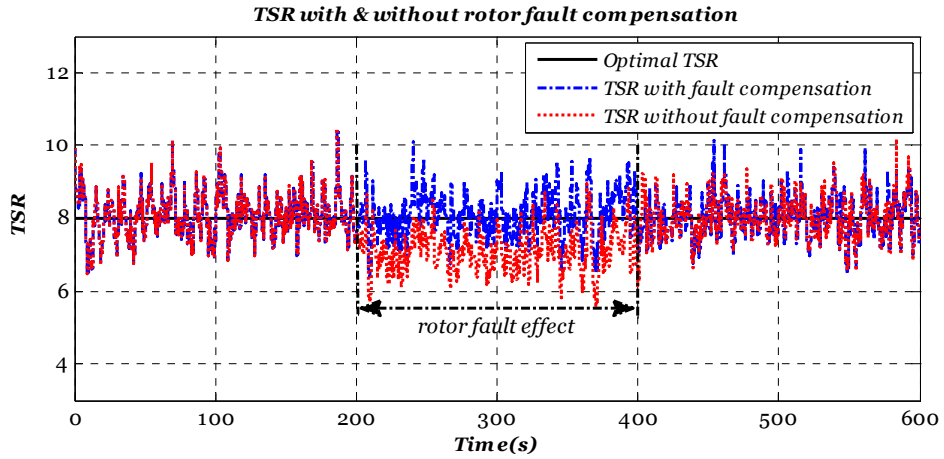

Figure 9-18: The effect of rotor scale fault on TSR

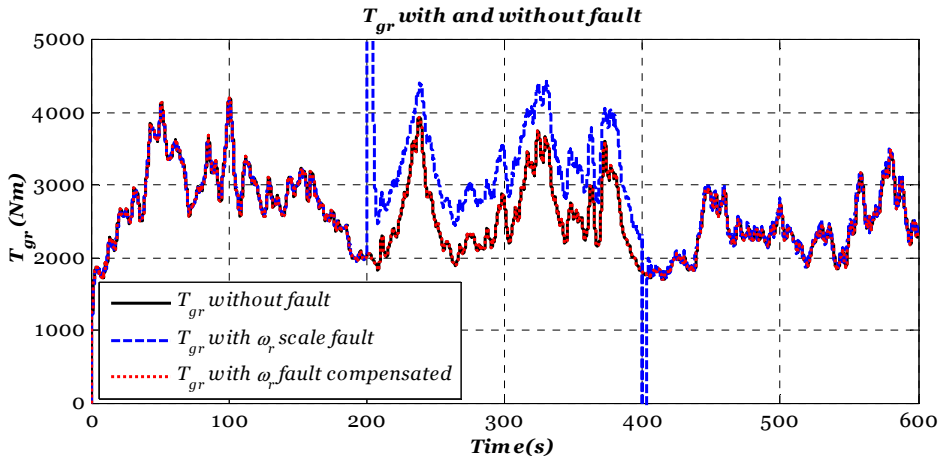

Figure 9-19: The effect of rotor scale fault on generator torque

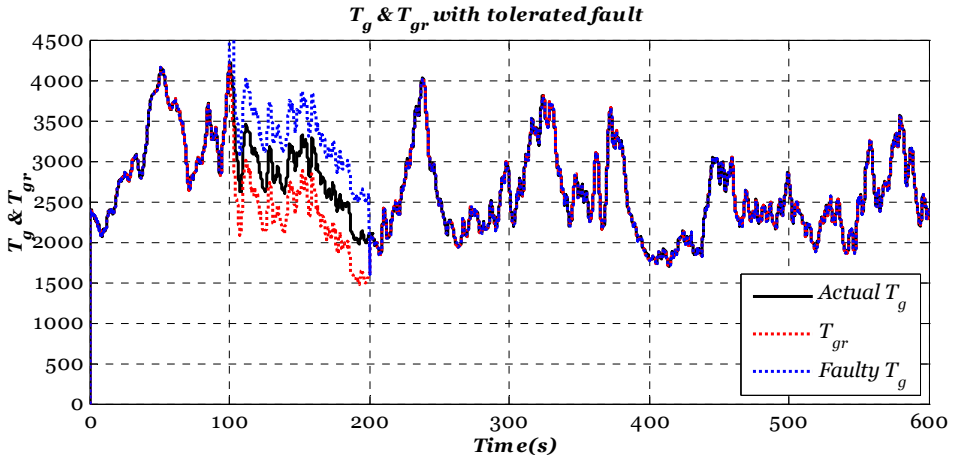

Figure 9-20: The ability of SMC to tolerate torque scale fault

9-6. SMC based sustainable OWTs within estimation and compensation framework with ESW estimation

The challenge involved within the strategy proposed in Section 9-5 is the uncertainty in the measured wind speed which can be overcome via the estimation of the EWS. To handle this challenge, the schematic of the proposed architecture is similar to the architecture proposed in Chapter 6 and Section 8-2-3 in Chapter 8. The control strategy designed to tolerate the effect of simultaneous generator and rotor sensor faults, overcome the SMC surface sensitivity to measurement noise and/or faults, tolerate generator torque scale fault via the inherent SMC robustness against matched uncertainty, and make use of the estimated EWS for optimal rotor speed computation. Therefore, to cope with these, the proposed adaptive SMC strategy presented in Section 9-4 is assisted by the estimated EWS and sensor fault estimate signals provided by *three* separate observers so that the overall control strategy takes on the structure shown in Figure 9-21.

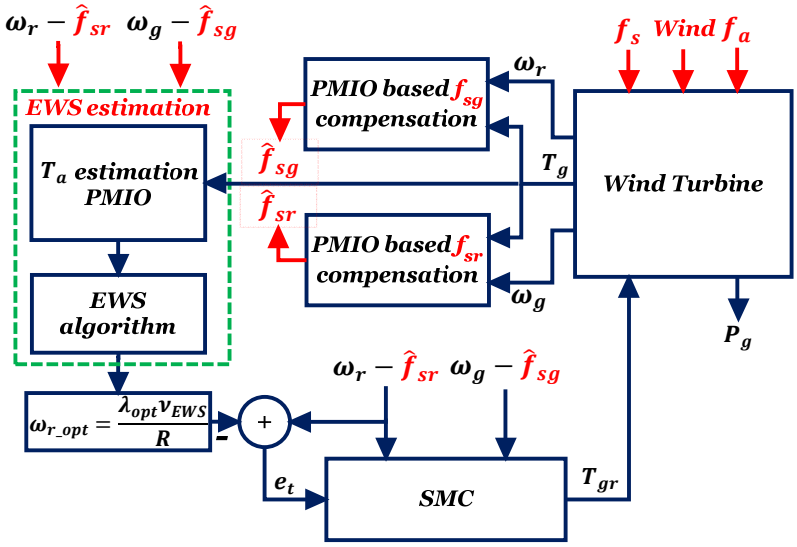

Figure 9-21: Schematic of the proposed strategy

The SMC have been already developed in Section 9-4. Moreover, the LMI-based design for the three estimators used for EWS and sensor faults estimation are given in Sections 8-2-3 and 9-5-1.

9-6-1. Simulation results

In this Section two severe sensor faults in the form of fixed measurements are considered for both ω_g and ω_r sensors simultaneously. The ω_g measurement stuck at 75(rad/s) within the period (200-400s), on the same time, ω_r measurement stuck at 1.4(rad/s). Moreover, the generator torque scale fault presented in Sections 9-4-1 and 9-5-2 is also considered in the time period (100-200s). Using the simultaneous state and sensor fault signals estimation of the two PMIOs, the third PMIO is designed to provide EWS estimation (see Figure 9-22) to be used for optimal rotor rotational speed calculation. Figure 9-23a shows the actual, measured, and estimated ω_g, whilst Figure 9-23b shows the actual, measured, and estimated ω_r. The fault estimation signal for both ω_g and ω_r measurements are shown in Figure 9-24 a &b. The scale generator torque fault and the ability of the SMC to inherently tolerate this fault is shown in Figure 9-25 a &b.

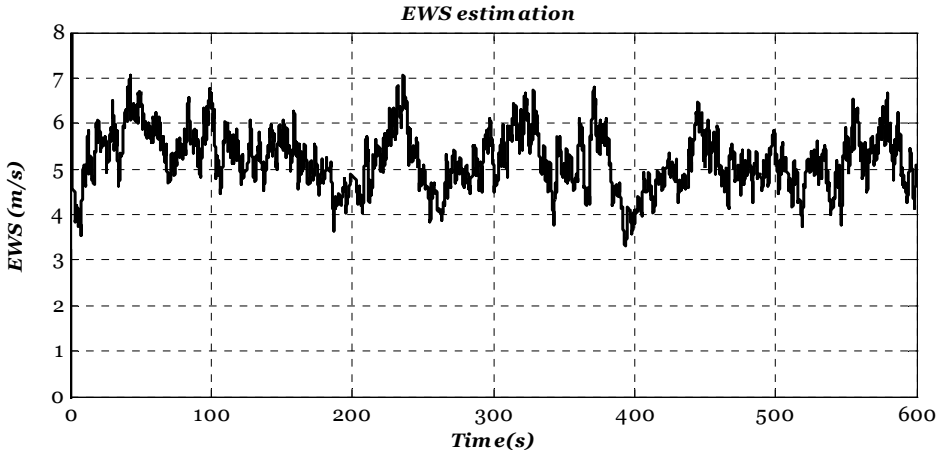

Figure 9-22: EWS estimation

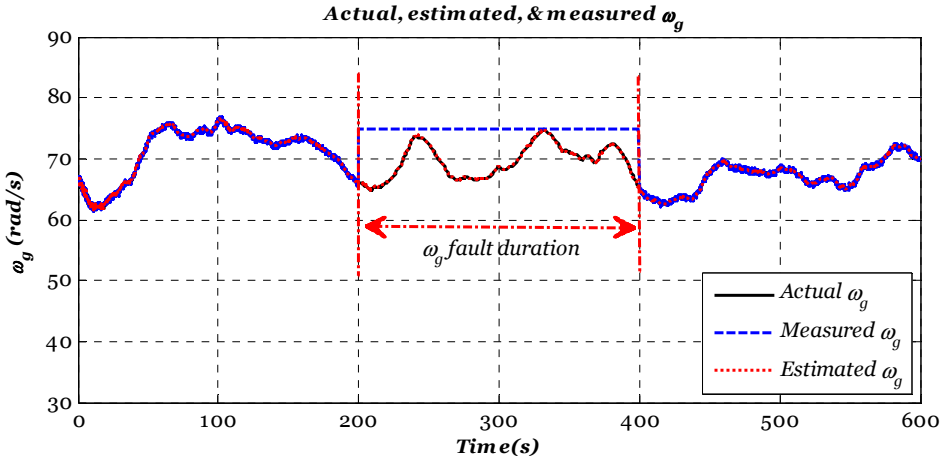

(a)

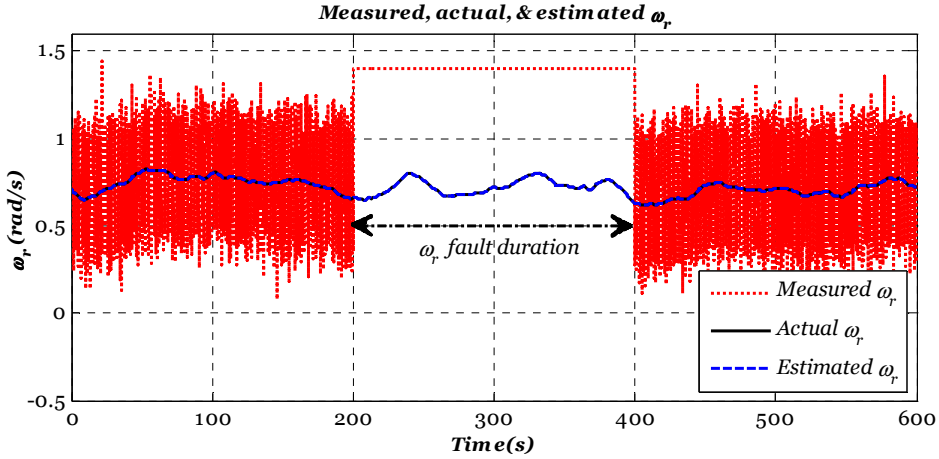

(b)

Figure 9-23: (a) Actual, measured, and estimated ω_g,

(b) Actual, measured, and estimated ω_r

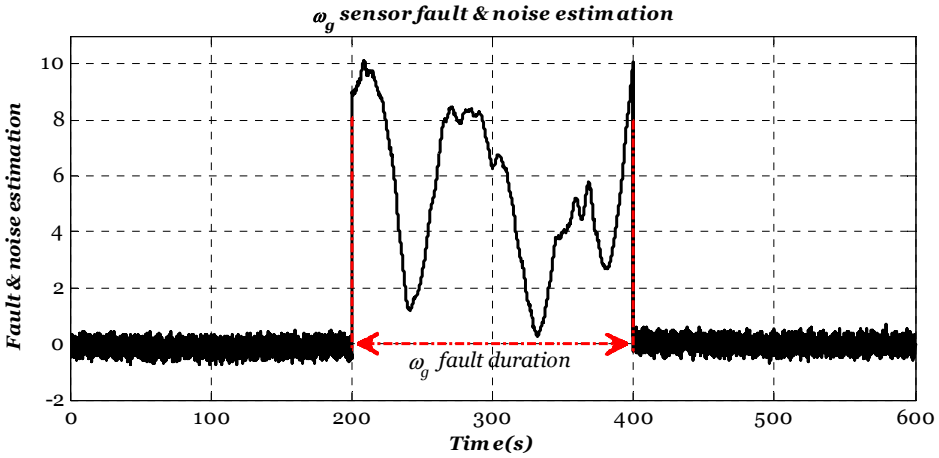

(a)

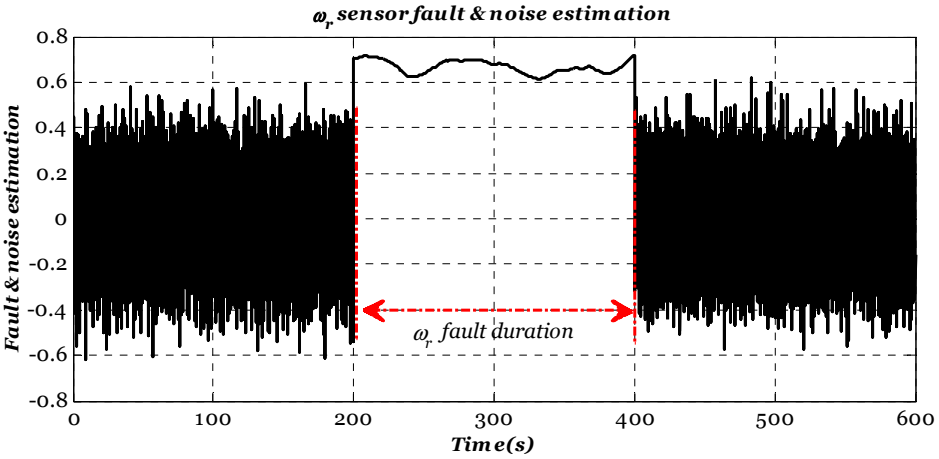

(b)

Figure 9-24 : (a) $\boldsymbol{\omega_g}$ sensor fault estimation, (b) ω_r sensor fault estimation

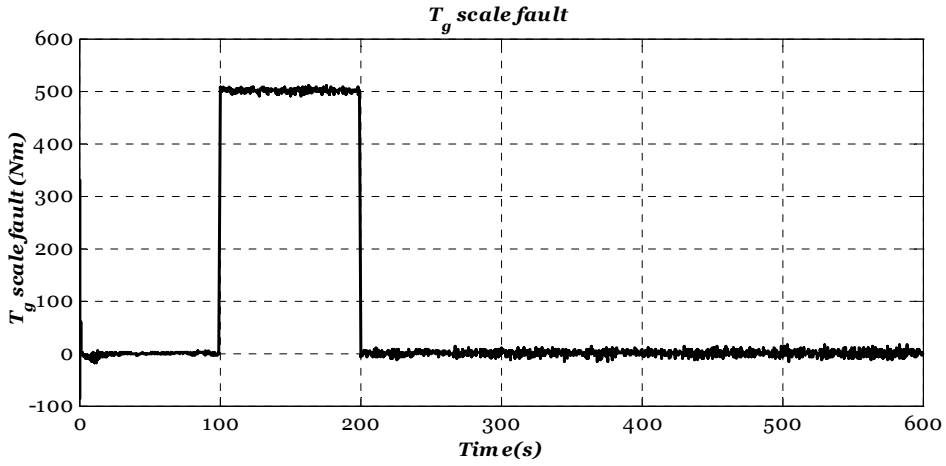

(a)

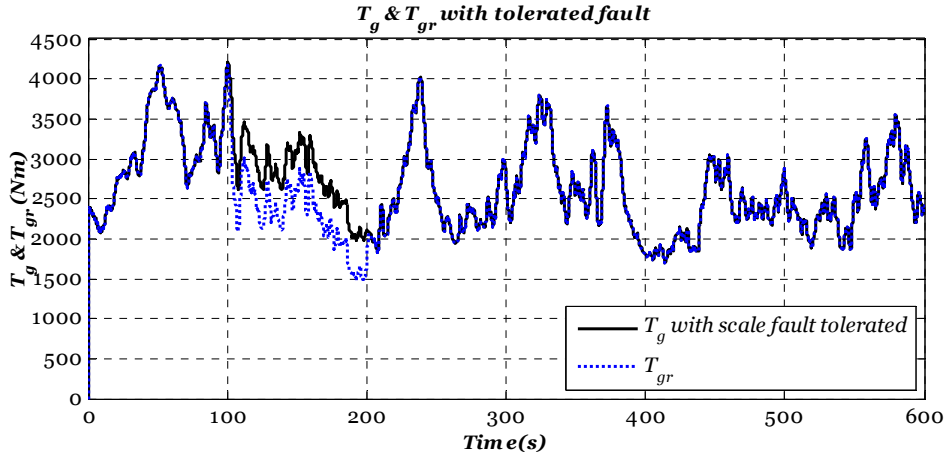

(b)

Figure 9-25 : (a) Generator torque scale fault, (b) T_{gr} tolerate the scale torque fault

9-7. Conclusion

In this Chapter different SMC strategies within the FTTC framework for sustainable operation of a wind turbine are proposed. SMC is a well-known robust control strategy. However, clear investigation of this strategy for different actuator and sensor faults has not been given in the literature. Based on the investigation of SMC robustness within the FTC framework presented in Section 9-3 the following facts are clarified:

1. Due to the discontinuous control action which maintains the closed-loop trajectory in the vicinity of the sliding surface, the SMC has inherent robustness against parametric and additive actuator faults.
2. Although the stuck actuator fault, from an SMC stand point, is similar to the effect of the match uncertainty, the SMC cannot tolerate this fault scenario due to the inability of the faulty actuator to deliver the control signal provided by the SMC.

3. The robustness of the SMC strategy against sensor faults depends on the appearance of the measured variable within the control signal. Specifically, the SMC can tolerate the effect of faulty measurement when it affects the linear component of the control signal. However, SMC lacks the ability to tolerate the effect of faulty measurement when it affect the discontinuous component of the control signal i.e. affects the sliding surface.
4. The sliding surface design is of vital important from FTC stand point. The design of this sliding surface with the minimum possible number of feedback signals offers advantageous features against some sensor faults.

Hence, the inherent robustness of the SMC against some actuator and sensor fault scenarios can be utilized as an FTC strategy that clearly obviates the need for FDI and/or fault estimation. This property of SMC is utilized in the strategy proposed in Section 9-4.

A combination of SMC with other FTC approaches is necessary to enhance the robustness of the SMC based closed-loop systems within an FTTC framework. This is the case of the strategy proposed in Section 9-5 in which the SMC is combined with the estimation and compensation concept in order to enhance the closed-loop robustness of OWTs against different fault scenarios. A further enhancement introduced in the strategy proposed in Section 9-6 via providing the closed-loop system with an estimation of the EWS signal to minimise the uncertainty in the reference optimal rotor speed.

Chapter 10 : Conclusions and future research suggestions

10-1. Conclusions and summary

10-1-1. T-S fuzzy estimation and control based AFTC

This thesis focuses on the development of active FTTC based on the concept of estimation and compensation for nonlinear systems via T-S fuzzy inference modelling. The main direction of the thesis has been shaped based on the common challenges encountered in the FTC for nonlinear systems which are:

(a) The FTC dependency on both accurate post-fault models provided by the FDD/FDI unit and/or accurate fault estimation signal.

(b) Minimizing the control reconfiguration time which is an important issue in practice where the time windows during which the system remains stable in the presence of a fault can be very short.

(c) Tolerate the simultaneous effect of actuators and sensor faults.

(d) Tackling system nonlinearity.

(e) Minimizing the complexity of the T-S fuzzy controller design.

(f) Applying the FTC strategies to application studies and stimulating interest in practical implementation. The work presented has made some contribution within each of the challenges outlined above.

The definitions of the fault, failure and faults classifications together with the explanation of both FTC and FDD methodologies have been reviewed in Chapter 1. Chapter 2 provides an introduction and overview of the traditional/modern AFTC. From the controlled system stand point, the current research interest is to develop FTC methods that have the capability to tackle the nonlinearity of the closed-loop system. Within this research trend, T-S fuzzy modelling and control is preferred over other nonlinear control strategies because, (1) T-S fuzzy control offers a systematic approach to control nonlinear systems via the a well-developed robust linear control strategy, (2)

The T-S fuzzy modelling methods can represent the nonlinear system accurately either globally or semi-globally through the use of the sector nonlinearity modelling approach. Moreover, (3) for the systems that are too difficult to be embodied in analytical models, the fuzzy modelling literature offers identification approaches to derive T-S fuzzy model. As a result, the T-S modelling and control method gives an opportunity to provide modelling of various nonlinear systems and hence it is decided to use this approach to handle system nonlinearity.

Chapter 3 presents an investigations of (a) the importance of LRMFC within the T-S fuzzy framework, and (b) how actuator and sensor faults impacts on the closed-loop performance for both regulator and tracking control problems. Via these investigations, the advantages of LRMFC and the challenges of FTC design within a regulator and tracking framework have been outlined. For example, the advantages gained by the use of LRMFC are: (i) The liner reference model has been used to overcome the hurdles associated with governing the closed-loop performance of nonlinear systems via multiple-modelling control (there is no need to use the LMI based pole-clustering), (ii) Offering more precise adjustment to the closed-loop eigenvalues if compared with LMI pole-clustering approach, and (iii) By on-line changing of the reference model response the impacts of actuator faults on closed-loop performance have been minimised.

The investigations have also shown that the regulator controllers are more immune against sensor parametric faults and can passively tolerate their effects, i.e. the steady-state value “hides” the parametric faults. Moreover, the importance of the sensor FTTC problem is attributed to the fact that, upon fault occurrence, the controller starts to direct the system according to the measurements that no longer represents the real system case. Hence, the FTTC problem is challenging from a design stand point especially for systems that are nonlinear and simultaneously affected by both actuator and sensor faults. Furthermore, it has also been shown that additive faults are a generalized fault representation that can additionally be used to assess the severity of sensor faults.

Motivated by the advantages of LRMFC and the design challenges within sensor FTTC, Chapter 4 proposed the design of three new FTTC strategies based on LRMFC. These are (i) integrated T-S fuzzy observer/VS based sensor FTTC, (ii) new T-S fuzzy PMIO based sensor FTTC, and (iii) new T-S fuzzy PPIO based actuator FTTC.

The T-S fuzzy observer/VS based sensor FTTC belongs to the control reconfiguration approach to AFTC. From the T-S framework stand point, this method cannot deal with premise variable sensor fault since handling this fault scenario will turn the design problem from measured to unmeasured premise variables design problem which requires good care against premise variable estimation error. However, this problem can be perfectly cope with by adding redundant sensors for the premise output(s) so that the fault tolerance is accomplished by switching the output to the fault-free sensor. Additionally, the method cannot tolerate the case in which the faulty parameter of the output matrix is continuously varying or similarly the problem of additive and state independent sensor faults. Consequently, the only possible solution is to turn the problem into a complete loss of measurement case provided that the detectability condition is still valid.

Consequently, the new T-S fuzzy PMIO based sensor FTTC offers more advantages if compared with VS approach such as (1) The T-S fuzzy PMIO has the capability to cope with unbounded sensor fault signals provided that its q^{th} derivative is bounded. (2) The method represents an integrated approach in which fault estimation and FTTC is performed without the need for an FDD unit. (3) Based on the fault estimation signal, an evaluation of fault severity is produce which in turn helps in managing maintenance operation. (4) Fault estimation signals can be used to compensate the effect of premise variable sensor fault so that the design problem remains as measured premise variable design. (5) The method can deal with external and state independent sensor faults as well as output matrix parametric change faults. Furthermore, the advantages of the T-S fuzzy PMIO based sensor FTTC provide enough motivation to develop similar approach for actuator FTTC whilst using T-S fuzzy PPIO instead of the PMIO proposed in sensor fault case.

As a result of the investigation and detailed discussion of the results presented in Chapter 4 for the three proposed strategies, the following points are obtained:

1. FTTC based on fault estimation and compensation approach can overcome the reconfiguration time problem arising in control reconfiguration-based FTTC. Furthermore, the inability of adaptive control-based FTTC to tolerate sensor faults means that fault estimation and compensation represents the best all round method for the sensor fault case of FTC.

2. The use of the estimation and compensation concept for FTTC represents an integrated FDD and FTC strategy. Moreover, information about fault severity is also available via the fault estimation signal.
3. The FTTC problem is challenging from a design stand point especially for systems that are nonlinear and simultaneously affected by both actuator and sensor faults.

Chapter 5 presents a novel FTTC strategy based on robust fault estimation and compensation of simultaneous actuator and sensor faults. A new architecture is proposed based on a combination of actuator and sensor T-S PMIO fault estimators together with a T-S observer-based state feedback control capable of time-varying reference tracking. The proposed architecture has the capability of taking into account some of the most challenging cases of AFTC. Firstly, it can maintain closed-loop system performance and nominal controller unchanged even in the case in which sensor and actuator faults simultaneously affect the system. Secondly, it can overcome the effects of time varying actuator and/or sensor faults with bounded q^{th} derivatives using the idea of fault estimation and compensation.

However, the main challenge encountered in this proposed method is the difficulty to satisfy the *separation principle*. Clearly, although the fuzzy controller is constructed using the local design structure, the feedback gains should be determined using global design conditions. Hence, the fuzzy control designer does not have freedom to assign the local system closed-loop poles anywhere in the stable complex plane (because of the global stability constraints). Therefore, the observer-based T-S state feedback control system suffers a major drawback in that the observer dynamics may not be assigned freely to satisfy closed-loop performance requirements. One of the possible solutions to this problem is the use of the model reference framework presented in Chapter 4 to govern the controller closed-loop system response whilst using LMI-based pole-clustering for the observer design. However, the use of LRMFC does not offer complete decoupling between the T-S controller and the T-S observer.

Chapter 6 follows the architecture proposed in Chapter 5. The proposed strategy involves the design of (i) a TSDOFC responsible for minimizing the tracking error between the reference and system output signals during nominal operation, and (ii) two T-S fuzzy observers dedicated to provide separate estimates of the actuator and sensor faults for the purpose of fault compensation. Clearly, the TSDOFC is proposed instead of the observer-based feedback controller in Chapter 5 to decouple the design of

controller and observer. Moreover, a combination of actuator and sensor T-S PPIO fault estimators have been designed to provide fast estimation of the actuator and sensor fault signals in order to compensate their effects from the input and outputs of the nonlinear system.

The significant attributes gained by using the FTTC system are:

1. The proposal of an FTTC system that robustly tolerates simultaneous sensor and actuator faults.
2. It provides an estimate time-varying actuator and sensor faults with bounded first time-derivatives using proportional and integral feedback PPIOs with T-S model structure.
3. It overcomes the hurdles imposed by the generally accepted use of T-S observer-based state estimate feedback.

While the proposed strategies in Chapter 4, 5 and 6 are based on the estimation and compensation approach, the main limitation of these strategies are summarized as follows:

- The performance of these methods is highly affected by fault estimation accuracy, the presence of any simultaneous faults, and the time behaviour of the fault.
- While estimation and compensation represents an excellent solution for different sensor fault scenarios, some limitations have been recognized in dealing with actuator faults specifically stuck fault and failure. In these cases the fault itself hides the compensation signal. These limitations open the opportunity to new research directions in the framework of simultaneous actuator and sensor faults for example the combination of control allocation and fault estimation and compensation. Moreover, in parametric actuator faults, adding compensation signals increases the faulty actuator load. This might causes the development of fault to failure faster than usual. The exception is, when the fault is just interpreted as an actuator fault (friction problem) whist in realty the actuator is still healthy. In this case, adding a compensation term is a good idea.

10-1-2. AFTC based sustainable OWTs

The last two decades have witnessed a fast growth in the use of wind energy due to some limitations inherent in the different kinds of well-known fossil fuel and nuclear

energy sources. There are several very significant challenges that characterize the design of wind turbine control systems such as the non-linearity of the aerodynamic subsystem and the dependence on a stochastic and uncontrollable EWS. Moreover, wind turbine systems demand a high degree of reliability and availability (sustainability) and at the same time are characterised by expensive and safety critical maintenance work. Actually, the recently developed OWTs are the foremost example, the OWT site accessibility and system availability is not always ensured during or soon after malfunctions, primarily due to changing weather conditions. Therefore, in Chapters 8 and 9 FTTC strategies have been proposed as a basis for sustainable OWTs.

The concept of wind turbine operation, the control problem, modes of operation and the non-linear and T-S fuzzy models of a wind turbine are presented in Chapter 7. Based on the investigation presented in this Chapter, several design constraints must be taken into account in the design of the wind turbine power maximization controller, these are: (a) Due to the non-linearity of the wind turbine aerodynamics and the stochastic and uncontrollable nature of the EWS, linear control strategies are unable to maintain acceptable performance over a wide range of wind speed. (b) T-S fuzzy estimation and control design complexity is highly reduced for this application due to the common input common output matrices of wind turbine model. (c) Accurate computation of optimal rotor speeds (the reference signal) requires an estimation of the EWS since this estimation overcomes the uncertainty in the measured wind speed. (d) Exact tracking leads to increased loading on the two drive train shafts and hence can shorten the drive train life time. It is thus very clear that the multi-objective approach cannot be avoided for robust wind turbine control design.

Chapter 8 gives an investigation of the effects of different fault scenarios on wind power conversion efficiency. Through this investigation, it has been shown how some sensor scaling faults emulate the effect of the λ_{opt} uncertainty problem due to wind turbine aging and blade deformation.

Three different FTTC strategies have been proposed to tolerate the effect of different scenarios of generator and rotor rotational speed sensor faults that affect the system in order to maintain maximization of the captured power while minimizing maintenance cost. The three proposed strategies are based on T-S fuzzy control and estimation. Specifically, the proposed strategies are: T-S observer-based state feedback sensor

FTTC, TSDOFC based sensor FTTC, and TSDOFC based sensor FTTC with EWS estimation.

Chapter 8 includes several contributions to the problem of sustainable wind turbine operation based on FTC can be summarized as follows: (1) the advantages of the proposed PMIO based state feedback sensor FTC over the generalized observer based sensor FTC proposed in the literature are (i) Obviate the need for residual evaluation and observer switching. (ii) Ability to tolerate simultaneous generator and rotor rotational speed sensor faults. (iii) The PMIO simultaneously estimates the states and the sensor fault signals. Hence, information about the fault severity can also be provided through the fault estimation signals. (2) The proposed TSDOFC based sensor FTTC with EWS estimation offers great simplification of the estimators. Moreover, it can deal with the cases of simultaneous unknown input (EWS) and unknown output (sensor fault and noise) estimation. (3) The use of PMIO to estimate the EWS offers high estimation accuracy since this estimator has the ability to provide good estimation of the unknown signals that contain fast and slow varying components.

It has been shown in Chapter 8 that sensor faults can lead to significant effects on optimizing the power harvested from wind. Moreover, stuck sensor faults may lead either to the turbine being brought to the cut-off or fast aerodynamic rotation which in turn stimulates structure vibration. Furthermore, the use of the estimation and compensation approach provides some information about fault severity and hence minimizes the need to protective, unscheduled and corrective maintenance whilst ensuring acceptable closed-loop performance over a wide range of operation conditions.

As a result, the main challenge highlighted in Chapter 8 is that the number of unknown input and output signals that affect the wind turbine system exceed the number of measurements making a challenging closed-loop robustness problem against unknown input and output signals. Specifically, the worst operation scenario of the wind turbine benchmark is that when the system is affected by the rotor and generator rotational speed sensor faults, the generator torque bias faults, as well as the recognized need for the estimation of the effective wind speed. Chapter 9 focuses on handling this challenging operation scenario by utilizing the inherent robustness of the SMC strategy within an AFTC framework to be applied to wind turbine benchmark for the power maximization problem. Based on the investigation of the robustness of the SMC against actuator and sensor faults clarifies the effectiveness of the SMC in tolerating some

actuator and sensor faults. It is clearly shown that SMC has the ability to tolerate sensor faults provided that the fault appears in the linear component of the control signal. Hence, three different FTC strategies have been proposed for sustainable OWTs utilizing (1) SMC alone, (2) combination of SMC and estimation and compensation concepts, and (3) combination of SMC and estimation and compensation concepts with EWS estimation.

10-2. Suggestions for future research

Although in this thesis new strategies have been proposed to overcome several challenges involved within the FTC framework, some improvements are still required to handle further challenges. Further research suggestions are addressed as follows:

1. As an approach to handle simultaneous actuator and sensor faults, a combination of adaptive control and robust sensor fault estimation and compensation together can be used as an alternative to the architecture proposed in Chapters 5 and 6. Clearly, the philosophy of adaptive control fits well with the AFTC approach due to the ability of adaptive control systems to adjust controller parameters on-line based on measured signals. Hence, involving the robust sensor fault estimation and compensation within the adaptive control framework enhances the overall closed-loop performance against actuator and sensor faults.
2. To cover more the challenges that arise from actuator fault scenarios, some control reconfiguration techniques can be included to the architecture presented in Chapters 5 and 6. For example, the control allocation technique can be utilized to redistribute the control action over the remaining healthy actuators during stuck or complete actuator fault.
3. As an alternative option to the interaction between the two observers proposed in Chapters 5 and, it is possible to modify the unknown input observer (UIO) type of FDD strategy to provide unknown input decoupling and fault estimation.
4. Owing to the presence of several redundant measurements in wind turbine systems, designing an integrated FDD/FTC based static VS is one of the approaches that can maintain the nominal performance of wind turbine control over a wide range of operation conditions.
5. The problem of uncertainty of λ_{opt} due to turbine aging and blade deformation together with the uncertainty in the measured wind speed represent real challenges

to power optimisation control problem. Therefore, robust estimation of these variables based on the wind turbine aerodynamic subsystem can ensure good power transformation performance.

References

Ahmed-Zaid, F., Ioannou, P., Gousman, K. & Rooney, R. 1991. Accommodation of failures in the F-16 aircraft using adaptive control. *IEEE Control Systems,* 11**,** 73-78.

Alwi, H. & Edwards, C. 2008. Fault tolerant control using sliding modes with on-line control allocation. *Automatica,* 44**,** 1859-1866.

Alwi, H., Edwards, C. & Hamayun, M. T. 2011. Nonlinear integral sliding mode fault tolerant longitudinal aircraft control. IEEE International Conference on Control Applications (CCA), 970-975. 28-30 Sept.

Alwi, H., Edwards, C. & Tan, C. P. 2009. Sliding mode estimation schemes for incipient sensor faults. *Automatica,* 45**,** 1679-1685.

Alwi, H., Edwards, C. & Tan, C. P. 2011. *Fault Detection and Fault-Tolerant Control Using Sliding Modes*, Springer-Verlag.

Amirat, Y., Benbouzid, M. E. H., Al-Ahmar, E., Bensaker, B. & Turri, S. 2009. A brief status on condition monitoring and fault diagnosis in wind energy conversion systems. *Renewable and Sustainable Energy Reviews,* 13**,** 2629-2636.

Andrawus, J. A., Watson, J. & Kishk, M. 2007. Wind turbine maintenance optimisation: principles of quantitative maintenance optimisation. *Wind Engineering,* 31(2)**,** 101-110.

Aouaouda, S., Chadli, M., Khadir, M. T. & Bouarar, T. 2012. Robust fault tolerant tracking controller design for unknown inputs T–S models with unmeasurable premise variables. *J. of Process Control,* 22**,** 861-872.

Archer, C. L. & Jacobson, M. Z. 2005. Evaluation of global wind power. *J. of geophysical research,* 110, D12110.

Ashari, A. E. & Sedigh, A. K. 2004. Reconfigurable controller design using eigenstructure assignment and genetic algorithms. SICE 2004 Annual Conference, 853-857. 4-6 Aug.

Bandyopadhyay, B., Deepak, F. & Kim, K.-S. 2009. *Sliding Mode Control Using Novel Sliding Surfaces*, Springer-Verlag.

Bartolini, G., Fridman, L., Pisano, A. & Usai, E. E. 2008. *Modern Sliding Mode Control Theory New Perspectives and Applications*, Springer-Verlag.

Bartoszewicz, A. & Nowacka-Leverton, A. 2009 *Time-Varying Sliding Modes for Second and Third Order Systems*, Springer-Verlag.

Benosman, M. & Lum, K. Y. 2010. Passive Actuators' Fault-Tolerant Control for Affine Nonlinear Systems. *IEEE Trans. on Control Systems Technology,* 18**,** 152-163.

Bianchi, D. F., De Battista, H. & Mantz, J. R. 2007. *Wind Turbine Control Systems: Principles, Modelling and Gain Scheduling Design*, Springer-Verlag.

Bin, J., Staroswiecki, M. & Cocquempot, V. 2006. Fault Accommodation for Nonlinear Dynamic Systems. *IEEE Trans. on Automatic Control,* 51**,** 1578-1583.

Bin, L., Yaoyu, L., Xin, W. & Zhongzhou, Y. 2009. A review of recent advances in wind turbine condition monitoring and fault diagnosis. IEEE Power Electronics and Machines in Wind Applications (PEMWA), 1-7. 24-26 June.

Blanke, M., Kinnaert, M., Lunze, J. & Staroswiecki, M. 2006. *Diagnosis and Fault-Tolerant Control*, Springer-Verlag.

Blanke, M., Staroswiecki, M. & Wu, N. E. 2001. Concepts and methods in fault-tolerant control. Proceedings of the American Control Conference, Arlington, Virginia, 2606-2620. 25-27 June.

Boskovic, J. D. & Mehra, R. K. 1999. Stable multiple model adaptive flight control for accommodation of a large class of control effector failures. Proceedings of the American Control Conference, San Diego, Califomia, 1920-1924. 2-4 June.

Boskovic, J. D. & Mehra, R. K. 2002. An adaptive retrofit reconfigurable flight controller. Proceedings of the 41st IEEE Conference on Decision and Control, Las Vegas, Nevada, 1257-1262. 10-13 Dec.

Bossanyi, E. A., Ramtharan, G. & Savini, B. 2009. The importance of control in wind turbine design and loading. 17th Mediterranean Conference on Control and Automation, Thessaloniki, Greece, 1269-1274. 24-26 June.

Boukhezzar, B., Lupu, L., Siguerdidjane, H. & Hand, M. 2007. Multivariable control strategy for variable speed, variable pitch wind turbines. *Renewable Energy,* 32**,** 1273-1287.

Boukhezzar, B. & Siguerdidjane, H. 2009. Nonlinear control with wind estimation of a DFIG variable speed wind turbine for power capture optimization. *Energy Conversion and Management,* 50**,** 885-892.

Boukhezzar, B. & Siguerdidjane, H. 2011. Nonlinear Control of a Variable-Speed Wind Turbine Using a Two-Mass Model. *IEEE Trans. on Energy Conversion,* 26**,** 149-162.

Boyd, S., El Ghaoui, L., Feron, E. & Balakrishnan, V. 1994. *Linear Matrix Inequalities in System and Control Theory*, Society for Industrial and Applied Mathematics (SIAM).

Burton, J. A. & Zinober, A. S. I. 1986. Continuous approximation of variable structure control. *Int. J. Systems Sci.,* 17**,** 876-885.

Burton, T., Sharpe, D., Jenkins, N. & Bossanyi, E. 2001. *Wind Energy Handbook*, John Wiley.

Calado, J., Korbicz, J., Patan, K., Patton, R. J. & Costa, J. 2001. Soft Computing Approaches to Fault Diagnosis for Dynamic Systems. *European J. of Control,* 7/2-3**,** 248-286.

Carriveau, R. 2011. *Fundamental and Advanced Topics in Wind Power.*

Caselitz, P. & Giebhardt, J. 2005. Rotor condition monitoring for improved operational safety of offshore wind energy converters. *J. of solar energy engineering,* 127**,** 253-261.

Çetin, N. S., Yurdusev, M. A. & Özdemir, A. 2005. Assessment of optimal tip speed ratio of wind turbines. *Mathematical and Computational Applications,* 10**,** 147-154.

Chadli, M. & El Hajjaji, A. 2010. Wind energy conversion systems control using T-S fuzzy modeling. 18th Mediterranean Conference on Control & Automation (MED), 1365-1370. 23-25 June 2010.

Chadli, M., Maquin, D. & Ragot, J. 2002. An LMI formulation for output feedback stabilization in multiple model approach. Proceedings of the 41st IEEE Conference on Decision and Control, Las Vegas, Nevada, 311-316. 10-13 Dec.

Chen, B.-S., Lee, C.-H. & Chang, Y.-C. 1996. H_∞ tracking design of uncertain nonlinear SISO systems: Adaptive fuzzy approach. *IEEE Trans. Fuzzy Syst.,* 4**,** 32-43.

Chen, B. & Liu, X. 2004. Reliable control design of fuzzy dynamic systems with time-varying delay. *Fuzzy Sets and Systems,* 146**,** 349-374.

Chen, J. & Patton, R. J. 1999. *Robust Model Based Fault Diagnosis for Dynamic Systems*, Kluwer Academic Publishers.

Chian-Song, C. 2010. T-S Fuzzy Maximum Power Point Tracking Control of Solar Power Generation Systems. *IEEE Trans. on Energy Conversion,* 25**,** 1123-1132.

Chian-Song, C. & Ya-Lun, O. 2011. Robust Maximum Power Tracking Control of Uncertain Photovoltaic Systems: A Unified T-S Fuzzy Model-Based Approach. *IEEE Trans. on Control Systems Technology,* 19**,** 1516-1526.

Chiang, L. H., Russell, E. L. & Braatz, R. D. 2001. *Fault Detection and Diagnosis in Industrial System*, Springer-Verlag.

Chilali, M. & Gahinet, P. 1996. H∞ design with pole placement constraints: an LMI approach. *IEEE Trans. on Automatic Control,* 41**,** 358-367.

Chun-Hsiung, F., Yung-Sheng, L., Shih-Wei, K., Lin, H. & Ching-Hsiang, L. 2006. A new LMI-based approach to relaxed quadratic stabilization of T-S fuzzy control systems. *IEEE Trans. on Fuzzy Systems,* 14**,** 386-397.

Corless, M. & Tu, J. a. Y. 1998. State and Input Estimation for a Class of Uncertain Systems. *Automatica,* 34**,** 757-764.

Corradini, M. L., Orlando, G. & Parlangeli, G. 2005. A fault tolerant sliding mode controller for accommodating actuator failures. 44th IEEE Conference on Decision and Control, and European Control Conference, Plaza de España Seville, 3091-3096. 12-15 Dec.

De Oca, S. M. & Puig, V. 2010. Fault-Tolerant Control design using a virtual sensor for LPV systems. Conference on Control and Fault-Tolerant Systems (SysTol), Nice, France, 88-93. 6-8 Oct.

Ding, S. X. 2008. *Model-based Fault Diagnosis Techniques Design Schemes, Algorithms, and Tools*, Springer-Verlag.

Dolan, D. S. L. & Lehn, P. W. 2006. Simulation Model of Wind Turbine 3p Torque Oscillations due to Wind Shear and Tower Shadow. *IEEE Trans. on Energy Conversion,* 2**,** 717-724.

Ducard, G. 2009. *Fault-tolerant Flight Control and Guidance Systems Practical Methods for Small Unmanned Aerial Vehicles*, Springer-Verlag

Edwards, C., Lombaerts, T. S. & Smaili, H. 2010. *Fault Tolerant Flight Control A Benchmark Challenge*, Springer-Verlag.

Edwards, C. & Spurgeon, S. 1998. *Sliding mode control: Theory and applications*, Taylor & Francis.

Edwards, C., Spurgeon, S. K. & Patton, R. J. 2000. Sliding mode observers for fault detection and isolation. *Automatica,* 36**,** 541-553.

Efimov, D., Cieslak, J. & Henry, D. 2012. Supervisory fault-tolerant control with mutual performance optimization. *Int. J. of Adapt. Control and Signal Processing***,** 00-00.

El Messoussi, W., Pages, O. & El Hajjaji, A. 2006. Observer-based robust control of uncertain fuzzy dynamic systems with pole placement constraints: an LMI approach. American Control Conference, Minneapolis, Minnesota 2203-2208. 14-16 June.

Esbensen, T., Jensen, B. T., Niss, M. O., Sloth, C. & Stoustrup, J. 2008. Joint Power and Speed Control of Wind Turbines. Aalborg: Aalborg University.

Esdu 1972. *Characteristics of wind speed in the lower layers of the atmosphere near the ground: Strong wind (neutral atmosphere)*, E.S.D.U. London.

Euntai, K. & Heejin, L. 2000. New approaches to relaxed quadratic stability condition of fuzzy control systems. *IEEE Trans. on Fuzzy Systems,* 8**,** 523-534.

Ezzeldin, M., Jokic, A. & Van Den Bosch, P. P. J. 2010. A parameter varying lyapunov function approach for tracking control for Takagi-Sugeno class of nonlinear systems. 8th IEEE International Conference on Control and Automation, Xiamen, China, 428-433. 9-11 June.

Falcoz, A., Henry, D. & Zolghadri, A. 2010. Robust Fault Diagnosis for Atmospheric Reentry Vehicles: A Case Study. *IEEE Trans. on Systems, Man and Cybernetics,* 40**,** 886-899.

Fang, L., Jian Liang, W. & Guang-Hong, Y. 2002. Reliable robust flight tracking control: an LMI approach. *IEEE Trans. on Control Systems Technology,* 10**,** 76-89.

Feng, G. 2010. *Analysis and Synthesis of Fuzzy Control Systems: A Model-Based Approach*, CRC Press.

Fu, Y.-P., Cheng, Y.-H., Jiang, B. & Yang, M.-K. 2011. Fault tolerant control with on-line control allocation for flexible satellite attitude control system. 2nd International Conference on Intelligent Control and Information Processing, Harbin, China, 42-46. 25-28 July.

Gao, Z. & Antsaklis, P. J. 1991. Stability of the pseudo-inverse method for reconfigurable control systems. *Int. J. of Control,* 53**,** 717-729.

Gao, Z. & Antsaklis, P. J. 1992. Reconfigurable control system design via perfect model following. *Int. J. of Control,* 56**,** 783-798.

Gao, Z. & Ding, S. X. 2007a. Actuator fault robust estimation and fault-tolerant control for a class of nonlinear descriptor systems. *Automatica,* 43**,** 912-920.

Gao, Z. & Ding, S. X. 2007b. Fault estimation and fault-tolerant control for descriptor systems via proportional, multiple-integral and derivative observer design. *IET, Control Theory & Applications,* 1**,** 1208-1218.

Gao, Z., Ding, S. X. & Ma, Y. 2007. Robust fault estimation approach and its application in vehicle lateral dynamic systems. *Optimal Control Applications and Methods,* 28**,** 143-156.

Gao, Z., Shi, X. & Ding, S. X. 2008. Fuzzy state/disturbance observer design for T-S fuzzy systems with application to sensor fault estimation. *IEEE Trans. on Systems, Man, and Cybernetics, Part B* 38**,** 875-880.

Gassara, H., El Hajjaji, A. & Chaabane, M. 2010. Observer-based robust H_∞ reliable control for uncertain T-S fuzzy systems with state time delay. *IEEE Trans. on Fuzzy Systems,* 18**,** 1027-1040.

Gayaka, S. & Bin, Y. 2011. Adaptive robust actuator fault-tolerant control in presence of input saturation. American Control Conference, San Francisco, 3766-3771. June 29-July 1.

Geromel, J. C., Bernussou, J. & De Oliveira, M. C. 1999. H_2 norm optimization with constrained dynamic output feedback controllers: decentralized and reliable control. *IEEE Trans. on Automatic Control,* 44**,** 1449-1454.

Gertler, J. 1998. *Fault Detection and Diagnosis in Engineering Systems*, Marcel Dekker

Goh, K. B., Spurgeon, S. K. & Jones, N. B. 2002. Fault diagnostics using sliding mode techniques. *Control Engineering Practice,* 10**,** 207-217.

Gopinathan, M., Boskovic, J. D., Mehra, R. K. & Rago, C. 1998. A multiple model predictive scheme for fault-tolerant flight control design. Proceedings of the 37th IEEE Conference on Decision and Control, San Diego, 1376-1381. 16-18 Dec.

Guang-Hong, Y. & Dan, Y. 2010. Reliable H_∞ Control of Linear Systems With Adaptive Mechanism. *IEEE Trans. on Automatic Control,* 55**,** 242-247.

Guang-Hong, Y., Si-Yang, Z., Lam, J. & Jianliang, W. 1998. Reliable control using redundant controllers. *IEEE Trans. on Automatic Control,* 43**,** 1588-1593.

Guelton, K., Bouarar, T. & Manamanni, N. 2009. Robust dynamic output feedback fuzzy Lyapunov stabilization of Takagi–Sugeno systems—A descriptor redundancy approach. *Fuzzy Sets and Systems,* 160**,** 2796-2811.

Guerra, T. M., Kruszewski, A., Vermeiren, L. & Tirmant, H. 2006. Conditions of output stabilization for nonlinear models in the Takagi-Sugeno's form. *Fuzzy Sets and Systems,* 157**,** 1248-1259.

Guerra, T. M. & Vermeiren, L. 2004. LMI-based relaxed nonquadratic stabilization conditions for nonlinear systems in the Takagi–Sugeno's form. *Automatica,* 40**,** 823-829.

Guo-Ping, J., Suo-Ping, W. & Wen-Zhong, S. 2000. Design of observer with integrators for linear systems with unknown input disturbances. *Electronics Letters,* 36**,** 1168-1169.

Hamayun, M. T., Edwards, C. & Alwi, H. 2011. An integral sliding mode augmentation scheme for fault tolerant control. American Control Conference, 3772-3777. June 29-July 1.

Hameed, Z., Hong, Y. S., Cho, Y. M., Ahn, S. H. & Song, C. K. 2009. Condition monitoring and fault detection of wind turbines and related algorithms: A review. *Renewable and Sustainable Energy Reviews,* 13**,** 1-39.

Hansen, A. D., Jauch, C., Sørensen, P., Iov, F. & Blaabjerg, F. 2003. Dynamic wind turbine models in power system simulation tool DIgSILENT. Roskilde, Denmark: Risø National Laboratory.

Henry, D. 2007. - Robust fault diagnosis of the microscope satellite micro-thrusters. *In:* Hong-Yue, Z. (ed.) *Fault Detection, Supervision and Safety of Technical Processes 2006.* Oxford: Elsevier Science Ltd.

Henry, D. & Zolghadri, A. 2005. Design of fault diagnosis filters: A multi-objective approach. *J. of the Franklin Institute,* 342**,** 421-446.

Ho Jae, L. & Do Wan, K. 2009. Fuzzy Static Output Feedback May Be Possible in LMI Framework. *IEEE Trans. on Fuzzy Systems* 17**,** 1229-1230.

Hsieh, C.-S. 2002. Performance gain margins of the two-stage LQ reliable control. *Automatica,* 38**,** 1985-1990.

Hu, S., Yue, D., Du, Z. & Liu, J. 2012. Reliable H_∞ non-uniform sampling tracking control for continuous-time non-linear systems with stochastic actuator faults. *IET, Control Theory & Applications,* 6**,** 120-129.

Huai-Ning, W. & Hong-Yue, Z. 2006. Reliable H_∞ fuzzy control for continuous-time nonlinear systems with actuator failures. *IEEE Trans. on Fuzzy Systems,* 14**,** 609-618.

Ibrir, S. 2004. Robust state estimation with q-integral observers. Proceedings of the American Control Conference, Boston, Massachusetts, 3466-3471. 30 June-2 July.

Ichalal, D., Marx, B., Ragot, J. & Maquin, D. 2012. New fault tolerant control strategies for nonlinear Takagi-Sugeno systems. *Int. J. Appl. Math. Comput. Sci.,* 22**,** 197–210.

Isermann, R. 2006. *Fault-Diagnosis Systems An Introduction from Fault Detection to Fault Tolerance*, Springer-Verlag.

Jelali, M. & Huang, B. 2010. *Detection and Diagnosis of Stiction in Control Loops: State of the Art and Advanced Methods*, Springer-Verlag.

Jiang, B., Gao, Z., Peng, S. & Yufei, X. 2010. Adaptive Fault-Tolerant Tracking Control of Near-Space Vehicle Using Takagi-Sugeno Fuzzy Models. *IEEE Trans. on Fuzzy Systems* 18**,** 1000-1007.

Jiang, B., Gao, Z., Shi, P. & Xu, Y. 2010. Adaptive Fault-Tolerant Tracking Control of Near-Space Vehicle Using Takagi-Sugeno Fuzzy Models. *IEEE Trans. on Fuzzy Systems,* 18**,** 1000-1007.

Jiang, B., Zhang, K. & Shi, P. 2011. Integrated Fault Estimation and Accommodation Design for Discrete-Time Takagi-Sugeno Fuzzy Systems With Actuator Faults. *IEEE Trans. on Fuzzy Systems,* 19**,** 291-304.

Jiang, J. I. N. 1994. Design of reconfigurable control systems using eigenstructure assignments. *Int. J. of Control,* 59**,** 395-410.

Jin, J. & Youmin, Z. 2006. Accepting performance degradation in fault-tolerant control system design. *IEEE Trans. on Control Systems Technology,* 14**,** 284-292.

Jin, X.-Z. & Yang, G.-H. 2009. Robust Adaptive Fault-tolerant Compensation Control with Actuator Failures and Bounded Disturbances. *Acta Automatica Sinica,* 35**,** 305-309.

Johnson, K. E. 2004. Adaptive torque control of variable speed wind turbines. National Renewable Energy Laboratory, NREL/TP-500-36265.

Johnson, K. E. & Fleming, P. A. 2011. Development, implementation, and testing of fault detection strategies on the National Wind Technology Center's controls advanced research turbines. *Mechatronics,* 21**,** 728-736.

Kamal, E., Aitouche, A., Ghorbani, R. & Bayart, M. 2012. Robust Fuzzy Fault-Tolerant Control of Wind Energy Conversion Systems Subject to Sensor Faults. *IEEE Trans. on Sustainable Energy,* 3**,** 231-241.

Kk-Electronic. Available: http://www.kk-electronic.com/Default.aspx?ID=9395 [Accessed 22/Mar/2012].

Klinkhieo, S. 2009. *On-line Estimation Approaches to Fault-Tolerant Control of Uncertain Systems.* Ph.D., The University of Hull.

Koenig, D. 2005. Unknown input proportional multiple-integral observer design for linear descriptor systems: application to state and fault estimation. *IEEE Trans. on Automatic Control,* 50**,** 212-217.

Konstantopoulos, I. K. & Antsaklis, P. J. 1996. Eigenstructure assignment in reconfigurable control systems. University of Notre Dame, ISIS-96-001.

Konstantopoulos, I. K. & Antsaklis, P. J. 1999. An optimization approach to control reconfiguration. *Dynamics and Control,* 9**,** 255-270.

Kuang-Yow, L. & Jeih-Jang, L. 2006. Output Tracking Control for Fuzzy Systems Via Output Feedback Design. *IEEE Trans. on Fuzzy Systems,* 14**,** 628-639.

Kuang-Yow, L., Liou, J. J. & Chien-Yu, H. 2006. LMI-based Integral fuzzy control of DC-DC converters. *IEEE Trans. on Fuzzy Systems,* 14**,** 71-80.

Larbah, E. & Patton, R. J. 2012. Robust decentralized control design using integral sliding mode control. UKACC International Conference on Control, Cardiff, UK, 81-86. 3-5 Sep.

Lescher, F., Zhao, J.-Y. & Borne, P. 2006. Switching LPV controllers for a variable speed pitch regulated wind turbine. *Int. J. of Comput., Communications & Control,* Vol.I 73-84.

Li, J. L. & Yang, G. H. 2012. Adaptive actuator failure accommodation for linear systems with parameter uncertainties. *IET Control Theory & Applications,* 6**,** 274-285.

Liang, B., Chang, T.-Q. & Wang, G.-S. 2011. Robust H_∞ Fault–tolerant Control against Sensor and Actuator Failures for Uncertain Descriptor Systems. *Procedia Engineering,* 15**,** 979-983.

Lin, C., Wang, Q.-G. & Heng Lee, T. 2005. Improvement on observer-based H[infinity] control for T-S fuzzy systems. *Automatica,* 41**,** 1651-1656.

Lopez-Toribio, C. J., Patton, R. J. & Daley, S. 2000. Takagi–Sugeno Fuzzy Fault-Tolerant Control of an Induction Motor. *Neural Computing & Applications,* 9**,** 19-28.

Lunze, J. & Steffen, T. 2006. Control Reconfiguration After Actuator Failures Using Disturbance Decoupling Methods. *IEEE Trans. on Automatic Control,* 51**,** 1590-1601.

Luqing, Y., Shengtie, W., Fengshan, B., Malik, O. P. & Yuming, Z. 2001. Control/maintenance strategy fault tolerant mode and reliability analysis for hydro power stations. *IEEE Trans. on Power Systems,* 16**,** 340-345.

Mansouri, B., Manamanni, N., Guelton, K. & Djemai, M. 2008. Robust pole placement controller design in LMI region for uncertain and disturbed switched systems. *Nonlinear Analysis: Hybrid Systems,* 2**,** 1136-1143.

Mansouri, B., Manamanni, N., Guelton, K., Kruszewski, A. & Guerra, T. M. 2009. Output feedback LMI tracking control conditions with H∞ criterion for uncertain and disturbed T–S models. *Information Sciences,* 179**,** 446-457.

Marcos, A., Ganguli, S. & Balas, G. J. 2005. An application of H∞ fault detection and isolation to a transport aircraft. *Control Engineering Practice,* 13**,** 105-119.

Maybeck, P. S. & Stevens, R. D. 1991. Reconfigurable flight control via multiple model adaptive control methods. *IEEE Trans. on Aerospace and Electronic Systems,* 27**,** 470-480.

Meskin, N. & Khorasani, K. 2011. *Fault Detection and Isolation Multi-Vehicle Unmanned Systems*, Springer New York Dordrecht Heidelberg London.

Munteanu, I., Bratcu, A., Cutululis, N.-A. & Ceanga, E. 2008. *Optimal Control of Wind Energy Systems: Towards a Global Approach* Springer-Verlag.

Niemann, H. & Stoustrup, J. 2005. Passive fault tolerant control of a double inverted pendulum—a case study. *Control Engineering Practice,* 13**,** 1047-1059.

Noura, H., Sauter, D., Hamelin, F. & Theilliol, D. 2000. Fault-tolerant control in dynamic systems: application to a winding machine. *IEEE Control Systems,* 20**,** 33-49.

Noura, H., Theilliol, D., Ponsart, J. & Chamseddine, A. 2009. *Fault-tolerant Control Systems Design and Practical Applications*, Springer-Verlag.

Odgaard, P. F. & Stoustrup, J. 2010. Unknown input observer based detection of sensor faults in a wind turbine. IEEE International Conference on Control Applications (CCA), 310-315. 8-10 Sept.

Odgaard, P. F., Stoustrup, J. & Kinnaert, M. 2009. Fault Tolerant Control of Wind Turbines: a Benchmark Model. 7th IFAC Symposium on Fault Detection, Supervision and Safety of Technical Processes *Safeprocess 2009*, Barcelona, 155-160. June 30 - July 3.

Østergaard, K. Z., Brath, P. & Stoustrup, J. 2007a. Estimation of effective wind speed Journal of Physics: Conference Series 75 012082.

Østergaard, K. Z., Brath, P. & Stoustrup, J. 2007b. Gain-scheduled Linear Quadratic Control of Wind Turbines Operating at High Wind Speed. IEEE International Conference on Control Applications, Singapore, 276-281. 1-3 Oct.

Østergaard, K. Z., Stoustrup, J. & Brath, P. 2009. Linear parameter varying control of wind turbines covering both partial load and full load conditions. *Int. J. of Robust and Nonlinear Control,* 19**,** 92-116.

Oudghiri, M., Chadli, M. & El Hajjaji, A. 2008. Robust observer-based fault-tolerant control for vehicle lateral dynamics. *Int. J. of Vehicle Design,* 48**,** 173-189.

Pao, L. Y. & Johnson, K. E. Year. A tutorial on the dynamics and control of wind turbines and wind farms. *In:* American Control Conference 2076-2089.

Pao, L. Y. & Johnson, K. E. 2011. Control of Wind Turbines. *IEEE Control Systems,* 31**,** 44-62.

Patton, R., Putra, D. & Klinkhieo, S. 2010a. Friction compensation as a fault-tolerant control problem. *Int. J. of Systems Science,* 41**,** 987-1001.

Patton, R. J. 1997a. Fault tolerant control: The 1997 situation. IFAC Safeprocess '97, Hull, United Kingdom., 1033-1055.

Patton, R. J. 1997b. Robustness in model-based fault diagnosis: The 1995 situation. *Annual Reviews in Control,* 21**,** 103-123.

Patton, R. J. & Chen, J. 1993. Optimal unknown input distribution matrix selection in robust fault diagnosis. *Automatica,* 29**,** 837-841.

Patton, R. J., Frank, P. M. & Clark, R. N. 1989. *Fault Diagnosis in Dynamic Systems: Theory and Application*, Prentice Hall.

Patton, R. J., Frank, P. M. & Clark, R. N. 2000. *Issues of fault diagnosis for dynamic systems*, Springer- Verlag.

Patton, R. J. & Klinkhieo, S. 2009. Actuator fault estimation and compensation based on an augmented state observer approach. Proceedings of the 48th IEEE Conference onDecision and Control, held jointly with the 28th Chinese Control Conference. CDC/CCC. , 8482-8487. 15-18 Dec.

Patton, R. J., Putra, D. & Klinkhieo, S. 2010b. Friction Compensation as a Fault-Tolerant Control Problem. *Int. J. of Systems Science,* 41.

Patton, R. J., Uppal, F. J., Simani, S. & Polle, B. 2010. Robust FDI applied to thruster faults of a satellite system. *Control Engineering Practice,* 18**,** 1093-1109.

Podder, T. K. & Sarkar, N. 2001. Fault-tolerant control of an autonomous underwater vehicle under thruster redundancy. *Robotics and Autonomous Systems,* 34**,** 39-52.

Pogoda, D. L. & Maybeck, P. S. 1989. Reconfigurable flight controller for the STOL F-15 with sensor/actuator failures. Proceedings of the IEEE National Aerospace and Electronics Conference, 318-324. 22-26 May.

Ponsart, J. C., Theilliol, D. & Aubrun, C. 2010. Virtual sensors design for active fault tolerant control system applied to a winding machine. *Control Engineering Practice,* 18**,** 1037-1044.

Puig, V. & Quevedo, J. 2001. Fault-tolerant PID controllers using a passive robust fault diagnosis approach. *Control Engineering Practice,* 9**,** 1221-1234.

Qing, W. & Mehrdad, S. 2010. Robust Fault Diagnosis of a Satellite System Using a Learning Strategy and Second Order Sliding Mode Observer. *IEEE Systems Journal* 4**,** 112-121.

Rahmat Ullah, N. & Thiringer, T. 2007. Variable speed wind turbines for power system stability enhancement. *IEEE Trans. on Energy Conversion,* 22**,** 52-60.

Rauch, H. E. 1995. Autonomous control reconfiguration. *IEEE Control Systems,* 15**,** 37-48.

Rhee, B.-J. & Won, S. 2006. A new fuzzy Lyapunov function approach for a Takagi–Sugeno fuzzy control system design. *Fuzzy Sets and Systems,* 157**,** 1211-1228.

Ribrant, J. & Bertling, L. M. 2007. Survey of Failures in Wind Power Systems With Focus on Swedish Wind Power Plants During 1997-2005. *IEEE Trans. on Energy Conversion,* 22**,** 167-173.

Richter, J. H. 2011. *Reconfigurable Control of Nonlinear Dynamical Systems A Fault-Hiding Approach*, Springer-Verlag.

Richter, J. H., Heemels, W., Van De Wouw, N. & Lunze, J. 2008. Reconfigurable control of PWA systems with actuator and sensor faults: Stability. 47th IEEE Conference on Decision and Control, 1060-1065. 9-11 Dec.

Richter, J. H., Heemels, W. P. M. H., Van De Wouw, N. & Lunze, J. 2011. Reconfigurable control of piecewise affine systems with actuator and sensor faults: Stability and tracking. *Automatica,* 47**,** 678-691.

Richter, J. H., Schlage, T. & Lunze, J. 2007. Control reconfiguration of a thermofluid process by means of a virtual actuator. *IET Control Theory & Applications,* 1**,** 1606-1620.

Rodrigues, M., Theilliol, D., Adam-Medina, M. & Sauter, D. 2008. A fault detection and isolation scheme for industrial systems based on multiple operating models. *Control Engineering Practice,* 16**,** 225-239.

Sami, M. & Patton, R. J. 2012a. Fault tolerant adaptive sliding mode controller for wind turbine power maximisation. 7th IFAC Symposium on Robust Control Design, Aalborg Congress & Culture Centre, Denmark, 499-504. 20-22 Jun.

Sami, M. & Patton, R. J. 2012b. A fault tolerant approach to sustainable control of offshore wind turbines. 2nd International Symposium On Environment Friendly Energies And Applications, Northumbria University, UK, 25–27 June.

Sami, M. & Patton, R. J. 2012c. Fault tolerant output feedback tracking control for nonlinear systems via T-S fuzzy modelling. 8th IFAC Symposium on Fault Detection, Supervision and Safety of Technical Processes, Mexico City, Mexico, 999-1004. 29-31 Aug.

Sami, M. & Patton, R. J. 2012d. An FTC approach to wind turbine power maximisation via T-S fuzzy modelling and control. 8th IFAC Symposium on Fault Detection, Supervision and Safety of Technical Processes, Mexico City, Mexico, 349-354. 29-31 Aug.

Sami, M. & Patton, R. J. 2012e. Global wind turbine FTC via T-S fuzzy modelling and control. 8th IFAC Symposium on Fault Detection, Supervision and Safety of Technical Processes, Mexico City, Mexico, 325-330. 29-31 Aug.

Sami, M. & Patton, R. J. 2012f. A multiple-model approach to fault tolerant tracking control for non-linear systems. 20th Mediterranean Conference on Control & Automation, Barcelona, 498-503. 3-6 July.

Sami, M. & Patton, R. J. 2012g. Wind turbine power maximisation based on adaptive sensor fault tolerant sliding mode control. 20th Mediterranean Conference on Control & Automation, Barcelona, 1183-1188. 3-6 July.

Sami, M. & Patton, R. J. 2012h. Wind turbine sensor fault tolerant control via a multiple-model approach. The 2012 UKACC International Conference on Control, Cardiff, 3-5 Sep.

Sanchez-Parra, M., Suarez, D. A. & Verde, C. 2011. Fault tolerant control for gas turbines. 16th International Conference on Intelligent System Application to Power Systems, 1-6. 25-28 Sept.

Seo, C.-J. & Kim, B. K. 1996. Robust and reliable H∞ control for linear systems with parameter uncertainty and actuator failure. *Automatica,* 32**,** 465-467.

Seron, M. M. & De Dona, J. A. 2009. Fault tolerant control using virtual actuators and invariant-set based fault detection and identification. Proceedings of the 48th IEEE Conference on Decision and Control, held jointly with the 28th Chinese Control Conference, 7801-7806. 15-18 Dec.

Seron, M. M., De Dona, J. A. & Martinez, J. J. 2009. Improved multisensor switching scheme for fault tolerant control. Proceedings of the 48th IEEE Conference on Decision and Control, held jointly with the 28th Chinese Control Conference, 7807-7812. 15-18 Dec.

Shengqi, S., Liang, D., Cuijuan, A. & Wenwei, L. 2009. Fault-tolerant control design for linear systems with input constraints and actuator failures. Chinese Control and Decision Conference, 5278-5283. 17-19 June.

Sijun, Y., Youmin, Z., Xinmin, W. & Rabbath, C. A. 2009. Robust Fault-Tolerant Control using on-line control re-allocation with application to aircraft. American Control Conference, 5534-5539. 10-12 June.

Šiljak, D. D. 1980. Reliable control using multiple control systems. *Int. J. of Control,* 31**,** 303-329.

Simani, S. & Patton, R. J. 2008. Fault diagnosis of an industrial gas turbine prototype using a system identification approach. *Control Engineering Practice,* 16**,** 769-786.

Sloth, C., Esbensen, T. & Stoustrup, J. 2010. Active and passive fault-tolerant LPV control of wind turbines. American Control Conference, 4640-4646. June 30 -July 2.

Sloth, C., Esbensen, T. & Stoustrup, J. 2011. Robust and fault-tolerant linear parameter-varying control of wind turbines. *Mechatronics,* 21**,** 645-659.

Slotine, J.-J. E. & Li, W. 1991. *Applied Nonlinear Control*, Prentice-Hall.

Soliman, M., Elshafei, A. L., Bendary, F. & Mansour, W. 2009. LMI static output-feedback design of fuzzy power system stabilizers. *Expert Systems with Applications,* 36**,** 6817-6825.

Song, B. & Hedrick, J. K. 2011. *Dynamic Surface Control of Uncertain Nonlinear Systems: An LMI*, Springer-Verlag.

Staroswiecki, M. 2005. Fault tolerant control using an admissible model matching approach. 44th IEEE Conference on Decision and Control, and European Control Conference, 2421-2426. 12-15 Dec.

Staroswiecki, M. 2006. Robust Fault Tolerant Linear Quadratic Control based on Admissible Model Matching. 45th IEEE Conference on Decision and Control, 3506-3511. 13-15 Dec.

Stefani, R. T., Shahian, B., Savant, C. J. & Hostetter, G. 2002. *Design of feedback control systems*, Oxford university press.

Steffen, T. 2005. *Control Reconfiguration of Dynamical Systems*, Springer-Verlag.

Steinberg, M. 2005. Historical overview of research in reconfigurable flight control. *Proceedings of IMechE, Part G: J. of Aerospace Engineering,* 219**,** 263-275.

Sugeno, M. & Kang, G. T. 1988. Structure identification of fuzzy model. *Fuzzy Sets and Systems,* 28**,** 15-33.

Sung, H. K., Lee, S. H. & Bien, Z. 2005. Design and implementation of a fault tolerant controller for EMS systems. *Mechatronics,* 15**,** 1253-1272.

Takagi, T. & Sugeno, M. 1985. Fuzzy Identification of Systems and Its Applications to Modeling and Control. *IEEE Trans. on Systems, Man, and Cybernetics,* 15**,** 116-132.

Tan, C. P. & Edwards, C. 2002. Sliding mode observers for detection and reconstruction of sensor faults. *Automatica,* 38**,** 1815-1821.

Tan, C. P. & Edwards, C. 2003. Sliding mode observers for robust detection and reconstruction of actuator and sensor faults. *Int. J. of Robust and Nonlinear Control,* 13**,** 443-463.

Tanaka, K., Hori, T. & Wang, H. O. 2003. A multiple Lyapunov function approach to stabilization of fuzzy control systems. *IEEE Trans. on Fuzzy Systems,* 11**,** 582-589.

Tanaka, K., Ikeda, T. & Wang, H. O. 1998. Fuzzy regulators and fuzzy observers: relaxed stability conditions and LMI-based designs. *IEEE Trans. on Fuzzy Systems,* 6**,** 250-265.

Tanaka, K. & Wang, H. O. 2001. *Fuzzy Control Systems Design and Analysis: A Linear Matrix Inequality Approach*, John Wiley.

Tao, G., Chen, S., Tang, X. & Joshi, S. M. 2004. Adaptive control of systems with actuator failures. *Int. J. of Robust and Nonlinear Control*.

Tao, G., Joshi, S. M. & Ma, X. 2001. Adaptive state feedback and tracking control of systems with actuator failures. *IEEE Trans. on Automatic Control,* 46**,** 78-95.

Technology, E. E. 2011. *http://eetweb.com/wind/wind-turbines-go-supersized-20091001/* [Online]. [Accessed 19/11/2011 2011].

Tehrani, E. S. & Khorasani, K. 2009. *Fault Diagnosis of Nonlinear Systems Using a Hybrid Approach*, Springer Science & Business Media.

Teixeira, M. C. M. & Zak, S. H. 1999. Stabilizing controller design for uncertain nonlinear systems using fuzzy models. *IEEE Trans. on Fuzzy Systems* 7**,** 133-142.

The World Wind Energy Association. 2012. Available: http://www.wwindea.org/technology/ch03/en/3_4_3.html [Accessed 27-March 2012].

Theilliol, D., C\, \#233, Join, D. & Zhang, Y. 2008. Actuator Fault Tolerant Control Design Based on a Reconfigurable Reference Input. *Int. J. Appl. Math. Comput. Sci.,* 18**,** 553-560.

Theilliol, D., Noura, H. & Sauter, D. 1998. Fault-tolerant control method for actuator and component faults. Proceedings of the 37th IEEE Conference on Decision and Control, Tampa, Florida USA, 604-609. 16-18 Dec.

Thiringer, T. O. & Petersson, A. 2005. control of a variable speed pitch regulated wind turbine. Goteborg, Sweden: Chalmers University of Technology.

Ting, Y., Tosunoglu, S. & Fernandez, B. 1994. Control algorithms for fault-tolerant robots. IEEE International Conference on Robotics and Automation, 910-915. 8-13 May.

Tong, S., Yang, G. & Zhang, W. 2011. Observer-based fault-tolerant control against sensor failures for fuzzy systems with time delays. *Int. J. of Appl. Math. and Comput. Sci.,* 21**,** 617-627.

Tseng, C.-S., Chen, B.-S. & Uang, H.-J. 2001. Fuzzy tracking control design for nonlinear dynamic systems via T-S fuzzy model. *IEEE Trans. on Fuzzy Systems,* 9**,** 381-392.

Tuan, H. D., Apkarian, P., Narikiyo, T. & Yamamoto, Y. 2001. Parameterized linear matrix inequality techniques in fuzzy control system design. *IEEE Trans. on Fuzzy Systems,* 9**,** 324-332.

Uppal, F. J. & Patton, R. J. 2005. Neuro-fuzzy uncertainty de-coupling: a multiple-model paradigm for fault detection and isolation. *Int. J. of Adapt. Control and Signal Processing,* 19**,** 281-304.

Utkin, V. I. 1992. *Sliding Modes in Control and Optimization*, Springer-Verlag.

Van Bussel, G. J. W. & Zaaijer, M. B. 2001. Reliability, Availability and Maintenance Aspects of Large-Scale Offshore Wind Farms, a Concepts Study. Marine Renewable Energies Conference, Newcastle, 119-126. 27-28 Dec.

Veillette, R. J. 1995. Reliable linear-quadratic state-feedback control. *Automatica,* 31**,** 137-143.

Veillette, R. J., Medanic, J. B. & Perkins, W. R. 1992. Design of reliable control systems. *IEEE Trans. on Automatic Control,* 37**,** 290-304.

Verbruggen, T. W. 2003. Wind turbine operation and maintenance based on condition monitoring. Energy Research Center of the Netherlands, Technical Report ECN-C-03-047.

Wang, H.-J., Lin, Y.-S., Xue, A.-K., Pan, H.-P. & Lu, R.-Q. 2008. Reliable Robust H∞ Tracking Control for a Class of Uncertain Lur e Singular Systems. *Acta Automatica Sinica,* 34**,** 893-899.

Wang, J. & Shao, H. 2000. Delay-dependent robust and reliable H_∞ control for uncertain time-delay systems with actuator failures. *J. of the Franklin Institute,* 337**,** 781-791.

Wei, X. & Liu, L. 2010. Fault estimation of large scale wind turbine systems. Proceedings of the 29th Chinese Control Conference, 4869-4874. 29-31 July.

Wei, X. & Verhaegen, M. 2008. Fault detection of large scale wind turbine systems: A mixed H∞/H- index observer approach. 16th Mediterranean Conference on Control and Automation, 1675-1680. 25-27 June.

Weng, Z., Patton, R. J. & Cui, P. 2007. Active fault-tolerant control of a double inverted pendulum. *J. of Systems and Control Engineering* 221**,** 221: 895.

Wilfrid, P. & Jean, P. B. 2002. *Sliding mode control in engineering*, Marcel Dekker.

Witczak, M., Dziekan, L., Puig, V. & Korbicz, J. 2008. Design of a fault-tolerant control scheme for Takagi-Sugeno fuzzy systems. 16th Mediterranean Conference on Control and Automation, Ajaccio, 280-285. 25-27 June.

Wright, A. D. & Balas, M. J. 2004. Design of Controls to Attenuate Loads in the Controls Advanced Research Turbine. ASME Wind Energy Symposium, Reno, Nevada January 5–8.

Www.Caithnesswindfarms.Co.Uk. 2012. Available: http://www.caithnesswindfarms.co.uk/ [Accessed 15-Feb 2012].

Www.Siemens.Co.Uk. 2012. *http://www.siemens.co.uk/pool/news_press/news_archive/2012/offshoreturbine.jpg* [Online]. [Accessed Feb. 2012].

Www.Smart-Energy.Com. 2012. *http://www.smart-energy.com/images/offshore-wind-turbine-installation01.jpg* [Online]. [Accessed Feb. 2012].

Xiaodong, L. & Qingling, Z. 2003. New approaches to H∞ controller designs based on fuzzy observers for T-S fuzzy systems via LMI. *Automatica,* 39**,** 1571-1582.

Xie, L. & De Souza Carlos, E. 1992. Robust H_∞ control for linear systems with norm-bounded time-varying uncertainty. *IEEE Trans. on Automatic Control,* 37**,** 1188-1191.

Xin, D. & Guang-Hong, Y. 2007. Switching control in adaptive state feedback tracking of systems with actuator failures. IEEE International Conference on Control Applications 622-627. 1-3 Oct.

Xuejing, C. & Fen, W. 2009. A robust fault tolerant control approach for LTI systems with actuator and sensor faults. Chinese Control and Decision Conference 890-895. 17-19 June.

Yang, G.-H. & Ye, D. 2011. *Reliable Control and Filtering of Linear Systems with Adaptive Mechanisms*, Taylor and Francis Group.

Yang, G. H., Wang, J. L. & Soh, Y. C. 2000. Reliable LQG control with sensor failures. *IEE Proceedings - Control Theory and Applications,* 147**,** 433-439.

Yang, H., Jiang, B. & Cocquempot, V. 2010. *Fault Tolerant Control Design for Hybrid Systems*, Springer-Verlag.

Ye, D. & Guang-Hong, Y. 2006. Adaptive Fault-Tolerant Tracking Control Against Actuator Faults With Application to Flight Control. *IEEE Trans. on Control Systems Technology,* 14**,** 1088-1096.

Yen, G. G. & Liang-Wei, H. 2003. Online multiple-model-based fault diagnosis and accommodation. *IEEE Trans. on Industrial Electronics,* 50**,** 296-312.

Yew-Wen, L., Der-Cheng, L. & Ti-Chung, L. 2000. Reliable control of nonlinear systems. *IEEE Trans. on Automatic Control,* 45**,** 706-710.

Yixin, D. & Passino, K. M. 2001. Stable fault-tolerant adaptive fuzzy/neural control for a turbine engine. *IEEE Trans. on Control Systems Technology,* 9**,** 494-509.

Zhang, K., Jiang, B. & Cocquempot, V. 2008. Adaptive Observer-based Fast Fault Estimation. *Int. J. of Control, Automation, & Systems,* 6**,** 320-326.

Zhang, K., Jiang, B. & Shi, P. 2009. A New Approach to Observer-Based Fault-Tolerant Controller Design for Takagi-Sugeno Fuzzy Systems with State Delay. *Circuits, Systems, and Signal Processing,* 28**,** 679-697.

Zhang, K., Jiang, B. & Staroswiecki, M. 2010. Dynamic Output Feedback-Fault Tolerant Controller Design for Takagi-Sugeno Fuzzy Systems With Actuator Faults. *IEEE Trans. on Fuzzy Systems,* 18**,** 194-201.

Zhang, Q., Ye, S., Li, Y. & Wang, X. 2011. An Enhanced LMI Approach for Mixed H2/H∞ Flight Tracking Control. *Chinese J. of Aeronautics,* 24**,** 324-328.

Zhang, Y. & Jiang, J. 2001. Integrated active fault-tolerant control using IMM approach. *IEEE Trans. on Aerospace and Electronic Systems,* 37**,** 1221-1235.

Zhang, Y. & Jiang, J. 2008. Bibliographical review on reconfigurable fault-tolerant control systems. *Annual Reviews in Control,* 32**,** 229-252.

Zhang, Y. M. & Jiang, J. 2002. Active fault-tolerant control system against partial actuator failures. *IEE Proceedings Control Theory and Applications,* 149**,** 95-104.

Zhao, Q. & Jiang, J. 1998. Reliable State Feedback Control System Design Against Actuator Failures. *Automatica,* 34**,** 1267-1272.

Zolghadri, A., Henry, D. & Monsion, M. 1996. Design of nonlinear observers for fault diagnosis: A case study. *Control Engineering Practice,* 4**,** 1535-1544.

Zou, A.-M. & Kumar, K. D. 2011. Adaptive fuzzy fault-tolerant attitude control of spacecraft. *Control Engineering Practice,* 19**,** 10-21.